Generalized continua and applications to finite deformations of quasi-inextensible fiber reinforcements

Marco Valerio D'Agostino

N° d'ordre 2015ISAL0061
Année 2015

Thèse

Generalized continua and applications to finite deformations of quasi-inextensible fiber reinforcements

Milieux continus généralisés: application aux grandes transformations des renforts de composites quasi-inextensibles

Présentée devant
L'institut national des sciences appliquées de Lyon

Pour obtenir
Le grade de docteur

Formation doctorale
Ecole doctorale Mécanique, Energétique, Génie Civil, Acoustique (MEGA)
Spécialité : Mécanique, génie mécanique

Par
Marco Valerio D'AGOSTINO

Soutenue le 07 Septembre 2015 devant la Commission d'examen

Jury

BOISSE Philippe	Pr. (LaMCoS, INSA Lyon-CNRS)	Directeur
CARON Jean-François	DR (Navier, Ecole des Ponts-CNRS)	Rapporteur
CHABRAND Patrick	Pr. (ISM, Aix-Marseille Université-CNRS)	Examinateur
DELL'ISOLA Francesco	Pr. (DISG, La Sapienza, Italie)	Examinateur
LIMAM Ali	Pr. (LGCIE, INSA Lyon)	Examinateur
MADEO Angela	McF HDR (LGCIE, INSA Lyon)	Co-encadrante
SEPPECHER Pierre	Pr. (IMath, Université de Toulon)	Rapporteur

LaMCoS - UMR CNRS 5259 - INSA de Lyon

20, avenue Albert Einstein, 69621 Villeurbanne Cedex (FRANCE)

INSA Direction de la Recherche - Ecoles Doctorales – Quinquennal 2011-2015

SIGLE	ECOLE DOCTORALE	NOM ET COORDONNEES DU RESPONSABLE
CHIMIE	**CHIMIE DE LYON** **http://www.edchimie-lyon.fr** Sec : Renée EL MELHEM Bat Blaise Pascal 3e etage 04 72 43 80 46 Insa : R. GOURDON secretariat@edchimie-lyon.fr	M. Jean Marc LANCELIN Université de Lyon – Collège Doctoral Bât ESCPE 43 bd du 11 novembre 1918 69622 VILLEURBANNE Cedex Tél : 04.72.43 13 95 directeur@edchimie-lyon.fr
E.E.A.	**ELECTRONIQUE, ELECTROTECHNIQUE, AUTOMATIQUE** **http://edeea.ec-lyon.fr** Sec : M.C. HAVGOUDOUKIAN Ecole-doctorale.eea@ec-lyon.fr	M. Gérard SCORLETTI Ecole Centrale de Lyon 36 avenue Guy de Collongue 69134 ECULLY Tél : 04.72.18 60.97 Fax : 04 78 43 37 17 Gerard.scorletti@ec-lyon.fr
E2M2	**EVOLUTION, ECOSYSTEME, MICROBIOLOGIE, MODELISATION** **http://e2m2.universite-lyon.fr** Sec : Safia AIT CHALAL Bat Atrium- UCB Lyon 1 04.72.44.83.62 Insa : S. REVERCHON Safia.ait-chalal@univ-lyon1.fr	M. Fabrice CORDEY Laboratoire de Géologie de Lyon Université Claude Bernard Lyon 1 Bât Géode – Bureau 225 43 bd du 11 novembre 1918 69622 VILLEURBANNE Cédex Tél : 04.72.44.83.74 Sylvie.reverchon-pescheux@insa-lyon.fr fabrice.cordey@ univ-lyon1.fr
EDISS	**INTERDISCIPLINAIRE SCIENCES-SANTE** **http://www.ediss-lyon.fr** Sec : Safia AIT CHALAL Bat Atrium – UCB Lyon 1 04 72 44 83 62 Insa : Safia.ait-chalal@univ-lyon1.fr	Mme Emmanuelle CANET-SOULAS INSERM U1060, CarMeN lab, Univ. Lyon 1 Bâtiment IMBL 11 avenue Jean Capelle INSA de Lyon 696621 Villeurbanne Tél : 04.72.11.90.13 Emmanuelle.canet@univ-lyon1.fr
INFOMATHS	**INFORMATIQUE ET MATHEMATIQUES** **http://infomaths.univ-lyon1.fr** Sec :Renée EL MELHEM Bat Blaise Pascal 3e etage infomaths@univ-lyon1.fr	Mme Sylvie CALABRETTO LIRIS – INSA de Lyon Bat Blaise Pascal 7 avenue Jean Capelle 69622 VILLEURBANNE Cedex Tél : 04.72. 43. 80. 46 Fax 04 72 43 16 87 Sylvie.calabretto@insa-lyon.fr
Matériaux	**MATERIAUX DE LYON** **http://ed34.universite-lyon.fr** Sec : M. LABOUNE PM : 71.70 –Fax : 87.12 Bat. Direction 1er et. Ed.materiaux@insa-lyon.fr	M. Jean-Yves BUFFIERE INSA de Lyon MATEIS Bâtiment Saint Exupéry 7 avenue Jean Capelle 69621 VILLEURBANNE Cedex Tél : 04.72.43 71.70 Fax 04 72 43 85 28 Ed.materiaux@insa-lyon.fr
MEGA	**MECANIQUE, ENERGETIQUE, GENIE CIVIL, ACOUSTIQUE** **http://mega.universite-lyon.fr** Sec : M. LABOUNE PM : 71.70 –Fax : 87.12 Bat. Direction 1er et. mega@insa-lyon.fr	M. Philippe BOISSE INSA de Lyon Laboratoire LAMCOS Bâtiment Jacquard 25 bis avenue Jean Capelle 69621 VILLEURBANNE Cedex Tél : 04.72 .43.71.70 Fax : 04 72 43 72 37 Philippe.boisse@insa-lyon.fr
ScSo	**ScSo*** **http://recherche.univ-lyon2.fr/scso/** Sec : Viviane POLSINELLI Brigitte DUBOIS Insa : J.Y. TOUSSAINT viviane.polsinelli@univ-lyon2.fr	Mme Isabelle VON BUELTZINGLOEWEN Université Lyon 2 86 rue Pasteur 69365 LYON Cedex 07 Tél : 04.78.77.23.86 Fax : 04.37.28.04.48 isavonb@dbmail.com

*ScSo : Histoire, Géographie, Aménagement, Urbanisme, Archéologie, Science politique, Sociologie, Anthropologie

Abstract

The micro-structure of materials is an essential feature for the design of engineering structures with improved performances. There are several possible approaches to the complex problem of considering the effect of microstructures on the overall mechanical behavior of real materials which basically belong to two philosophical categories:

- start from the description of the micro-scale to arrive to the description of the macro-scale,
- directly start from the description of the macro-scale somehow accounting for the presence of micro-scales.

We refrain here from a deep analysis of the two "philosophies", limiting ourselves to discuss some of their advantages and disadvantages. Indeed, a remarkable literature exists based on the adoption of the first viewpoint: start from the microscopic properties of complex materials to arrive to the homogenized ones. With this respect, one can cite so-called homogenization models, multi-scale methods, upscaling procedures and so on. The common idea to all such approaches is to establish "a priori" the characteristics of the microstructure (e.g. topology, mechanical stiffnesses, distribution of different phases, etc.) and develop suitable tools for arriving to the global mechanical properties at higher scales. The main advantage of this type of methods is that they allow to directly know how the macroscopic parameters are related to the microscopic ones. It is clear that such kind of information is a really useful tool since it suffices to observe the characteristics of a given microstructure to arrive to the homogenized descriptors which can henceforth be used to describe the material behavior at higher scales. Nevertheless, some drawbacks can also be reported about such methods which are substantially related to the fact that some simplifying assumptions about the characteristics of the microstructure are sometimes needed and often become too restrictive to be able to give rise to a homogenized behavior which is fully representative of the real material at higher scales. For example, some standard homogenization techniques intrinsically need the imposition of boundary conditions between representative cells and it is difficult to establish wether one type of boundary conditions is more realistic than another. As a result, we can summarize by saying that it is true that the homogenized system keeps in its memory some informations about the microscopic characteristics of the system itself, but often the simplifying hypotheses which have been made at the level of the microstructure are too restrictive to assure that the obtained homogenized system is fully able to describe the real macroscopic material behavior. The second possible type of approach is to start directly from the description of the macroscopic scale by developing models which are able to describe the average mechanical behavior of the considered material by means of a relatively small set of macroscopic descriptors. The main advantage of this kind of approach is that real material behaviors can be described by means of few constitutive parameters at those macroscopic scales which are often interesting from an engineering point of view. Moreover, the efficacy of the adopted macroscopic theory can be easily compared with experiments which can be precisely conceived and reproduced on specimens which have reasonable sizes to be handled without problems related e.g. to the smallness of the samples themselves. Finally, the real material behavior being described by a limited number of parameters, it is conceivable to design structures which have rather sophisticated shapes and large dimensions just relying on few equations describing the global mechanical behavior

of the considered structure. On the other hand, the drawbacks of such a type of procedures are twofold

- one must know that, even if in a simplified macroscopic framework, the global theory must be complemented with some additional macroscopic descriptors if one wants to model some macroscopic manifestations of the microstructure and
- it is often hard to accomplish the inverse task of relating the proposed macroscopic descriptors to precise characteristics of the microstructure.

In summary, if such macroscopic models are able to be more easily handled at scales which are peculiar of engineering design, some difficulties arise when one needs to relate the used macroscopic descriptors to detailed microscopical properties. Generalized continuum theories belong to the second of the quoted categories and, in this memoir, we will try to analyze wether their possible use can provide some advantages when dealing with real engineering problems. We are of course aware that the first category previously discussed is as legitimate as the second one for approaching a wealthy of problems, but its study will not be the object of the present manuscript. Instead, we will focus on a discussion about the use of generalized continuum theories to model materials with microstructure: we regard such theories as a reasonable "engineering" compromise between the complexity of the model which we want to use and the detail at which microstructures can be described. In the framework of continuum theories, the systematic use of continuum Cauchy theories may sometimes represent a too drastic simplification of reality since some essential characteristics related to the heterogeneity of microstructures are implicitly neglected in such models. Every material is actually heterogeneous if one considers sufficiently small scales: it suffices to go down to the molecular or atomic level to be aware of such heterogeneity. Nevertheless, very often, the effect of microstructure cannot be detected at the engineering scale. In such cases, continuum Cauchy theory is a suitable choice for modeling the mechanical behavior of considered materials in the simplest and more effective way. However, there are some cases in which the considered materials are heterogeneous even at relatively large scales and, as a consequence, the effect of microstructure on the overall mechanical behavior of the medium cannot be neglected. In such situations, Cauchy continuum theory may not be useful to fully describe the mechanical behavior of considered materials. It is in fact well known that such continuum theory is not able to catch significant phenomena related to concentrations of stress and strain and to specific deformation patterns in which high gradients of deformation occur and which are, in turn, connected to particular phenomena which take place at lower scales. Moreover, Cauchy models are not able to catch in an appropriate way the dynamical response of some micro-structured materials showing dispersive behaviors or even frequency band-gaps. Generalized continuum theories may be good candidates to model such micro-structured materials in a more appropriate way (both in the static and dynamic regime) since they are able to account for the description of the macroscopic manifestation of the presence of microstructure in a rather simplified way.
The present manuscript is organized as follows:

- In chapter 1 a general description of fibrous composite reinforcements is given, with particular attention to the introduction of standard experimental tests which are used to characterize the micro- and macro-structural mechanical properties of such materials.
- In chapter 2 some fundamental issues concerning classical continuum mechanical models are recalled. Moreover, second gradient continuum models are introduced and discussed by means of the Principle of Virtual Work. Since the applications targeted in this manuscript are limited to static cases, we refrain here to treat the more general case including inertia effects.
- In chapter 3 we start analyzing some discrete and continuum models for the description of the mechanical behavior of 2D woven composites. At this stage of the manuscript, we want to show

how some discrete numerical simulations allowed us to unveil some very special deformation modes related to the effect of the local bending of fibers on the overall macroscopic deformation of fibrous composite reinforcements. Such discrete simulations showed rather clearly that microscopic bending of the fibers cannot be neglected when considering the deformation of fibrous composite reinforcements. For this reason, we subsequently introduced a continuum model which is able to account for such microstructure-related effects by means of second gradient terms appearing in the strain energy density.

- In chapter 4 we reduce the general continuum mechanical framework introduced in Chapter 2 to the particular case of 2D continua. We put a strong accent on the geometric interpretation of second gradient deformation measures which are seen to be directly related to the the in-plane curvatures of suitable coordinate lines. Such coordinate lines will be interpreted in the next chapters are the yarns of the considered 2D woven composite, so acquiring a direct physical sense.

- In chapter 5 we introduce a strong kinematical hypothesis on the admissible deformations, assuming that the yarns composing the woven reinforcements are inextensible. Such assumption allows us to build-up a simplified first gradient model for the behavior of 2D woven reinforcements which is still representative of their mechanical behavior. A constrained least Action principle is proposed and the associated integral Euler-Lagrange equations are presented. A numerical method allowing to show some solutions concerning the case of bias extension test is implemented in Mathematica® and the obtained results are discussed.

Résumé

La microstructure des matériaux constitue un outil essentiel pour optimiser les propriétés mécaniques des structures et ainsi améliorer leurs performances. Il existe plusieurs approches qui prennent en compte les effets de la micro-structure sur le comportement macroscopique des matériaux, elles appartiennent à l'une des catégories suivantes :

- description du comportement à l'échelle macroscopique à partir d'une description de celui-ci à l'échelle microscopique,
- description directe du comportement macroscopique tenant indirectement compte de la présence d'une micro-structure.

Ne voulant pas aborder ici le problème délicat de l'analyse approfondie de ces deux approches qui sont philosophiquement distinctes, on se limitera à mettre en évidence leurs principaux avantages et inconvénients. En effet, il existe une littérature abondante qui se fonde sur le premier point de vue : obtenir les propriétés homogénéisées du comportement mécanique des matériaux complexes à l'échelle macroscopique en partant d'une description détaillée de leurs propriétés microscopiques. On peut citer à ce propos les méthodes d'homogénéisation, les méthodes multi-échelles, les procédures de upscaling, etc. L'idée commune à toutes ces approches consiste à établir a priori les caractéristiques de la microstructure (par exemple la topologie, les propriétés mécaniques, la distribution des phases, etc.) et d'en déduire les propriétés mécaniques aux échelles supérieures en développant les outils adaptés. L'avantage principal de ce type de méthode se situe dans la connaissance directe des liens entre les paramètres microscopiques et macroscopiques. Ce type d'information est alors très utile puisqu'il suffira de prendre en compte les caractéristiques d'une microstructure donnée pour obtenir les caractéristiques homogénéisées permettant de décrire le comportement du matériau à l'échelle macroscopique. Cependant, on doit aussi mentionner les limites de ce type d'approches micro-macro, limites pour la plupart liées aux hypothèses simplificatrices nécessaires pour la description de la microstructure. Celles-ci peuvent être excessives et ne plus permettre de représenter correctement le comportement macroscopique. Par exemple, certaines techniques d'homogénéisation standard nécessitent l'introduction de conditions aux limites adaptées entre les cellules élémentaires et il est difficile de connaître a priori le type de conditions aux limites les plus réalistes. On peut en conclure que si le système homogénéisé conserve bien une mémoire de la microstructure sous-jacente, les hypothèses associées à sa description sont souvent trop restrictives pour permettre la reconstruction complète du comportement réel du matériau. Le deuxième type d'approche possible consiste à partir directement de la description à l'échelle macroscopique en développant des modèles capables de décrire le comportement moyen du matériau par un ensemble relativement limité de paramètres. L'avantage fondamental de ce type d'approche réside dans la possibilité de décrire le comportement du matériau microstructuré à partir de l'introduction, à l'échelle macroscopique, de ce nombre restreint de paramètres, ce qui est d'un grand intérêt pour les sciences de l'ingénieur. En outre, la validité du modèle macroscopique adopté peut être directement évaluée par l'intermédiaire d'essais mécaniques effectués sur des échantillons dont les dimensions sont suffisamment grandes pour être réalisés facilement. On peut ainsi décrire le comportement global de structures de dimensions importantes et de géométries complexes, en utilisant peu de paramètres et peu d'équations. Il existe néanmoins quelques inconvénients liés à ces approches purement macroscopiques :

- il faut être conscient que le modèle global doit être complété par des paramètres supplémentaires permettant de décrire certains effets de la microstructure et
- il est souvent compliqué de relier explicitement ces paramètres macroscopiques aux propriétés de la micro- structure.

En résumant, on peut dire que ces dernières approches sont plus faciles d'utilisation aux échelles habituelles des sciences de l'ingénieur, mais il est alors plus difficile d'établir le lien entre les paramètres et la microstructure. Les théories des milieux continus généralisés appartiennent à la deuxième classe des modèles cités. On essaiera d'analyser dans ce travail les situations dans lesquelles leur utilisation permet d'apporter des avantages évidents. Même si la première classe de modèles permet aussi la description de certains comportements, leur analyse ne fait pas partie de l'objet de ce manuscrit. On se focalisera plutôt sur l'utilisation des théories de milieux continus généralisés pour la description du comportement mécanique de certains matériaux microstructurés, en considérant ces théories comme un compromis raisonnable entre d'une part la complexité du modèle, et d'autre part le niveau de détail auquel les microstructures peuvent être décrites. Dans le cadre des théories des milieux continus généralisés, l'utilisation systématique d'une théorie dite de Cauchy conduit souvent à des simplifications trop fortes de la réalité. En effet, certaines caractéristiques de la microstructure sont implicitement négligées dans ces approches. Cependant, même si tous les matériaux sont hétérogènes à une échelle suffisamment petite et possèdent donc une microstructure, celle-ci n'induit pas forcément un comportement spécifique à une échelle macroscopique. Dans ce cas, la théorie de Cauchy sera parfaitement adaptée à leur description. D'autres matériaux en revanche, possèdent des microstructures à une échelle beaucoup plus grande (micron, millimètre, centimètre), dont l'effet se répercute sur le comportement macroscopique. Le modèle de Cauchy est alors insuffisant pour décrire leur comportement global spécifique, lié par exemple à la concentration d'efforts ou de déformations, ou encore à des modes de déformations particuliers caractérisés par de forts gradients locaux induisant des comportements eux-mêmes liés à ce qui se passe à des échelles plus petites. Les modèles de Cauchy ne sont pas non plus adaptés à la description de la réponse dynamique de certains matériaux microstructurés montrant des comportements dispersifs ou des band-gaps. Les théories de milieux continus généralisés peuvent être de bonnes candidates pour modéliser ces matériaux d'une façon plus précise et plus réaliste, aussi bien en statique qu'en dynamique, puisqu'elles peuvent décrire, même d'une façon simplifiée, la manifestation macroscopique de la présence d'une microstructure. Dans l'état actuel des connaissances et de la technologie, il est intéressant de faire porter les efforts sur la concep- tion de matériaux microstructurés pouvant présenter des propriétés originales afin d'améliorer et d'optimiser les réponses des structures qui les utilisent. En effet, ces structures conçues en utilisant de tels matériaux microstructurés – aussi connus sous le nom de matériaux architecturés ou metamatériaux – peuvent présenter des résistances améliorées, des facilités de mise en forme, des poids minimisés, etc. Elles peuvent également posséder des propriétés innovantes dans le domaine du contrôle des vibrations ou dans le domaine de la furtivité. Certaines microstructures génèrent en effet des propriétés très particulières vis à vis de la propagation d'ondes, ce qui confère aux structures résultantes des solutions de choix comme écran ou absorbeur d'ondes. Le nouveau concept de metamatériaux est en train d'intéresser de plus en plus les physiciens et les mécaniciens. Ces matériaux sont obtenus par l'assemblage optimal de plusieurs éléments individuels disposés en sous-structures périodiques ou quasi-périodiques et permettent ainsi l'obtention de propriétés très originales. En effet, la forme, la géométrie, les dimensions, le contraste des propriétés mécaniques, l'orientation et la disposition de ces éléments peuvent influencer par exemple la propagation d'ondes, d'une façon telle qu'aucun matériau naturel n'est capable de concurrencer. Les propriétés ainsi créées peuvent certainement donner lieu à des applications innovantes en ingénierie.
Un des domaines d'application les plus prometteurs des théories de milieux continus généralisés concerne l'étude du comportement mécanique des renforts tissés de composites. Cette classe de metamatériaux est en effet constituée par le tissage de mèches (constituées de nombreuses fibres plus fines), dont les rigidités sont très différentes en traction et en cisaillement : les mèches sont

très raides en traction mais l'angle entre deux mèches peut varier très facilement. Ce contraste très marqué des propriétés mécaniques de la meso-structure du matériau permet de décrire ses propriétés homogénéisées dans le cadre d'une théorie de deuxième gradient. En effet, les théories de Cauchy standard ne sont pas à même de décrire certains motifs de déformation qui sont souvent observés comme par exemple, des concentrations de gradients de déformation dans des couches limites très fines reliées aux déformations en flexion des mèches, et donc indirectement aux déformations en flexion des fibres. Il est important de noter qu'en aucun cas une théorie de Cauchy ne peut tenir compte des conséquences des mécanismes de déformation de flexion de la meso-structure sur le comportement mécanique global d'une pièce, alors même qu'il est facile de comprendre que ces mécanismes de déformation ont un effet macroscopique notamment lors de conditions aux limites ou de conditions de chargement particuliers. La manifestation macroscopique de la meso-structure peut en effet jouer un rôle majeur lors de la mise en forme des renforts de composites puisque ces renforts sont contraints de prendre des formes très particulières pour permettre la réalisation d'éléments structuraux de géométrie complexe. Lors du processus de mise en forme, la rigidité en flexion des mèches joue certainement un rôle très important sur la déformation globale de la pièce. C'est pour cette raison, principalement, qu'une théorie de milieux continus généralisés devient un outil important pour la modélisation. Des raisonnements du même type que ceux exposés jusqu'ici peuvent être formulés pour les composites constitués par des renforts fibreux englobés dans une matrice molle. Dans ce cas, les théories de milieux continus généralisés s'appliquent lorsque l'on considère l'ensemble du matériau fini : renfort fibreux + matrice molle.
Ce manuscrit est organisé comme suit :

- Dans le chapitre 1 nous introduisons les aspects généraux de la mécanique des renforts fibreux de composites avec une attention particulière à la description des tests mécaniques standards qui sont souvent utilisés pour caractériser les propriétés micro et macro de ces matériaux.

- Dans le chapitre 2 nous rappelons certains concepts fondamentaux concernant la mécanique des milieux continus classiques. De plus, nous introduisons les théories de deuxième gradient à l'aide du Principe des Travaux Virtuels.

- Dans le chapitre 3 nous nous proposons de présenter une première modélisation des renforts fibreux de composites en mettant en place des modèles numériques discrets. Cette modélisation discrète permet de rendre compte de certains effets de la microstructure des renforts fibreux sur leur comportement macroscopique global. En particulier, il sera montré que la flexion locale des mèches à l'échelle mesoscopique a un effet non-négligeable sur le comportement macroscopique global de ces matériaux. Dans un deuxième moment nous introduisons une modélisation continue de deuxième gradient pour la description des mêmes matériaux et nous montrons que les termes d'ordre supérieur permettent une description satisfaisante des effets de flexion locale sur-cités.

- Dans le chapitre 4 on particularise le cadre général de la mécanique des milieux continus introduit dans le chapitre 2 au cas particulier des milieux continus 2D. On mettra un accent fort sur l'interprétation géométrique des mesures de déformation de deuxième gradient qui seront directement reliées aux courbures dans le plan de certaines lignes matérielles. Ces lignes matérielles seront ensuite interprétées dans les chapitres suivantes comme décrivant les mèches des renforts fibreux de composites qu'on se propose d'étudier.

- Dans le chapitre 5 nous introduisons une hypothèse cinématique forte sur les déformations admissibles, en supposant que les mèches du renfort considéré sont inextensibles. Cette hypothèse nous permettra de construire un modèle simplifié de premier gradient pour le comportement des renforts de composites 2D qui est encore représentatif de leur comportement mécanique. Une méthode numérique permettant de montrer certaines solutions concernant le cas du bias extension test est codée en Mathematica® et les résultats obtenus sont discutés.

General Introduction

It is today well accepted that a major scientific challenge is that of finding innovative ways of assembling different components in periodic or quasi-periodic patterns in order to design new metamaterials showing better performances and new functionalities. We are more and more accustomed to expressions such as complex materials, architectured materials, metamaterials, smart materials and so on. With all such expressions one wants to generally indicate materials exhibiting different mechanical responses at different scales due to different levels of heterogeneity. The main characteristic of such materials is that their overall mechanical behavior of is macroscopically influenced by the underlying microstructure, especially in presence of particular loading and/or boundary conditions. It is then clear that the fact of understanding the mechanics of meso- and micro-structured materials is becoming a fundamental issue in engineering and science. Complex metamaterials may exhibit superior mechanical properties with respect to more commonly used engineering materials, also providing some advantages as easy formability processes, light weight and exotic behaviors with respect to wave propagation. In this manuscript we address the problem of the description of the mechanical behavior of a class of complex engineering materials which are known as woven fibrous composite reinforcements. These materials possess a hierarchical microstructure, since they are constituted by woven tows which are themselves made up of thousand of fibers. The high contrast between the high tension stiffness of the yarns and the very low resistance to angle variations is a fundamental characteristic of such materials which contributes to the need of using a second gradient theory for their mechanical description (see e.g. PIERRE ALIBERT). We will show that the micro-structure of fibrous composites actually has a strong impact on the overall mechanical behavior of the macroscopic engineering piece. In particular, according to the approach followed in this work, the macroscopic manifestation of the microstructure of such materials is accounted for by

- the use of suitable orthotropic constitutive laws which allow for the description of two privileged directions in the material corresponding to warp and weft and
- the introduction of second gradient terms in the strain energy density which permit to take into account the bending stiffness of the yarns.

A first gradient continuum orthotropic model is not able, alone, to take into account all the possible effects that the microstructure of considered materials have on their macroscopic deformation. More precisely, as we will show, some particular loading conditions, associated to particular types of boundary conditions may cause some microstructure-related deformation modes which are not fully taken into account in first gradient continuum theories. One way to deal with the description of such microstructure-induced deformations, while remaining in the framework of a macroscopic theory, is to consider so-called "generalized continuum theories". Such generalized theories allow for the introduction of a class of internal actions which is wider than the one which is accounted for by classical first gradient Cauchy continuum theory. These more general contact actions excite additional deformation modes which can be seen to be directly related with the properties of the microstructure of the considered materials. The main aim of the present work is to explicitly show the interest of using second gradient theories for the modeling of the mechanical behavior of fibrous composite reinforcements. This task will be accomplished by structuring the present manuscript as follows:

- In chapter 1 a general description of fibrous composite reinforcements is given, with particular attention to the introduction of standard experimental tests which are used to characterize the micro- and macro-structural mechanical properties of such materials.

- In chapter 2 some fundamental issues concerning classical continuum mechanical models are recalled. Moreover, second gradient continuum models are introduced and discussed by means of the Principle of Virtual Work. Since the applications targeted in this manuscript are limited to static cases, we refrain here to treat the more general case including inertia effects.

- In chapter 3 we start analyzing some discrete and continuum models for the description of the mechanical behavior of 2D woven composites. At this stage of the manuscript, we want to show how some discrete numerical simulations allowed us to unveil some very special deformation modes related to the effect of the local bending of fibers on the overall macroscopic deformation of fibrous composite reinforcements. Such discrete simulations showed rather clearly that microscopic bending of the fibers cannot be neglected when considering the deformation of fibrous composite reinforcements. For this reason, we subsequently introduced a continuum model which is able to account for such microstructure-related effects by means of second gradient terms appearing in the strain energy density.

- In chapter 4 we reduce the general continuum mechanical framework introduced in Chapter 2 to the particular case of 2D continua. We put a strong accent on the geometric interpretation of second gradient deformation measures which are seen to be directly related to the the in-plane curvatures of suitable coordinate lines. Such coordinate lines will be interpreted in the next chapters are the yarns of the considered 2D woven composite, so acquiring a direct physical sense.

- In chapter 5 we introduce a strong kinematical hypothesis on the admissible deformations, assuming that the yarns composing the woven reinforcements are inextensible. Such assumption allows us to build-up a simplified first gradient model for the behavior of 2D woven reinforcements which is still representative of their mechanical behavior. A constrained least Action principle is proposed and the associated integral Euler-Lagrange equations are presented. A numerical method allowing to show some solutions concerning the case of bias extension test is implemented in Mathematica® and the obtained results are discussed. We finally compare the obtained numerical solutions with an analogous model implemented in COMSOL® in order to be sure that the COMSOL® model gives the same results as the Mathematica® code.

Contents

Chapter 1

Composite materials

Contents

1.1 Introduction

By composite materials we generally mean all materials that are composed at least of two distinct constituents, which can have very different physical or chemical properties, assembled in a specific way that gives to the final material specific characteristics which differ significantly from those of every individual component. Composite materials are usually constituted by two phases, namely the reinforcement and the matrix. These two phases posses different functionalities: the reinforcement gives the fundamental mechanical properties to the material and the matrix plays the role of cohesion between the different components. There exists several examples of natural or artificial materials which respect the definition given above and which can henceforth be classified as composite materials. Among them we can list, for example

- ***Carbon-fiber-reinforced polymers:*** they are composed of a woven fibrous reinforcement in which a polymeric resin is injected to give rise to the final engineering piece.

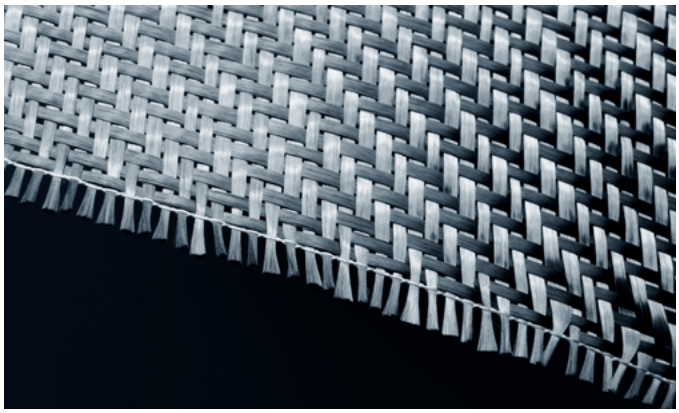

Figure 1.1: Example of carbon fabric

- ***Concrete:*** it consists of loose stones held with a matrix of cement.

Figure 1.2: Concrete

- ***Sandwich structure panel:*** it is a material realized attaching two stiff thin skins to a thick lightweight core.

Figure 1.3: Sandwich panel used at NASA

- ***Plywood:*** it is a sheet material realized from thin layers of wood veneer that are glued together rotated up to 90 degrees to one another.

Figure 1.4: Plywood used in construction

- ***Bone tissue:*** it is constituted by a hydroxyapatite matrix reinforced with collagen fibres.

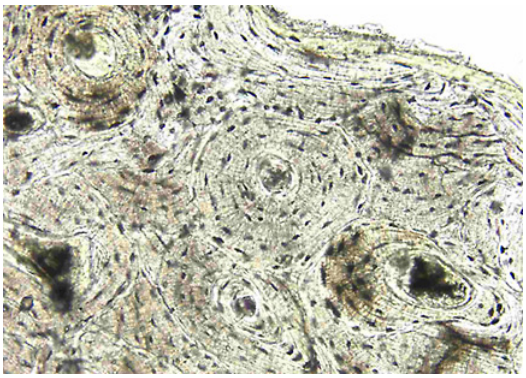

Figure 1.5: Bone tissue structure

In this manuscript we will focus our attention on the description of the mechanical behavior of some particular composite materials which are known as woven fiber-reinforced composites. Such materials

are conceived by molding the raw fiber reinforcement into the desired shape and then injecting a polymeric resin which confers the final stiffness to the engineering piece. In the framework of the present manuscript we will study of the mechanical behavior of the raw woven reinforcement alone, before the injection of the polymeric resin. This fact is of crucial interest for an accurate description of the forming process of such reinforcements. The tools which are needed to develop a complete theoretical framework for the description of the behavior of such materials are not trivial since different complicated aspects must be taken into account, such as:

- development of suitable hyperelastic constitutive laws which allow for the description of an average material behavior at large strains,
- development of a generalized continuum theory which is able to account for the effect of the presence of the mesostructure on the overall mechanical behavior of the considered material.

In this chapter we introduce composite materials, in general and fibrous composite reinforcements, in particular. We then explicitly show that fibrous composite reinforcements are materials with hierarchical microstructure and this fact confers them peculiar mechanical properties. Indeed, different scales of heterogeneities may be identified, namely the microscopic scale (scale of the fiber), the mesoscopic scale (of the yarns) and the macroscopic scale (of the engineering piece). The micro- and meso-structure of the materials considered in this thesis play a crucial role on the overall mechanical behavior of the material at the macroscopic scale. We try here to specify which are the main characteristics of the micro- and meso-structures which have a macroscopic manifestation on the overall behavior of woven fibrous composite reinforcements. We presented some simple and standard mechanical tests which allow to characterize some basic macroscopic deformation modes as related to the meso- and microscopic ones. All the considerations exposed in this chapter are at the basis of the conception of suitable macroscopic hyperelastic constitutive laws to be used in the modeling of fibrous composite reinforcements in the framework of a continuum theory.

1.2 Carbon fiber reinforced polymer: production method

In this work we will consider only composite materials in which the reinforcement is constituted by carbon fibers which are suitably woven together in order to give rise to materials which are very easily molded in complex shapes. More particularly, we will focus on the description of the composite alone during its forming process before that the polymeric resin is injected and cured. In this section we analyze the process of fabrication of these reinforcements explaining briefly the various production steps. The understanding of such processes is important to understand which are the mechanical properties which can be conferred to the reinforcement by changing the production process.

In order to obtain the final engineering pieces usually employed in aeronautical engineering the following steps are implemented:

1. fiber manufacturing,
2. obtaining of yarns by assembling the single fibers together,
3. weaving of the yarns to get the reinforcement,
4. molding of the reinforcement into the desired shape,
5. injection of the polymeric resin,
6. solidification of the resin.

In what follows, we analyze in some detail certain aspects of the manufacturing process of fiber composite materials.

1.2.1 Fibers and yarns

There are mainly two ways to manufacture carbon fibers:

- starting from polyacrylonitrile fibers (PAN),
- starting from pitch fibers.

In the first case, the carbon fibers are made by conversion of a precursor in polyacrylonitrile. The filaments are first spun from the precursor heated to its oxidation temperature, then held under tension, and then carbonized in a nitrogen atmosphere at about 1 200 C°. The non-carbon elements volatilize, leaving mainly carbon. The fibers obtained after this step are called high resistance fibers (RH). An additional step of graphitization at 2500 C° allows to perfect the structure and obtain so-called high-modulus fibers (MH). Variations during step graphitization lead to different types of fibers.
For the case of pitch fibers, the filaments are cooked, after spinning, at 600 C°, then carbonized in a nitrogen atmosphere at 2500 C° to enrich them with carbon. The obtained fibers show a very good level of carbon. However, the difficulty of removing impurities in the original pitch gives them a lower tensile stiffness.
The last step before obtaining usable fibers is the textile sizing. This operation consists of treating the fiber surface and it plays a leading role in their lifetime. Its main function is to achieve better compatibility and greater cohesion between fiber and matrix to optimize the mechanical properties of the final piece. Its composition may vary significantly from one producer to another.

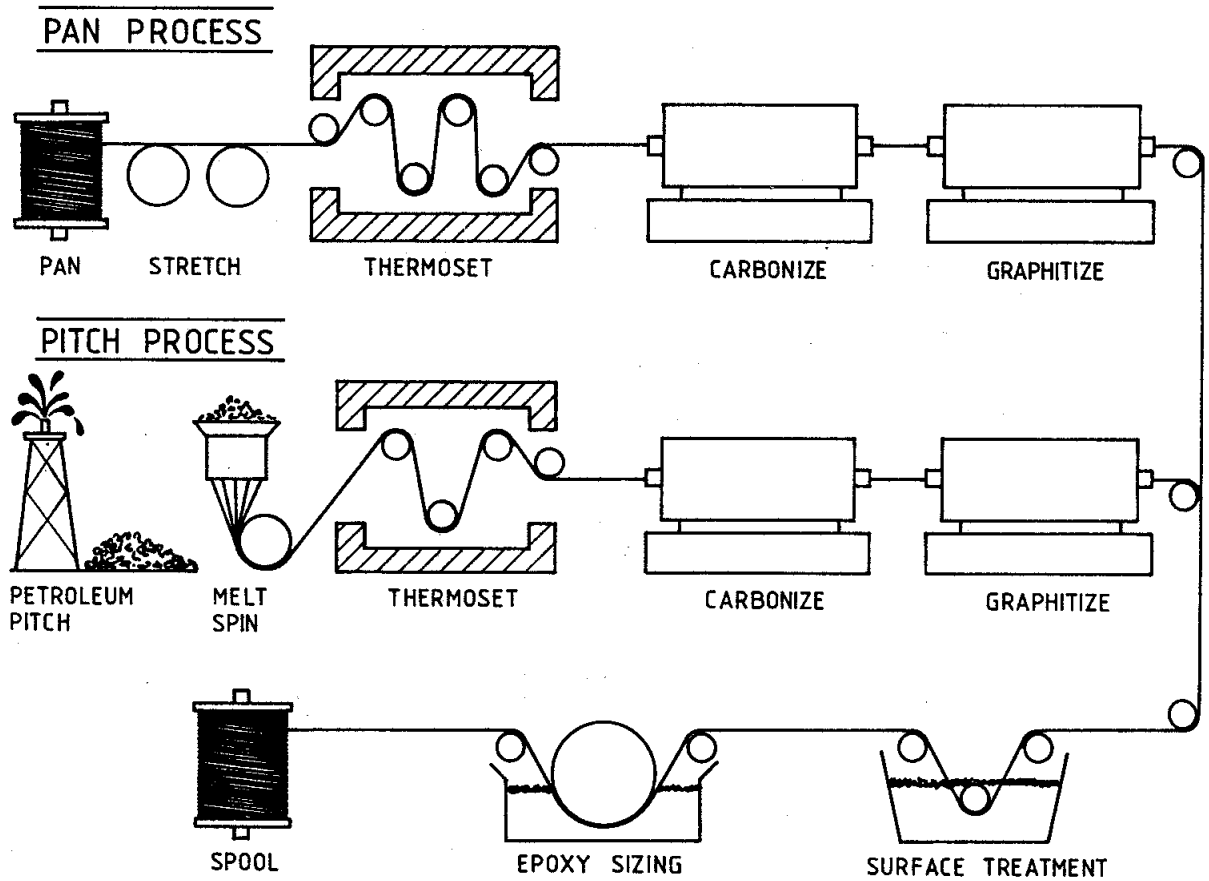

Figure 1.6: PAN and pitch based carbon fiber manufacturing procedure.

The obtained fibers can undergo treatments or transformations in order to give them new properties (see Fig. 1.6). In our case, they are assembled into yarns, with possible additional treatments.

Once assembled, the strands of carbon fibers generally contain between 3,000 and 48,000 fibers. The characteristic quantities generally used to describe a yarn are: material, type of assembly, number of fibers, fiber diameter, linear density, rigidity and tensile strength.

1.2.2 Reinforcement

The reinforcements studied in this manuscript are assemblies of carbon yarns obtained by weaving. Weaving can be 2D (surface), 2.5D (interlocks) or 3D (three-dimensional). The first ones are obtained interlacing the yarns in two perpendicular preferred directions called warp and weft. The type of arrangement used is said armor of the reinforcement. For the 2D case, the traditional armor of the textile industry are used. For 3D weaving, a third direction is added to the thickness of reinforcement. Finally, the weavings called 2.5D, are situated on the border between woven 2D and 3D.

A reinforcement armor is obtained from a weaving machine (loom), in the same way as clothing textiles. The weaving process requires a number of steps performed by specific parts of the weaving machine as schematically shown in Figure 1.2.2.

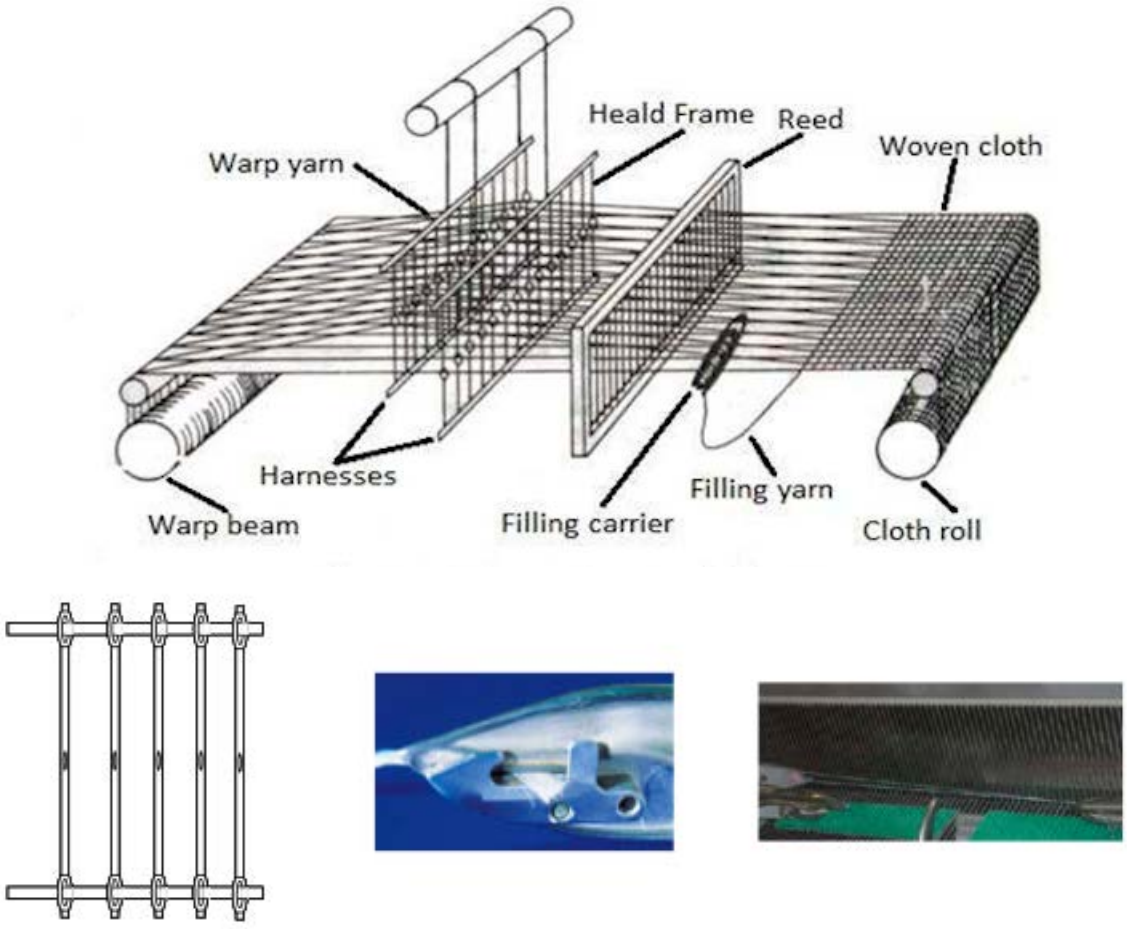

Figure 1.7: Basic structure of a loom

Regarding the 2D fabrics, there are three main armors (see Fig.1.8):

- plain weave, it is the simplest armor: each warp yarn passes alternately above and below each weft yarn,
- twill $N \times M$: the weft yarns pass over N warp yarns then under M warp yarns, shifting of one yarn to each passage,

- satin: the weft yarn passes over N warp yarns then below 1 warp yarn.

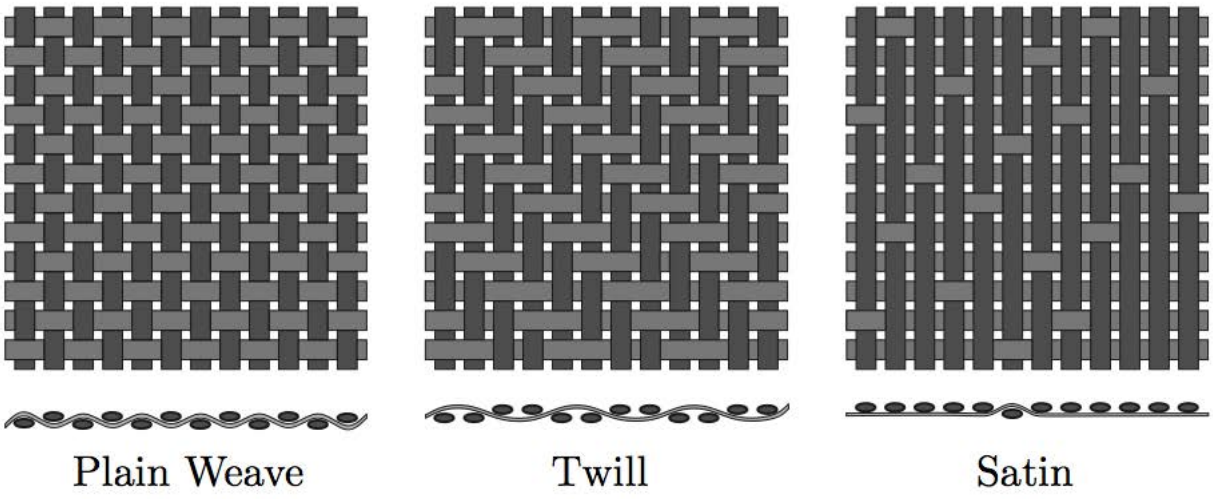

Figure 1.8: Schemes of weaving for fibrous composite reinforcements

The combination of these three families of armors with the plurality of available geometries and materials constituting the yarns, allows to obtain a wide variety of woven reinforcements. If the reinforcement is the same in the warp and weft direction, we will talk about balanced fabric. Generally, a fabric can be characterized by his armor, the relative arrangement of warp and weft yarns and the shrinkage that is the relative difference between the length of the fabric in one direction and the length of a yarn in the same direction. The shrinkage is given by:

$$\text{shrinkage} = \frac{l_{\text{yarn}} - l_{\text{fabric}}}{l_{\text{yarn}}}.$$

Thick specimens can be obtained superimposing these 2D armors. The resulting structure is laminar in the sense that the various lamina have no links other than the resin. These materials are then highly susceptible to delamination that can lead to a collapse of the structure. To overcome the problems peculiar of 2D armors, thick woven reinforcements were designed. These reinforcements can be seen as the superposition of different lamina structurally assembled during the weaving. Instead of continually intersects in the same plane, the weft yarns intersect several planes of warp yarns within the thickness of material (see Figure 1.5). The obtained woven fabric can then reach thicknesses of the order of ten centimeters (see e.g. Figs. 1.8,1.9).

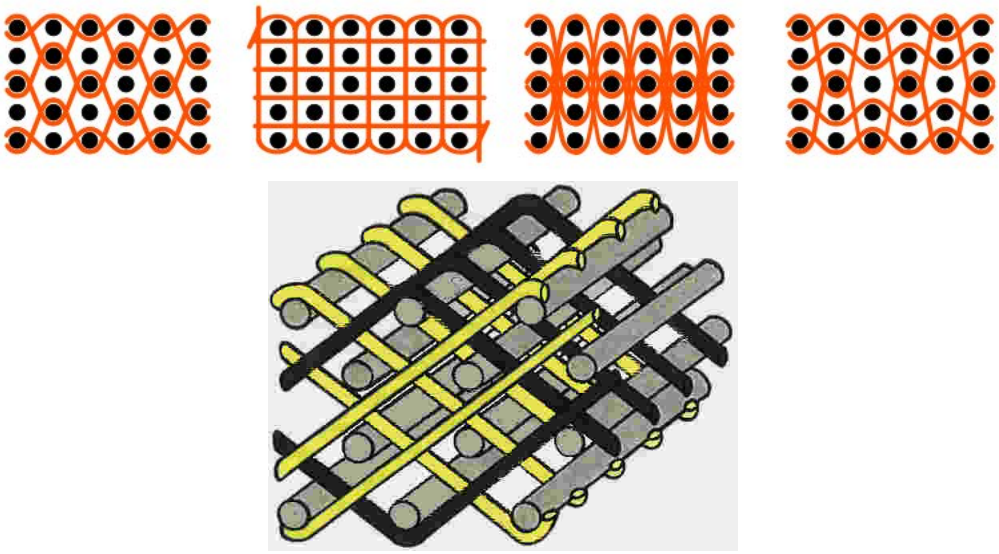

Figure 1.9: Examples of thick woven reinforcements

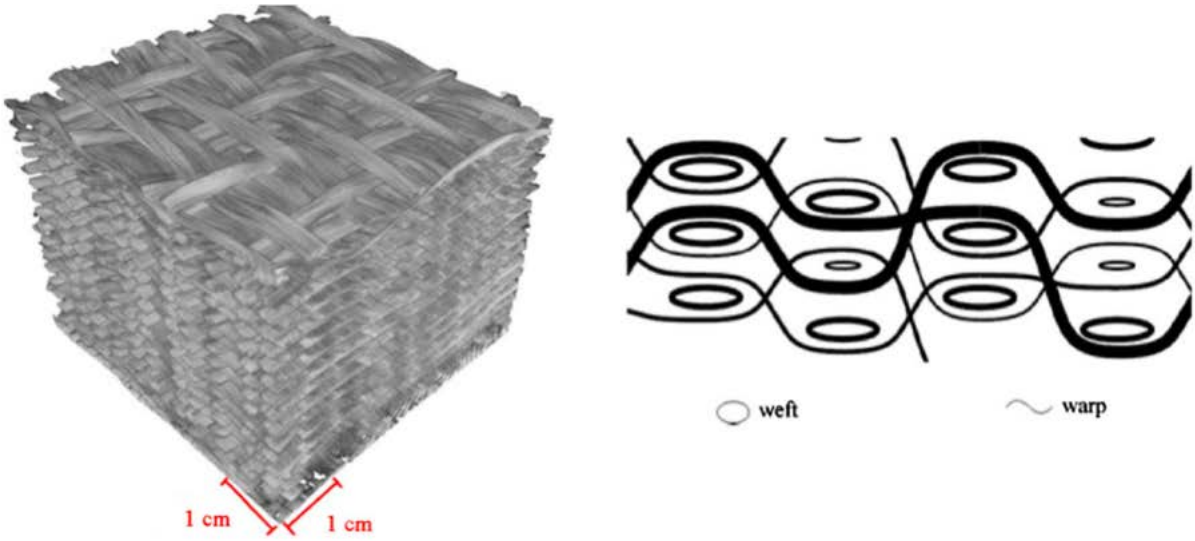

Figure 1.10: 2.5D woven composite interlock

1.3 Multi-scale mechanical behavior of fibrous composite reinforcements

As we have already pointed out, woven composite reinforcements are multi-scale materials and their macroscopic mechanical behavior is strongly influenced by the different scales presented by the materials themselves. The hierarchical heterogeneity of composite reinforcements is illustrated in Fig. 1.11, in which three different scales can be recognized:

- the macroscopic scale (left): scale of the engineering piece;
- the mesoscopic scale (center): scale of the yarn;
- the microscopic scale (right): scale of the fibre.

The meso- and micro-structural characteristics of composite reinforcements have visible effects on their overall mechanical behavior at the macroscopic scale. Such influence of the microstructure on the macroscopic behavior of the material has a twofold nature related to:

- the orthotropy conferred to the material by the presence of the woven yarns and
- the effect of some mesostructural properties (as the effect of the bending stiffness of the yarns) on the macroscopic deformation mechanisms.

We will show in this manuscript how the first point concerning the orthotropy of the material can be approached in a continuum framework by means of the use of suitable constitutive laws, while the second point can be addressed by using generalized, second gradient, continuum theories. Another possible approach which can give interesting informations about the behavior of fibrous reinforcements is the use of discrete models, which is what we do in this manuscript to complete our continuum analysis.

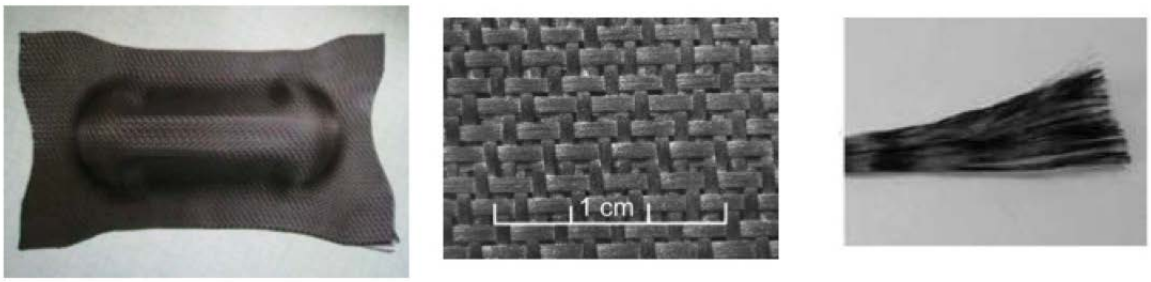

Figure 1.11: Hierarchical microstructure of fibrous composite reinforcements.

It is clear at this point that the macroscopic behavior of fibrous composite reinforcements is related to specific deformations mechanisms associated to the deformation of the yarns at the mesoscopic scale. Such mesoscopic deformation mechanisms are, in turn, influenced by the microscopic structure of the material, i.e. by the behavior of the fibers which constitute the yarns.
In order to be able to understand the intrinsic behavior of fibrous composite reinforcements, one needs to catch which are the deformation mechanisms which take place at the mesoscopic scale. To do so, it is sensible to describe some basic experimental tests which are used in the community of woven fiber reinforcements and which allow for the measurement of simple mechanical parameters related to simple deformation mechanisms at the mesoscopic and microscopic scales. We present anddiscuss such experimental tests with the twofold aim of

- better understanding the deformation mechanisms which may take place at the mesoscopic (and also microscopic) scale
- proposing some simple procedures to measure some mechanical characteristics of the material at the mesoscopic (or microscopic) scale.

The experimental tests introduced in this chapter will be a basis to propose a procedure to measure first and second gradient elastic coefficients in the last chapter of this manuscript.

1.3.1 Tensile behavior of the Yarns

The yarns, as already remarked above, are constituted by many fibers. When a yarn is subjected to tension, a nonlinear behavior can be recognized which is due to the fact that the fibers are not all stretched simultaneously. Nevertheless, when reaching a certain threshold load, corresponding to which the fibers are all stretched, the yarn starts showing a very high stiffness. When the transition from the nonlinear behavior to the acquisition of the complete stiffness of the yarn does

not have significant effects on the macroscopic material behavior of the woven fabric, one can also consider, as a limit case that the fibers are inextensible which is what we do starting from Chapter 5. The study of the material behavior of woven composite reinforcements based on such simplifying hypothesis (inextensibility) is of interest in order to obtain some "reference" material behaviors starting from which one can then conceive and propose some experimental procedures for measuring first and second gradient coefficients mainly related to angle variation and to bending of the yarns. In this manuscript, and in particular in Chapter 5, we will see that, although such study of the inextensible case introduces conceptual difficulties related to the fact that the ratio between the value of the tension stiffness and that of the shear stiffness tends to infinity, suitable solutions cans be found for the bias extension test. These findings, will allow us to propose in Chapter 6 a simple procedure to identify the relevant first and second gradient parameters which intervene in the observed phenomena.

1.3.2 Compaction of the Yarn in the Transverse Plane

The compaction of the yarn is defined as the change of the area in the transversal plane to the yarn, which is the plane orthogonal to the fibers directions. When the yarn is compressed in the direction orthogonal to its main direction the internal fibers are more closely packed together and fill the voids initially present in the transversal section of the fibers. We remark that the behavior of the material in compaction presents an asymptotical behavior: after an initial phase in which the fibers re-organize themselves in such a way that the voids are filled, the material shows an increased stiffness. In particular, the stiffness of the yarn finally tends to the stiffness of the material constituting the fibers. In addition, is it worth noting that this type of mechanism is difficult to characterize from an experimental point of view due to the fact that a pure compaction test is difficult to be realized and reproduced. For this reason, throughout this manuscript, we will assume that the compaction deformation mechanism does not have a significant impact on the macroscopic deformation of the considered specimens.

1.3.3 Shear Behavior of the Yarn

Two types of shear modes can be individuated in the yarns

- the distortion: this deformation mode occurs in the transversal plane of the yarn;
- the transverse shear: this deformation mode occurs in the direction of the fibers.

The first deformation mode is characterized by the fact that the cross section of the yarn changes its shape without activating compaction deformation modes. Such deformation mode is due to the fact that the fibers constituting the yarn slide one with respect to the other in order to adapt the overall imposed deformation. So, if one considers, for example, a yarn with cross sections which are initially, let us say, vertical and if a bending deformation is imposed to the yarns, the fibers are forced to slide one with respect to the other in order to let the yarn assume the desired form and, at the same time, let the fibers respect the quasi-inextensibility constraint. This internal sliding of the fibers can be interpreted as a motion of the cross sections (for example a rotation). It is worth noting that a coupling mechanism can be recognized between the compaction of the yarn and its distortion: when the yarn is compacted the distortion of the yarn occurs with increased difficulty. This is sensible since when the fibers are compacted friction mechanisms are more pronounced which render sliding more difficult.
The transverse shear is a deformation mode in the direction of the fibers and corresponds to a sliding between the fibers in the direction of the fibers themselves. As for the distortion, an increased compaction of the yarn causes a stiffening effect on the transversal shear. It can be also understood that, being the two quoted deformation modes of the yarns based on the same microscopic mechanism of fibers', a coupling exists between them. Both these types of deformation are difficult

to be characterized from an experimental point of view, in particular the stiffening effects due to compaction.

1.3.4 Behavior of the Yarn Subject to Bending

There exist only few studies which concern the behavior of the yarns subjected to bending. This type of studies, however, is interesting since the bending properties of the yarns can affect the macroscopical behavior of the specimen. In particular, as we will see in the next chapters, the fact of neglecting the effect of the bending stiffness of the yarns (and so of the fibers), produces macroscopic models that are not able to describe all the experimental evidences. As it will be shown in detail in the remainder of this manuscript, a Cauchy continuum theory is not able to account for the effect of bending stiffness of the yarns on the macroscopic behavior of the fabric. It is for this reason that generalized continuum theories (second gradient) may be introduced to palliate this inconvenience. Such theories are indeed able to account for the macroscopic manifestation of the mesoscopic bending of the yarns, still remaining in the framework of a continuum theory. I

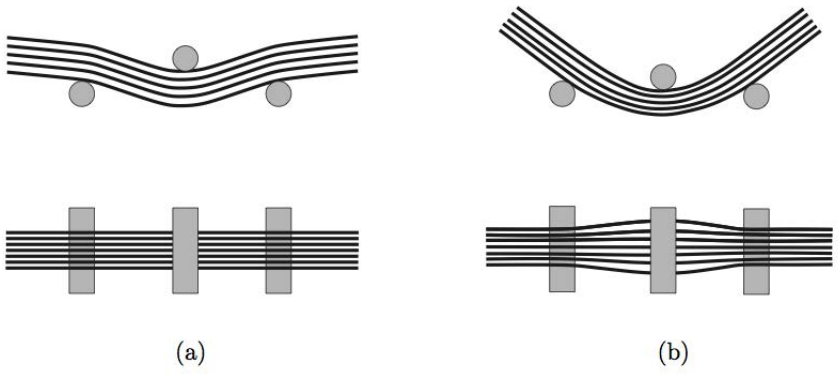

Figure 1.12: Bending of the yarn before the lateral expansion (a) and after (b).

When the yarn is subjected to a three point bending test, three different types of mechanism are turned on, that are (see Fig. 1.12)

- the transversal shear of the yarn;
- the bending of the fibers which constitute the yarn;
- the lateral expansion of the fibers in correspondence of the central support.

The first mechanism is activated due to the internal sliding of the fibers which takes pace as a consequence of the fact that they are bending together and that they are almost inextensible. The activation of the second mechanism is evidently easy to understand. As for the third mechanism, one can imagine that the contact with the central support can induce the fibers to rearrange themselves in the horizontal plane.

1.4 Macroscopic Behavior

In this section we present and discuss some elementary material tests that are commonly used to characterize the macroscopic mechanical behavior of woven fibrous composite reinforcements. Such tests are an indispensable tool for the correct comprehension of the mechanical behavior of fibrous composite reinforcements as influenced by the presence of their micro- and meso-structure.

1.4.1 Uniaxial Extension Test

The behavior of the fibrous composite reinforcements subjected to uniaxial tension test results to be nonlinear. This nonlinearity is due to the compaction of the yarns and the undulation of the tissue with the subsequent straightening (decrimping). More particularly, when an uniaxial tension test is performed on a given specimen, two successive phenomena can be observed

- a reduction of the undulation in the direction of the solicitation up to arrive to a complete straightening of the yarns (decrimping)
- the elongation of the yarns in the direction of the solicitation.

These two mechanisms give an easy interpretation of the diagram obtained from experimental measurements in the plane force vs imposed displacement (see [13, 59]). In the first phase, corresponding to the reduction of the undulation of the yarns in the direction of the solicitation, the material possesses a stiffness that increases as the undulation decreases. When the complete straightening of the solicited yarns is reached, the material offers a constant stiffness which corresponds to an increasing force measured in function of the elongation of the yarns. A small elongation of the macroscopic specimen will be observed due to decrimping phenomena. On the other hand, if the fibers are not parallel to the side of the specimen (and hence to the applied load) the resistance to tension is much lower and significant macroscopic elongations can be observed which are substantially due to pantographic motions of the yarns (see Fig. 1.13).
In the second part of this thesis we will introduce the hypothesis of inextensibility of the yarns, so implicitly assuming that decrimping phenomena and yarns' elongations are not the predominant deformation mechanisms intervening in the deformation process of a fibrous composite reinforcements.

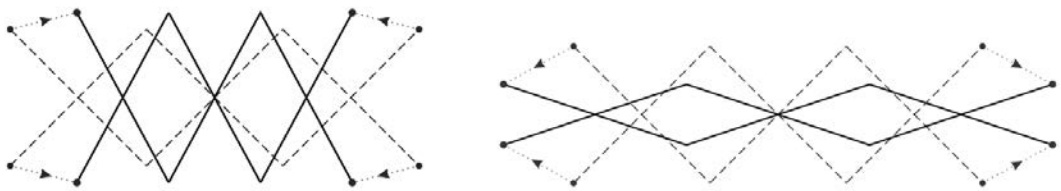

Figure 1.13: Pantographic motions of the yarns.

1.4.2 Biaxial Extension Test

The biaxial extension test is performed by soliciting to tension the material simultaneously in the warp and weft directions. If one denotes the deformation in one of the solicited observed direction as ε_{obs} (i.e. warp or weft) and the deformation in the orthogonal direction as $\varepsilon_{\text{orth}}$, is possible to define the coefficient of the biaxial extension test as

$$k = \frac{\varepsilon_{\text{orth}}}{\varepsilon_{\text{obs}}}$$

from which different cases of solicitation can be identified

- $k = 0$ or $k = \infty$ corresponds to a limit case in which the biaxial test degenerates into an uniaxial one;
- $k = 1$corresponds to an equal solicitation in both direction;
- $k = r$ with $r \in \mathbb{R}$corresponds to a solicitation case in which the deformation in the orthogonal direction is r times the deformation in the observed one.

The results of the test, naturally, depend on the chosen value of the coefficient k and one can experimentally observe that when $k = 1$ the deformation in the observed direction is due to the compaction of the yarns, indeed when$k = 0$ or $k = \infty$ the deformation is due to the reduction of the undulation (that involves the shear of the yarns in its transversal plane). When $k = r$ the two mechanism are in competition. The biaxial extension test can be hence used if one wants to understand better which is the effect of such two deformation mechanisms on the overall mechanical behavior of the macroscopic piece.
In this manuscript we will only focus our attention on some deformation patterns in which the two family of fibers are equally solicited in the two directions. More than that, when considering the inextensibility constraint, such deformation mechanisms will be considered to be unessential.

1.4.3 Shear Tests in the Plane of the Reinforcement

The main deformation mechanism in fibrous composite reinforcements is certainly associated to shear, i.e. to the change of the angle between yarns at the mesoscopic scale. The behavior of the reinforcement subjected to shear in the plane, results to be highly nonlinear. Some studies based on the technique of the image correlation [27, 26] have shown that, in an initial phase of the test, the two families of yarns rotate in a relative way (like rigid bodies connected by internal pivots) and hence the shear force associated to this deformation is relatively low. When the shear angle variation between yarns becomes larger than 40° (and lower than 50°) a stiffening in the shear behavior is observed and the mechanism of deformation drastically changes. In this second phase the relative motions described above are replaced by a lateral contact between the yarns (and their relative lateral compaction), so this fact corresponds to an increased stiffness. Two simple tests permit the study of the behavior of the composite reinforcement subjected to shear in the plane: the picture frame test and the bias extension test. Due to the important effect that such macroscopic deformation mode has on the deformation of specimens subjected to more complex loading conditions it is essential to set up experimental procedures which are able to give precise informations in this sense.

1.4.3.1 Picture Frame Test

In the picture frame test the composite reinforcement is placed into an articulated quadrilateral structure, that initially possesses a square shape. By imposing a displacement d at one node of the structure, see Figs. 1.14,1.15, the reinforcement is subjected to pure shear and a simple kinematical relation furnishes the shear angle variation as a function of the imposed displacement d and the length L of the edge of the articulated square:

$$\gamma = \frac{\pi}{2} - 2\arccos\left(\frac{2d + \sqrt{2}L}{2L}\right) \tag{1.1}$$

It has been experimentally shown that the picture frame test is not the more suitable one to correctly measure the shear angle resistance since some parasite tensions take place which render the measure of the force not reliable. More particularly, the measured force is not due only to the shear stiffness, but also to a big extent to such parasite tensions. Due the occurrence of such problems during the picture frame tests, a second test for the measure of the shear stiffness was conceived which is known as bias extension test.

1.4.3.2 Bias Extension Test

The bias extension test is performed on rectangular samples of composite reinforcements, with the height (in the loading direction) relatively greater (at least twice) than the width, and the yarns initially oriented at ±45-degrees with respect to the loading direction. The specimen is clamped at its two ends, one of which is maintained fixed and the second one is displaced of a given amount.

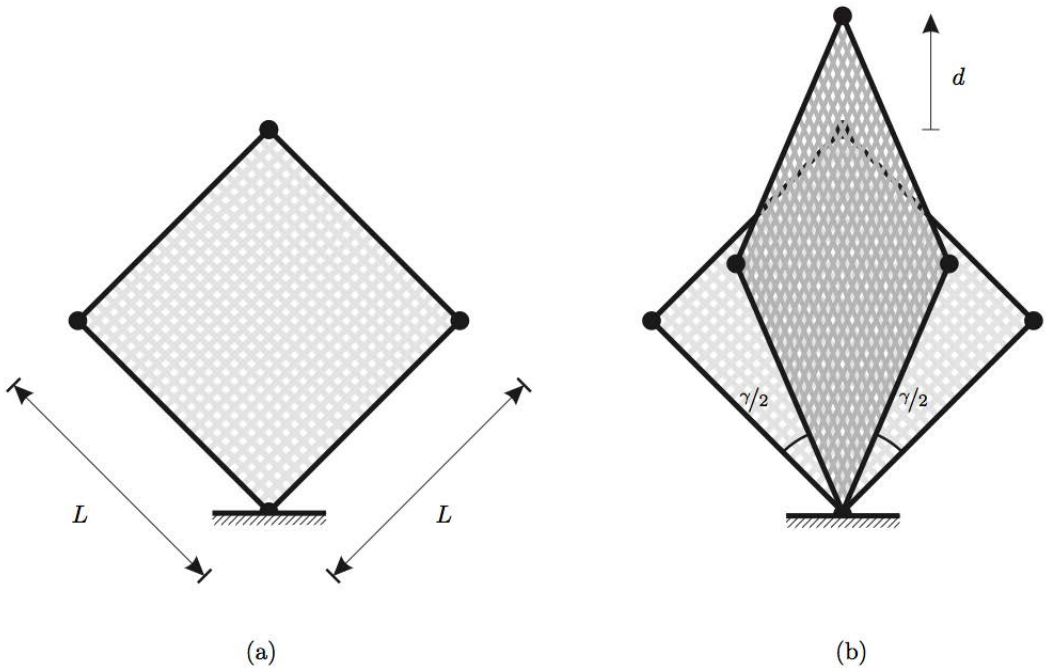

Figure 1.14: Kinematic of the picture frame test. (a) Specimen before the deformation (b) specimen after the imposed displacement d.

The relative displacement of the two ends of the specimen generates angle variations between the warp and weft: the creation of three different regions A, B and C, in which the shear angle between fibers remains almost constant after deformation, can be detected (see Figs. 1.16 and 3.3).
In particular, the fibers in regions C remain undeformed, i.e. the angle between fibers remains at 45° also after deformation. On the other hand, the angle between yarns becomes much smaller than 45° in regions A and B, but it keeps almost constant in each of them. In particular if in the zone A the angle is γ it will be of $\gamma/2$ in the zone B . Also in this case, a simple kinematical relation furnishes the shear angle variation as function of the imposed displacement and of the geometry of the specimen:

$$\gamma = \frac{\pi}{2} - 2\arccos\left(\frac{\sqrt{2}}{2}\left(1 + \frac{d}{L_0 - w_0}\right)\right). \tag{1.2}$$

It is worth noting that the kinematical relations (1.1) and (1.2) are deduced by implicitly using the assumption that the yarns are inextensible so that only pantographic motions are activated at the scale of the yarns which allow to univocally relate the angle variation to the geometry of the specimen and the imposed displacement. As we will show in the remainder of this manuscript, other deformation mechanisms actually intervenes in the bias extension test which are related to the bending of the yarns at the mesoscopic scale. Such mesoscopic bending actually creates transition layers between the regions A, B and C which allow to shift from one value of the angle to the other. It is for this reason that the bias extension test, when simulated in the framework of second gradient theories, contains useful additional informations about the bending stiffness of the yarns.

1.4.4 Transversal Shear Test

This test is performed in order to characterize the behavior of the composite reinforcement when it is subjected to transversal shear. The machine, depicted in Fig. 1.17, imposes on the specimen (shaped as a parallelepiped) a kinematic of pure transversal shear in order to solicit the only transversal shear deformation mode. The test is usually performed twice by orienting the specimen in the direction

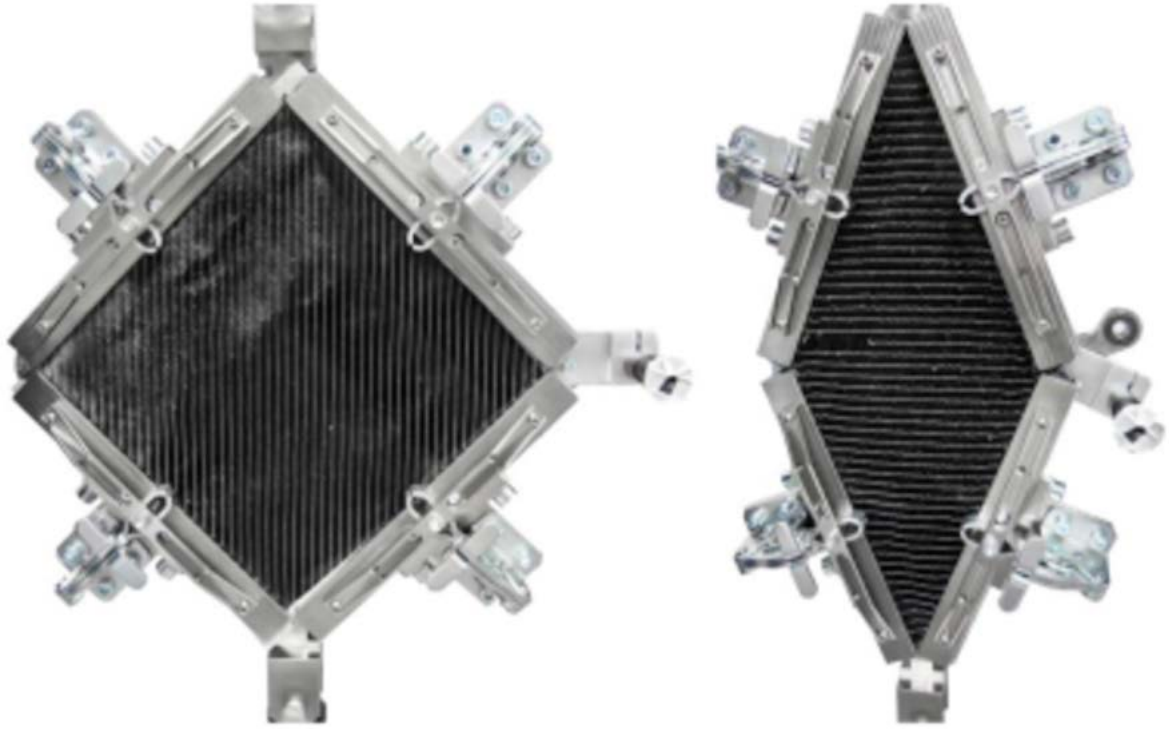

Figure 1.15: Experimental set-up for a picture frame test.

of the warp and weft, since the material, if not perfectly balanced, may have different stiffnesses in these two directions.

1.5 2D fibrous composite reinforcements: main deformation mechanisms and essential experimental tests.

In this thesis we will mainly focus on the modeling of the mechanical behavior of 2D fibrous composite reinforcements trying to isolate the fundamental deformation mechanisms which intervene in the deformation of such complex materials. Indeed, as we have seen in the first part of this chapter, different deformation mechanisms related to the microstructure of such materials can be identified. Nevertheless, the relative importance of such deformations with respect to the overall behavior of the material is not the same for each deformation mode. More particularly, we can argue that the main deformation mode intervening in the deformation of 2D fibrous composite reinforcements is the variation of the angle between the warp and weft direction which results in panthographic-type deformations (see Figs. 1.18,1.19).
For this reason, starting from chapter 5, we will introduce in our arguments the hypothesis of inextensibility of the yarns, so allowing the simplification of excluding elongation deformation modes. This will allow us to focus our attention on a unique first gradient deformation mode: the shear angle variation. On the other hand, we will show by means of the bias extension test that some particular boundary and loading conditions can be applied to the material that trigger second gradient deformation modes which are mainly associated to the local bending of the fibers. We will hence be able at the end of this manuscript to propose a very simple second gradient model with inextensible fibers which can guide us towards the identification of first and second gradient parameters from an experimental point of view. More particularly, a bias extension test will be proposed to calibrate first and second gradient elastic parameters on observable quantities.
Before thinking about an effective way of evaluating second gradient parameters, a suitable way of measuring first gradient ones must be individuated. This is what is done from several years to

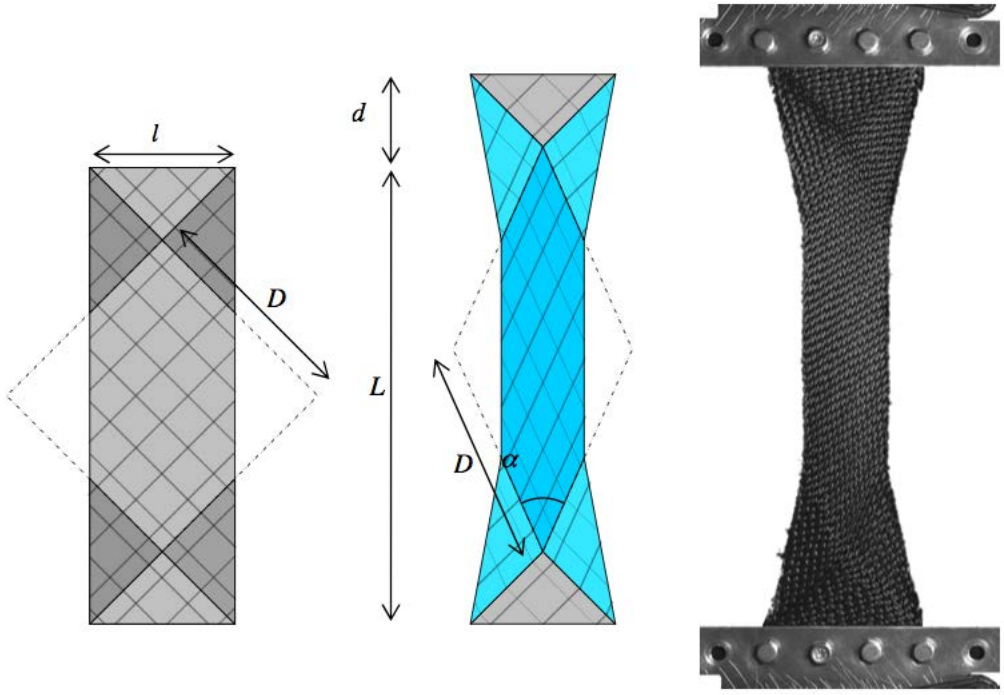

Figure 1.16: Kinematics of the bias extension test.

measure the shear stiffness in 2D woven reinforcements. The main idea is to try to conceive a test in which the shear angle variation is the sole intervening deformation mode. To this purpose, the picture frame test was conceived.

1.5.1 The picture frame test is not the best test to evaluate shear stiffness

Even if, from a theoretical point of view, the picture frame test is the most suitable way of measuring the shear angle variation and the associated shear stiffness, this is not indeed the case when trying to do so experimentally. If one looks at Fig. 1.14, it could seem evident that only an affine deformation of the frame takes place and that the only deformation mechanism of the tested reinforcement is the shear angle variation. Nevertheless, when trying to set up the experimental test (Fig. 1.15), it is not evident how one can fix the composite to the frame without creating parasite tensions in the yarns. The desirable situation would be that of having a pivot linking each yarn to the frame: this would allow rotations of the yarns so avoiding parasite tensions. Since such experimental configuration is difficult to be set up, the picture frame test is nowadays less used for the determination of the shear stiffness. Another test was conceived to this task which is the bias extension test already described above.

1.5.2 Bias extension test is suitable for the evaluation of the shear stiffness and for the local bending stiffness of the fibers

As already pointed out, the bias extension test was originally conceived to give an alternative to the picture frame test for measuring the shear stiffness of 2D fibous reinforcements. indeed (see Fig. 1.16) the central zone C of the specimen can be seen as equivalent to the picture frame specimen. The advantage of the bias extension test is that each yarn of the specimen has at least a free end and this fact is sufficient to avoid tensions in the yarns themselves. Nevertheless, what was less clear until recently is that a secondary, microstructure-related, deformation mechanism takes place in a bias extension test which was not fully evidenced. Such deformation mechanism is the bending

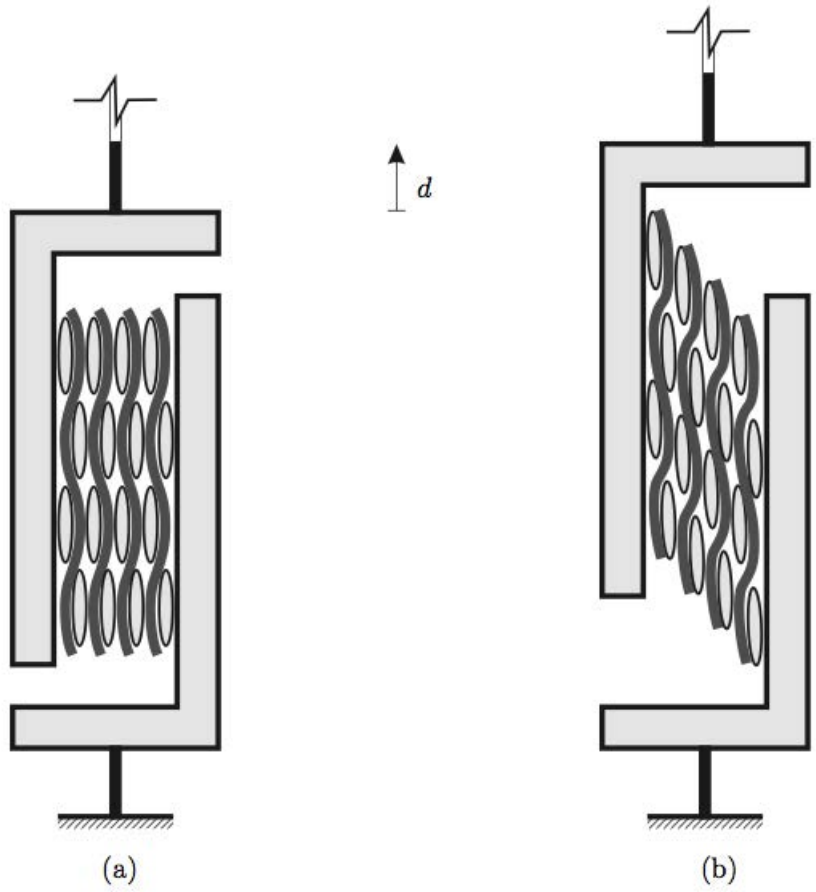

Figure 1.17: Kinematic of the transversal shear test. (a) Specimen before the deformation (b) specimen after the imposed displacement d.

of the yarns corresponding to the transition zones from one region at constant angle variation to the adjacent one (see Fig. 3.4). Although one could think that the energy associated to such local bending is not quantitative relevant, this is indeed not the case. We will show at the end of this manuscript (Chapter 6) how with a simple second gradient model with inextensible fibers, we can set up a very neat procedure to measure both first and second gradient elastic parameters as follows:

- We calibrate the second gradient parameter (associated to local bending) in order to fit the thickness of the transition layer between the zones A and B
- We calibrate the first gradient parameter (associated to shear angle variations) in order to fit the experimental force-displacement curve.

We will show that, contrarily to what one could expect, the second gradient energy related to the local bending of the fibers can range from the 5 to the 10% of the total energy associated to such test. This means that when performing a bias-extension test a macroscopic error can be committed if one ignores such bending phenomena and a second gradient theory can avoid such imprecisions. We are henceforth proposing a clear procedure to quantitatively measure for the first time first and second gradient coefficients of fibrous reinforcements by means of a unique test.

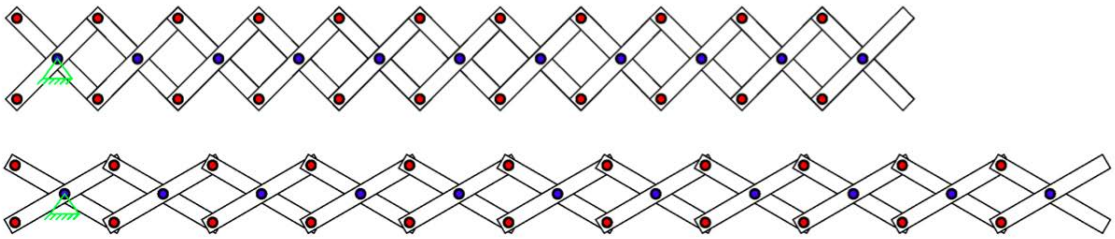

Figure 1.18: Example of pantographic motions.

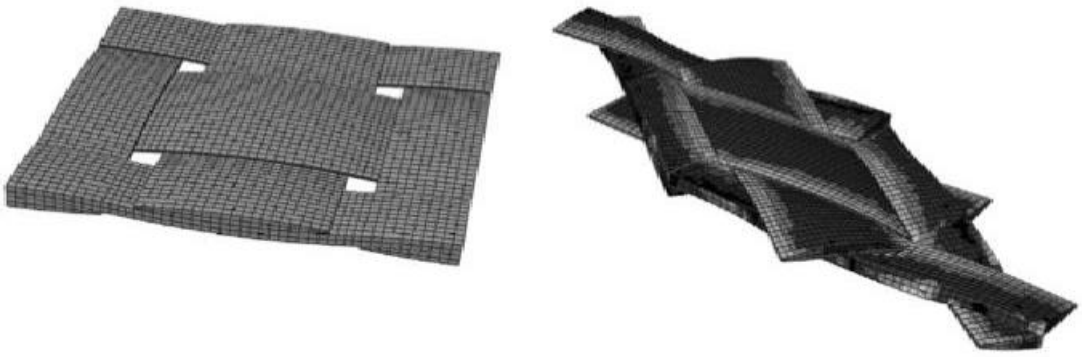

Figure 1.19: Pseudo-panthographic motions in 2D fibrous composite reinforcements.

Chapter 2

Generalized continuum mechanics

In this chapter we will present and discuss some well assessed facts concerning first and second gradient theories. First of all, the kinematics of such continua is introduced by defining the space of configurations and of admissible virtual displacements together with the deformation measures which will used throughout this thesis.
As a second step the concept of hyperelasticity is introduced since it is useful for the modeling of materials which undergo to large elastic strains as it is the case for fibrous composite reinforcements. The concepts of objectivity and of material symmetries are then introduced and their effect on the form of the strain energy density are discussed.
Representation theorems for isotropic, transversally isotropic and orthotropic continua are recalled. Finally, we will set up the principle of virtual powers for first and second gradient continua, so naturally introducing the equilibrium problem for such continua in weak and strong form.

Contents

2.1 Kinematics

In the framework of mechanical engineering, there are two fundamental objects that we have to specify in order to rigorously formulate our models: that of deformable body and that of physical space. The choice of an appropriate mathematical representative for deformable bodies and physical space is a very delicate point since, in addition to reflect the intuitive properties that a material body must have, such choice must also allow us to be able to apply a certain number of mathematical techniques, such as integration by parts. The definition of material body that we adopt in this work is as follows:

Definition 1. A ***deformable body*** $\mathscr{B}$ is a compact connected topological 3-manifold with boundary such that:

- $\mathring{\mathscr{B}}$ can be covered with a single chart,
- there exists a homeomorphism $\varpi : \mathscr{B} \to \mathbb{R}^3$ such that $\varpi(\mathscr{B}) \subseteq \mathbb{R}^3$ is a subset of $\mathbb{R}^3$ with a piece-wise $\mathscr{C}^k$-regular boundary, i.e., there exist a finite number of $\mathscr{C}^1$-regular curves $\{\gamma_\alpha\}_{\alpha=1}^{h\in\mathbb{N}_*}$ defined on compact intervals $[a_\alpha, b_\alpha]$, that can be intersected each other only at the images of the boundary points of the intervals, such that, if we call $\hat{\Gamma} = \bigcup_\alpha^h \gamma_\alpha \subseteq \partial\mathscr{B}$ (the skeleton of the boundary) we have that $\partial\mathscr{B} \setminus \hat{\Gamma}$ consists of a finite number of $\mathscr{C}^k$-regular disjoint surfaces $\{\Sigma_\beta\}_{\beta=1}^{k\in\mathbb{N}_*}$.

A point $p \in \mathscr{B}$ is said ***material particle***.

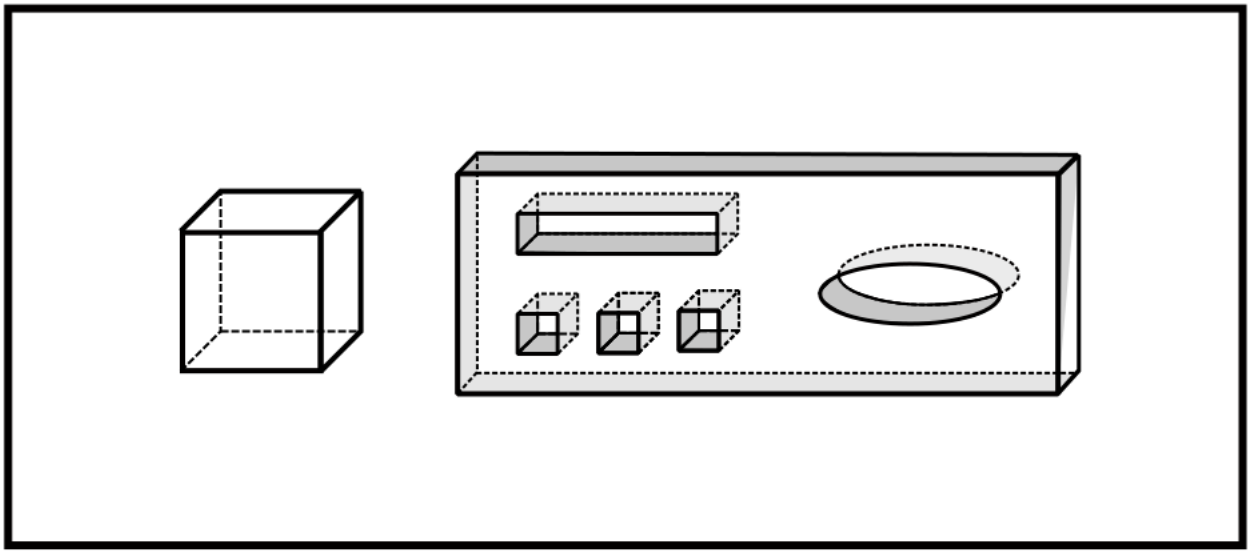

Figure 2.1: Examples of piecewise $\mathscr{C}^k$-regular boundary

This definition of deformable body is sufficiently general to include a large part of the objects of interest in engineering context. For example Figs. (2.2),(2.1) give simple examples of deformable bodies in our definition.
The choice of physical space, in which our deformable bodies manifest themselves, is not univocal but it is related to the kind of phenomenon that we want to describe. In dealing exclusively with static problems, the choice that seems most appropriate for the physical space $\mathscr{S}$ is that of three-dimensional Euclidean space.

The deformable body $\mathscr{B}$ manifests itself in the physical space $\mathscr{S}$ thanks to suitable functions:

Figure 2.2: Example of admissible deformable body

Definition 2. A ***configuration*** φ is an embedding of $\mathscr{B}$ in $\mathscr{S}$ such that $\varphi \circ \varpi^{-1}$ is a $\mathscr{C}^k$-diffeomorphism[1]. We call, ***space of admissible configurations,*** a suitable subset[2] $\mathcal{Q}$ of the set of all configurations.

In the space of admissible configurations, we can consider a map $\varphi_\star$ that we call ***Lagrangian configuration.***
In this way, setting $\mathscr{B}^\star := \varphi_\star(\mathscr{B}) \subseteq \mathscr{S}$ we can refer every admissible configuration directly to $\mathscr{B}^\star$ considering the composition maps

$$\chi_\varphi := \varphi \circ \varphi_\star^{-1} : \mathscr{S} \supseteq \mathscr{B}^\star \to \mathscr{S}, \quad \forall \varphi \in \mathcal{Q}.$$

With an abuse of notation, we will refer also to the set $\mathscr{B}^\star$ as Lagrangian configuration, to maps χ_φ as configurations and we will use the symbol $\mathcal{Q}$ to indicate both the set of admissible $\{\varphi\}$ and $\{\chi_\varphi\}$. When there is no danger of confusion, we will write simply χ instead of χ_φ. The image of $\mathscr{B}^\star$ with respect to the configuration χ is called ***Eulerian or current configuration*** of the deformable body $\mathscr{B}$ in $\mathscr{S}$.

With the specific choice of an Euclidean structure for the physical space, we can associate, to every configuration χ, a vector field u defined on $\mathscr{B}^\star$ as follows:

$$u(\varphi_\star(p)) := \chi(\varphi_\star(p)) - \varphi_\star(p).$$

We call the vector field u, the ***displacement field*** associated to χ.

2.2 Deformation measures

In this section we introduce the classical deformation measure tensors which will be used in the following to establish the constitutive laws for the considered continua. In order to do this, it is convenient to consider two cartesian systems of coordinates[3] $\mathcal{O}_{\mathbf{X}}$ and $\mathcal{O}'_{\boldsymbol{x}}$ on $\mathscr{S}$ thanks to which we

[1] Sometimes can be also useful to ask a piece-wise $\mathscr{C}^k$-regularity

[2] The specific nature of the space of configurations is specified for any particular physical problem. In particular, it is a subset of the set of all configurations when imposing specific kinematical boundary conditions on a measurable subset of the boundary.

[3] The coordinates $\mathbf{X} = (X^1, X^2, X^3)$ of $\mathcal{O}_{\mathbf{X}}$ are called Lagrangian coordinates, while the coordinates $\boldsymbol{x} = (x^1, x^2, x^3)$ of $\mathcal{O}'_{\boldsymbol{x}}$ are called Eulerian coordinates

can associate, to every material particle, two triples of real numbers that represent its position in the Lagrangian and Eulerian configuration. Thanks to the identifications induced by $\mathcal{O}_{\mathbf{X}}$ and $\mathcal{O}'_{\boldsymbol{x}}$ of $\mathscr{S}$ with $\mathbb{R}^3$, we can regard a configuration χ as a map $\boldsymbol{\chi}$ from $\mathbb{R}^3$ to $\mathbb{R}^3$ such that:

$$\boldsymbol{\chi}(\mathbf{X}) = \boldsymbol{x}$$

that transforms triples of real numbers (the coordinates[4] $\mathbf{X}_{(p)}$ of the image $\varphi_\star(p) \in \mathscr{B}^\star$ of a material particle $p \in \mathscr{B}$ in the coordinate system $(\mathscr{S}, \mathcal{O}_{\mathbf{X}})$) in triples of real numbers (the coordinates of the images $\boldsymbol{\chi}(\mathbf{X})$ in $(\mathscr{S}, \mathcal{O}'_{\boldsymbol{x}})$).
It is very important to point out that, in general, we can consider two different coordinate systems on $\mathscr{S}$ that give us two different identifications of this Euclidean space with $\mathbb{R}^3$.
A gradient[5] of order $n \leq k$ of a regular $\mathscr{C}^k$ map $\boldsymbol{\chi}$ defined on a domain of $\mathbb{R}^3$ at a point $\mathbf{X}_0$ is the multilinear function

$$\nabla^n \boldsymbol{\chi}(\mathbf{X}_0) : \underbrace{\mathbb{R}^3 \times \ldots \times \mathbb{R}^3}_{n-times} \to \mathbb{R}^3$$

whose components, in the natural tensorial base, are

$$\chi^i_{,A_1 \ldots A_k}(\mathbf{X}_0) = \frac{\partial^k \chi^i}{\partial X^{A_1} \ldots \partial X^{A_k}}(\mathbf{X}_0),$$

where from now on we label with capital letters the Lagrangian components and with small letters the Eulerian components of the considered tensor.

Definition 3. We call ***deformation gradient*** the 2-point tensor $\nabla\boldsymbol{\chi}$ of order $\begin{bmatrix} 0 & 1 \\ 1 & 0 \end{bmatrix}$ that we will indicate with $\mathbf{F}$.

If we indicate with $T_{\mathbf{X}}\mathscr{B}^\star$ the tangent space to the Lagrangian configuration at the point $\mathbf{X}$ and with $T_{\boldsymbol{x}}\boldsymbol{\chi}(\mathscr{B}^\star)$ the tangent space to the Eulerian configuration at the point $\boldsymbol{x}$, the deformation gradient $\mathbf{F}$ of $\boldsymbol{\chi}$ maps elements of $T_{\mathbf{X}}\mathscr{B}^\star$ (Lagrangian tangent vectors) in elements of $T_{\boldsymbol{x}}\boldsymbol{\chi}(\mathscr{B}^\star)$ (Eulerian tangent vectors) i.e.

$$\forall \boldsymbol{U} \in T_{\mathbf{X}}\mathscr{B}^\star,\ \mathbf{F} \cdot \boldsymbol{U} = \boldsymbol{u} \in T_{\boldsymbol{x}}\boldsymbol{\chi}(\mathscr{B}^\star).$$

The deformation gradient gives a linear approximation of the deformation of an infinitesimal cube around a point of coordinates $\mathbf{X}$ in $\mathscr{B}^\star$. The action of this tensor on the cube had been deeply understood and it is sealed in the polar decomposition theorem for non singular isomorphism:

Polar decomposition theorem. *Let us consider a configuration $\boldsymbol{\chi}$ with deformation gradient $\mathbf{F}$. We can find two unique tensor fields, one Lagrangian purely symmetric positive definite $\mathbf{U}$, and one two-point orthogonal*[6] *$\mathbf{R}$ of order $\begin{bmatrix} 0 & 1 \\ 1 & 0 \end{bmatrix}$, such that for every $\mathbf{X} \in \mathscr{B}^\star$ we have*

$$\mathbf{F}(\mathbf{X}) = \mathbf{R}(\mathbf{X}) \cdot \mathbf{U}(\mathbf{X}).$$

[4] If there is no danger of confusion, we will simply write $\mathbf{X}$ instead of $\mathbf{X}_{(p)}$.

[5] All the k-order gradients are, in the language of differential geometry, 2-point tensors that are k-times covariant in the Lagrangian part and 1-times contra-variant in the Eulerian part. We remember that if we have a differentiable map ψ between two differentiable manifolds $\mathcal{M}$ and $\mathcal{N}$, a 2-point tensor of order $\begin{bmatrix} p & r \\ q & s \end{bmatrix}$, over the map ψ, is a section $\mathcal{T} \in \Gamma\left(\mathcal{M}, T^p_q\mathcal{M} \otimes_{\mathcal{M}} T^r_s\psi^*(T\mathcal{N})\right)$ of the vector bundle $T^p_q\mathcal{M} \otimes_{\mathcal{M}} T^r_s\psi^*(T\mathcal{N})$ on $\mathcal{M}$ where $T^p_q\mathcal{M}$ is the (p,q)-tensor bundle on $\mathcal{M}$ and $T^r_s\psi^*(T\mathcal{N})$ is the (r,s)-tensor bundle on the pullback of the tangent bundle $T\mathcal{N}$. In the Language of continuum mechanics, the sections of are $T^p_q\mathcal{M}$ are said Lagrangian tensor fields and the sections of $T^r_s\psi^*(T\mathcal{N})$ Eulerian tensor fields.

[6] A two point $\begin{bmatrix} 0 & 1 \\ 1 & 0 \end{bmatrix}$ tensor field $\mathbf{R}$, over a map ψ between two Riemannian manifolds $(\mathcal{M}, g_{\mathcal{M}})$ (the Lagrangian configuration) and $(\mathcal{N}, g_{\mathcal{N}})$ (the Eulerian configuration), is said ***orthogonal*** if for every $p \in \mathcal{M}$ we have that $\mathbf{R}^t(\mathbf{X}) \cdot \mathbf{R}(\mathbf{X}) = \mathbb{1}_{\mathcal{M}}$ and $\mathbf{R}(\mathbf{X}) \cdot \mathbf{R}^t(\mathbf{X}) = \mathbb{1}_{\mathcal{N}}$, with $\mathbb{1}_{\mathcal{M}}$ identity on the tangent space $T_p\mathcal{M}$ to $\mathcal{M}$ at p and $\mathbb{1}_{\mathcal{N}}$ identity on the tangent space $T_{\psi(p)}\mathcal{N}$ to $\mathcal{N}$ at $\psi(p)$. The transpose tensor field $\mathbf{R}^t$, of $\mathbf{R}$, is the unique two point $\begin{bmatrix} 1 & 0 \\ 0 & 1 \end{bmatrix}$ tensor field such that: $g_{\mathcal{N},\psi(p)}\left(\mathbf{R}_p \cdot \boldsymbol{U}_p, \boldsymbol{v}_{\psi(p)}\right) = g_{\mathcal{M},p}\left(\boldsymbol{U}_p, \mathbf{R}^t_{\psi(p)} \cdot \boldsymbol{v}_{\psi(p)}\right)$ $\forall p \in \mathcal{M}$, $\boldsymbol{U}_p \in T_p\mathcal{M}$, $\boldsymbol{v}_{\psi(p)} \in T_{\psi(p)}\mathcal{N}$, where $\mathbf{R}_p : T_p\mathcal{M} \to T_{\psi(p)}\mathcal{N}$ and $\mathbf{R}^t_{\psi(p)} : T_{\psi(p)}\mathcal{N} \to T_p\mathcal{M}$ are linear functions.

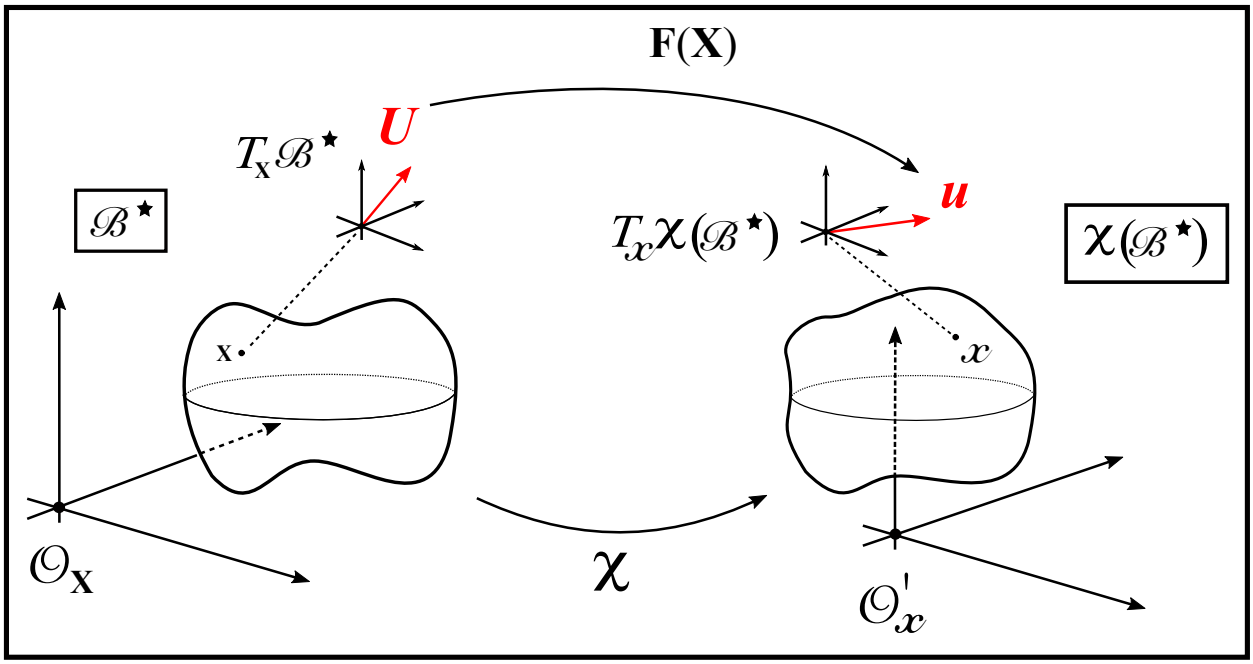

Figure 2.3: 2-point tensor and tangent spaces

The polar decomposition theorem states that every deformation gradient can be always decomposed in an unique way as a composition of a rotation and a purely deformation map at every point of the Lagrangian configuration.

Figure 2.4: Geometric interpretation of the action of $\mathbf{R}$ and $\mathbf{U}$ on an infinitesimal cube

In the theory of elasticity the energy cost is related only to the symmetric part of the deformation gradient. This means that the rotations are energy free. So this suggests the introduction of a new kinematical quantity that takes into account only the deformative symmetric part of $\mathbf{F}$.

Definition 4. We call the Lagrangian tensor field $\mathbf{C}(\mathbf{X}) := \mathbf{F}^t(\mathbf{X})\,\mathbf{F}(\mathbf{X}) = \mathbf{U}^2(\mathbf{X})$ the ***right Cauchy-Green tensor***.

In coordinates we have

$$C^A_B = \left(F^t\right)^A_i F^i_B.$$

The Cauchy-Green tensor transforms Lagrangian tangent vectors in Lagrangian tangent vectors.

Remark 5. Considering the scalar product $\langle \mathbf{u}, \mathbf{v} \rangle$ in $\mathscr{S}$, we can obtain canonical isomorphism between spaces of tensors. For example it can be easily proved that[7]

$$T^0_2(T\mathscr{B}^\star) \overset{\flat}{\underset{\langle\cdot,\cdot\rangle}{\sim}} T^1_1(T\mathscr{B}^\star) \overset{\sharp}{\underset{\langle\cdot,\cdot\rangle}{\sim}} T^2_0(T\mathscr{B}^\star),$$

where $T^0_2(T\mathscr{B}^\star)$ is the bundle of 2-covariant tensors, $T^1_1(\mathscr{B}^\star)$ the bundle of 1-contravariant 1-covariant tensors and $T^2_0(T\mathscr{B}^\star)$ is the bundle of 2-contravariant tensors and $\flat$ and $\sharp$ are the musical isomorphisms associated to the metric given by the scalar product. So, we can always associate to $\mathbf{C}$ a corresponding tensor completely contravariant or covariant. In indicial notation we set

[7] We remember the formal construction of a general bundle of (p,q)-tensors on a smooth manifold $\mathcal{M}$: $T^p_q(T\mathcal{M}) := (T\mathcal{M})^{\otimes_p} \otimes_{\mathcal{M}} (T^*\mathcal{M})^{\otimes_q}$. Moreover, in the smooth case, it results that the space of (p,q)-tensor fields is equivalent to a tensor product of modules over the algebra of smooth functions: $\Gamma\left(\mathcal{M}, T^p_q(T\mathcal{M})\right) \cong \left(\mathfrak{X}^\infty(\mathcal{M})\right)^{\otimes_p} \otimes \left(\Omega^1(\mathcal{M})\right)^{\otimes_q}$, where $\mathfrak{X}^\infty(\mathcal{M})$ is the module of smooth vector fields over $\mathscr{C}^\infty(\mathcal{M})$ and $\Omega^1(\mathcal{M})$ is the module of 1-forms over $\mathscr{C}^\infty(\mathcal{M})$.

$$\begin{cases} \mathbf{C}^{\flat} := \flat\left(\mathbf{C}\right) & C_{AB} = \delta_{AC} C^{C}_{B} \\ \\ \mathbf{C}^{\sharp} := \sharp\left(\mathbf{C}\right) & C^{AB} = \delta^{AC} C^{B}_{C} \end{cases}$$

where δ_{AC} and $\delta^{AC}$are Kronecker delta.

Remark 6. The fundamental theorem concerning the spectral decomposition of a self-adjoint automorphism of a finite dimensional vector space with scalar product, states that there exists an orthonormal basis of eigenvectors such that the matrix representing the automorphism in this basis is diagonal, and the diagonal elements are the eigenvalues. In mechanics, the eigenvalues of $\mathbf{C}$ are said ***principal stretches*** and the corresponding eigenvectors ***principal directions***. The deviation of the eigenvalues from the unity measures the amount of strain in a deformation.

Remark 7. In term of differential geometry language, the tensor $\flat\mathbf{C}$ is a metric tensor on the Lagrangian configuration $\mathscr{B}^{\star}$ obtained thanks to the pull-back χ^{*} of the standard Euclidean metric on $\mathscr{S}$. For this reason, it can be easily proved that the induced curvature tensor vanishes.

Definition 8. We call the Lagrangian tensor field $\mathbf{E}\left(\mathbf{X}\right) := \frac{1}{2}\left(\mathbf{C}\left(\mathbf{X}\right) - \mathbb{1}_{\mathcal{L}}\right)$, ***Green-Lagrange tensor field***.

2.3 Hyperelastic formulation

An hyperelastic model, of the behavior of a material, consists to give a triple $(\mathcal{Q}, \mathscr{L}, \mathscr{A})$ where:

- $\mathcal{Q}$ is a suitable space of admissible configurations,
- $\mathscr{L} : \mathbb{R}^{N} \supseteq A \to \mathbb{R}$ is a real values function from a subset of $\mathbb{R}^{N}$, with $N \in \mathbb{N}^{*}$, called ***Lagrangian density or stored energy function***,
- $\mathscr{A} : \mathcal{Q} \to \mathbb{R}$ is a functional (in general not linear) called ***action functional or Lagrangian energy*** functionally related to the Lagrangian density.

A mechanical phenomenon is modeled, in a hyperelastic framework, specifying these three objects. In the following we analyze in detail the so called n-th gradient model for hyperelastic materials, with great attention to the first and second gradient.

The choice of the Lagrangian density is said the ***constitutive law*** of the model.

Once specified the functional dependence of $\mathscr{A}$ from $\mathscr{L}$, the action functional associates to every configuration a real number that represent its "energetic cost".
Our objective is so to detect the configuration, if it exists, that minimizes the energetic cost, and so the configuration $\boldsymbol{\chi}_{\star}$ such that

$$\mathscr{A}\left[\boldsymbol{\chi}_{\star}\right] \leq \mathscr{A}\left[\boldsymbol{\chi}\right] \qquad \forall \boldsymbol{\chi} \in \mathcal{Q}. \tag{2.1}$$

This is exactly the content of the last action principle.

2.3.1 First gradient model

An hyperelastic model is a ***first gradient hyper-elastic model*** if the Lagrangian density is of the following type:

$$\mathscr{L} : \underbrace{\mathbb{R}^{3} \times \mathbb{R}^{3} \times \mathbb{R}^{3\times 3}}_{\sim \mathbb{R}^{15}} \to \mathbb{R}, \qquad \text{with} \qquad \mathscr{L} \in \mathscr{C}^{h}\left(\mathbb{R}^{15}\right)$$

for a suitable $h \in \mathbb{N}$. In this case we will say that the Lagrangian density is a ***first gradient Lagrangian density***.
If we consider a configuration $\boldsymbol{\chi}$, we can evaluate the Lagrangian density only at the points in $\mathscr{B}^\star \times \mathbb{R}^3 \times \mathscr{G}l_3(\mathbb{R}) \subseteq \mathbb{R}^{15}$ of the form $(\mathbf{X}, \boldsymbol{\chi}(\mathbf{X}), \nabla\boldsymbol{\chi}(\mathbf{X}))$. In this way we can associate to every configuration $\boldsymbol{\chi}$ a $\mathscr{C}^{\min\{h,k-1\}}$ real valued function $\mathscr{L}_{\boldsymbol{\chi}}$ defined on $\mathscr{B}^\star$ as

$$\mathscr{L}_{\boldsymbol{\chi}}(\mathbf{X}) := \mathscr{L}(\mathbf{X}, \boldsymbol{\chi}(\mathbf{X}), \nabla\boldsymbol{\chi}(\mathbf{X}))$$

The action functional is then defined as

$$\mathscr{A} : \mathcal{Q} \to \mathbb{R}, \qquad \mathscr{A}[\boldsymbol{\chi}] := -\int_{\mathscr{B}^\star} \mathscr{L}_{\boldsymbol{\chi}} dm = -\int_{\mathscr{B}^\star} \mathscr{L}(\mathbf{X}, \boldsymbol{\chi}, \nabla\boldsymbol{\chi})\, dm, \tag{2.2}$$

where dm is the volume form on $\mathscr{B}^\star$ induced by the Euclidean structure of $\mathscr{S}$.

Definition 9. We will call ***first gradient body*** the couple $(\mathscr{B}^\star, \mathscr{L})$, where $\mathscr{L}$ is a first gradient Lagrangian density.

2.3.2 Second gradient model

In a second gradient model, the Lagrangian density is more complex depending also to the second gradient of the configuration. For this reason the domain of $\mathscr{L}$ has to be larger:

$$\mathscr{L} : \underbrace{\mathbb{R}^3 \times \mathbb{R}^3 \times \mathbb{R}^{3\times3} \times \mathbb{R}^{3\times3\times3}}_{\sim\mathbb{R}^{42}} \to \mathbb{R}, \qquad \text{with} \qquad \mathscr{L} \in \mathscr{C}^h\left(\mathbb{R}^{42}\right), \quad h \in \mathbb{N}$$

As in the first gradient model, we can associate to every configuration a $\mathscr{C}^{\min\{h,k-1\}}$ real valued function $\mathscr{L}_{\boldsymbol{\chi}}$ defined on $\mathscr{B}^\star$ thanks to the relation

$$\mathscr{L}_{\boldsymbol{\chi}}(\mathbf{X}) := \mathscr{L}\left(\mathbf{X}, \boldsymbol{\chi}(\mathbf{X}), \nabla\boldsymbol{\chi}(\mathbf{X}), \nabla^2\boldsymbol{\chi}(\mathbf{X})\right).$$

In this case, the action functional will be

$$\mathscr{A}[\boldsymbol{\chi}] := -\int_{\mathscr{B}^\star} \mathscr{L}\left(\mathbf{X}, \boldsymbol{\chi}, \nabla\boldsymbol{\chi}, \nabla^2\boldsymbol{\chi}\right) dm. \tag{2.3}$$

Definition 10. A couple $(\mathscr{B}^\star, \mathscr{L})$ in which $\mathscr{L}$ is a second gradient Lagrangian density is said to be a ***second gradient body***.

2.4 Material symmetries, Galilean invariance and homogeneity.

In this paragraph, we want to formalize the observation according to which the mechanical response of certain materials is independent of the direction (or a subset of directions) of the imposed external solicitation and also by the point of application.
Moreover, every physical theory has to be independent by a specified class of observers. In our contest we will consider only the invariance with respect to the Galilean reference system. This means that the proposed formulation of the physical phenomenon, has to be invariant by the right orthogonal group action.

2.4.1 Material symmetries

In the proposed framework, the material symmetry at a given point $\mathbf{X}$ of a Lagrangian density $\mathscr{L}$ of a first gradient body $\mathscr{B}^\star$ can be formulated as follows:

Definition 11. Let $\mathscr{G}$ be a subgroup of the group of invertible orientations preserving matrices $\mathscr{G}l_3(\mathbb{R})$. We say that a first gradient body $(\mathscr{B}^\star, \mathscr{L})$ is ***$\mathscr{G}$-symmetric at $\mathbf{X}$ with symmetry group*** $\mathcal{G}_{\mathbf{X}} = \mathscr{G}$ if we have

$$\mathscr{L}(\mathbf{X}, \mathbf{F}\cdot\mathbf{Q}) = \mathscr{L}(\mathbf{X}, \mathbf{F}) \quad \forall \mathbf{Q} \in \mathscr{G}. \tag{2.4}$$

In components the relation (2.4) becomes

$$\mathscr{L}\left(X^A, F^i_A Q^A_I\right) = \mathscr{L}\left(X^A, F^i_I\right) \quad \forall \mathbf{Q} \in \mathscr{G}.$$

In an analogous way, we can adapt the given definition for a second gradient material. We follow the approach done in [28]. Let $\mathscr{G}$ be a subgroup of the group of invertible orientation preserving matrices $\mathscr{G}l_3(\mathbb{R})$ and $\mathcal{S}$ a subgroup of the group of the $(1,2)$-tensors, symmetric with respect to covariant indices $\left(G^A_{IJ} = G^A_{JI} \quad \forall\, I, J\right)$. We can consider a subgroup $\mathscr{H}$ of the cartesian product $\mathscr{G}l_3(\mathbb{R}) \times \mathcal{S}$ with respect to the following operation $\odot$:

$$(\mathbf{Q}_3, \mathbf{G}_3) = (\mathbf{Q}_1, \mathbf{G}_1) \odot (\mathbf{Q}_2, \mathbf{G}_2) = \left(\mathbf{Q}_1\cdot\mathbf{Q}_2, (\mathbf{G}_1\cdot\mathbf{Q}_2)^{tt}\cdot\mathbf{Q}_2 + \mathbf{Q}_1\cdot\mathbf{G}_2\right),$$

where the transposition operation tt of the three-order tensor $\mathbf{G}_1\cdot\mathbf{Q}_2$ is understood to act on the last two indices. In components we have

$$\begin{cases} (\mathbf{Q}_3)^A_I = (\mathbf{Q}_1)^A_B (\mathbf{Q}_2)^B_I \\ \\ (\mathbf{G}_3)^A_{IJ} = (\mathbf{G}_1)^A_{BC} (\mathbf{Q}_2)^B_I (\mathbf{Q}_2)^C_J + (\mathbf{Q}_1)^A_B (\mathbf{G}_2)^B_{IJ} \end{cases} \tag{2.5}$$

The identity element with respect to the introduced operation is $(\mathbb{1}, \mathbf{0})$. In this way it can be easy proved that $(\mathscr{H}, \odot, (\mathbb{1}, \mathbf{0}))$ is a group.

Definition 12. Let $(\mathscr{H}, \odot, (\mathbb{1}, \mathbf{0}))$ be a subgroup of $\mathscr{G}l_3(\mathbb{R}) \times \mathcal{S}$. We say that a second gradient body $(\mathscr{B}^\star, \mathscr{L})$ is ***$\mathscr{H}$-symmetric at $\mathbf{X}$ with symmetry group*** $\mathcal{G}_{\mathbf{X}} = \mathscr{H}$ if we have

$$\mathscr{L}\left(X^A, F^i_A Q^A_I, F^i_{A,B} Q^A_I Q^B_J + F^i_A G^A_{IJ}\right) = \mathscr{L}\left(X^A, F^i_I, F^i_{I,J}\right) \quad \forall\, (\mathbf{Q}, \mathbf{G}) \in \mathscr{H}. \tag{2.6}$$

2.4.1.1 Derivation of second gradient material symmetry definition

In this paragraph we want to understand how the group operation (2.5) (and so the definition of material symmetry for a second gradient material) has been conceived. In order to do this, we have the exigence of considering a curvilinear orientation preserving coordinate system $\mathcal{O}''_{\mathbf{Y}}$ on $\mathscr{S}$. Chosen a point $p \in \mathscr{B}$ we assume that the origins $\mathcal{O}$ and $\mathcal{O}''$ are coincident with $\varphi_\star(p)$ and, moreover, that

$$\nabla_{\mathbf{X}}\mathbf{Y} = \mathbf{Q}(\mathbf{X}) \qquad \text{with} \qquad \mathbf{Q} \in S\mathbb{O}_3(\mathbb{R}) \ \forall \mathbf{X} \in \mathscr{B}^\star.$$

If we indicate with $\mathbf{F}$ the gradient of $\boldsymbol{\chi}$ respect to $\mathbf{X}$ and with $\mathbf{H}$ the gradient of $\boldsymbol{\chi}$ respect to $\mathbf{Y}$, we obtain the following relations:

$$\mathbf{F}(\mathbf{X}) = \nabla_{\mathbf{X}}\boldsymbol{\chi}(\mathbf{Y}(\mathbf{X})) = \nabla_{\mathbf{Y}}\boldsymbol{\chi}(\mathbf{Y})\cdot\nabla_{\mathbf{X}}\mathbf{Y} \qquad \Longrightarrow \qquad \mathbf{F}(\mathbf{X}) = \mathbf{H}(\mathbf{Y}(\mathbf{X}))\cdot\mathbf{Q}(\mathbf{X}) \quad \forall \mathbf{X} \in \mathscr{B}^\star$$

and

$$\nabla_{\mathbf{X}}\mathbf{F}(\mathbf{X}) = \nabla_{\mathbf{X}}\left(\nabla_{\mathbf{Y}}\boldsymbol{\chi}(\mathbf{Y}(\mathbf{X}))\cdot\nabla_{\mathbf{X}}\mathbf{Y}\right) =$$

$$= \left(\nabla^2_{\mathbf{Y}}\boldsymbol{\chi}(\mathbf{Y}(\mathbf{X}))\cdot\nabla_{\mathbf{X}}\mathbf{Y}\right)^{tt}\cdot\nabla_{\mathbf{X}}\mathbf{Y} + \nabla_{\mathbf{Y}}\boldsymbol{\chi}(\mathbf{Y}(\mathbf{X}))\cdot\nabla^2_{\mathbf{X}}\mathbf{Y} =$$

$$= \left(\nabla_{\mathbf{Y}}\mathbf{H}(\mathbf{Y}(\mathbf{X}))\cdot\mathbf{Q}(\mathbf{X})\right)^{tt}\cdot\mathbf{Q}(\mathbf{X}) + \mathbf{H}(\mathbf{Y}(\mathbf{X}))\cdot\nabla_{\mathbf{X}}\mathbf{Q}(\mathbf{X}).$$

So finally we find that the invariants for a second gradient continuum reads:

$$\mathscr{L}\left(\mathbf{X},\mathbf{F}\left(\mathbf{X}\right),\nabla_{\mathbf{X}}\mathbf{F}\left(\mathbf{X}\right)\right)=$$

$$=\begin{cases}\mathscr{L}\left(\mathbf{X},\mathbf{H}\left(\mathbf{Y}\left(\mathbf{X}\right)\right)\cdot\mathbf{Q}\left(\mathbf{X}\right),\left(\nabla_{\mathbf{Y}}\mathbf{H}\left(\mathbf{Y}\left(\mathbf{X}\right)\right)\cdot\mathbf{Q}\left(\mathbf{X}\right)\right)^{tt}\cdot\mathbf{Q}\left(\mathbf{X}\right)+\mathbf{H}\left(\mathbf{Y}\left(\mathbf{X}\right)\right)\cdot\nabla_{\mathbf{X}}\mathbf{Q}\left(\mathbf{X}\right)\right)\\ \\ \check{\mathscr{L}}\left(\mathbf{Y},\mathbf{H}\left(\mathbf{Y}\right),\nabla_{\mathbf{Y}}\mathbf{H}\left(\mathbf{Y}\right)\right).\end{cases}$$

where $\check{\mathscr{L}}$ is the expression of the Lagrangian with respect to the curvilinear coordinate system $\mathcal{O}'_{\mathbf{Y}}$.

2.4.2 Galilean invariance

The class of observers considered this work is that of Galileian observers. This means that every Lagrangian density, to be physically admissible, has to verify the following condition

$$\mathscr{L}\left(\mathbf{X},\boldsymbol{\chi},\mathbf{F},\nabla\mathbf{F}\right)=\mathscr{L}\left(\mathbf{X},\mathbf{Q}\cdot\boldsymbol{\chi}\left(\mathbf{X}\right)+\mathbf{b},\mathbf{Q}\cdot\mathbf{F},\mathbf{Q}\cdot\nabla\mathbf{F}\right)\quad\forall\mathbf{Q}\in S\mathbb{O}_3\left(\mathbb{R}\right),\mathbf{b}\in\mathbb{R}^3.\tag{2.7}$$

Definition 13. Every Lagrangian density that verifies the condition (2.7) is said to be ***objective***.

The imposed condition implies that any objective Lagrangian density cannot depend on $\boldsymbol{\chi}\left(\mathbf{X}\right)$ and so it will be of the form

$$\mathscr{L}\left(\mathbf{X},\mathbf{F},\nabla\mathbf{F}\right).$$

The invariance under the left action of $S\mathbb{O}_3\left(\mathbb{R}\right)$ on $\mathbf{F}$ and $\nabla\mathbf{F}$ allow us to prove the following proposition [21]:

Proposition 14. *If $\mathscr{L}$ is an objective Lagrangian density then there exists another function $\hat{\mathscr{L}}:\underbrace{\mathbb{R}^3\times\mathbb{R}^6\times\mathbb{R}^{18}}_{\sim\mathbb{R}^{27}}\to\mathbb{R}$ such that, for every $\mathbf{F}\in\mathscr{G}l_3\left(\mathbb{R}\right)$, we have*

$$\mathscr{L}\left(\mathbf{X},\mathbf{F},\nabla\mathbf{F}\right)=\hat{\mathscr{L}}\left(\mathbf{X},\mathbf{U},\nabla\mathbf{U}\right),$$

where $\mathbf{U}$ is the symmetric part of $\mathbf{F}$ in its polar decomposition.

Corollary 15. *Given an objective Lagrangian density $\mathscr{L}$, it is always possible to find two functions $\tilde{\mathscr{L}}$ and $\bar{\mathscr{L}}$ such that*

$$\mathscr{L}\left(\mathbf{X},\mathbf{F},\nabla\mathbf{F}\right)=\hat{\mathscr{L}}\left(\mathbf{X},\mathbf{U},\nabla\mathbf{U}\right)=\tilde{\mathscr{L}}\left(\mathbf{X},\mathbf{C},\nabla\mathbf{C}\right)=\bar{\mathscr{L}}\left(\mathbf{X},\mathbf{E},\nabla\mathbf{E}\right),$$

where $\mathbf{U}$ is the symmetric part of $\mathbf{F}$, $\mathbf{C}$ is the Cauchy tensor and $\mathbf{E}$ is the Green-Lagrange tensor.

2.4.3 Homogeneity

Informally, a body is said homogeneous if we can describe its behavior with an energy density that does not depend explicitly on a considered point.

Definition 16. We say that a deformable first gradient body $(\mathscr{B}^\star,\mathscr{L})$ is homogeneous if there exists a Lagrangian density $\mathscr{L}^{\hom}:\mathbb{R}^3\times\mathbb{R}^{3\times3}\to\mathbb{R}^3$ such that

$$\mathscr{L}\left(\mathbf{X},\boldsymbol{\chi}\left(\mathbf{X}\right),\nabla\boldsymbol{\chi}\left(\mathbf{X}\right)\right)=\mathscr{L}^{\hom}\left(\boldsymbol{\chi}\left(\mathbf{X}\right),\nabla\boldsymbol{\chi}\left(\mathbf{X}\right)\right)\qquad\forall\mathbf{X}\in\mathscr{B}^\star.$$

In an analogous way the notion of homogeneity is introduced for second gradient continua.

2.4.4 Representation theorems for first gradient energies

In this section, we follow the ideas presents in [15] and [75]. In order to exhibit the principal results of this section, we remember the definition of the principal invariants of a matrix of order three.

Definition 17. Given a matrix[8] $\mathbf{A} \in \mathbb{M}_3(\mathbb{R})$, its ***principal invariants*** are the coefficients $\iota_1, \iota_2, \iota_3$ appearing in the characteristic polynomial of $\mathbf{A}$.

From the definition of characteristic polynomial of a matrix $\mathbf{A} = (a_{ij})$

$$\det(\mathbf{A} - \lambda \mathbb{1}) = -\lambda^3 + \iota_1 \lambda^2 - \iota_2 \lambda + \iota_3,$$

the following useful relations can be easily established:

$$\begin{cases} \iota_1 = \operatorname{tr}(\mathbf{A}) = \lambda_1 + \lambda_2 + \lambda_3 \\ \\ \iota_2 = \dfrac{1}{2}\left[\operatorname{tr}^2(\mathbf{A}) - \operatorname{tr}\left(\mathbf{A}^2\right)\right] = \operatorname{tr}(\mathbf{Cof}\,\mathbf{A}) = \lambda_1\lambda_2 + \lambda_2\lambda_3 + \lambda_3\lambda_1 \\ \\ \iota_3 = \det(\mathbf{A}) = \lambda_1\lambda_2\lambda_3 \end{cases}$$

where $\lambda_1, \lambda_2, \lambda_3$ are the eigenvalues of the considered matrix. We will indicate with

$$\boldsymbol{\iota}^3_{\mathbf{A}} = (\iota_1, \iota_2, \iota_3)$$

the triple of the principal invariants of the considered matrix $\mathbf{A}$. If we have the necessity of specifying the dependence of the principal invariants by the chosen matrix, we will write $\iota_1(\mathbf{A}), \iota_2(\mathbf{A}), \iota_3(\mathbf{A})$.

In what follows, we will need to introduce other invariants of a generic matrix $\mathbf{A}$ and, for this reason, we give the following definition:

Definition 18. We call ***invariant*** of a matrix $\mathbf{A} \in \mathbb{M}_3(\mathbb{R})$, with respect to a subgroup $\mathscr{G}$ (said the subgroup of invariance) of $\mathscr{G}l_3(\mathbb{R})$, any real valued function $f : \mathbb{M}_3(\mathbb{R}) \to \mathbb{R}^m$ such that $f\left(\mathbf{B}^{-1}\mathbf{A}\mathbf{B}\right) = f(\mathbf{A}) \quad \forall \mathbf{B} \in \mathscr{G}$.

In the spirit of definition (18) we can reinterpret the introduced principal invariants as real valued functions[9]:

$$\iota_1, \iota_2, \iota_3 : \mathbb{M}_3(\mathbb{R}) \to \mathbb{R}$$

and

$$\boldsymbol{\iota}^3 : \mathbb{M}_3(\mathbb{R}) \to \mathbb{R}^3$$

as vector valued function.
It is known that $\iota_1, \iota_2, \iota_3$ are invariant with respect to $\mathscr{G}l_3(\mathbb{R})$ according to the given definition.

2.4.4.1 Representation theorem for isotropic materials

Definition 19. A first gradient body $(\mathscr{B}^\star, \mathscr{L})$ is ***isotropic at a point*** $\mathbf{X}$ if it is $S\mathbb{O}_3(\mathbb{R})$-symmetric at $\mathbf{X}$. If $(\mathscr{B}^\star, \mathscr{L})$ is also homogeneous ($\mathscr{G}_{\mathbf{X}} = S\mathbb{O}_3(\mathbb{R}) \quad \forall \mathbf{X} \mathscr{B}^\star$) then we will say that it is ***isotropic.***

It can be proved the following result

[8] $\mathbb{M}_3(\mathbb{R})$ is the set of all the real 3×3 matrices.
[9] With an abuse of notation we indicate the values and the functions with the same symbol.

Theorem 20. *Given a first gradient body $(\mathscr{B}^\star, \mathscr{L})$, under the assumption that $\mathscr{L}$ is objective, we have that $(\mathscr{B}^\star, \mathscr{L})$ is isotropic at a point $\mathbf{X}$ if and only if there exist a function*[10] $\mathscr{L}^{iso} : \boldsymbol{\iota}^3\left(\mathbb{S}_3^>\right) \to \mathbb{R}$ *such that*

$$\mathscr{L}\left(\mathbf{X}, \mathbf{F}\right) = \tilde{\mathscr{L}}\left(\mathbf{X}, \mathbf{C}\right) = \mathscr{L}^{iso}\left(\mathbf{X}, \boldsymbol{\iota}^3\left(\mathbf{F}^t\mathbf{F}\right)\right) = \mathscr{L}^{iso}\left(\mathbf{X}, \boldsymbol{\iota}^3\left(\mathbf{C}\right)\right) \qquad \forall \mathbf{F} \in \mathscr{G}l_3\left(\mathbb{R}\right).$$

In this way, we have that the energy density $\mathscr{L}$ does not depend arbitrarily and entirely on $\mathbf{C}$, but only on three scalar invariants of such tensor field.

2.4.4.2 Representation theorem for transversally-isotropic materials

Definition 21. A first gradient body $(\mathscr{B}^\star, \mathscr{L})$ is ***transversally-isotropic at a point*** $\mathbf{X}$ ***with respect to a given unitary vector*** $\mathbf{D} \in T_{\mathbf{X}}\mathscr{B}^\star$, if it is $\mathscr{G}$-symmetric at $\mathbf{X}$ with

$$\left\{\mathbf{Q} \in S\mathbb{O}_3\left(\mathbb{R}\right) : \mathbf{Q} \cdot \mathbf{D} = \pm\mathbf{D}\right\} \subseteq \mathscr{G}. \tag{2.8}$$

If the relation (2.8) is verified for every[11] $\mathbf{X} \in \mathscr{B}^\star$ we will call $(\mathscr{B}^\star, \mathscr{L})$ ***transversally-isotropic with respect to*** $\mathbf{D}$.

In order to formulate a representation theorem for the class of transversally-isotropic materials, we have to introduce another two invariants, in the spirit of definition 18, for a matrix. Indeed as transverse isotropy is less restrictive than isotropy, we need more variables in order to find the correct domain of a suitable representation energy $\mathscr{L}^{\text{tran}}$. In this case, however, the subgroup of invariance will be $S\mathbb{O}_3\left(\mathbb{R}\right)$ instead of $\mathscr{G}l_3\left(\mathbb{R}\right)$.
We define the two following functions

$$\iota_4, \iota_5 : \mathbb{S}_3^> \times \mathbb{R}^3 \to \mathbb{R}, \qquad \iota_4\left(\mathbf{C}, \mathbf{D}\right) = \left\langle \mathbf{C} \cdot \mathbf{D}, \mathbf{D} \right\rangle, \quad \iota_5\left(\mathbf{C}, \mathbf{D}\right) = \left\langle \mathbf{C}^2 \cdot \mathbf{D}, \mathbf{D} \right\rangle.$$

If there is not possibility of confusion, we will omit the explicit dependance by the chosen unitary vector. It is immediate to verify that

$$\forall \mathbf{Q} \in S\mathbb{O}_3\left(\mathbb{R}\right) \qquad \iota_\alpha\left(\mathbf{Q}^{-1} \cdot \mathbf{C} \cdot \mathbf{Q}\right) = \iota_\alpha\left(\mathbf{Q}^t \cdot \mathbf{C} \cdot \mathbf{Q}\right) = \iota_\alpha\left(\mathbf{C}\right) \text{ with } \alpha = 1, \ldots, 5.$$

In this way also the function

$$\boldsymbol{\iota}^5 : \mathbb{S}_3^> \to \mathbb{R}^5, \qquad \boldsymbol{\iota}^5\left(\mathbf{C}\right) = \left(\iota_1\left(\mathbf{C}\right), \ldots, \iota_5\left(\mathbf{C}\right)\right)$$

is invariant with respect to $S\mathbb{O}_3\left(\mathbb{R}\right)$.

Remark 22. Remarking that

$$\iota_5\left(\mathbf{C}\right) = \left\langle \mathbf{C} \cdot \mathbf{D}, \mathbf{C} \cdot \mathbf{D} \right\rangle = \left\| \mathbf{C} \cdot \mathbf{D} \right\|^2 \geq \iota_4\left(\mathbf{C}\right),$$

we can conclude that $\boldsymbol{\iota}^5\left(\mathbb{S}_3^>\right)$ is a strict subset of $\left(\mathbb{R}_*^+\right)^5$, where $\mathbb{R}_*^+$ is the subset of $\mathbb{R}$ of strictly positive real numbers.
Finally we can give the desired representation theorem:

Theorem 23. *Given a first gradient body $(\mathscr{B}^\star, \mathscr{L})$, under the assumption that $\mathscr{L}$ is objective, we have that $(\mathscr{B}^\star, \mathscr{L})$ is transversally-isotropic at a point $\mathbf{X}$ with respect to the unitary vector $\mathbf{D} \in T_{\mathbf{X}}\mathscr{B}^\star$ if and only if there exist a function $\mathscr{L}^{tran} : \boldsymbol{\iota}^5\left(\mathbb{S}_3^>\right) \to \mathbb{R}$ such that*

$$\mathscr{L}\left(\mathbf{X}, \mathbf{F}\right) = \tilde{\mathscr{L}}\left(\mathbf{X}, \mathbf{C}\right) = \mathscr{L}^{tran}\left(\mathbf{X}, \boldsymbol{\iota}^5\left(\mathbf{C}\right)\right) \qquad \forall \mathbf{F} \in \mathscr{G}l_3\left(\mathbb{R}\right).$$

Then, the representation theorem for transversally isotropic materials states that the energy depends on five scalar invariants.

[10] $\mathbb{S}_3^>$ is the subset of $\mathbb{M}_3\left(\mathbb{R}\right)$ of symmetric definite positive 3×3 matrices.
[11] Thanks to the canonical parallelism always defined in Euclidean spaces.

2.4.4.3 Representation theorem for orthotropic materials with two orthogonal preferred directions

We consider two orthogonal unitary vectors $\mathbf{D}_1$ and $\mathbf{D}_2$ in the tangent space to $\mathscr{B}^\star$ at $\mathbf{X}$. Associated with these two vectors, we can consider the two matrices $\mathbf{R}_{\mathbf{D}_1}, \mathbf{R}_{\mathbf{D}_2}$ denoting the rotations with axis respectively $\mathbf{D}_1$ and $\mathbf{D}_2$ and angle π.

Definition 24. A first gradient body $(\mathscr{B}^\star, \mathscr{L})$ is ***orthotropic at a point*** $\mathbf{X}$ ***with respect to orthogonal vectors*** $\mathbf{D}_1$ ***and*** $\mathbf{D}_2$ if it is $\mathscr{G}$-symmetric at $\mathbf{X}$ with

$$\{\mathbf{R}_{\mathbf{D}_1}, \mathbf{R}_{\mathbf{D}_2}\} \subseteq \mathscr{G}. \tag{2.9}$$

If the relation (2.9) is verified for every $\mathbf{X} \in \mathscr{B}^\star$ we will call $(\mathscr{B}^\star, \mathscr{L})$ ***orthotropic with respect to*** $\mathbf{D}_1$ ***and*** $\mathbf{D}_2$.

In this case, after introducing the following functions

$$\begin{cases} \iota_4 : \mathbb{S}_3^> \to \mathbb{R}, & \iota_4(\mathbf{C}) = \langle \mathbf{C} \cdot \mathbf{D}_1, \mathbf{D}_1 \rangle \\ \iota_6 : \mathbb{S}_3^> \to \mathbb{R}, & \iota_6(\mathbf{C}) = \langle \mathbf{C} \cdot \mathbf{D}_2, \mathbf{D}_2 \rangle \\ \iota_8 : \mathbb{S}_3^> \to \mathbb{R}, & \iota_8(\mathbf{C}) = \langle \mathbf{C} \cdot \mathbf{D}_1, \mathbf{D}_2 \rangle \\ \iota_9 : \mathbb{S}_3^> \to \mathbb{R}, & \iota_9(\mathbf{C}) = \langle \mathbf{C} \cdot (\mathbf{D}_1 \wedge \mathbf{D}_2), \mathbf{D}_1 \rangle \\ \iota_{10} : \mathbb{S}_3^> \to \mathbb{R}, & \iota_{10}(\mathbf{C}) = \langle \mathbf{C} \cdot (\mathbf{D}_1 \wedge \mathbf{D}_2), \mathbf{D}_2 \rangle, \end{cases}$$

where $\mathbf{D}_1 \wedge \mathbf{D}_2$ is the vector product of $\mathbf{D}_1$ and $\mathbf{D}_2$, it is immediately clear that, in the basis $\{\mathbf{D}_1, \mathbf{D}_2, \mathbf{D}_1 \wedge \mathbf{D}_2\}$, the endomorphism $\mathcal{C}$, that in the standard basis is represented by the matrix $\mathbf{C}$, is represented by the symmetric matrix

$$\begin{bmatrix} \iota_4(\mathbf{C}) & \iota_8(\mathbf{C}) & \iota_9(\mathbf{C}) \\ \iota_8(\mathbf{C}) & \iota_6(\mathbf{C}) & \iota_{10}(\mathbf{C}) \\ \iota_9(\mathbf{C}) & \iota_{10}(\mathbf{C}) & \iota_1(\mathbf{C}) - (\iota_4(\mathbf{C}) + \iota_6(\mathbf{C})) \end{bmatrix}.$$

As a consequence, there exists a function $\mathscr{L}^{\mathrm{orth}}$ such that

$$\mathscr{L}(\mathbf{X}, \mathbf{F}) = \tilde{\mathscr{L}}(\mathbf{X}, \mathbf{C}) = \check{\mathscr{L}}^{\mathrm{orth}}\left(\mathbf{X}, \boldsymbol{\iota}^{\mathrm{orth}}(\mathbf{C})\right) \qquad \forall \mathbf{F} \in \mathscr{G}l_3(\mathbb{R}),$$

where $\boldsymbol{\iota}^{\mathrm{orth}}(\mathbf{C})$ is the function

$$\boldsymbol{\iota}^{\mathrm{orth}} : \mathbb{S}_3^> \to \mathbb{R}^6, \qquad \boldsymbol{\iota}^{\mathrm{orth}}(\mathbf{C}) = (\iota_1(\mathbf{C}), \iota_4(\mathbf{C}), \iota_6(\mathbf{C}), \iota_8(\mathbf{C}), \iota_9(\mathbf{C}), \iota_{10}(\mathbf{C})).$$

The main result of this section concerns the possibility of restricting the codomain of $\boldsymbol{\iota}^{\mathrm{orth}}$. In order to do this, we can first remark that the matrix

$$\begin{bmatrix} \iota_4 & \iota_8 & \iota_9 \\ \iota_8 & \iota_6 & \iota_{10} \\ \iota_9 & \iota_{10} & \iota_1 - (\iota_4 + \iota_6) \end{bmatrix}$$

has to be positive definite. This implies that, writing the explicit expression of the principal minors, we have

$$\begin{cases} \iota_4 > 0 \\ \iota_4\iota_6 - \iota_8^2 > 0 \\ \left(\iota_4\iota_6 - \iota_8^2\right)(\iota_1 - (\iota_4 + \iota_6)) - \iota_4\iota_{10}^2 - \iota_6\iota_9^2 + 2\iota_8\iota_9\iota_{10} > 0, \end{cases}$$

from which it follows immediately that $\iota_1 > 0$ and $\iota_6 > 0$. On the contrary, $\iota_8, \iota_9, \iota_{10}$ need not to be positive and so $\boldsymbol{\iota}^{\text{orth}}\left(\mathbb{S}_3^{>}\right) \subseteq \left(\mathbb{R}_*^+\right)^3 \times \mathbb{R}^3$. The representation theorem for orthotropic material states that:

Theorem 25. *Given a first gradient body $(\mathscr{B}^\star, \mathscr{L})$, under the assumption that $\mathscr{L}$ is objective, we have that $(\mathscr{B}^\star, \mathscr{L})$ is orthotropic at a point $\mathbf{X}$ with respect to the unitary vectors $\mathbf{D}_1$ and $\mathbf{D}_2$ if and only if there exist a function $\mathscr{L}^{orth} : \left|\boldsymbol{\iota}^{orth}\right|\left(\mathbb{S}_3^{>}\right) \to \mathbb{R}$ such that*

$$\mathscr{L}(\mathbf{X}, \mathbf{F}) = \tilde{\mathscr{L}}(\mathbf{X}, \mathbf{C}) = \mathscr{L}^{tran}\left(\mathbf{X}, \left|\boldsymbol{\iota}^{orth}\right|(\mathbf{C}), sgn(\iota_8\iota_9\iota_{10})\right) \qquad \forall \mathbf{F} \in \mathscr{G}l_3(\mathbb{R}),$$

where $\left|\boldsymbol{\iota}^{orth}\right| : \mathbb{S}_3^{>} \to \left(\mathbb{R}_*^+\right)^6$ defined as $\left|\boldsymbol{\iota}^{orth}\right|(\mathbf{C}) = (\iota_1, \iota_4, \iota_6, |\iota_8|, |\iota_9|, |\iota_{10}|)$.

2.5 First and second variation of the action functional

We have already pointed out that we assume the validity of the least action principle. So we are assuming that the effective deformation consequent to the application of certain external conditions, will be the configuration that minimizes in the sense of (2.1), if this configuration exists, the action functional. In this perspective, it is fundamental to dispose of the opportune instruments to determine the eventual minimum.
From the mathematical point of view, one only needs to readapt the standard notions of differentiation, developed in the contest of vector valued function of several variables, to functionals. This leads to the formulation of the notions of Fréchet and Gâteaux differential[12]

In this contest, we will call ***first variation of the action*** its Gâteaux differential[13].
Informally, the Gâteaux differential allows us to regard the behavior of the action functional when we perturb a little bit the configuration on which it is calculated. So the first variation works on a couple $[\boldsymbol{\chi}, \delta\boldsymbol{u}]$ formed by a configuration χ and a virtual displacement field $\delta\boldsymbol{u}$ (the small variation). For a first gradient model, the first variation of an action functional at a configuration χ is[14]

$$\delta\mathscr{A}[\boldsymbol{\chi}; \delta\boldsymbol{u}] = -\int_{\mathscr{B}^\star} \mathscr{D}_F\mathscr{L}_{\boldsymbol{\chi}} \mid \nabla\delta\boldsymbol{u}\, dm = -\int_{\mathscr{B}^\star} \frac{\partial\mathscr{L}_\chi}{\partial F^i_A}\delta u^i_{,A} dm$$

where the symbol $\mid$ indicates the total contraction of interested tensors.

[12]Given two normed vector spaces $\left(\mathbb{X}_\alpha, \|\cdot\|_\alpha\right)$, $\left(\mathbb{X}_\beta, \|\cdot\|_\beta\right)$ and a map $\Phi : \mathbb{X}_\alpha \to \mathbb{X}_\beta$, we say that Φ is Fréchet differentiable at $\xi_0 \in \mathbb{X}_\alpha$ if there exists a linear continuous map $\Phi_{*\xi_0} : \mathbb{X}_\alpha \to \mathbb{X}_\beta$ such that

$$\lim_{\xi\to 0} \frac{\|\Phi(\xi + \xi_0) - \Phi(\xi_0) - \Phi_{*\xi_0} \cdot \xi\|_\beta}{\|\xi\|_\alpha} = 0.$$

We say that $\Phi : \mathbb{X}_\alpha \to \mathbb{X}_\beta$ is Gâteaux differentiable at $\xi_0 \in \mathbb{X}_\alpha$ if there exists, for every $\eta \in \mathbb{X}_\alpha$, the following limit:

$$\lim_{t\to 0} \frac{1}{t}\left[\Phi(t\eta + \xi_0) - \Phi(\xi_0)\right] =: \delta\Phi[\xi_0; \eta] \in \mathbb{X}_\beta.$$

It can be easily proved, thanks to the mean value theorem for normed spaces, that Fréchet differentiability always implies the Gâteaux one.

[13]There are many results concerning the regularity of functionals of type (2.2) and (2.3). For example it can be proved that: let $[a, b]$ be a real interval and $\left(\mathscr{C}^n[a, b], \|\cdot\|_{n,\infty}\right)$ the set of n-times differentiable real valued maps with the sup-norm of order n. Let also $\mathscr{L} : [a, b] \times \mathbb{R}^{n+1} \to \mathbb{R}$ be a $\mathscr{C}^{n+1}$ function. Then the integral functional

$$\mathscr{A}[f] := \int_a^b \mathscr{L}\left(x, f(x), \ldots, f^{(n)}(x)\right) dx$$

is continuous and Fréchet differentiable at every $f \in \mathscr{C}^n[a, b]$.

[14]In what follows, considering the objective first gradient Lagrangian density $\mathscr{L} : \mathbb{R}^3 \times \mathbb{R}^9 \ni (\mathbf{X}, F) \mapsto \mathscr{L}(\mathbf{X}, F) \in \mathbb{R}$, we indicate with $\mathscr{D}_F\mathscr{L}$ the gradient of $\mathscr{L}$ with respect to F-variables. So $\mathscr{D}_F\mathscr{L}_{\boldsymbol{\chi}}$ indicates the F-gradient of $\mathscr{L}$ evaluated in the points $(\mathbf{X}, \nabla\boldsymbol{\chi}(\mathbf{X})) = (\mathbf{X}, \mathbf{F}(\mathbf{X}))$ of $\mathbb{R}^3 \times \mathbb{R}^9$.

From the obtained expression, we can define the ***first Piola-Kirchhoff stress tensor*** $\boldsymbol{\mathcal{P}}$ as

$$\boldsymbol{\mathcal{P}} := P_i^A dx^i \otimes \frac{\partial}{\partial X^A}, \qquad \text{with} \qquad P_i^A = \frac{\partial \mathscr{L}_\chi}{\partial F_A^i}.$$

In same way, the first variation of a second gradient action is[15]

$$\delta\mathscr{A}\left[\boldsymbol{\chi}; \delta\boldsymbol{u}\right] = -\int_{\mathscr{B}^\star} \left[\mathscr{D}_F\mathscr{L}_{\boldsymbol{\chi}} \mid \nabla\delta\boldsymbol{u} + \mathscr{D}_G\mathscr{L}_{\boldsymbol{\chi}} \mid \nabla^2\delta\boldsymbol{u}\right] dm =$$

$$= -\int_{\mathscr{B}^\star} \left[\frac{\partial \mathscr{L}_{\boldsymbol{\chi}}}{\partial F_A^i}\delta u^i_{,A} + \frac{\partial \mathscr{L}_{\boldsymbol{\chi}}}{\partial F_{AB}^i}\delta u^i_{,AB}\right] dm.$$

How it was done for the first Piola-Kirchhoff stress tensor, we define the ***iper-stress tensor*** $\boldsymbol{\mathfrak{M}}$ as

$$\boldsymbol{\mathfrak{M}} := \mathfrak{M}_i^{AB} dx^i \otimes \frac{\partial}{\partial X^A} \otimes \frac{\partial}{\partial X^B}, \qquad \text{with} \qquad \mathfrak{M}_i^{AB} = \frac{\partial \mathscr{L}_\chi}{\partial G_{AB}^i}.$$

In elementary calculus classes, it is proved that, for regular functions, the property of being a stationary point is a necessary condition for being an extremum. In the contest of functional, we find the same situation.

Definition 26. A configuration $\boldsymbol{\chi}_\star \in \mathcal{Q}$ is a ***stationary point*** for an action functional $\mathscr{A}$ if

$$\delta\mathscr{A}\left[\boldsymbol{\chi}_\star; \delta\boldsymbol{u}\right] = 0$$

for any admissible[16] virtual displacement $\delta\boldsymbol{u}$.

Once the stationary points have been found, the extremum can be detected regarding the hessian of the function evaluated at these points. It is possible to adapt to functionals also the notion of hessian.
In our case, we have that the second Gâteaux differential[17] for action functionals of the type (2.2) and (2.3) is:

$$\delta^2\mathscr{A}\left[\boldsymbol{\chi}; \delta\boldsymbol{u}, \delta\mathbf{v}\right] = -\int_{\mathscr{B}^\star} \mathscr{D}^2_{FF}\mathscr{L}_{\boldsymbol{\chi}} \mid (\nabla\delta\boldsymbol{u} \otimes \nabla\delta\mathbf{v})\, dm = -\int_{\mathscr{B}^\star} \frac{\partial^2 \mathscr{L}}{\partial F_A^i \partial F_B^j}\delta u^i_{,A}\delta v^j_{,B} dm$$

for a first gradient functional and

[15] where, considering the objective second gradient Lagrangian density $\mathscr{L} : \mathbb{R}^3 \times \mathbb{R}^9 \times \mathbb{R}^{27} \ni (\mathbf{X}, F, G) \mapsto \mathscr{L}(\mathbf{X}, F, G) \in \mathbb{R}$, we indicate with $\mathscr{D}_G\mathscr{L}$ the gradient of $\mathscr{L}$ with respect to G-variables. So $\mathscr{D}_G\mathscr{L}_{\boldsymbol{\chi}}$ indicates the G-gradient of $\mathscr{L}$ evaluated in the points $\left(\mathbf{X}, \nabla\boldsymbol{\chi}(\mathbf{X}), \nabla^2\boldsymbol{\chi}(\mathbf{X})\right) = \left(\mathbf{X}, \mathbf{F}(\mathbf{X}), \nabla\mathbf{F}(\mathbf{X})\right)$ of $\mathbb{R}^3 \times \mathbb{R}^9 \times \mathbb{R}^{27}$.

[16] Roughly speaking, an admissible virtual displacement $\delta\boldsymbol{u}$ is a vector field such that, given a configuration $\boldsymbol{\chi} \in \mathcal{Q}$, we have that $\boldsymbol{\chi} + \delta\boldsymbol{u}$ is still in $\mathcal{Q}$. Considering for example a Dirichlet boundary problem, in which $\mathcal{Q}$ is determined by the imposition of the condition $\boldsymbol{\chi} \equiv \boldsymbol{\psi}_0$ on a measurable subset Γ of the boundary $\partial\mathscr{B}^\star$, in the language of differential geometry we have that $\mathcal{Q}$ has the structure of a Banach manifold and the set of admissible virtual displacements at $\boldsymbol{\chi} \in \mathcal{Q}$ is an open subset (one in which the exponential map is a diffeomorphism) of the tangent space $T_{\boldsymbol{\chi}}\mathcal{Q} = \left\{\delta\boldsymbol{u} : \mathscr{B}^\star \to T\boldsymbol{\chi}(\mathscr{B}^\star) \mid \pi \circ \delta\boldsymbol{u} = \boldsymbol{\chi} \;\&\; \delta\boldsymbol{u}|_\Gamma = (\boldsymbol{\chi}(\mathbf{X}), \mathbf{0})\right\}$, where π is the projection of tangent bundle $T\boldsymbol{\chi}(\mathscr{B}^\star)$ on $\boldsymbol{\chi}(\mathscr{B}^\star)$.

[17] The second order Gâteaux differential, for a map $\Phi : \mathbb{X}_\alpha \to \mathbb{X}_\beta$ between two normed vector spaces $\left(\mathbb{X}_\alpha, \|\cdot\|_\alpha\right)$ and $\left(\mathbb{X}_\beta, \|\cdot\|_\beta\right)$, is defined as follows:

$$\delta^2\Phi\left[\xi_0; \eta, \zeta\right] := \delta\delta\Phi\left[\left[\xi_0; \eta\right], \zeta\right] = \lim_{t\to 0} \frac{1}{t}\left[\delta\Phi\left[\xi_0 + t\zeta; \eta\right] - \delta\Phi\left[\xi_0; \eta\right]\right]$$

if such limit exists for every $\eta, \zeta \in \mathbb{X}_\alpha$.

$$\delta^2\mathscr{A}\left[\boldsymbol{\chi};\delta\boldsymbol{u},\delta\mathbf{v}\right]=-\int_{\mathscr{B}^\star}\Big[\mathscr{D}^2_{FF}\mathscr{L}_{\boldsymbol{\chi}}\mid(\nabla\delta\boldsymbol{u}\otimes\nabla\delta\mathbf{v})+\mathscr{D}^2_{GG}\mathscr{L}_{\boldsymbol{\chi}}\mid\left(\nabla^2\delta\boldsymbol{u}\otimes\nabla^2\delta\mathbf{v}\right)+$$

$$+\mathscr{D}^2_{FG}\mathscr{L}_{\boldsymbol{\chi}}\mid\left(\nabla\delta\boldsymbol{u}\otimes\nabla^2\delta\mathbf{v}\right)+\mathscr{D}^2_{GF}\mathscr{L}_{\boldsymbol{\chi}}\mid\left(\nabla^2\delta\boldsymbol{u}\otimes\nabla\delta\mathbf{v}\right)\Big]\,dm=$$

$$=-\int_{\mathscr{B}^\star}\Bigg[\frac{\partial^2\mathscr{L}}{\partial F^i_A\partial F^j_B}\delta u^i_{,A}\delta v^j_{,B}+\frac{\partial^2\mathscr{L}}{\partial G^i_{AB}\partial G^j_{CD}}\delta u^i_{,AB}\delta v^j_{,CD}+$$

$$+\frac{\partial^2\mathscr{L}}{\partial F^i_A\partial G^j_{BC}}\delta u^i_{,A}\delta v^j_{,BC}+\frac{\partial^2\mathscr{L}}{\partial G^i_{AB}\partial F^j_C}\delta u^i_{,AB}\delta v^j_{,C}\Bigg]dm.$$

for a second gradient one.

Remark 27. The tensor field $\mathscr{D}^2_{FF}\mathscr{L}$ of order $\left[\begin{smallmatrix}2 & 0\\ 0 & 2\end{smallmatrix}\right]$ is the fourth order elasticity tensor.
This is a fundamental result in theory of functionals:

Theorem 28. *Let $\Phi:\mathbb{X}\to\mathbb{R}$ be a functional 2-times Gâteaux differentiable on a normed space $\mathbb{X}$. Then*
1) if Φ has a local (global) minimum in $\xi_0\in\mathbb{X}$ then $\delta\Phi\left[\xi_0;\eta\right]=0\quad\forall\eta\in\mathbb{X}$,
2) if $\xi_0\in\mathbb{X}$ is a stationary point for Φ and $\delta^2\Phi\left[\xi;\eta,\eta\right]\geq 0\quad\forall\eta\in\mathbb{X},\forall\xi\in\mathbb{B}_r\left(\xi_0\right)$ $(\forall\xi\in\mathbb{X})$, Φ has a local (global) minimum in ξ_0.

2.5.1 General assumption on stored energy function and the problem of convexity

In mathematical literature, there are many useful theorems that guarantee the existence of a solution for the variational problem (2.1) under suitable conditions on the Lagrangian density. One of the most powerful tool, stated in the following theorem, demands the convexity of the stored energy function.

Theorem 29. *Let be $\mathscr{B}^\star$ a domain in $\mathbb{R}^n$ with boundary $\partial\mathscr{B}^\star$, and let*[18]

$$\mathscr{L}:\mathscr{B}^\star\times\mathbb{M}_{n,m}\left(\mathbb{R}\right)\to[a,+\infty]\subseteq\mathbb{R}^\infty$$

be a function with the following properties:

1) **Convexity:** *for almost all $\mathbf{X}\in\mathscr{B}^\star$ the function $\mathscr{L}\left(\mathbf{X},\cdot\right):\mathbb{M}_{n,m}\left(\mathbb{R}\right)\ni\mathbf{F}\to\mathscr{L}\left(\mathbf{X},\mathbf{F}\right)\in[a,+\infty]$ is convex.*

2) **Continuity and measurability:** *for almost all $\mathbf{X}\in\mathscr{B}^\star$ the function $\mathscr{L}\left(\mathbf{X},\cdot\right):\mathbb{M}_{n,m}\left(\mathbb{R}\right)\ni\mathbf{F}\to\mathscr{L}\left(\mathbf{X},\mathbf{F}\right)\in[a,+\infty]$ is continuos and the function $\mathscr{L}\left(\cdot,\mathbf{F}\right):\mathscr{B}^\star\ni\mathbf{X}\to\mathscr{L}\left(\mathbf{X},\mathbf{F}\right)\in[a,+\infty]$ is measurable $\forall\,\mathbf{F}\in\mathbb{M}_{n,m}\left(\mathbb{R}\right)$.*

3) **Coerciveness:** *there exist constants $\alpha>0$ and $c>1$ such that $\mathscr{L}\left(\mathbf{X},\mathbf{F}\right)\geq\alpha\left\|\mathbf{F}\right\|^c+a$ for almost all $\mathbf{X}\in\mathscr{B}^\star$ and $\forall\,\mathbf{F}\in\mathbb{M}_{n,m}\left(\mathbb{R}\right)$.*
Let us indicate with ds the surface measure on the boundary, and let us also to consider a ds-measurable subset Γ_0 of $\partial\mathscr{B}^\star$ with $ds\left(\Gamma_0\right)>0$ and a measurable function $\boldsymbol{\chi}_0:\Gamma_0\to\mathbb{R}^m$ such that the resulting configuration space[19]

$$\mathcal{Q}=\left\{\boldsymbol{\chi}\in W^{1,p}\left(\mathscr{B}^\star,\mathbb{R}^m\right):\boldsymbol{\chi}\overset{a.e.}{\equiv}_{\Gamma_0}\boldsymbol{\chi}_0\right\}$$

[18] $\mathbb{R}^\infty:=\mathbb{R}\cup\{\infty\}$.
[19] $W^{1,p}\left(\mathscr{B}^\star,\mathbb{R}^m\right)$ is a Sobolev space.

is not empty. Then, if we consider the action functional $\mathscr{A} : \mathcal{Q} \to \mathbb{R}$ *defined as*

$$\mathscr{A}[\boldsymbol{\chi}] := \int_{\mathscr{B}^\star} \mathscr{L}(\mathbf{X}, \nabla\boldsymbol{\chi})\, dm - F[\boldsymbol{\chi}]$$

with F *linear and continuous functional on* $W^{1,p}(\mathscr{B}^\star, \mathbb{R}^m)$*, and assume that* $inf_{\boldsymbol{\chi}\in\mathcal{Q}}\{\mathscr{A}[\boldsymbol{\chi}]\} < +\infty$*, we have that there exists at least one function* $\boldsymbol{\chi}_\star \in \mathcal{Q}$ *such that*

$$\mathscr{A}[\boldsymbol{\chi}_\star] = inf_{\boldsymbol{\chi}\in\mathcal{Q}}\{\mathscr{A}[\boldsymbol{\chi}]\}.$$

In this paragraph we want to understand if this theorem can be useful in the contest of the hyper-elasticity. The crucial point consists to establish if the hypothesis of convexity for the Lagrangian density can be reasonable from a physical point of view.

2.5.1.1 Suitable mathematical conditions for physically reasonable energies

Many physical evidences suggest that a good hyper-elastic formulation of the mechanical behavior of an elastic body has to take into account the intuitive idea that, if the stress tends to infinity, also the corresponding strain should tend to infinity. We briefly see how to consider, in our framework, such consideration. A possible choice is as follows: we require that the Lagrangian density $\mathscr{L}$ approaches $+\infty$ if any one of the eigenvalues $\lambda_\mu(\mathbf{C})$ tends to 0 or $+\infty$. Under a suitable regularity for $\mathscr{L}$, we can expect, thanks to the mean value theorem, that $\|\nabla_F \mathscr{L}(\mathbf{X}, \mathbf{F})\|$ tends to $+\infty$. If two of the eigenvalues $\lambda_{\mu_1}(\mathbf{C})$ and $\lambda_{\mu_2}(\mathbf{C})$ are kept confined in a compact interval of $(0, +\infty)$ it can be easily proved that:

$$\begin{cases} \lambda_{\mu_3}(\mathbf{C}) \to 0^+ \Longleftrightarrow \det(\mathbf{F}) \to 0^+ \\ \lambda_{\mu_3}(\mathbf{C}) \to +\infty \Longleftrightarrow \|\mathbf{F}\| \to +\infty \\ \lambda_{\mu_3}(\mathbf{C}) \to +\infty \Longleftrightarrow \|\mathbf{Cof}\,\mathbf{F}\| \to +\infty \\ \lambda_{\mu_3}(\mathbf{C}) \to +\infty \Longleftrightarrow \det(\mathbf{F}) \to +\infty \end{cases}$$

and so we are naturally led to make the following two requests to provide a criterion for determining what functions can actually represent physical reasonable energies:

$$\begin{cases} \mathscr{L}(\mathbf{X}, \mathbf{F}) \to +\infty \text{ as } \det(\mathbf{F}) \to 0^+ \\ \mathscr{L}(\mathbf{X}, \mathbf{F}) \to +\infty \text{ as } \|\mathbf{F}\| + \|\mathbf{Cof}\,\mathbf{F}\| + \det(\mathbf{F}) \to +\infty \end{cases}$$

The proposed conditions have so the following physically meaning: an infinite energy is needed for expanding a continuous body in an infinite range or to annihilate the volume loosing one or more dimensions.

2.5.1.2 Comparison between the introduced conditions and the convexity.

Now we want to understand if the introduced suitable mathematical conditions for physical reasonable energies are compatibles with the assumption of convexity of the stored energy function. In order to answer, we have first the necessity to introduce the following object:

Definition 30. Given a first gradient body $(\mathscr{B}^\star, \mathscr{L})$ and considering a map $\boldsymbol{\chi} : \mathscr{B}^\star \to \mathbb{R}^3$, we will call ***Cauchy stress tensor*** the quantity

$$\boldsymbol{\mathcal{T}} := (\det(\nabla\boldsymbol{\chi}))^{-1}\, \boldsymbol{\mathcal{P}} \cdot \flat\left(\nabla\boldsymbol{\chi}^t\right)$$

where the contraction is intended on the Lagrangian parts of the two considered tensors.

Remark 31. From given definition, we can remark that the the Cauchy stress tensor is an Eulerian tensor of order $(0,2)$. In indicial notation we have

$$\mathcal{T}_{ij} = (\det(\nabla\boldsymbol{\chi}))^{-1}\,\mathcal{P}_i^A\delta_{AB}F_j^B.$$

Theorem 32. *Let us consider a first gradient body $(\mathscr{B}^\star, \mathscr{L})$ and let us assume that, for $\mathbf{X} \in \mathscr{B}^\star$, the Lagrangian density*

$$\mathscr{L}(\mathbf{X}, \cdot) : \mathscr{G}l_3^+(\mathbb{R}) \ni \mathbf{F} \to \mathscr{L}(\mathbf{X}, \mathbf{F}) \in \mathbb{R}$$

is a convex function in $\mathbf{F}$. Then

1) *this property is incompatible with the property $\mathscr{L}(\mathbf{X}, \mathbf{F}) \to +\infty$ as $\det\mathbf{F} \to 0^+, \mathbf{F} \in \mathscr{G}l_3^+(\mathbb{R})$.*
2) *The axiom of frame indifference implies that, $\forall\,\boldsymbol{\chi} : \mathscr{B}^\star \to \mathbb{R}^3$ and $\forall\,\mathbf{X} \in \mathscr{B}^\star$, the eigenvalues of the Cauchy stress tensor $\boldsymbol{\mathcal{P}}(\boldsymbol{x})$ evaluated at $\boldsymbol{x} = \boldsymbol{\chi}(\mathbf{X})$ have to satisfy the following inequalities:*

$$\lambda_1 + \lambda_2 \geq 0, \quad \lambda_2 + \lambda_3 \geq 0, \quad \lambda_1 + \lambda_3 \geq 0.$$

In the light of theorem (32), it seems that it is not possible to have convex energies which are also reasonable.

Example 33. For example, the condition 2) of theorem (32) is not respected in we consider a sphere subjected to a uniform pressure.

For these reasons, John Ball has introduced the notion of polyconvex function. Indeed this is a weaker requirement with respect to the convexity that does not conflict with any reasonable physical assumption. For completeness we give the definition of polyconvex function:

Definition 34. Let be $\mathscr{G}$ a subset of $\mathbb{M}_3(\mathbb{R})$. A function $\mathscr{L} : \mathscr{G} \to \mathbb{R}$ is polyconvex if there exist a convex function $\mathbb{L} : \mathbb{U} \to \mathbb{R}$, where

$$\mathbb{U} := \{(\mathbf{F}, \mathbf{Cof}\,\mathbf{F}, \det(\mathbf{F})) \in \mathscr{G} \times \mathbb{M}_3(\mathbb{R}) \times \mathbb{R}\}$$

such that

$$\mathscr{L}(\mathbf{F}) = \mathbb{L}(\mathbf{F}, \mathbf{Cof}\,\mathbf{F}, \det(\mathbf{F}))$$

for every $\mathbf{F} \in \mathscr{G}$.

2.6 Irreducible form for the first variation for the action functional and external forces

From a mathematical point of view, there are not a priori restrictions on the possible choice of the kinematical constraints. From a mechanical point of view, on the other hand, fixed the degree of the theory, we are interested to consider only those kinematical constraints that have a counter part in term of external forces. This means that, if we consider a kinematical constraint, we want also an external force that works on this constrain. One of the most relevant advantage of adopting a variational formulation is that it is directly possible to identify the external forces sustainable by the considered continuum, by only imposing compatible kinematical constraints. The technical tool that allows us to do so, is the integration by parts. The initial definition of a material body is so designed to allow this integration by parts.

2.6.1 First gradient

We start analyzing the standard case of first gradient theory. From the first variation of the action functional

$$\delta\mathscr{A}\left[\boldsymbol{\chi};\delta\boldsymbol{u}\right]=-\int_{\mathscr{B}^\star}\frac{\partial\mathscr{L}_\chi}{\partial F^i_A}\delta u^i_{,A}dm,$$

integrating by parts, we arrive to

$$\delta\mathscr{A}\left[\boldsymbol{\chi};\delta\boldsymbol{u}\right]=\int_{\mathscr{B}^\star}\left(\frac{\partial\mathscr{L}_\chi}{\partial F^i_A}\right)_{,A}\delta u^i dm-\int_{\partial\mathscr{B}^\star}\frac{\partial\mathscr{L}_\chi}{\partial F^i_A}\delta u^i N_A ds$$

where the N_A are the components of the 1-form $\boldsymbol{N}^*$ dual of the external Lagrangian normal $\boldsymbol{N}$ to the surface $\partial\mathscr{B}^\star$, where it is defined. In compact form we have

$$\delta\mathscr{A}\left[\boldsymbol{\chi};\delta\boldsymbol{u}\right]=\int_{\mathscr{B}^\star}\left\langle\mathrm{Div}\boldsymbol{\mathcal{P}},\delta\boldsymbol{u}\right\rangle dm-\int_{\partial\mathscr{B}^\star}\left\langle\boldsymbol{\mathcal{P}}\cdot\boldsymbol{N}^*,\delta\boldsymbol{u}\right\rangle ds.$$

From the found expression, we can remark how the only sustainable forces, in a first gradient model, are volume and surface ones. The only kinematical constraint compatible with this forces is that of assigning the displacement on a subregion of the boundary. Even farther we can remark how in a first gradient theory the surface actions depend only on the normal of the considered surface. Setting

$$\mathfrak{f}^{int}:=\mathrm{Div}\boldsymbol{\mathcal{P}}\qquad\text{and}\qquad\mathfrak{g}^{int}:=\boldsymbol{\mathcal{P}}\cdot\boldsymbol{N}^*$$

for the internal actions, the external work will be of the form

$$\mathcal{W}^{ext}\left[\delta\boldsymbol{u}\right]=\int_{\mathscr{B}^\star}\mathfrak{f}^{ext}\cdot\delta\boldsymbol{u}\,dm-\int_{\partial\mathscr{B}^\star}\mathfrak{g}^{ext}\cdot\delta\boldsymbol{u}\,ds,$$

where $\mathfrak{f}^{ext}$ and $\mathfrak{g}^{ext}$ are prescribed external forces.
The principle of virtual works is expressed as

$$\mathcal{W}^{int}\left[\boldsymbol{\chi};\delta\boldsymbol{u}\right]-\mathcal{W}^{ext}\left[\delta\boldsymbol{u}\right]=\delta\mathscr{A}\left[\boldsymbol{\chi};\delta\boldsymbol{u}\right]-\mathcal{W}^{ext}\left[\delta\boldsymbol{u}\right]=$$

$$=\int_{\mathscr{B}^\star}\left(\mathfrak{f}^{int}-\mathfrak{f}^{ext}\right)\cdot\delta\boldsymbol{u}\,dm-\int_{\partial\mathscr{B}^\star}\left(\mathfrak{g}^{int}-\mathfrak{g}^{ext}\right)\cdot\delta\boldsymbol{u}\,ds=$$

$$=\int_{\mathscr{B}^\star}\left(\mathrm{Div}\boldsymbol{\mathcal{P}}-\mathfrak{f}^{ext}\right)\cdot\delta\boldsymbol{u}\,dm-\int_{\partial\mathscr{B}^\star}\left(\boldsymbol{\mathcal{P}}\cdot\boldsymbol{N}^*-\mathfrak{g}^{ext}\right)\cdot\delta\boldsymbol{u}\,ds=0,\qquad\forall\text{ compatible }\delta\boldsymbol{u}.$$

2.6.2 Second gradient

Applying the same procedure to a theory of the second gradient, it turns out that the family of sustainable contact actions is richer.
Furthermore, the dependence of the boundary contact actions by the shape of the $\partial\mathscr{B}^\star$, it is not merely related to the vector field of external normals $\boldsymbol{N}$ but also to the curvature (and so to $\nabla\boldsymbol{N}$). The following calculation towards the irreducible form for the internal work of a second gradient continuum closely follow those presented in [52] and [3].
Let us so consider the first variation of the second gradient action functional:

$$\delta\mathscr{A}\left[\boldsymbol{\chi},\delta\boldsymbol{u}\right]=-\int_{\mathscr{B}^\star}\left[\frac{\partial\mathscr{L}_{\boldsymbol{\chi}}}{\partial F^i_A}\delta u^i_{,A}+\frac{\partial\mathscr{L}_{\boldsymbol{\chi}}}{\partial G^i_{AB}}\delta u^i_{,AB}\right]dm.$$

If we integrate by parts, we obtain

$$\delta\mathscr{A}\left[\boldsymbol{\chi},\delta\boldsymbol{u}\right]=+\int_{\mathscr{B}^\star}P^A_{i,A}\delta u^i dm-\int_{\partial\mathscr{B}^\star}P^A_i\delta u^i N_A ds+$$

$$+\underbrace{\int_{\mathscr{B}^\star}\mathfrak{M}^{AB}_{i,B}\delta u^i_{,A}dm}_{I}-\underbrace{\int_{\partial\mathscr{B}^\star}\mathfrak{M}^{AB}_{i}\delta u^i_{,A}N_B ds}_{II}$$

Considering the two addends I and II of the first variation, it is clear that we can integrate them by parts once again. We start with the term I:

$$\int_{\mathscr{B}^\star}\mathfrak{M}^{AB}_{i,B}\delta u^i_{,A}dm=-\int_{\mathscr{B}^\star}\mathfrak{M}^{AB}_{i,AB}\delta u^i dm+\int_{\partial\mathscr{B}^\star}\mathfrak{M}^{AB}_{i,B}n_A\delta u^i ds=$$

$$=-\int_{\mathscr{B}^\star}\mathrm{Div}\left(\mathrm{Div}\left(\mathfrak{M}\right)\right)\cdot\delta\boldsymbol{u}\,dm+\int_{\partial\mathscr{B}^\star}\left(\mathrm{Div}\left(\mathfrak{M}\right)\cdot\boldsymbol{N}^*\right)\cdot\delta\boldsymbol{u}\,ds$$

Now we proceed with the term II. We need to introduce the two Lagrangian tensors, $\mathfrak{T}$ and $\mathfrak{N}$, of order (1,1), called respectively tangent and normal projector[20] defined as follows:

$$\mathfrak{T}:=\boldsymbol{N}\otimes\boldsymbol{N}^*,\qquad\mathfrak{N}:=\mathbb{1}-\boldsymbol{N}\otimes\boldsymbol{N}^*.$$

So, in coordinates, we have

$$\delta^C_B=\left(\mathfrak{T}^C_B+\mathfrak{N}^C_B\right)$$

Thanks to the two introduced projectors, we can rewrite the term II as follows:

$$\int_{\partial\mathscr{B}^\star}\left(\mathfrak{M}^{AB}_i N_B\right)\delta u^i_{,A}ds=\int_{\partial\mathscr{B}^\star}\left(\mathfrak{M}^{AB}_i N_B\right)\delta u^i_{,C}\delta^C_A ds=\int_{\partial\mathscr{B}^\star}\left(\mathfrak{M}^{AB}_i N_B\right)\delta u^i_{,C}\left(\mathfrak{T}^C_A+\mathfrak{N}^C_A\right)ds$$

$$=\underbrace{\int_{\partial\mathscr{B}^\star}\left(\mathfrak{M}^{AB}_i N_B\right)\delta u^i_{,C}\left(\mathfrak{T}^C_D\mathfrak{T}^D_A\right)ds}_{\clubsuit}+\underbrace{\int_{\partial\mathscr{B}^\star}\left(\mathfrak{M}^{AB}_i N_B\right)\delta u^i_{,C}\left(\mathfrak{N}^C_D\mathfrak{N}^D_A\right)ds}_{\spadesuit},$$

being so able to decompose II as sum of the two sub-terms $\clubsuit$ and $\spadesuit$. We can easily remark that $\clubsuit$ is the tangential part of the tensor $\nabla\delta\boldsymbol{u}$ which has only 4 non zero components. In this way, we can regard such quantity as an intrinsic superficial one, and so we are authorized to use the divergence theorem for Riemannian manifold with boundary on every regular components of $\partial\mathscr{B}^\star$:

$$\int_{\partial\mathscr{B}^\star}\left(\mathfrak{M}^{AB}_i N_B\right)\delta u^i_{,C}\left(\mathfrak{T}^C_D\mathfrak{T}^D_A\right)ds=\int_{\partial\mathscr{B}^\star}\left(\mathfrak{M}^{AB}_i N_B\mathfrak{T}^D_A\delta u^i_{,C}\right)\mathfrak{T}^C_D ds=$$

$$=\int_{\left(\bigcup_\beta\Sigma_\beta\right)\cup\left(\bigcup_\alpha\gamma_\alpha\right)}\left(\mathfrak{M}^{AB}_i N_B\mathfrak{T}^D_A\delta u^i_{,C}\right)\mathfrak{T}^C_D ds=$$

[20] This tensor fields have to be defined in an adapted tubular neighborhood of the boundary.

$$= \int_{(\bigcup_\beta \Sigma_\beta)\cup(\bigcup_\alpha \gamma_\alpha)} \left(\mathfrak{M}_i^{AB} N_B \delta u^i \mathfrak{T}_A^D\right)_{,C} \mathfrak{T}_D^C ds - \int_{(\bigcup_\beta \Sigma_\beta)\cup(\bigcup_\alpha \gamma_\alpha)} \left(\mathfrak{M}_i^{AB} N_B \mathfrak{T}_A^D\right)_{,C} \delta u^i \mathfrak{T}_D^C ds =$$

$$= \int_{\bigcup_\alpha \gamma_\alpha} [\![\left(\mathfrak{M}_i^{AB} N_B \delta u^i\right) \underbrace{\mathfrak{T}_A^C \left(V_\alpha\right)_C}_{(V_\alpha)_A}]\!] dl - \int_{(\bigcup_\beta \Sigma_\beta)\cup(\bigcup_\alpha \gamma_\alpha)} \left(\mathfrak{M}_i^{AB} N_B \mathfrak{T}_A^D\right)_{,C} \mathfrak{T}_D^C \delta u^i ds =$$

$$= \int_{\bigcup_\alpha \gamma_\alpha} [\![\boldsymbol{\mathfrak{M}} \cdot (\boldsymbol{N}^* \otimes \boldsymbol{V}_\alpha^*) \cdot \delta \boldsymbol{u}]\!] \, dl - \int_{(\bigcup_\beta \Sigma_\beta)\cup(\bigcup_\alpha \gamma_\alpha)} ([\nabla \left(\boldsymbol{\mathfrak{M}} \cdot \boldsymbol{N}^*\right) \cdot \boldsymbol{\mathfrak{T}}] : \boldsymbol{\mathfrak{T}}) \cdot \delta \boldsymbol{u} \, ds,$$

where, for any α, $\boldsymbol{V}_\alpha^*$ is the Lagrangian 1-form dual to the normal $\boldsymbol{V}_\alpha$ to γ_α tangent to Σ_β where $\beta \in [\gamma_\alpha]$ and $[\gamma_\alpha]$ represents the set of indices labeling the surfaces Σ_β concurring in γ_α.
Given expression ♠ , remembering that we set $\boldsymbol{\mathfrak{N}} := \boldsymbol{N} \otimes \boldsymbol{N}^*$ or equivalently in index notation $N_A^C = n_A n^C$, we have:

$$\int_{\partial \mathscr{B}^\star} \left(\mathfrak{M}_i^{AB} N_B\right) \delta u^i_{,C} \left(\mathfrak{N}_D^C \mathfrak{N}_A^D\right) ds = \int_{\partial \mathscr{B}^\star} \left(\mathfrak{M}_i^{AB} N_B\right) \delta u^i_{,C} \left(N^C N_D N^D N_A\right) ds =$$

$$= \int_{\partial \mathscr{B}^\star} \left(\mathfrak{M}_i^{AB} N_B N_A\right) \delta u^i_{,C} N^C ds = \int_{\partial \mathscr{B}^\star} \underbrace{\boldsymbol{\mathfrak{M}} \cdot (\boldsymbol{N}^* \otimes \boldsymbol{N}^*)}_{\text{1eulerian covector}} \cdot \underbrace{\nabla_{\mathbf{n}} \delta \boldsymbol{u}}_{\text{1 eul vec}} \, ds$$

We can hence finally introduce the irreducible form for the internal work as:

$$\delta \mathscr{A}\left[\boldsymbol{\chi}, \delta \boldsymbol{u}\right] = + \int_{\mathscr{B}^\star} \underbrace{\left(P_{i,A}^A - \mathfrak{M}_{i,AB}^{AB}\right)}_{=\left(P_i^A - \mathfrak{M}_{i,B}^{AB}\right)_{,A}} \delta u^i dm - \int_{\partial \mathscr{B}^\star} \left(P_i^A N_A - \mathfrak{M}_{i,B}^{AB} N_A - \left(\mathfrak{M}_i^{AB} N_B \mathfrak{T}_A^D\right)_{,C} \mathfrak{T}_D^C\right) \delta u^i ds$$

$$- \int_{\partial \mathscr{B}^\star} \left(\mathfrak{M}_i^{AB} N_B N_A\right) \delta u^i_{,C} N^C ds - \int_{\partial \partial \mathscr{B}^\star} \left(\mathfrak{M}_i^{AB} N_B \delta u^i\right) V_A dl,$$

or equivalently in compact form:

$$\delta \mathscr{A}\left[\boldsymbol{\chi}, \delta \boldsymbol{u}\right] = \int_{\mathscr{B}^\star} \mathrm{Div}(\boldsymbol{\mathcal{P}} - \mathrm{Div}\left(\boldsymbol{\mathfrak{M}}\right)) \cdot \delta \boldsymbol{u} \, dm +$$

$$- \int_{\partial \mathscr{B}^\star} ((\boldsymbol{\mathcal{P}} - \mathrm{Div}\left(\boldsymbol{\mathfrak{M}}\right)) \cdot \boldsymbol{N}^* - [\nabla \left(\boldsymbol{\mathfrak{M}} \cdot \boldsymbol{N}^*\right) \cdot \boldsymbol{\mathfrak{T}}] : \boldsymbol{\mathfrak{T}}) \cdot \delta \boldsymbol{u} \, ds +$$

$$- \int_{\partial \mathscr{B}^\star} \boldsymbol{\mathfrak{M}} \cdot (\boldsymbol{N}^* \otimes \boldsymbol{N}^*) \cdot \nabla_{\mathbf{n}} \delta \boldsymbol{u} \, ds - \int_{\partial \partial \mathscr{B}^\star} \boldsymbol{\mathfrak{M}} \cdot (\boldsymbol{N}^* \otimes \boldsymbol{V}^*) \cdot \delta \boldsymbol{u} \, dl.$$

If we set

$$\begin{cases} \mathfrak{f}^{int} = \mathrm{Div}\left(\boldsymbol{\mathcal{P}} - \mathrm{Div}\left(\boldsymbol{\mathfrak{M}}\right)\right) \\ \mathfrak{g}^{int} = \left(\boldsymbol{\mathcal{P}} - \mathrm{Div}\left(\boldsymbol{\mathfrak{M}}\right)\right) \cdot \boldsymbol{N}^* - [\nabla \left(\boldsymbol{\mathfrak{M}} \cdot \boldsymbol{N}^*\right) \cdot \boldsymbol{\mathfrak{T}}] : \boldsymbol{\mathfrak{T}} \\ \mathfrak{b}^{int} = \boldsymbol{\mathfrak{M}} \cdot (\boldsymbol{N}^* \otimes \boldsymbol{N}^*) \\ \mathfrak{t}^{int} = \boldsymbol{\mathfrak{M}} \cdot (\boldsymbol{N}^* \otimes \boldsymbol{V}^*) \end{cases}$$

with $\mathfrak{f}^{int}, \mathfrak{g}^{int}, \mathfrak{b}^{int}, \mathfrak{t}^{int} \in \Omega^1\left(\boldsymbol{\chi}\left(\mathscr{B}^\star\right)\right)$, we can rewrite the internal work in the simple form:

$$\delta\mathscr{A}\left[\chi;\delta\boldsymbol{u}\right] = \int_{\mathscr{B}^\star} \mathfrak{f}^{int}\cdot\delta\boldsymbol{u}\,dm - \int_{\partial\mathscr{B}^\star} \mathfrak{g}^{int}\cdot\delta\boldsymbol{u}\,ds - \int_{\partial\mathscr{B}^\star} \mathfrak{b}^{int}\cdot\nabla_{\mathbf{n}}\delta\boldsymbol{u}\,ds - \int_{\partial\partial\mathscr{B}^\star} \mathfrak{t}^{int}\cdot\delta\boldsymbol{u}\,dl.$$

So in a second gradient model, the external actions compatibles with the introduced form of the internal work are

- forces per unite volume,
- forces per unite area,
- forces per unite line,
- double-forces per unite area, i.e., objects that expend work on the normal derivative of virtual displacements.

Therefor the external work which has to be introduced in a second gradient theory, has the following general form:

$$\mathcal{W}^{ext}\left[\delta\boldsymbol{u}\right] = \int_{\mathscr{B}^\star} \mathfrak{f}^{ext}\cdot\delta\boldsymbol{u}\,dm - \int_{\partial\mathscr{B}^\star} \mathfrak{g}^{ext}\cdot\delta\boldsymbol{u}\,ds - \int_{\partial\mathscr{B}^\star} \mathfrak{b}^{ext}\cdot\nabla_{\mathbf{n}}\delta\boldsymbol{u}\,ds - \int_{\partial\partial\mathscr{B}^\star} \mathfrak{t}^{ext}\cdot\delta\boldsymbol{u}\,dl,$$

where

- $\mathfrak{f}^{ext}$ is the external force per unite volume,
- $\mathfrak{g}^{ext}$ is the external force per unite area,
- $\mathfrak{b}^{ext}$ is the external double-force for unite area,
- $\mathfrak{t}^{ext}$ is the external force for unite line.

Chapter 3

Discrete and continuum models for 2D fabrics

As it happens for every mathematical model intended to be used for natural phenomena, the continuum model of deformable bodies developed following Cauchy's point of view, although may be very effective to carefully describe a wealthy of systems, cannot be universally applied. As a matter of fact, already at a very early stage of Cauchy formulation of the basic ideas of continuum models, Gabrio Piola [19], with a stringent mathematical study, analyzed its limits and proposed some more general models which are nowadays widely used. More than one century later Piola's ideas resurfaced (for a discussion of these phenomena of re-discovery the interested reader should consult the work by Russo [79]) and a group of scientists (Mindlin [55, 56, 57], Toupin [86, 87], Green and Rivlin [39, 37, 38, 40], Germain [35, 36] Eringen and Suhubi [30, 31]) reformulated, accepted and understood the objections and observations pushed forward by Piola and re-started and developed his work. Although, for some reasons to be investigated, the impetus of this flow of ideas was relented until the beginning of XXI century, they are now flourishing and constitute those fields which are variously named as: generalized continuum models, multi-scale models, second or higher gradient (or higher grade) continua, microstructured continua, multipolar continua, enhanced continuum models and so on (see e.g. [18, 9, 10, 60]).
In this work we propose to show that such generalized continuum models can be useful to characterize mechanical systems composed by nearly inextensible fibers with relatively low bending stiffness. To these systems was dedicated the interesting work [83], which represents an unavoidable reference in the field. Such work has been followed by several researchers (e.g., [74, 54]) .
We start by presenting two discrete models which are inspired by, but do not exactly coincide with, some woven fabrics constituted by nearly inextensible fibers (see e.g. [33, 7, 11]):

- A simple two-dimensional structure consisting of (long) elasticae (as models for nearly inextensible fibers) connected to each other by means of perfect internal pivots, in the manner of a pantographic lattice (the internal pivots do not interrupt the continuity of the fibers). These fibers, and associated pivots, are assumed to be uniformly distributed in the plane. We assume that the fibers are (nearly-)inextensible elasticae with equal flexural stiffnesses. Once a corresponding homogenized model is introduced we get a generalization of Pipkin's theory of perfectly flexible inextensible nets with shear resistance [65, 66, 72], the latter manifesting itself as a dependence of the strain-energy function on the shear angle between intersecting fibers. This type of shear resistance vanishes in the present model of ideal pantographic lattices characterized by ideal pivots in which there is no concentrated rotational elastic stiffness. Similar structures that exhibit such *floppy modes* (modes with vanishing associated energy) are discussed comprehensively in [49] and closely resemble those studied in [2]. Here, we recall that (see [24]) the compatibility of the first gradient of the deformation is shown to imply a direct connection between the *gradient of fiber shear* and the *fiber bending strains*: this effect is as-

sociated with the second gradient of deformation. Accordingly, the *pantographic substructure* leads naturally to a particular second-gradient continuum theory of elasticity. This is indeed a very particular generalized continuum, where no extra kinematical descriptor is introduced: the only difference of the model which we present here when compared with standard Cauchy continua consists in the introduction of second gradient of displacement as an independent variable in the constitutive equation for deformation energy.

- Another way to model a metamaterial with a microstructure consisting of nearly inextensible fibers is given by the introduction of local constraints in the discrete continuum model at the finite element (FE) level. More particularly, the elementary cell of the discretization is composed by standard quadrilateral elements with the addition of very stiff diagonal bar elements joining the opposite corner nodes (mimicking the behavior of fibers) with an axial stiffness which is very high with respect to the in-plane stiffness of the considered FE. Basically, this strategy consists in a penalty for the deformations along particular directions in the plane of the material, (TPM, Truss Penalty Method). This strategy is a weak version of the one presented in [41] in which the authors have implicitly imposed the inextensibility constraint locally at each Gauss points of the FE. The strategy presented in this work imposes the inextensibility constraint globally at the element level. Moreover, in this way it is possible to generalize the method for a n-family of constrained directions. In this work we presents a 2-family fiber reinforcement that in the following is denoted by TPM-2 and which will be seen to be useful for the description of so-called bias extension test.

On the basis of the informations obtained by means of the considered discrete models we finally investigate the continuum description of fibrous composite reinforcements and we end up with the conclusion that a second gradient theory is indeed necessary in order to account for the bending stiffness of fibers at the microscopic level. We are of course aware that the particular second gradient continuous model which we present here may not be general enough to describe carefully all the macroscopic phenomenology of considered mechanical systems: we may need to introduce continua endowed with microstructure fields (see e.g. [31]) as, for instance, directors. Moreover, the most general constitutive modeling of 2D anisotropic structures made of flexible nets of fibers should rely on the methods based on the material symmetry groups. Inertial, damage, plastic deformation or dislocation effects are not included in the present model. The phenomenology of fibrous reinforcements is rich of instability and bifurcation phenomena due to the interest which has to be directed towards their large deformation configurations (see e.g. [6, 7, 43, 48, 91]). Indeed, one can observe wrinkling (see e.g [8, 48]), plies and plastic deformations etc.
When presenting the numerical simulations associated to the introduced continuum models, we will point out that some numerical errors related to the high contrast between the tensile stiffness and the bending stiffness of yarns may arise. These phenomena are known as tension locking phenomena (see e.g.[42]) and are mitigated here by choosing suitably refined meshes and finite elements of suitably high order.

Contents

3.1 Materials with strong contrast of the mechanical properties at the microscopic level

It is known (see e.g. [80]) that materials which have strong contrasts of the mechanical properties at the microscopic level are likely to behave as generalized continua when subjected to particular loading and/or boundary conditions. It has been recently shown (see [33]) that a particular class of engineering materials, known as fibrous composite reinforcements, show exotic mechanical properties when considering particular loading conditions and kinematical constraints. Fibrous composite reinforcements are woven fabrics which present a very high tension stiffness in the warp and weft directions together with a very low shear stiffness. In other words, the yarns constituting such materials are very stiff in tension, while the angle variation between two superimposed yarns (warp and weft) can occur very easily. These characteristics make fibrous composite reinforcements a topical example to better understand which types of microstructures must be considered in order to obtain second or higher order continua at the homogenized level.
In virtue of the importance of the mechanical modeling of these materials for engineering, it is essential to establish which theoretical and numerical models must be adopted to better describe their macroscopic and mesoscopic properties.

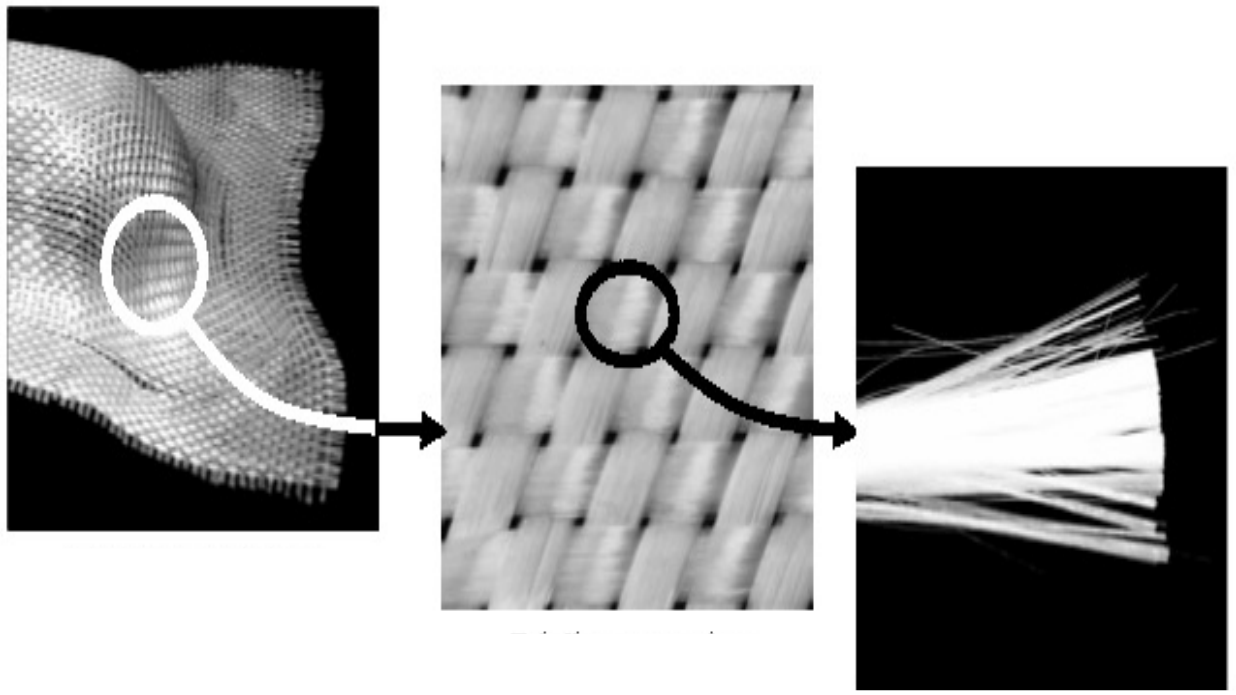

Figure 3.1: Macroscopic, mesoscopic and microscopic scale of a woven fabric.

Figure 3.1 shows the macroscopic engineering component of fibrous composite reinforcement, its mesoscopic scale (warp and weft) and the microstructure of each yarn. We are interested here to the mesoscopic and macroscopic scale of such materials and we will try to model from a theoretical and a numerical point of view some peculiar deformation patterns of 2D woven composites at the

scale of warp and weft and then at the scale of the whole engineering component. As already discussed, we propose here to address the modeling of the mechanical behavior of 2D fibrous composite reinforcements both by considering

- discrete mechanical systems mimicking at best the characteristics of the underlying mesostructures,
- continuum models which are able to correctly catch the overall mechanical behavior of such systems.

We will show the limits of the considered discrete modeling while capturing from them some essential features which are needed to understand the correct way of exploiting generalized continuum theories via finite element methods.
In this work, we target to reproduce a very common experimental test on woven composites which is known as bias extension test: we will use this example as a reference case for testing the efficacy of all the introduced discrete and continuum models. The bias extension test is a mechanical test which is widely used in the field of fibrous composite materials. This test is useful to characterize the mechanical behavior of woven fibrous composites undergoing large shear deformations.

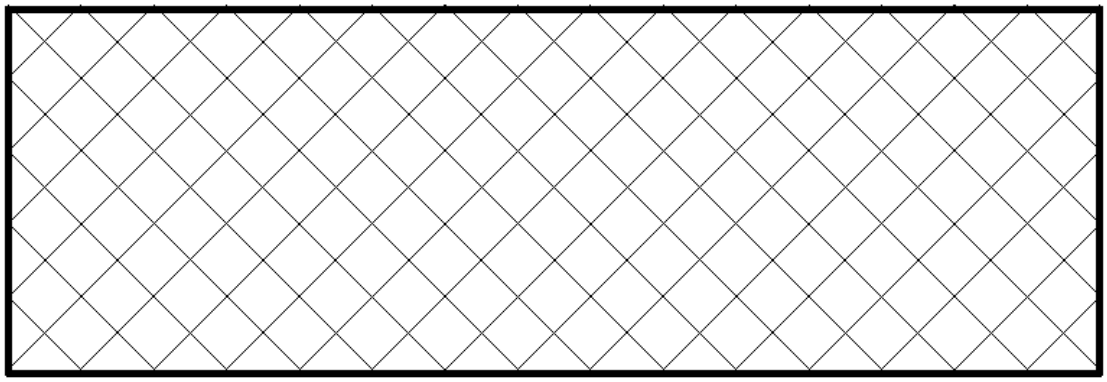

Figure 3.2: Reference configuration of a specimen of fibrous composite reinforcement for a bias-extension test.

The bias extension test is performed on rectangular samples of woven composites, with the height (in the loading direction) relatively greater (at least twice) than the width, and the yarns initially oriented at $\pm$ 45-degrees with respect to the loading direction (see Fig.3.2). The specimen is clamped at two ends: one end is maintained fixed and the second one is gradually displaced of a given amount. The relative displacement of the two ends of the specimen generates angle variations between the warp and weft. The deformed configuration consists of three different regions A, B and C, in which the shear angle between the yarns remains almost constant (see Fig.3.3 and references [6, 11, 44]). More particularly, the fibers in regions C remain undeformed, i.e. the angle between fibers remains at 45° also after deformation. As far as considering the other regions A and B, the angle between fibers becomes much smaller than 45°, but it keeps almost constant in each region. The main characteristics of the bias extension test are summarized in Fig. 3.3 in which both the undeformed and deformed shapes of the considered specimen are schematically depicted. In [33] it has also been put in evidence that another important phenomenological aspect of the bias extension test must be taken into account. In particular, at the transition lines between two different regions at constant shear angle the presence of thin transition layers can be identified which allow a smooth transition from a region with constant shear angle to the adjacent one (see Fig.3.4).
These layers will be called shear transition layers and their thickness can be associated to the gradient of shear angle variation between yarns (or equivalently to the in-plane bending stiffness of the yarns).

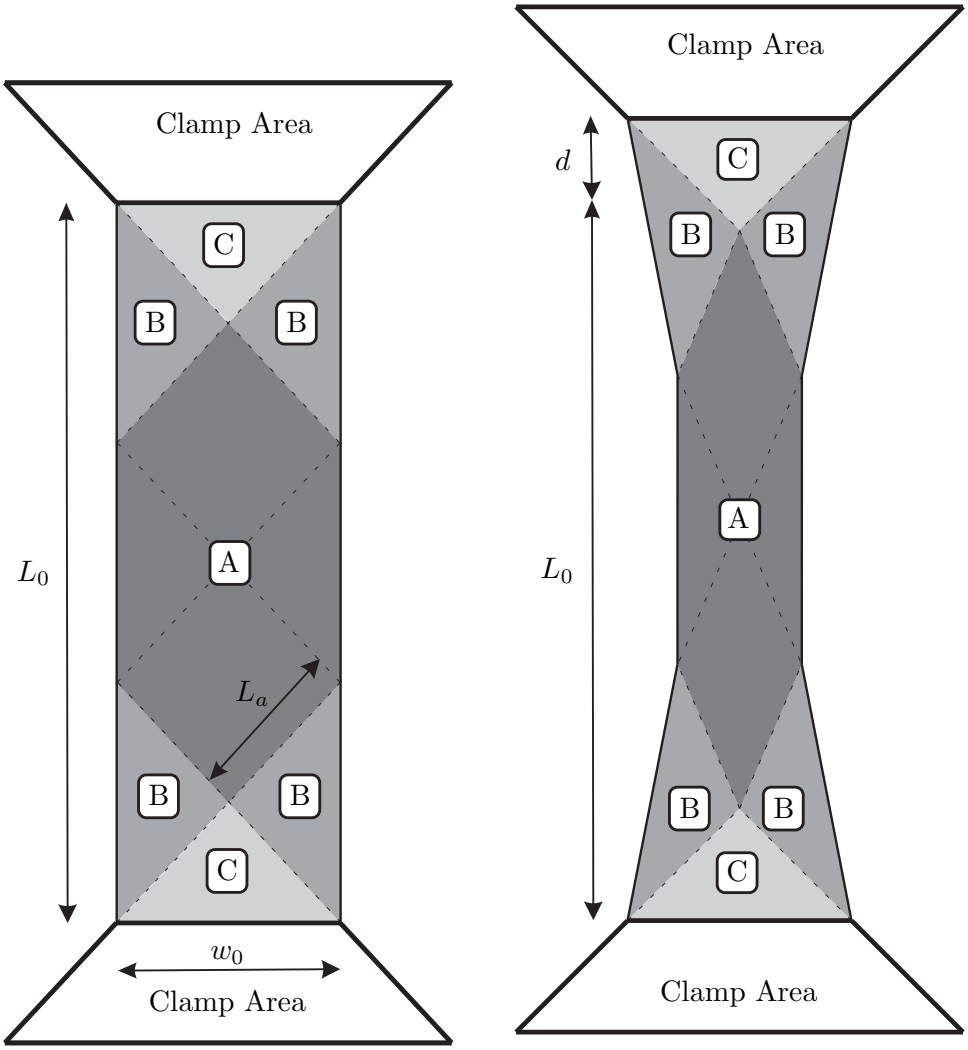

Figure 3.3: Simplified description of the deformation pattern in the bias extension test.

It is clear that a complete predictive model of the bias extension test must necessarily include an accurate description of such shear transition layers.
In the reminder of this work, we will propose different discrete and continuum models for the description of the bias extension test and we will point out which ones of the main characteristics of this test are well described (or not) in each model.

3.2 Discrete mechanical systems including strong contrast at lower scales

As it has been previously discussed, fibrous composite reinforcements exhibit a strong contrast between the tension and the shear stiffnesses at the mesoscopic level. In this section we propose two different discrete systems which can be built-up by means of available softwares and which include the possibility of accounting for such kinds of strong contrasts.

3.2.1 Pantographic lattices

As a first example of discrete modeling of fibrous networks, we introduce a modular pantographic structure which can be described, at the mesoscopic level, as a structure constituted by nearly in-

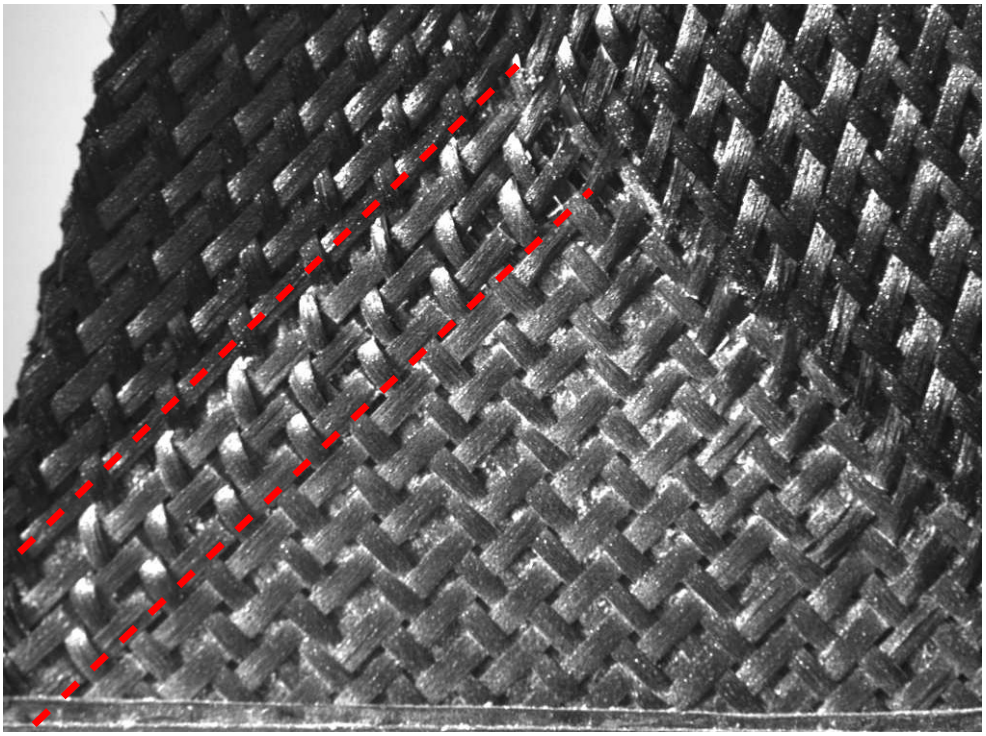

Figure 3.4: Shear transition layers in a fibrous composite reinforcement subjected to a bias extension test.

extensible but flexible Euler-Bernouilli beams connected by pivots at their intersection points. It is worth noting that the considered structure is different from a truss-like structure since the internal pivots do not interrupt the continuity of each beam. In other words, in presence of appropriate loading and boundary conditions, the bending moment in each beam is not vanishing as in truss structures, but it is instead fundamental to characterize the global structural response. The considered beams have an elliptical cross section, in which the major and minor axis are respectively denoted by D_1 and D_2: the major axis lies in the considered plane and the orientation of the beams is at $\pm 45^\circ$ with respect to the global reference frame (see Fig.3.5). The yarns are supposed to be constituted by carbon fibers and the used elastic and geometric parameters are summarized in table 3.1.

E	ν	D_1	D_2
$[GPa]$	$[-]$	$[mm]$	$[mm]$
6	0.3	1.5	0.6

Table 3.1: Properties of the bars constituting the pantographic lattice.

The considered beams are linear-elastic beams i.e. no geometrical nor material linearities are included in this model. We assume that external actions and external constraints are applied at intersection nodes only. In the next section we will show numerical simulations in which this pantographic lattice is used to model a bias extension test and we will discuss the obtained results.
The reason for which the presented discrete lattice cannot be regarded as an always effective model of the fiber reinforcements considered e.g. in [11] is simple. Indeed, it is true that the fibers which form these fabrics may effectively be individually modeled as beams and that their contact can be in some circumstances be modeled as pivots (see e.g. [88]): however, as they have a section whose diameter can be comparable with the distance between two closest contact zones, the model of Euler

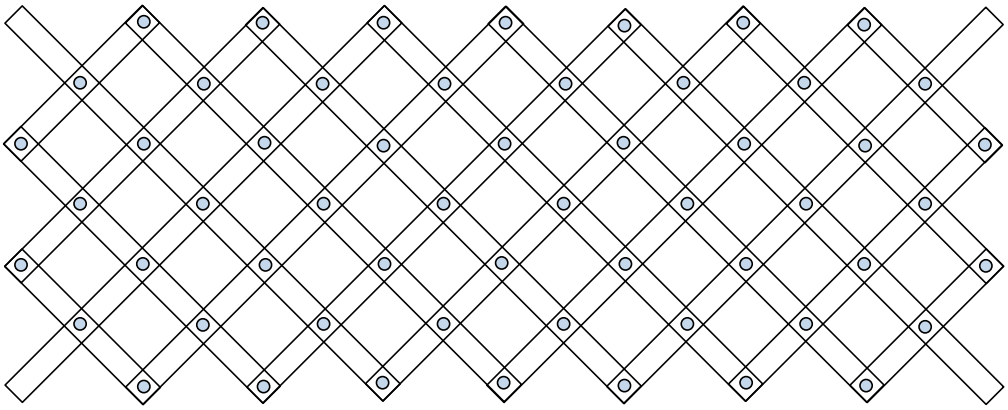

Figure 3.5: Module of the pantographic lattice.

beam does not seem always applicable for describing their behavior when they are included in woven fabrics. On the other hand, in the next subsection, we present a structure constituted by elasticae whose section is small when compared to the distance between the closest introduced pivots which are inter-connecting them, so that every fiber can be always effectively modeled as Euler beam.

3.2.2 Truss Penalty Model

A second way to model networks of almost inextensible yarns is the Truss Penalty Model (TPM). The discretization of the problem is obtained by constraining in a suitable way a standard quadrilateral shell element available in a software like ADINA. In particular, we choose to constrain a quadrilateral shell finite element by means of two rigid bars which are connected to the corners of the element by means of internal pivots. The rigid diagonal bars are not connected by an internal hinge at their intersection, as for the pantographic lattices case, but they are free to slide in a relative motion (see Fig.3.6). We call the obtained finite element TPM-2. We choose this kind of finite element because it is very robust and accurate. Moreover, this finite element is formulated with a full quadrature scheme (using all Gauss points) so in this way a specific strategy to control the in-plane hour-glass mode is not necessary. It is worth noting that, this kind of finite element is a shell-element, but in this numerical investigation the out-of-plane displacement of the element are forbidden and then the rotational degree of freedom are not activated for the plane geometry and in-plane load condition considered. Summarizing, only the in-plane deformation part is considered and the inextensibility constraint in the fiber direction is accounted for by adding rigid bars as diagonals of the finite element. The introduction of the diagonal truss element constraint penalizes some deformation modes of the finite element: in particular, the global shear deformation mode with respect to the spatial reference frame at the element level.
The admissible deformation modes associated to TPM-2 elements are depicted in Fig. 3.6: it can be noticed that the presence of the diagonal rigid bars forbids the classical shear modes of the element thus reducing the degrees of freedom from 8 to 6. We can summarize with reference to Fig.3.6 by saying that the TPM-2 element only allows the three rigid modes (1,2,3), the extensional deformation mode (4) and the two hour-glass deformation modes (5,6). The introduced penalty method can be interesting for further developments oriented towards the design of specific finite elements. For example, it is possible to conceive a quadrilateral finite element in which the inextensibility constraint along the two diagonals can be implicitly formulated, adopting a reduced integration scheme to overcome the in-plane shear locking and adopting a stabilization strategy for the hour-glass modes analogously to [41, 42], (or introducing in-plane bending stiffness). In the numerical simulations based on the TPM-2 elements which will be presented in the next section, the considered constitutive model for the bars is simply linear elastic. Table 3.2 summarizes the values used for the Young modulus E_m of the membrane, for the Young modulus E_b of the internal bars and for

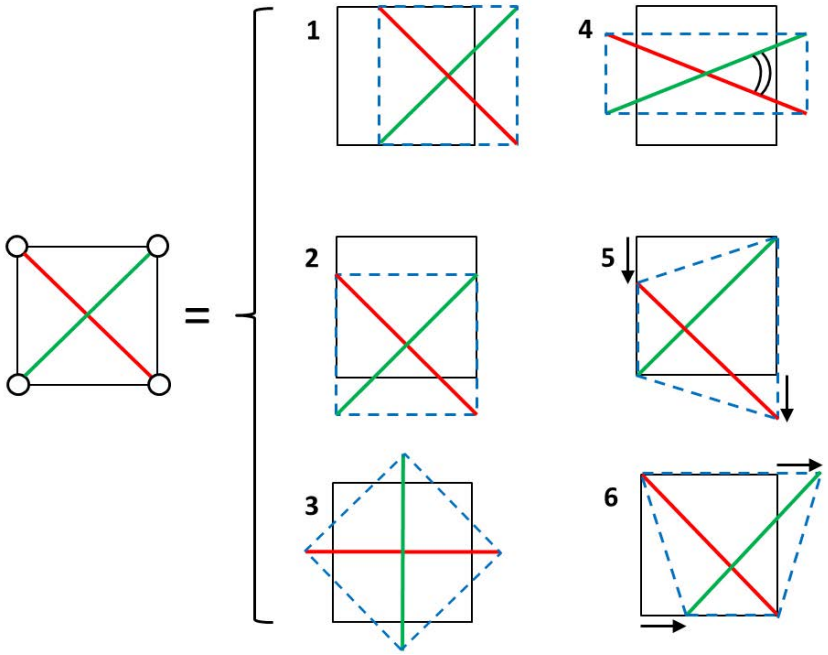

Figure 3.6: TPM-2: Deformation modes for the base cell obtained by means of the constrained finite element.

the corresponding Poisson ratios ν_m and ν_b. Moreover, the diameter D of the bars is also given in this table. This linear constitutive assumption will be shown to be sensible for relatively small imposed displacements, but will be seen to be too restrictive to describe the bias extension test for high imposed displacements of the top surface.

E_m	E_b	ν_m	ν_b	D
$[MPa]$	$[GPa]$	$[-]$	$[-]$	$[mm]$
0.168	20	0.3	0.3	0.6

Table 3.2: Elastic properties of the TPM-2 bars.

The main advantages of this strategy used to account for the inextensibility conditions are: i) the numerical implementation is very easy to be performed, ii) the inextensibility condition is not imposed locally at the Gauss points, but a global formulation of the inextensibility conditions is considered for the whole finite element, and iii) it is possible to obtain a parametric modulation of the stiffness of the constraining bars in order to obtain solutions which are close to the experimental deformed shapes. On the other hand, only linear constitutive equations have been implemented in this model for the sake of simplicity. This fact limits the applicability of the TPM-2 to the case of imposed displacements of the top surface which only activate geometric non-linearities and not material ones. Indeed, as it will be more deeply discussed, geometrical non-linearities are not sufficient to describe large shear angle variations in the bias test which are associated to high displacements of the top surface. In order to catch such strongly non-linear behavior, material non-linearities have also to be introduced in the constitutive model.
Notwithstanding these limits of the considered TPM-2 finite element for what concerns the highly non-linear regime, we show that it is indeed well adapted to describe the overall behavior of 2D fibrous composites at moderate strains. Of course, a generalization of the considered FE including the possibility of material non-linearities is possible, but is not attempted in the present work. Such generalization would, in fact, lead to the difficulty of choosing the correct material behavior and, in a second time, induce a long procedure of calibration of the introduced parameters to fit at best

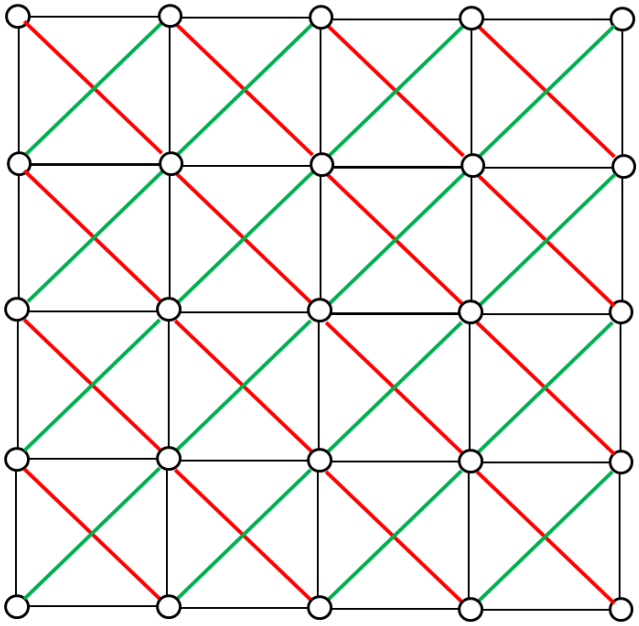

Figure 3.7: A periodic modular pattern of TPM-2 discretization (2-family inextensible directions).

the experimental behavior at high strains. The main task of the present work being that of showing the limits of the considered discrete model with respect to the description of the observed transition layers, we limit ourselves to consider a simplified linear case.

3.3 Equilibrium shapes of introduced discrete systems

In this section we show the results of the numerical investigations obtained with the different discrete methods presented above. In the next sections, we will instead present two continuum models which will be seen to be better adapted than the discrete ones to the description of the mechanical behavior of 2D fibrous composites also at high strains. In Fig. 3.8 we schematically present the three different approaches which we use in this work to simulate the bias extension test: two particular discrete systems and a continuum approach. The characteristic sizes of the specimen are the same for all numerical simulations treated in this work:

- basis: $100\,mm$
- height: $300\,mm$

In this section we show the strong and weak points of the proposed discrete approaches and we leave to the following sections the treatment of the bias extension test by means of continuum theories.

3.3.1 Pantographic lattices

Employing the discrete pantographic lattice model introduced in section 3.2.1, we compute the equilibrium shape of the specimen subjected to an imposed displacement of the top surface. Figure 3.9 displays the current configuration of the testing sample for an imposed displacement of 55 mm: the color distribution indicates, for each yarn, the angle variation field of the yarn itself with respect to its reference configuration. In particular, we can see that the three characteristic regions denoted by A, B and C in Fig. 3.3 are recovered in the considered discrete numerical simulation. The portion of yarns lying in the triangle C basically stay undeformed and indeed the angle rotation of each fiber with respect to its reference configuration is vanishing as it can be easily deduced from Fig. 3.9.

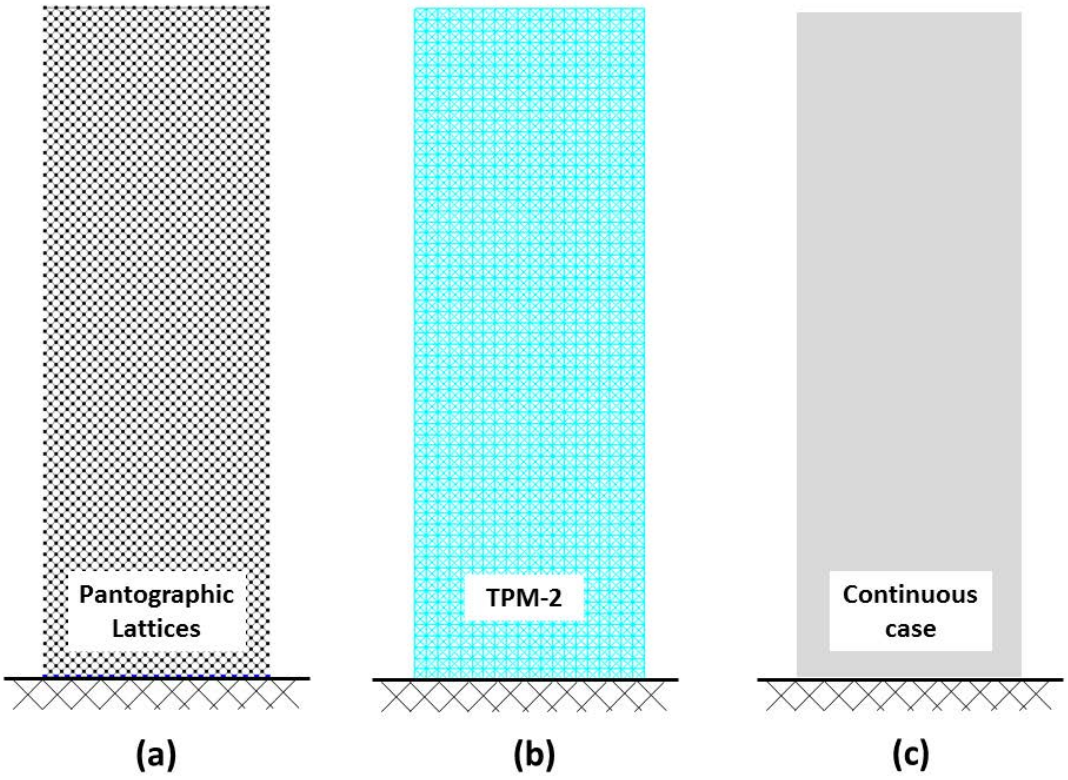

Figure 3.8: Schematic representation of the bias extension test simulated with the discrete and continuum models. Basis: $100\,mm$, height: $300\,mm$.

The two orders of fibers lying in the region A actually rotate of the same amount (almost 20°) with respect to their reference configuration: this is equivalent to say that the total angle variation in the region A is of almost 40°. The situation is slightly different for the portion of yarns lying in the region B. Indeed, it can be recognized that one order of yarns almost remains parallel to the reference configuration (no angle variation). On the other hand, the second order of fibers rotates of almost 20° with respect to the reference configuration: this means that the total angle variation in the region B is of almost 20°. Clearly, it is possible to directly relate the angle variation to the in-plane cross-section rotation of beams due to the fact that the beams are bending in a small transition zone from one triangle at constant shear strain to the adjacent one. Indeed, it is possible to remark that in Fig. 3.9 the presence of the so called shear transition layer can be detected. The thickness of this transition layer is directly related to the in-plane bending stiffness of fibers. The performed numerical simulations on the pantographic lattice structure allow us to conclude that the presence of the shear transition layer at the macroscopic level is indeed naturally stemming from the particular mesostructure of the considered medium. In particular, we are able to claim that the onset of such transition layers is due to the fact that the shear angle gradually varies from one constant value to another constant value: this variation is made in a thin transition zone in which a rapid gradient of the shear angle variation can be observed. The thickness of such transition layers is clearly related to the in-plane bending stiffness of the fibers. These observations fit with the theoretical results presented in [24] in which a direct relationship between the in-plane bending strain of fibers and the gradient of shear strain is found. It is hence possible to claim that, in this context, the need of a higher gradient theory is directly stemming from micro-structural effects.
Figure 3.3.1 shows the bending energy and the axial energy of the pantographic lattice, respectively. As we could expect, it can be noticed that the bending energy is concentrated in the shear transition

layer which determines the transition between two regions at constant shear angle. On the other hand, the axial energy is concentrated on few beams close to the corners of the specimen.

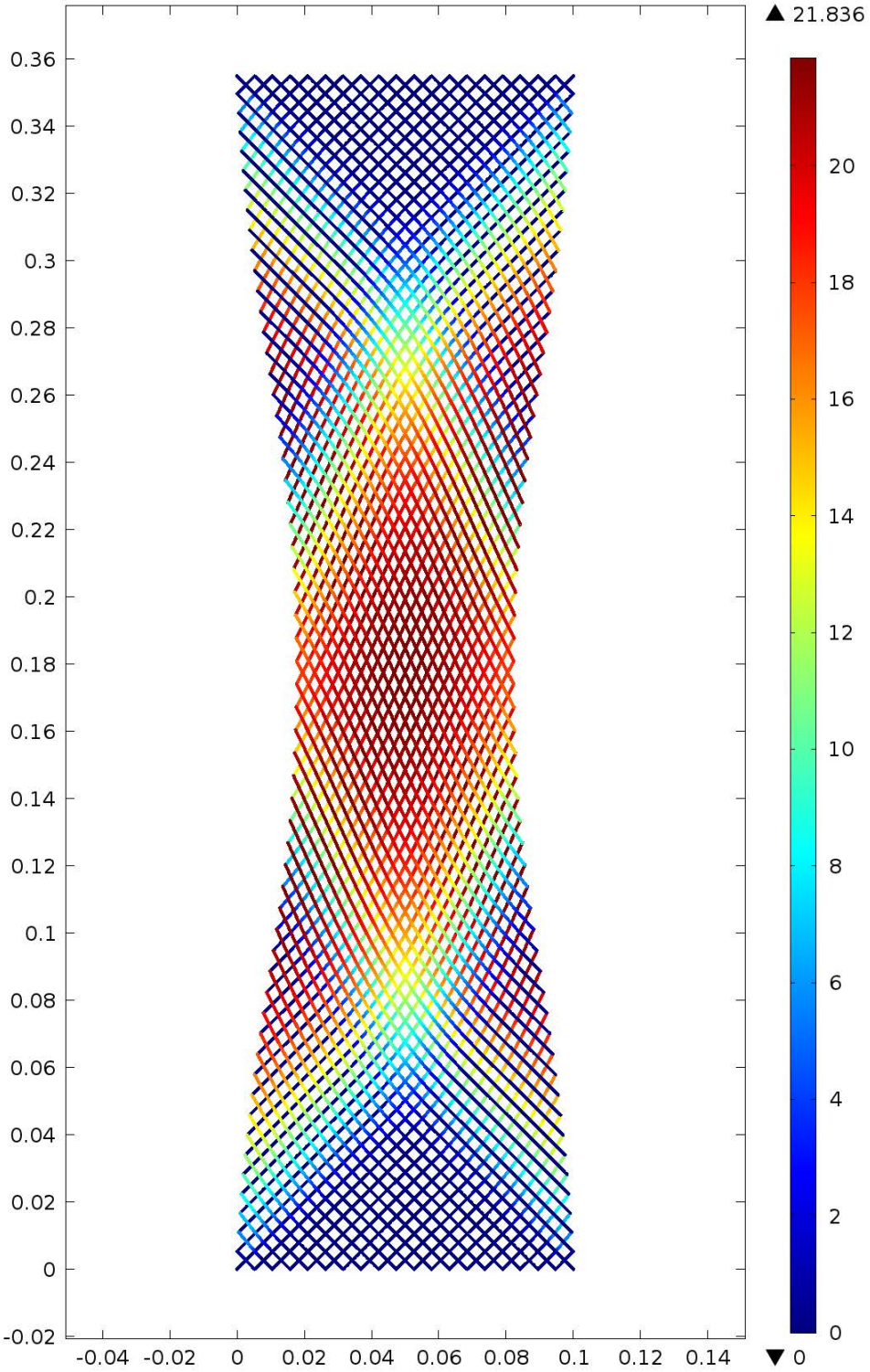

Figure 3.9: Fiber angle variation in the pantographic lattice for a displacement of 55 mm.

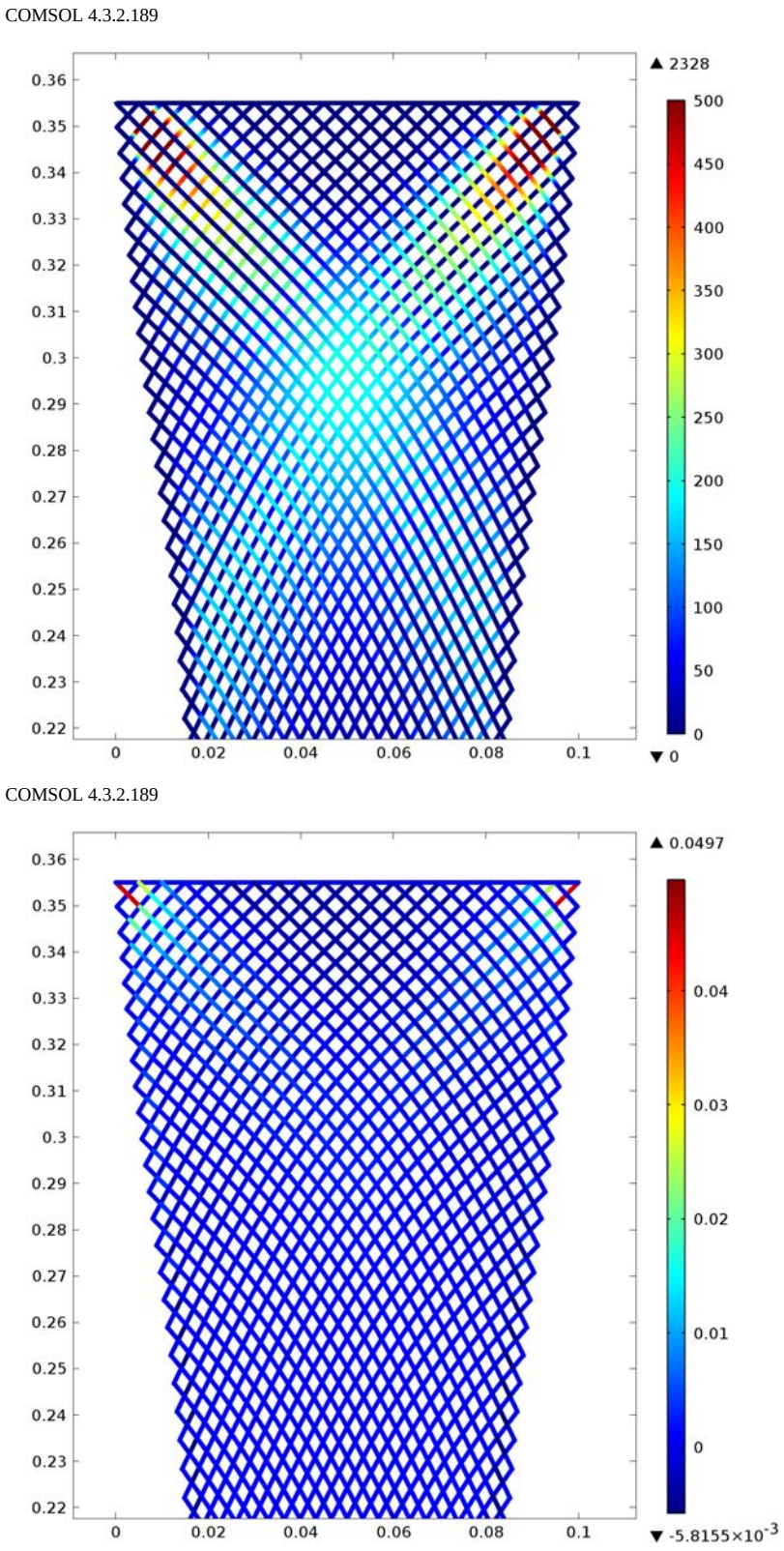

Figure 3.10: From left to right: bending energy (J/m) and axial energy (J/m) of the pantographic structure.

3.3.2 TPM elements: mesh-dependence of the thickness of the shear transition layer

In figure 3.11, we consider the set up for the problem in study by means of TPM-2 finite elements.

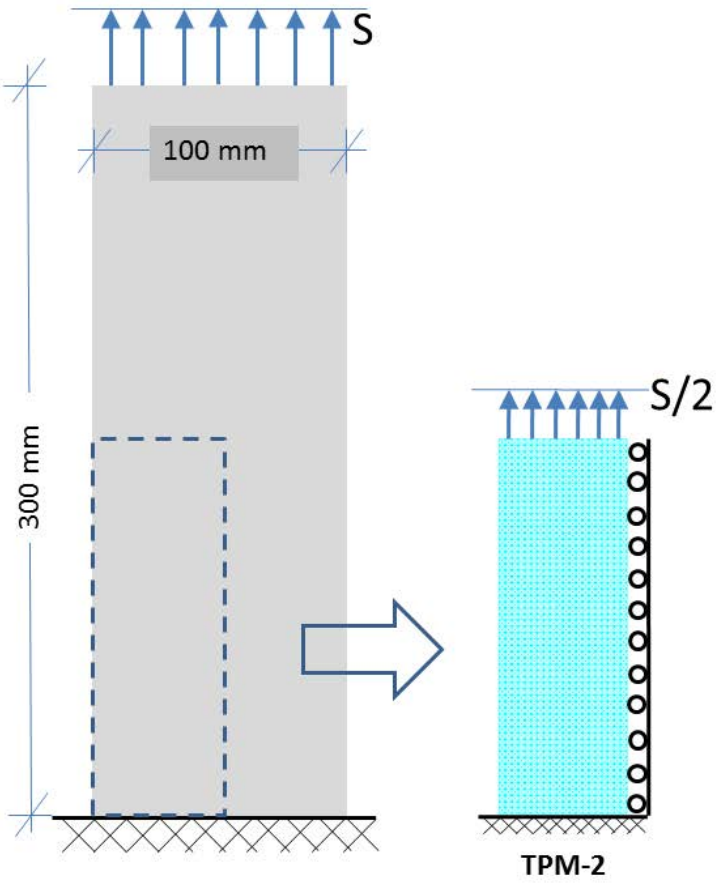

Figure 3.11: Set up of the problem and its discretization by TPM-2 mesh

We remark that, in virtue of symmetry, we are able to implement only one fourth of the structure (see Fig. 3.11). Figure 3.12 shows simultaneously the undeformed configuration for the TPM-2 material, the deformed one and a schematic representation of the solution for the bias test in which the three zones at constant shear angle are indicated here as 1, 2 and 3 (see also Fig.3.3). Large deformation assumption is accounted for in the numerical simulations only because of geometrical non-linearities. More precisely, the constitutive relations for the single beams are the classical linear-elastic ones (quadratic energy in the deformation measures), but the considered strain measures are nonlinear.

The obtained solution (Fig. 3.12(b)) reproduces quite precisely the solution for the bias test on a fibrous composite reinforcement, at least for imposed displacements up to $50 - 55\,mm$. The obtained solution presents the previously discussed three different zones at constant shear angle: these zones being characterized by a homogeneous deformation process, they show constant strain (or stress) field. It is worth noticing that the representative deformation modes which allow for the transition from one region to the adjacent one are the hour-glass deformation modes 5 and 6 as indicated in figure 3.6. More particularly, these deformation modes are also influenced from the imposed boundary conditions which indeed fix two of the four sides of the TPM-2 elements which remain undeformed. In this context, it is evident how the thickness of the transition layer which is responsible of the transition between two zones at constant shear angle strongly depends on the

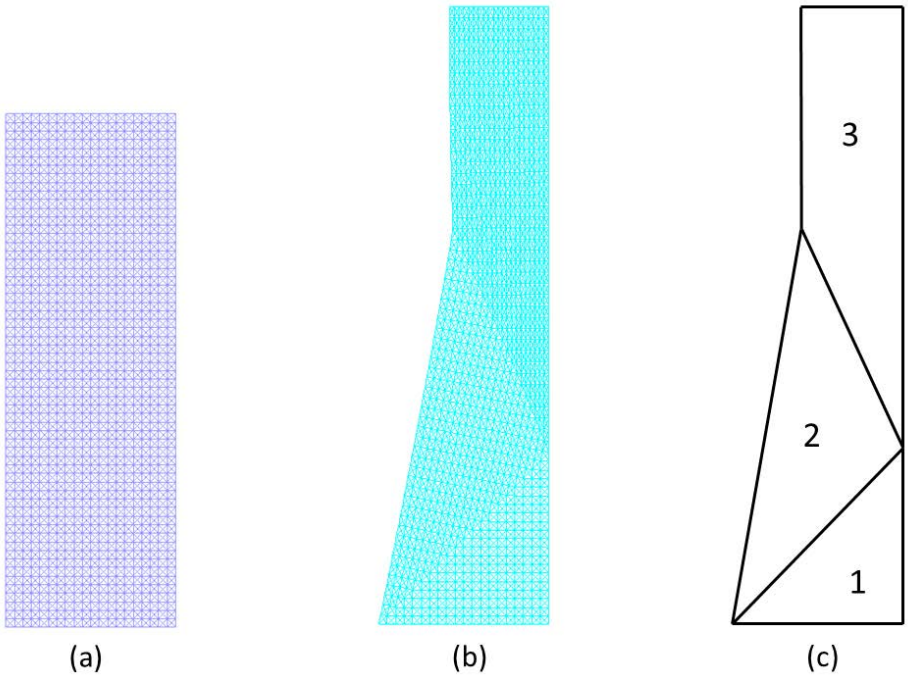

Figure 3.12: Initial configuration (a); final configuration (b); homogeneous strain zones (c).

size of the chosen elements: the transition always occurs on one and only finite element. This fact is underlined in Fig.3.13 in which the transition deformation strips are highlighted by means of a different color. This fact must systematically be taken into account when looking for FEM solutions for the bias extension test: a model in which each finite element deforms independently of the deformation of the adjacent ones cannot account for the description of the transition zone in which high gradients of the shear angle variation occur.
The three in-plane Cauchy stress components obtained by means of the TPM-2 model are shown in figure 3.14. In this figure one can appreciate the homogeneity of the response and the high strain jumps corresponding to the two transition zones are also evident. Furthermore, we observe that in the limit of very high axial stiffness for the truss there are strong concentrations of the reaction forces in the corners of the specimen, as it is indicated in figure 3.15: all the other reactions are negligible in comparison with respect to those which are highlighted in this picture. This is coherent with the results obtained by means of the panthographic structure model. We explicitly remark that the main features of the obtained response strongly depend on the ratio between the stiffness of the internal diagonal truss and that of the membrane. When decreasing the truss stiffness, all the observed peculiarities of the solution vanish and a standard elastic solution is recovered.
In fact, as it is depicted e.g. in figure 3.16, decreasing the stiffness of the truss of the TPM-2 discretization, the strong gradients disappear compared to the previous high stiffness case. Analogously, the strong concentration at the corners of the reaction field disappears as well. These results allow us to deduce that the typical solution of the bias extension test in which three zones at constant shear angle are present, is indeed deeply related to the strong contrast between the high tensile stiffness of the yarns and the low shear angle variation stiffness. Consequently, this strong contrast of the mechanical properties at the mesoscopic level is also responsible for the onset of shear transition layers between the transition zones: these transition zones cannot be properly taken into account by the considered TPM-2 model. As suggested by the homogenization techniques proposed in [2], when considering truss structures with strong contrasts of the mechanical properties, one possible solution to correctly model the structure itself is to consider a second (or higher) gradient continuum model. On the light of these considerations, we are led to the conclusion that one possible strategy for the

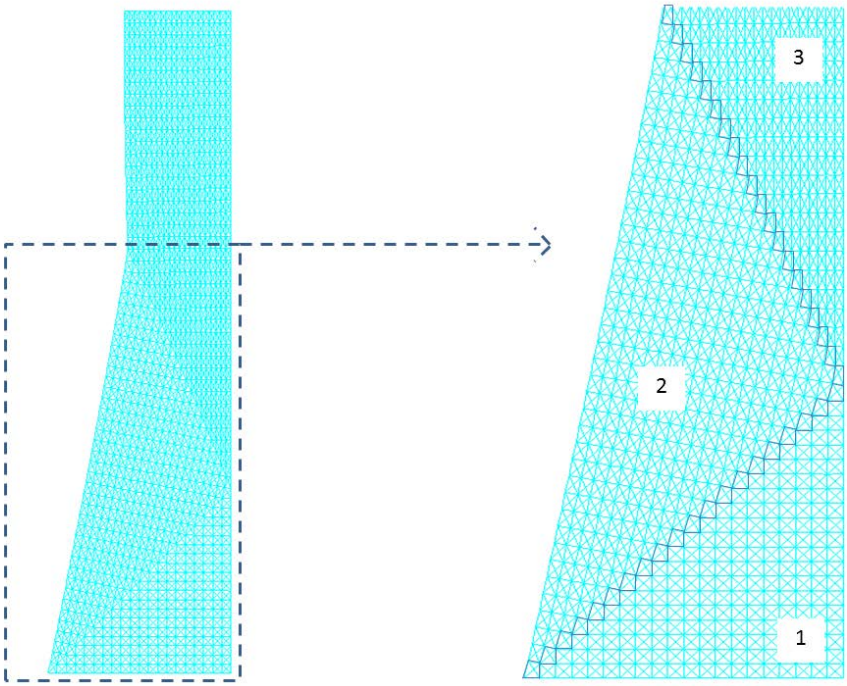

Figure 3.13: Transition deformation zones.

correct modeling of 2D woven fabrics is indeed that of considering a generalized continuum theory which allows for the description of high strain gradients concentrated in thin transition layers. The development of such continuum theory will be presented in the next section.
In summary, the TPM-2 model is able to catch the basic features of the bias extension test, but it is not able to correctly describe the thickness of shear transition layers. The geometric non-linearities included in the TPM-2 model allow us to test here the material behavior for imposed displacements up to $55\,mm$. The solutions obtained by means of the proposed finite elements are reliable and no tension locking problems are encountered.

3.4 Generalized continuum modeling of fibrous composite reinforcements

In this section we introduce and discuss the interest of using continuum models for the description of the mechanical behavior of fibrous composite reinforcements, also by comparison with the previously discussed discrete numerical simulations. Continuous approaches have been widely used in the last decades to model such class of engineering materials (see e.g.[88, 91, 4, 41, 8, 34, 25, 48]). Nevertheless, when modeling with a continuum theory materials which have strong discontinuities of the mechanical properties at the microscopic scale, then a standard Cauchy continuum theory may not be sufficient to fully describe their mechanical behavior at the homogenized scale (see [2]). This is the case for woven composite reinforcements, at least for certain cases in which particular boundary and/or loading conditions are applied to the considered specimen. Indeed, an orthotropic, first gradient, constitutive law which is able to account for the presence of privileged directions with very high tension stiffness, is not sufficient to catch all the characteristic deformation patterns which woven fabrics may experience. In order to describe the experimentally observed shear strain high gradients related to the bending of fibers at the mesoscopic level, one has to complete the orthotropic continuum model by considering a generalized, second gradient, continuum theory.
The anisotropic behavior of woven composites, due to the presence of very stiff yarns in the warp

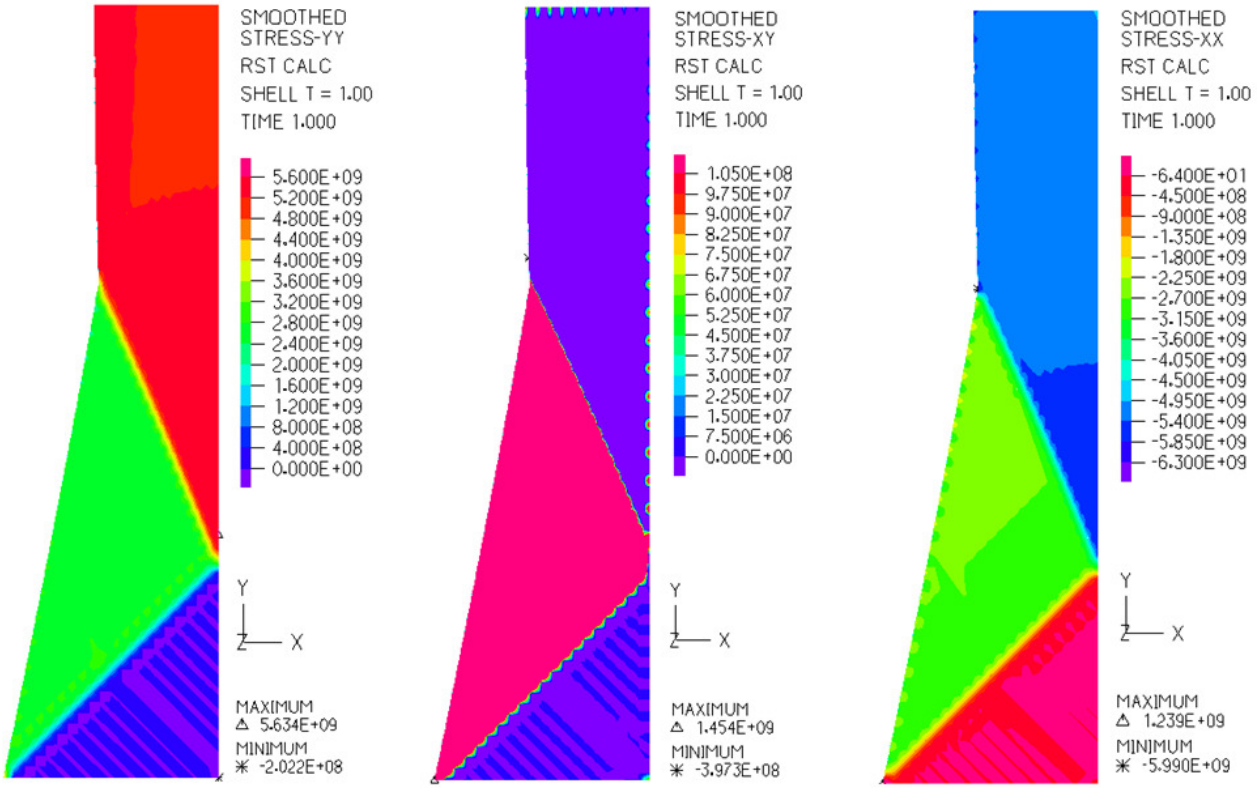

Figure 3.14: Stress components of the membrane obtained by means of the TPM-2 discretization approach: σ_{YY} (left), σ_{XY} (center), σ_{XX} (right).

and weft directions, can be modeled in a continuum framework by means of well established representation theorems (see e.g. [75, 33, 12, 14] and references there cited). These theorems state that orthotropic material behaviors can be described in a continuum framework by choosing constitutive relations which express the strain energy density as function of some invariants of the Cauchy-Green deformation tensor which also take into account the presence of particular orthotropic directions. In particular, for an in-plane 2D problem the quoted orthotropic invariants can be introduced as

$$i_4 = \mathbf{m}_1 \cdot \mathbf{C} \cdot \mathbf{m}_1, \quad i_6 = \mathbf{m}_2 \cdot \mathbf{C} \cdot \mathbf{m}_2, \quad i_8 = \mathbf{m}_1 \cdot \mathbf{C} \cdot \mathbf{m}_2, \tag{3.1}$$

where $\mathbf{m}_1$ and $\mathbf{m}_2$ are orthonormal vectors in the warp and weft directions, $\mathbf{C} = \mathbf{F}^T \cdot \mathbf{F}$ is the classical Cauchy-Green deformation tensor and $\mathbf{F} = \nabla \boldsymbol{\chi}$ is the gradient of the placement map $\boldsymbol{\chi}$. Clearly, the displacement field can be also introduced as a function of $\boldsymbol{\chi}$ as: $\mathbf{u} = \boldsymbol{\chi} - \mathbf{X}$, where $\mathbf{X}$ is the Lagrangian position of material particles in the reference configuration Ω of the body. It is worth noticing that the first two invariants i_4 and i_6 are related to changes of length in the directions $\mathbf{m}_1$ and $\mathbf{m}_2$ respectively, while the invariant i_8 is a measure of the angle variation between two yarns. Indeed, it can be checked that the total angle variation γ of two superimposed yarns with respect to the reference configuration can be directly related to the introduced invariants by means of the relation

$$\gamma = \arcsin\left(\frac{i_8}{\sqrt{i_4 i_6}}\right).$$

It is worth noticing that when one wants to consider orthotropic materials which experience plastic deformations, then an evolution of the considered anisotropy should be taken into account. This

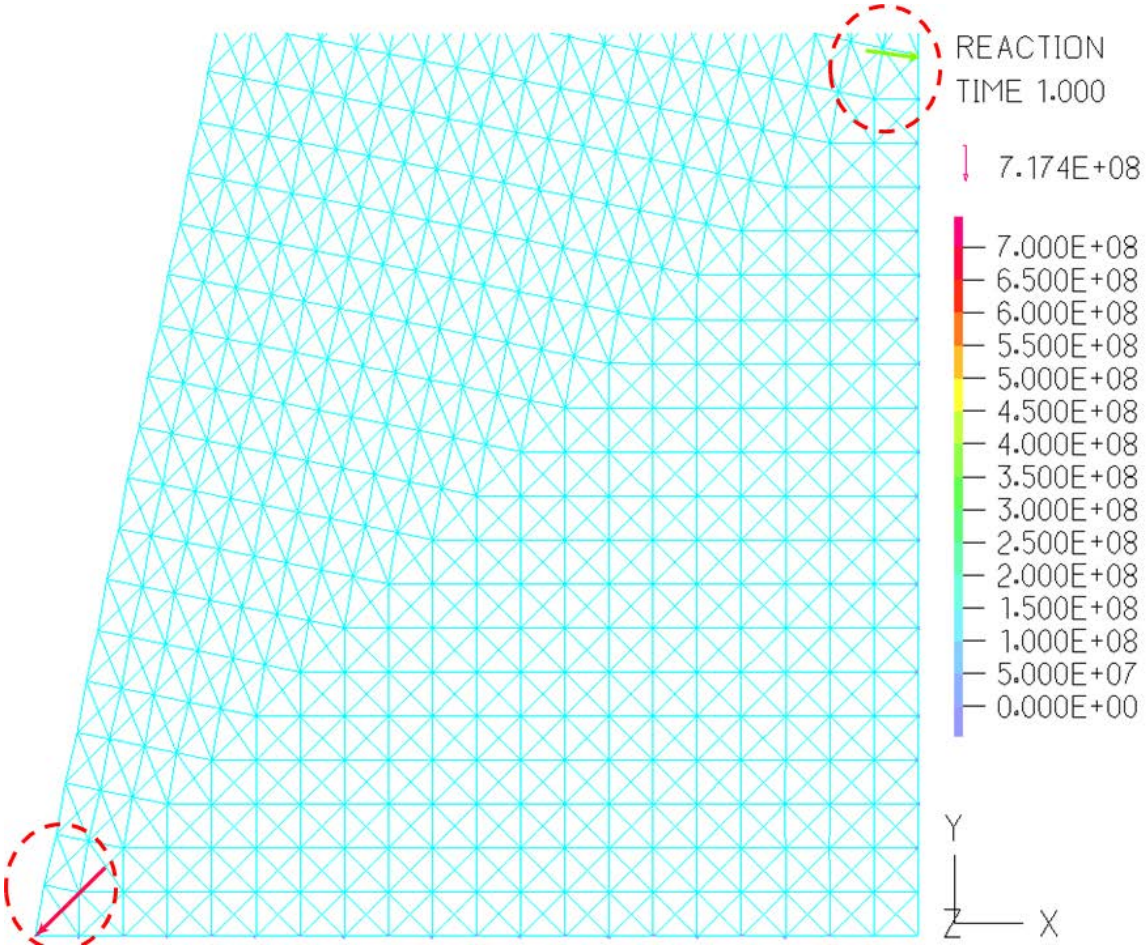

Figure 3.15: Reactions force concentration in the TPM-2 model.

would lead to the definition of a more general constitutive framework with respect to the one considered in this work (see e.g. [16]). Different 2D orthotropic materials can be modeled by choosing particular constitutive expressions of the strain energy density in terms of the three introduced invariants. Indeed, orthotropic constitutive relations are able to account for the presence of an orthotropic mesostructure in the considered continua, but they are not able to fully describe the effect of this mesostructure on the macroscopic deformation of the continuum when concentrations of stress and strain occur. For example, it has already been remarked that, when considering the bias extension test, thin transition layers exhibiting concentration of strain appear at the transition between two regions at constant shear angle. We also remarked, on the basis of the discrete models presented in the present work, that the thickness of these transition layers is directly related to the bending stiffness of the fibers. Moreover, when considering the TPM-2 element, we highlighted the fact that the size of the shear transition layer is directly related to the size of the considered mesh. On the other hand, when considering the pantographic structure, the size of the transition layer is seen to be well described and to directly depend on the bending stiffness of considered beams. In order to be able to describe the onset of shear transition layers in the framework of a continuum theory, higher gradient theories are known to be needed. On the basis of the quoted remarks and of other phenomenological considerations on the bias test, the constitutive expression of the strain energy density considered in this work is of the form

$$W = \frac{K_4}{2}\left(i_4 - 1\right)^2 + \frac{K_6}{2}\left(i_6 - 1\right)^2 + \frac{K_8}{2}\left(i_8\right)^2 + \frac{A_8}{2}\left(i_8\right)^8 + \frac{\alpha}{2}\nabla i_8 \cdot \nabla i_8. \tag{3.2}$$

The coefficients K_4 and K_6 represent the tensile rigidity in the $\mathbf{m}_1$ and $\mathbf{m}_2$ directions respectively,

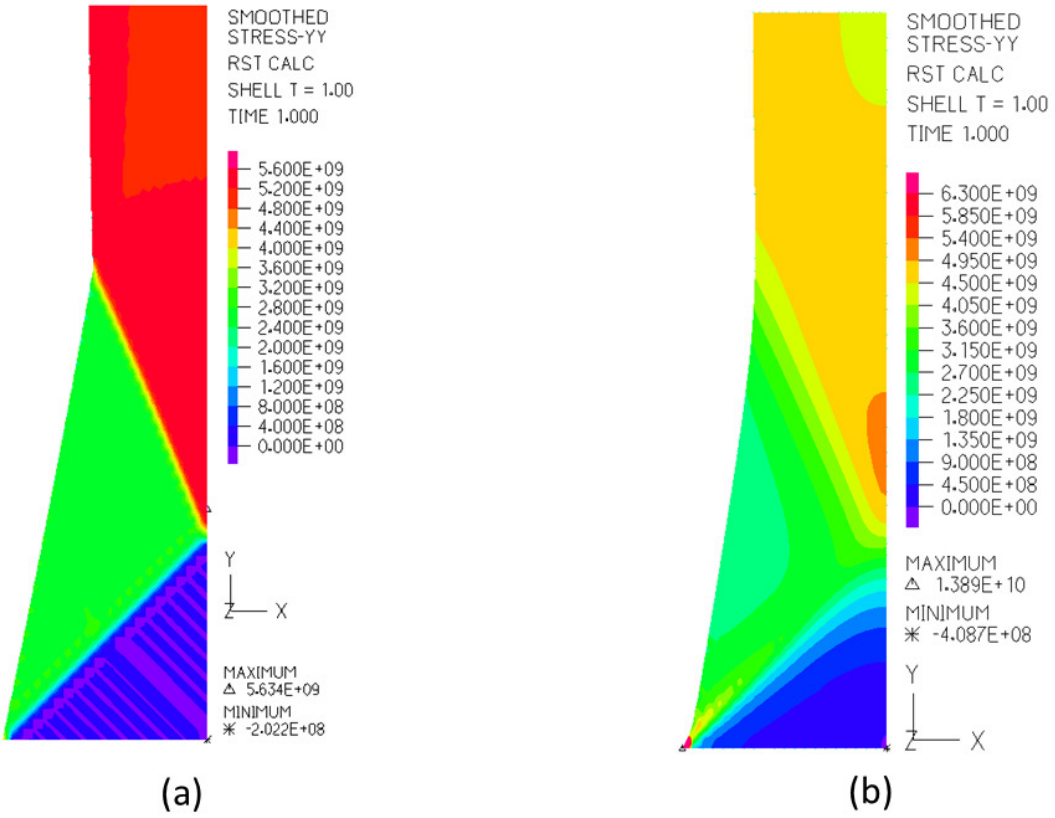

Figure 3.16: TPM-2 Model: (a) High diagonal truss stiffness; (b) Low diagonal truss stiffness.

K_8 is the shear angle variation stiffness which is valid for small strains (up to an imposed external displacement of 55 mm) and A_8 is instead the shear stiffness for the non-linear regime (external displacements higher than 55 mm). Finally, the coefficient α is the second gradient elastic coefficient which allows to account for high gradients of the shear angle variation and which is capable to describe the onset of shear transition layers.

3.4.1 Principle of virtual powers and equations in weak form

In this subsection, the least action principle needed to describe the mechanical behavior of fibrous composite reinforcements in the quasi-static regime is set up. In particular, the action functional for our generalized orthotropic continuum can be written as

$$\mathcal{A} = \int_{\Omega} W\left(i_4, i_6, i_8, \nabla i_8\right)\, d\Omega,$$

where Ω is the volume occupied by the fibrous specimen in its reference configuration and the constitutive expression for the strain energy density W is given in Eq. (3.2). It is worth noticing that considering this expression for the action functional, we are implicitly assuming that all inertial effects can be neglected and that the phenomenon that we are studying can be considered to be quasi-static. As classically done, the power of internal forces of the considered generalized continuum can be written as the first variation of the action functional as: $\mathcal{P}^{int} = \delta\mathcal{A}$. Relying on the principle of virtual powers we can hence write the governing equations for the considered fibrous system in the following weak form

$$\delta\mathcal{A} = \mathcal{P}^{ext}, \tag{3.3}$$

where $\mathcal{P}^{ext}$ is the power of external forces that, in the framework of the considered second gradient model, we choose to take the particular form

$$\mathcal{P}^{ext} = \int_{\partial\Omega} \left(\mathbf{f}^{ext} \cdot \delta\mathbf{u}\right) + \int_{\partial\Omega} \left(\tau_4 \cdot \delta i_4 + \tau_6 \cdot \delta i_6 + \tau_8 \cdot \delta i_8\right),$$

where $\delta\mathbf{u}$ is the virtual displacement field, while δi_4, δi_6 and δi_8 are the virtual variations of the three invariants introduced in Eq. (3.1). The virtual variations of these invariants can clearly be expressed in terms of the virtual variation of displacement and of its space derivatives by means of the definitions (3.1). The quantities τ_4, τ_6, and τ_8, represent the external actions expending power on the elongation of the two orders of fibers and on the shear angle variation respectively, while $\mathbf{f}^{ext}$ is the classical surface external force.

3.4.2 Numerical simulations

The numerical simulations of the continuum model presented in the previous subsection are intended to be directly implemented in the weak form (3.3) by using the code COMSOL Multiphysics. Indeed, in order to improve the stability of the numerical simulation, the second gradient simulations are implemented via the constrained micromorphic approach presented in [33] to which, to the sake of simplicity, we refer for details on the relation between second gradient and constrained micromorphic theories. Indeed, it is known that second gradient theories can be obtained as suitable limits of micromorphic theories subjected to precise kinematical restrictions (see e.g. [53, 58]).

K_4	K_6	K_8	A_8	α
$[GPa]$	$[GPa]$	$[MPa]$	$[MPa]$	$[MPa \times m^2]$
6	6	0.0428	0.18	2×10^{-5}

Table 3.3: First and second gradient constitutive parameters for the considered orthotropic continuum model.

Table 3.3 shows the values of the first and second gradient parameters appearing in Eq. (3.2) which are used in the numerical simulations proposed here. The geometry of the problem in study is of the same type as the one considered in the discrete approaches. More particularly, we consider a rectangular specimen of the same dimensions as the ones considered for the discrete numerical simulations (see Fig. 3.8). As for the boundary conditions we choose:

- vanishing displacement of the bottom surface ($\delta\mathbf{u} = \{0, 0\}$),
- imposed vertical displacement of the top surface ($\delta\mathbf{u} = \{0, 55\,mm\}$),
- vanishing angle variation at the bottom and top surfaces ($\delta i_8 = 0$),
- vanishing double-tractions at the top and bottom surfaces ($\tau_4 = 0$, $\tau_6 = 0$).

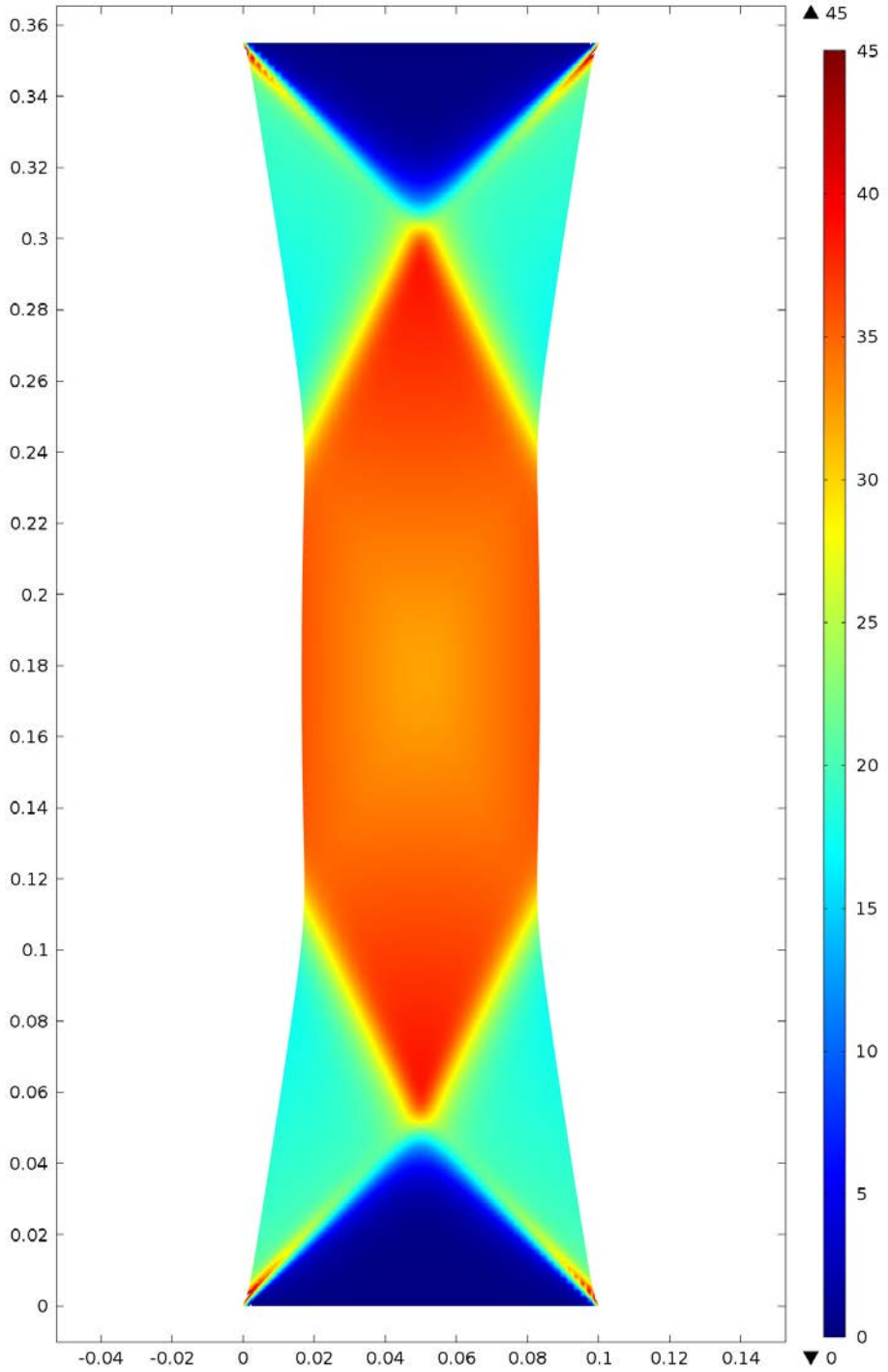

Figure 3.17: Total angle variation γ for an imposed displacement of 55 mm: first gradient theory.

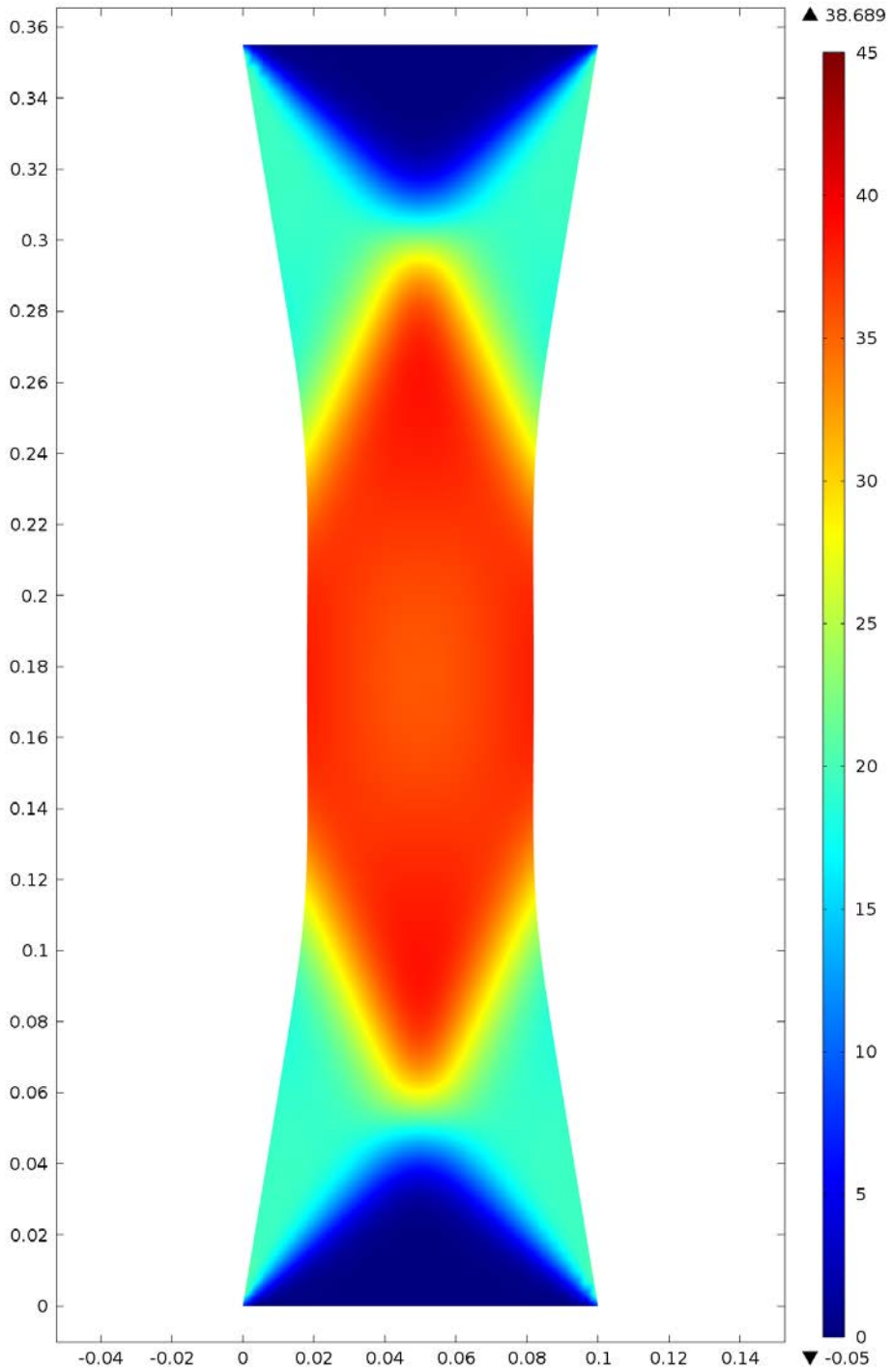

Figure 3.18: Total angle variation γ for an imposed displacement of $55\,mm$: second gradient theory.

It is worth to discuss with some more details how the aforementioned problem and, in particular, the used boundary conditions have been implemented in the numerical code. The continuum numerical simulations presented in this work have been performed via the code COMSOL Multiphysics by directly implementing the principle of virtual powers (3.3). The boundary conditions listed above have been imposed in weak form as well by means of suitable Lagrange multipliers. More precisely, instead of imposing locally that the displacement is vanishing on one side of the specimen, we impose a global integral constraint on the whole line by using a Lagrange multiplier. This approach allows us to directly obtain the value of the resultant reaction force on the basis of the specimen which

is indeed directly the value of the introduced Lagrange multiplier. This approach permits to avoid numerical errors in the post-processing phase related to line integrations of the reaction force field on the basis of the specimen.
We start showing the results for the total angle variation obtained via the first and second gradient theory. Indeed, figure 3.17 shows the total angle variation between yarns when imposing a displacement of the top surface of $55\,mm$. Figure 3.18 shows the same quantity obtained by using a second gradient theory. As already proven in [33], it can be seen that when considering the numerical simulation obtained by using a classical first gradient Cauchy theory (see Fig.3.17), the solution sensibly deviates from the experimental one, especially for what concerns the description of the shear transition layers. Indeed, as it will be better pointed out in the remainder of this section, the size of the transition layer which is obtained in the framework of a first gradient theory strongly depends on the size of the considered elements. Figure 3.18 shows the second gradient solution for the total angle variation: it can be seen that the description of the transition layer is much more accurate and the transition between two zones at constant shear angle actually takes place on smooth transition layers. Moreover, the thickness of the transition layer is seen to be mesh-independent when considering a second gradient theory. Figure 3.19 shows in detail how the thickness of the transition layers strongly depend on the size of the considered mesh in the case of the first gradient solution, while Fig. 3.20 actually shows that this mesh-dependency disappears in the case of second gradient solution when a sufficiently small mesh is considered. It is in fact clear that the characteristic size of the used mesh must be smaller of the thickness of the transition layer in order to obtain the correct solution in the transition layer region. It is for this reason that a sufficiently fine mesh is necessary also in the case of second gradient solution in order to be able to catch the correct solution of the considered problem.

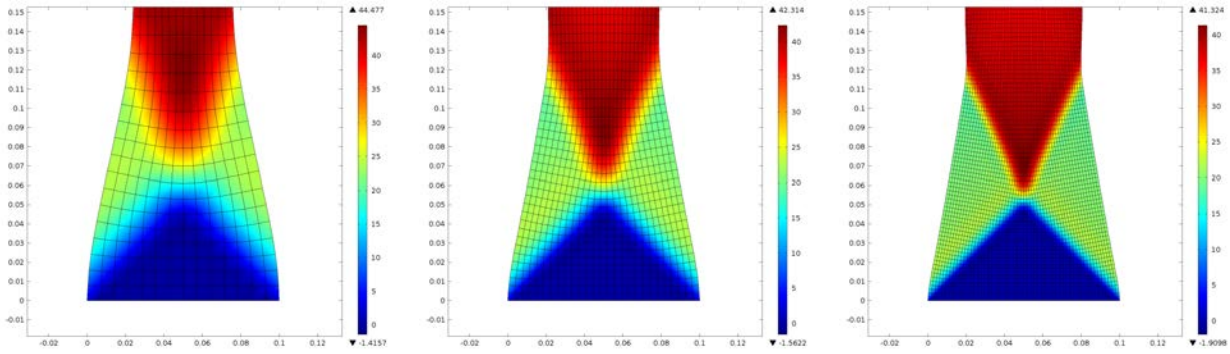

Figure 3.19: Dependency of the first gradient solution on the size of the considered mesh.

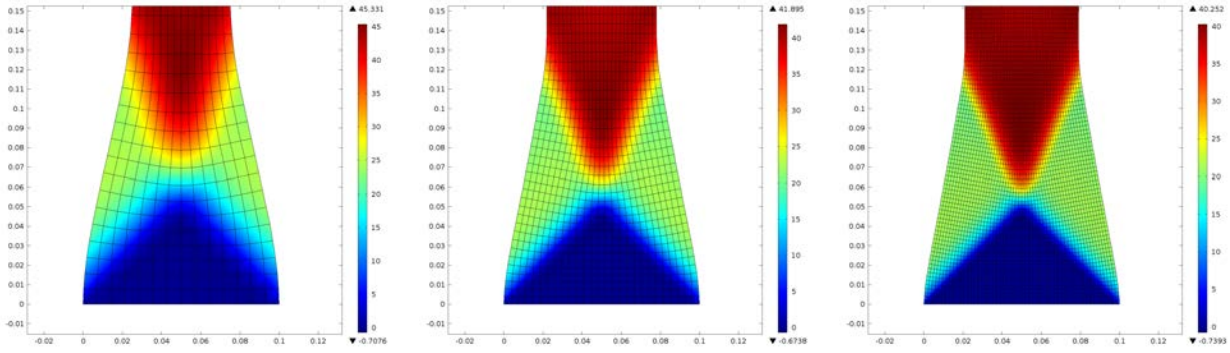

Figure 3.20: Independency of the second gradient solution on the size of the considered mesh.

More particularly, it can be remarked that, independently of the size of the considered mesh, in the

first gradient solution the thickness of the transition layer is always comparable to the size of one element of the considered mesh (as happened for the TPM-2 solution), while in the second gradient solution, as far as the mesh is small enough to catch the characteristic features of the considered phenomenon, the thickness of the transition layer keeps constant also when considering smaller and smaller meshes. This phenomenon of mesh-dependency is better underlined in figures 3.21 and 3.22 in which the solution restricted to one section passing across the transition layer is depicted for three different mesh sizes.

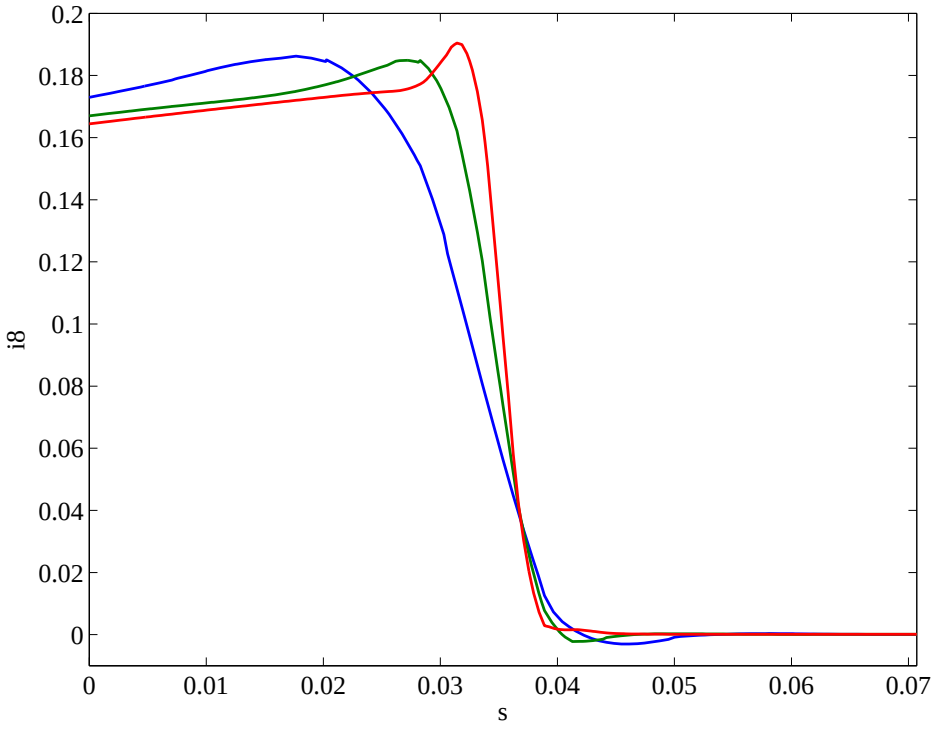

Figure 3.21: Dependency of the first gradient solution on the size of the considered mesh.

In these figures the blue line corresponds to the shear angle variation obtained by means of the coarser mesh, while the green and the red line represent the solution corresponding to the medium and the finer mesh respectively. The discussed mesh-independency related to the second gradient solution appears clearly in Fig. 3.22: indeed, the solutions obtained with the medium and finer mesh (green and red lines) are almost perfectly superimposed.

3.5 Force-displacement curves: discussion about the occurrence of tension locking and comparison of discrete and continuum models

An important physical parameter which directly allows for the comparison of the numerical simulations with the experimental tests is the evolution of the overall force on the bottom surface of the specimen as a function of the displacement imposed at the top surface. Indeed, the force calculated starting from finite element solutions based on continuum models is seen to be often subjected to what is called numerical tension locking (see e.g. [42]). In particular, the search of a numerical solution for a system which exhibits strong differences between the tension stiffness and the shear angle variation stiffness can lead to numerical errors which give rise to equilibrium configurations in which the fibers appear to be artificially stretched. This implies that the calculated values of the reaction force on the basis of the specimen appear to be of many orders of magnitude bigger than

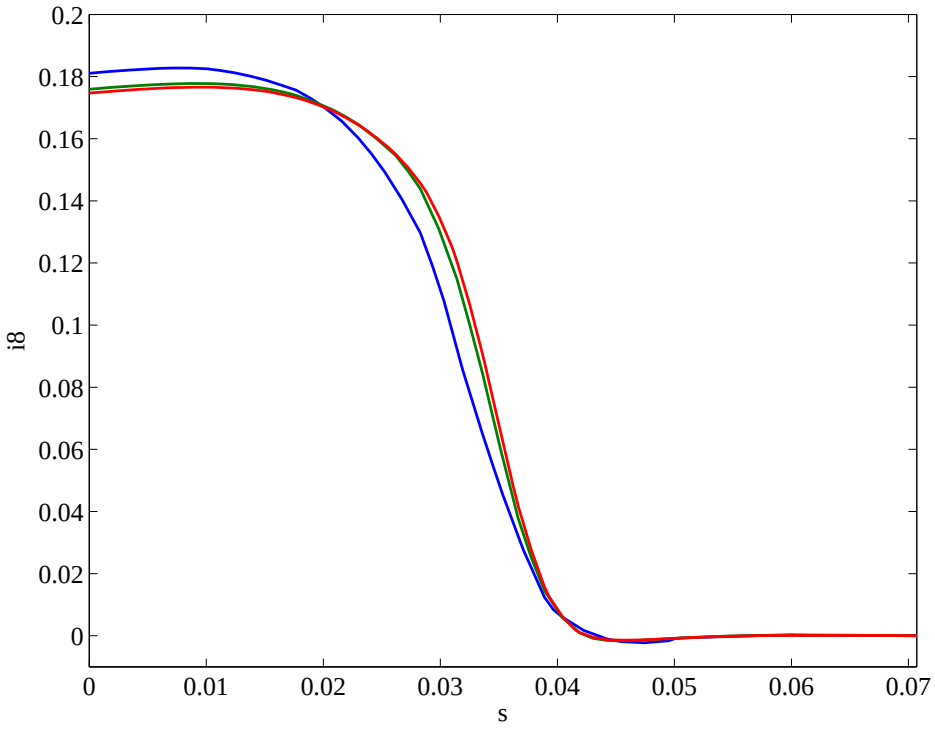

Figure 3.22: Independency of the second gradient solution on the size of the considered mesh.

the expected ones. In [42] the authors show that the phenomenon of tension locking can be avoided when using bi-linear finite elements, by means of i) meshes adapted to the directions of the fibers and ii) stabilization techniques based on reduced integration. Indeed, the phenomenon of tension locking can be also seen to be related to i) the non-linearity of the considered constitutive behavior and ii) the type and order of considered finite elements.
Figure 3.23 shows that, when considering bi-linear Lagrange square finite elements in the first gradient continuum simulation, the force-displacement curve is over-estimating of three orders of magnitude the expected values of force which is normally included between 0 and $30\,N$. When decreasing the mesh size one gets better and better approximation of the calculated force-displacement curve in spite of an increment of calculation time. On the other hand, Fig. 3.24 shows that when considering quadratic Lagrange elements the convergence to the expected solution is much quicker than in the case of linear elements.
We can summarize by saying that the fact of using continuum theories with constitutive equations of the type (3.2) in which strong contrasts of the mechanical properties at the mesoscopic level are present, may give rise to numerical errors which are known as tension locking phenomena. This is why the convergence of the calculated solution must always be checked by controlling the corresponding force-displacement curve. The continuum model proposed in the present work do not show tension locking when considering quadratic elements with a reasonably refined mesh.
Once that the convergence of the continuum solution has been checked, it can be compared with the discrete solutions.
Figure 3.25 shows the comparison of the force-displacement curve in the linear regime $(0 - 55\,mm)$ as obtained with the pantographic structure, the TPM-2 and the continuum first gradient model respectively. It can be seen that, when considering a range of small imposed displacements $(0 - 55\,mm)$, then the discrete models and the first gradient continuum one are all suitable to describe the force-displacement curve for the bias extension test. It is worth to remark that solution obtained with the pantographic lattice slightly overestimates the value of the force and that the force-displacement behavior is perfectly linear. The perfectly linear behavior of the force-displacement curve obtained

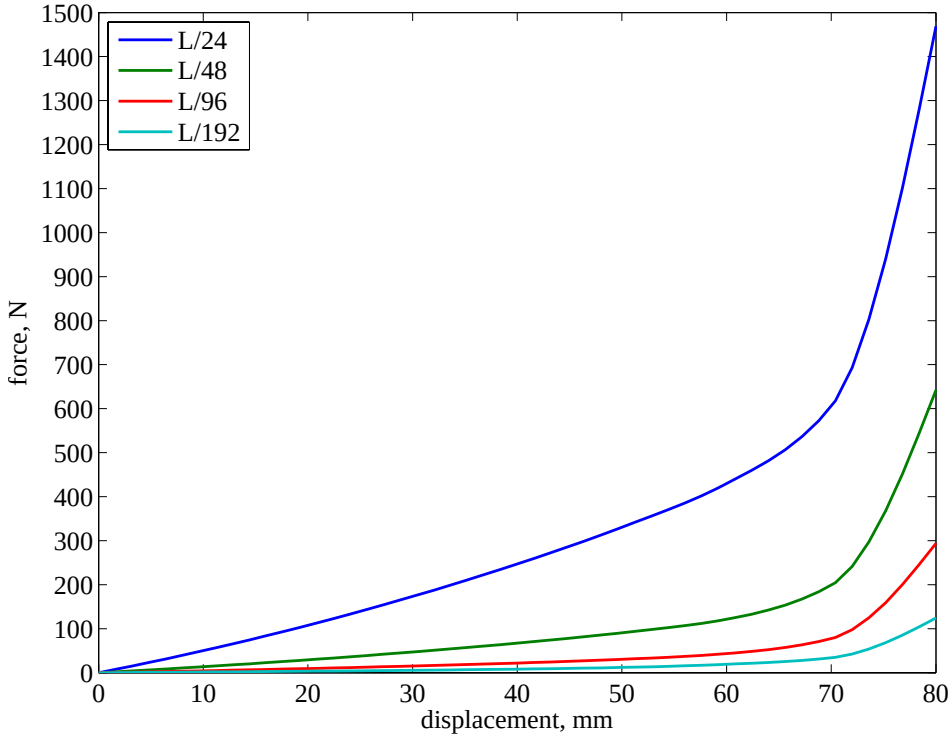

Figure 3.23: Comparison of the force-displacement curves for different mesh sizes: the case of bi-linear square finite elements.

via the pantographic lattice is related to the fact that the deformation measures of the considered Euler-Bernouilli beams are linearized. On the other hand, the solutions obtained via the TPM-2 and the continuum model show a slightly non-linear behavior which is related to the presence of geometric non-linearities. As already observed, material non-linearities have not been implemented in the pantographic lattice and in the TPM-2 models, while they are taken into account in the continuum model by means of a non-linear constitutive equation for the deformation energy density ($A_8 \neq 0$ in Eq. (3.2)). Fig.3.26 shows the comparison of the first gradient ($\alpha = 0$) continuum solution with linear and non-linear material behavior.
The value of the non-linear coefficient A_8 has been calibrated in order to fit at best the experimental force-displacement curve.
Finally, we want to highlight which is the effect of the second gradient constitutive behavior ($\alpha \neq 0$) on the force-displacement curve. To this task, we refer to Fig. 3.27

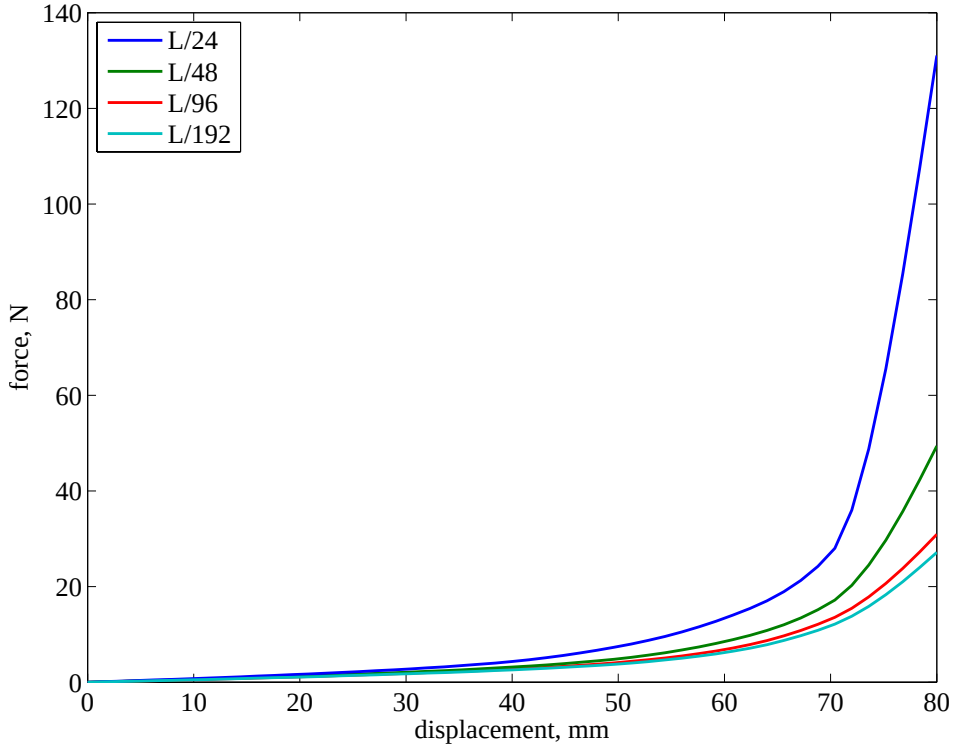

Figure 3.24: Comparison of the force-displacement curves for different mesh sizes: the case of bi-quadratic square finite elements.

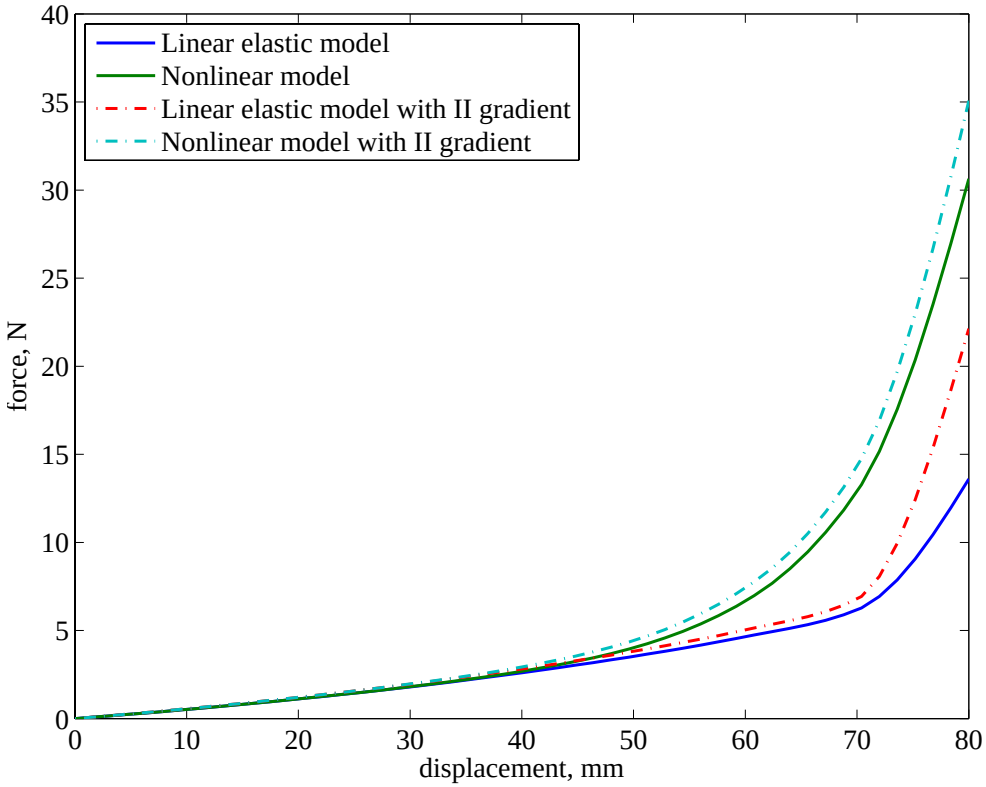

Figure 3.27: Force-displacement curves obtained via the continuum first gradient theory: linear and non-linear constitutive assumption.

in which the first and second gradient solutions are depicted both for the linear and non-linear

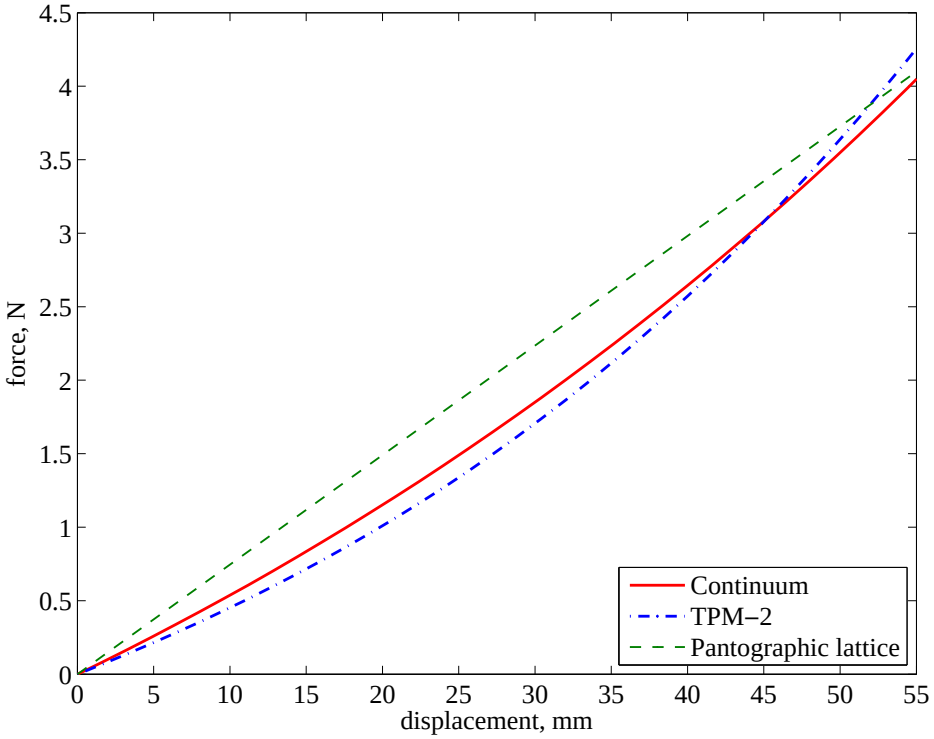

Figure 3.25: Comparison of the force-displacement curve obtained via TPM-2 elements and via the continuum first gradient theory: the case of small imposed displacements (up to $55\,mm$).

case. It can be immediately noticed that the global effect of adding a second gradient term in the constitutive equation is that of obtaining a stiffer material, at least for what concerns high imposed displacements. This stiffening effect is much more evident when considering a linear first gradient model ($A_8 = 0$) than in the non-linear case ($A_8 \neq 0$). The stiffening effect related to second gradient can be associated to the fact that the model accounts for the bending stiffness of the yarns at the mesoscopic level differently to what happens in the first gradient case.

3.6 Conclusions and Perspectives

In this work it is proven that simple physical mesostructures (which resembles closely some mesostructures used in the technology of fiber reinforced composites) can induce, in the corresponding macroscopic continuum model, a dependence of deformation energy on strain gradient (second gradient theory). The second gradient macroscopic constitutive equation for deformation energy is heuristically determined in terms of the geometry and the mechanical properties of the considered fibrous material. The results obtained in the present work urge to be rigorously framed in the context of mathematical homogenization techniques of the kind presented in [2].
On the basis of the comparison between discrete and continuum models, we conclude that one possible way to correctly describe the behavior of fibrous composite reinforcements is to use a simplified continuum macroscopic description of microscopically complex (i.e. constituted by heterogeneous parts connected following a specific geometric pattern) mechanical systems. One of the main physical feature which leads to conclude that a fibrous composite reinforcement must indeed be modeled as a second gradient continuum is represented by the strong contrast between the very high tensile stiffness of the yarns constituting the lattice and the very low shear angle variation stiffness. Indeed, the yarns of considered woven fabrics can be considered to be almost inextensible, while two superimposed yarns can easily rotate one with respect to the other. In the limit case of inextensibility the

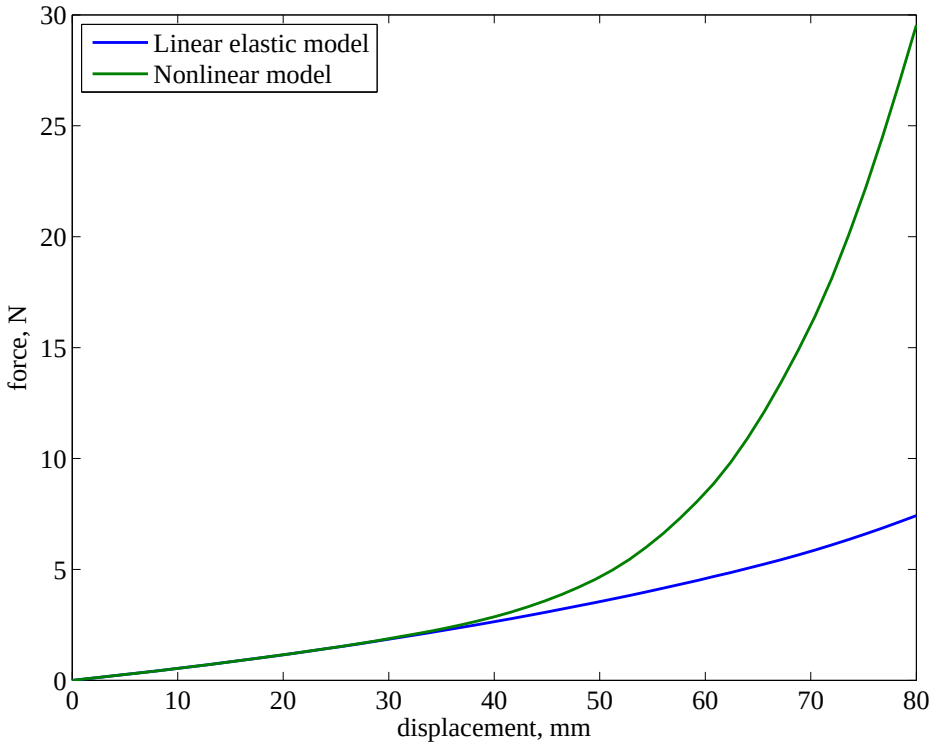

Figure 3.26: Force-displacement curves obtained via the continuum first gradient theory: linear and non-linear constitutive assumption.

introduction of suitable Lagrange multipliers (remarked already by Piola [19]) cannot be avoided. In the present work we limit ourselves to consider models in which the tensile stiffness of the yarns is much higher than the shear stiffness. The study of the limit case of inextensible networks by the introduction of Lagrange multipliers presents numerous conceptual difficulties which need to be carefully addressed. We henceforth leave the investigation of this delicate case to future work. In this work, we show how the fact of considering strong contrasts of the mechanical properties at the mesoscopic level actually leads to the conclusion that a second gradient deformation energy must be introduced at the homogenized level. We hence focus on the description of the so-called bias extension test by means of the introduced discrete and continuum models. We find out that:

- The pantographic lattice discrete model is able to account for the description of the basic features of the bias extension test on woven composites, including the description of the onset of shear transition layers. This is possible since each yarn is modeled as an unique Euler-Bernouilli beam with its own bending stiffness: the connection between different beams is realized via perfect internal pivots which do not interrupt the continuity of each yarn. The basic information provided by this discrete model is that if one wants to use a continuum model for the description of the bias extension test, then the possibility of the description of shear transition layers related to the bending stiffness of the yarns at the mesoscopic level must necessarily be taken into account. This result naturally leads to the conclusion that the thickness of the shear transition layers which are observed at the macroscopic scale is indeed directly related to the bending stiffness of the yarns at the mesoscopic scale. This fact must be accounted for when considering a continuum theory for the description of the bias extension test. In particular, following the reasonings presented in [24], higher gradients of the shear strain must be considered in order to describe the effect of bending stiffness of the yarns on the overall mechanical behavior of the material at the macroscopic level.

- The TPM-2 model is suitable to account for the basic features of the bias extension test, but it

shows some limits related to the fact that TPM-2 elements are not actually able to mimic the continuity of yarns. Indeed, the connections between two elements is made by internal pivots, but the bars constituting the rigid truss are not continuous when passing from one element to the adjacent one. This interruption of the continuity of yarns does not create particular problems for the description of the overall behavior of the bias extension test, but it forbids the correct description of the onset of shear transition layers. This limit is related to the fact that no shear angle gradients can be accounted for due to interruption of yarns' continuity. Indeed, we show that the transition from one region at constant shear angle to the adjacent one is made on one single finite element: non-local bending of fibers is not allowed in the TPM-2 model. This means that the solution is mesh-dependent for what concerns the description of the thickness of the shear transition layers. The main information provided by this discrete model is that when using finite elements, non-local material behaviors must be conceived in order to be able to describe gradual bending of the yarns on more than one element. This information can be added to the preceding ones to conclude that higher order theories are needed for the correct modeling of woven fabrics.

- Continuum models are seen to be suitable to describe in a satisfactory way the basic features of the bias extension test. First gradient models are able to catch most of the features of the considered solution, except for what concerns the correct description of transition layers. Indeed, the thickness of the transition layers predicted by means of the first gradient model strongly depend on the size of the considered mesh (the transition layer is always localized on one element as happened for the TPM-2 model). On the other hand, a second gradient continuum model is able to cure this mesh dependency and the thickness of the shear transition layer remains indeed fixed when decreasing the mesh size. The fact of introducing higher gradients of shear strain in the proposed continuum theory has been seen to be necessary on the basis of precise mesoscopic considerations. In particular the fact of considering such higher gradients of the shear strain allows to account for the bending stiffness of the yarns at the mesoscopic level.

In virtue of the aforementioned remarks, we can conclude that a second gradient continuum model is a possible framework to precisely treat the bias extension test from a theoretical and also from a numerical point of view. Nevertheless, one must be aware of the fact that when looking for finite element solutions of continuum models in which such strong contrasts of the mechanical properties exist, numerical errors related to so-called locking phenomena can be easily introduced (see e.g. [42]). As a consequence, the numerical integration schemes to be used, in order to apply the formulated model to technologically relevant problems (e.g. bias tests [44, 85], shear tests [45] or (pre)forming of reinforcements [4, 43, 6, 25, 91]) need to be able to confront the corresponding difficulties. In particular, the convergence of the solution must be carefully checked when considering highly-contrasted media, for example by checking that the obtained solution does not change when refining the mesh of the considered domain.
Further investigations will involve some immediate and interesting developments of presented analysis. These will include the study of:

- pantographic lattices constituted by inextensible fibers by using Lagrange multipliers
- pantographic lattices constituted by different kinds of fibers, having for instance different bending stiffnesses, and showing eventually material gradients of mechanical properties, so that their continuum modeling may require the introduction of inhomogeneous constitutive equations
- more general microstructures with different inextensibility directions in order to more closely aid the design of new meta-materials

- dynamics of pantographic lattices, including eventually phenomena of excitation of internal degrees of freedom
- well-posedness properties (e.g. of the kind studied in for the class of nonstandard deformation energies arising in the class of generalized continua we introduced here.

Chapter 4

2D models: reduced kinematics and geometric interpretation of first and second gradient deformation measures

In this chapter, we introduce the particular case of 2D continua and we explicitly show that in such case we can finally give a direct interpretation of the first and second gradient of the placement field in the light of differential geometry.
Moreover, we explicitly point out that, when assuming the introduced coordinate system to coincide with two preferential mutually orthogonal material directions (orthotropic media), then the components of the second gradient of the placement can be thought to have precise physical meanings associated to elementary deformation modes. When considering the particular case of inextensible fibers both the kinematics and the expression of the introduced deformation measures appear to be ulteriorly simplified. This drastic simplification allows the possibility of setting up reduced mechanical models which account for the predominant deformation mechanisms of particular orthotropic systems.

Contents

4.1 First and second gradient of 2D placement fields

In this subsection we try to give a geometrical interpretation of the components of the second gradient of the displacement field with reference to a suitable Lagrangian basis $\{\mathbf{D}_1, \mathbf{D}_2\}$ which, in general, may or may not coincide with preferential material directions. The coordinate of Lagrangian material particles in such basis will be denoted by (ζ_1, ζ_2). The following considerations are inspired by [**?**] and [76].
Let us consider a two-dimensional material body $\mathscr{B}$. As usually done, we will keep the hypothesis that the physical space $\mathscr{S}$ is a two-dimensional Euclidean space.
Hereafter, we will consider that the placement $\mathbf{r} : \mathscr{B}^\star \to \mathbb{R}^2$ is a $\mathscr{C}^2$ diffeomorphism mapping the Lagrangian configuration in the current one. Our primary objective is here to give a geometrical interpretation of the second gradient (the hessian) of the map $\mathbf{r}$ and then prove the Rivlin decomposition under the assumption of inextensibility. Denoting $\{\mathbf{D}_1, \mathbf{D}_2\}$ a Lagrangian orthonormal basis, the vector valued map $\mathbf{r}$can be decomposed as

$$\mathbf{r}(\zeta_1, \zeta_2) = r_1(\zeta_1, \zeta_2)\,\mathbf{D}_1 + r_2(\zeta_1, \zeta_2)\,\mathbf{D}_2,$$

where r_1 and r_2 are the components of $\mathbf{r}$ in the considered basis. With such notations, we can write the matrix representation of the first gradient of placement as

$$\mathbf{F} = \nabla\mathbf{r} = \begin{bmatrix} \nabla r_1(\zeta_1, \zeta_2) \\ \\ \nabla r_2(\zeta_1, \zeta_2) \end{bmatrix} = \begin{bmatrix} \dfrac{\partial r_1}{\partial \zeta_1} & \dfrac{\partial r_1}{\partial \zeta_2} \\ \\ \dfrac{\partial r_2}{\partial \zeta_1} & \dfrac{\partial r_2}{\partial \zeta_2} \end{bmatrix} = \begin{bmatrix} r_{1,1} & r_{1,2} \\ r_{2,1} & r_{2,2} \end{bmatrix} = \begin{bmatrix} \mathbf{d}_1 & \mathbf{d}_2 \end{bmatrix},$$

where we simultaneously introduce different notations for the partial derivatives which will be equivalently used in the following.
It can be checked that the compact tensorial expression for the first gradient of placement takes the form

$$\nabla\mathbf{r}(\zeta_1, \zeta_2) = \mathbf{d}_1 \otimes \mathbf{D}_1 + \mathbf{d}_2 \otimes \mathbf{D}_2,$$

where

$$\mathbf{d}_1 = \frac{\partial \mathbf{r}}{\partial \zeta_1} = \mathbf{F} \cdot \mathbf{D_1} \qquad \text{and} \qquad \mathbf{d}_2 = \frac{\partial \mathbf{r}}{\partial \zeta_2} = \mathbf{F} \cdot \mathbf{D_2}. \tag{4.1}$$

At this point, we want to create a sort of grid on our body in order to be able to follow its deformation and to assign to the components of the second gradient of displacement particular geometrical meanings. To do so, we consider, for the sake of simplicity, the case in which the body is a convex set, so that a simple representative grid can be defined introducing the coordinate lines as (see also fig 4.1)

$$\begin{cases} l_{\bar{\zeta}_1} := \left\{(\zeta_1, \zeta_2) \in \mathscr{B}^\star : \zeta_1 = \bar{\zeta}_1\right\} \\ \\ l_{\bar{\zeta}_2} := \left\{(\zeta_1, \zeta_2) \in \mathscr{B}^\star : \zeta_2 = \bar{\zeta}_2\right\}. \end{cases}$$

It can be remarked that, in general, due to the shape of the body, the projections of the coordinate lines on the two axes, vary when varying the considered coordinate line. When considering a vertical coordinate line $l_{\bar{\zeta}_1}$, we will denote by $\mathfrak{D}_{\bar{\zeta}_1}$ its projection on the ζ_2 axis and, analogously, fixed a horizontal coordinate line $l_{\bar{\zeta}_2}$, by $\mathfrak{D}_{\bar{\zeta}_2}$ its projection on the ζ_1 axis.
We set the block matrix representation of the hessian to take the form:

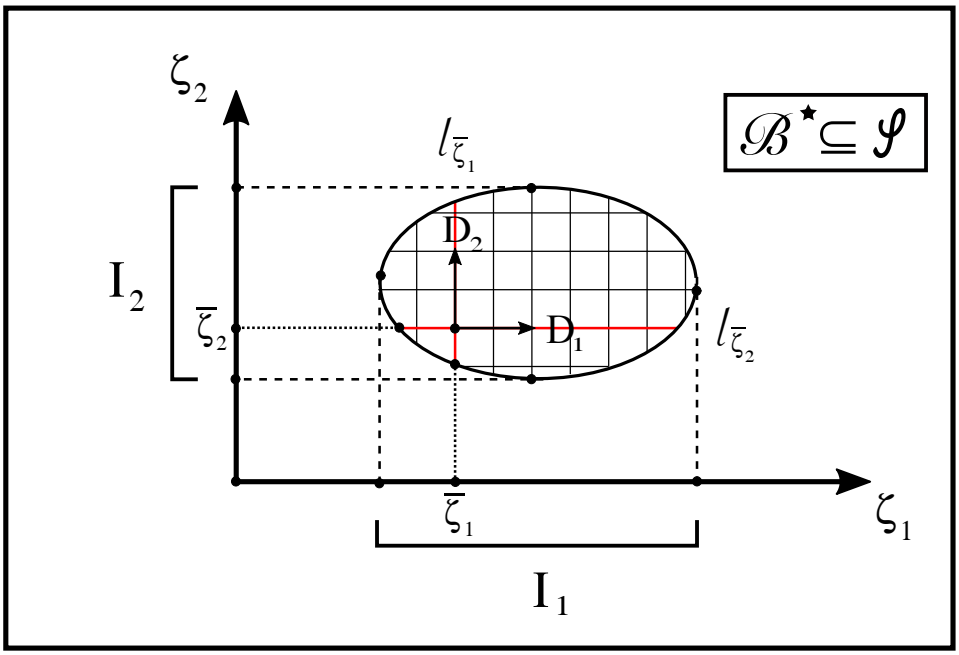

Figure 4.1: Images of coordinates lines, tangent vectors and projections

$$\nabla^2\mathbf{r}\left(\zeta_1,\zeta_2\right)=\begin{bmatrix}\nabla^2 r_1\left(\zeta_1,\zeta_2\right)\\ \\ \nabla^2 r_2\left(\zeta_1,\zeta_2\right)\end{bmatrix}=\begin{bmatrix}\begin{bmatrix}\dfrac{\partial^2 r_1}{\partial\zeta_1^2} & \dfrac{\partial^2 r_1}{\partial\zeta_2\partial\zeta_1}\\ \\ \dfrac{\partial^2 r_1}{\partial\zeta_1\partial\zeta_2} & \dfrac{\partial^2 r_1}{\partial\zeta_2^2}\end{bmatrix}\\ \\ \begin{bmatrix}\dfrac{\partial^2 r_2}{\partial\zeta_1^2} & \dfrac{\partial^2 r_2}{\partial\zeta_2\partial\zeta_1}\\ \\ \dfrac{\partial^2 r_2}{\partial\zeta_1\partial\zeta_2} & \dfrac{\partial^2 r_2}{\partial\zeta_2^2}\end{bmatrix}\end{bmatrix}=\begin{bmatrix}\begin{bmatrix}r_{1,11} & r_{1,21}\\ \\ r_{1,12} & r_{1,22}\end{bmatrix}\\ \\ \begin{bmatrix}r_{2,11} & r_{2,21}\\ \\ r_{2,12} & r_{2,22}\end{bmatrix}\end{bmatrix}, \tag{4.2}$$

while its tensorial expression can be recognized to take the form

$$\nabla^2\mathbf{r}=\mathbf{g}_1\otimes\mathbf{D}_1\otimes\mathbf{D}_1+\mathbf{g}_2\otimes\mathbf{D}_2\otimes\mathbf{D}_2+\boldsymbol{\Gamma}\otimes\left(\mathbf{D}_1\otimes\mathbf{D}_2+\mathbf{D}_2\otimes\mathbf{D}_1\right), \tag{4.3}$$

where we set[1]

$$\mathbf{g}_1=\left(\frac{\partial^2 r_1}{\partial\zeta_1^2},\frac{\partial^2 r_2}{\partial\zeta_1^2}\right),\qquad \mathbf{g}_2=\left(\frac{\partial^2 r_1}{\partial\zeta_2^2},\frac{\partial^2 r_2}{\partial\zeta_2^2}\right),\qquad \boldsymbol{\Gamma}=\left(\frac{\partial^2 r_1}{\partial\zeta_1\partial\zeta_2},\frac{\partial^2 r_2}{\partial\zeta_1\partial\zeta_2}\right). \tag{4.4}$$

Now, we will explicitly proceed towards the geometric interpretation of the three vectors $\mathbf{g}_1,\mathbf{g}_2,\boldsymbol{\Gamma}$ appearing in Eq. (4.3). To do so, we indicate with π_1 and π_2 the two projections of $\mathscr{B}^\star$ on the coordinate axes and with I_1 and I_2 the image of these projections (see also Fig. 4.1), i.e.

$$I_1:=\pi_1\left(\mathscr{B}^\star\right)\qquad\text{and}\qquad I_2:=\pi_2\left(\mathscr{B}^\star\right).$$

The pure geometrical meaning of the gradient and second gradient of the placement field may allow us to describe how the coordinates lines are deformed.

[1]Remember that for the Schwartz theorem, being $\mathbf{r}$ $\mathscr{C}^2$ regular, we have $r_{1,21}=r_{1,12}$ and $r_{2,21}=r_{2,12}$

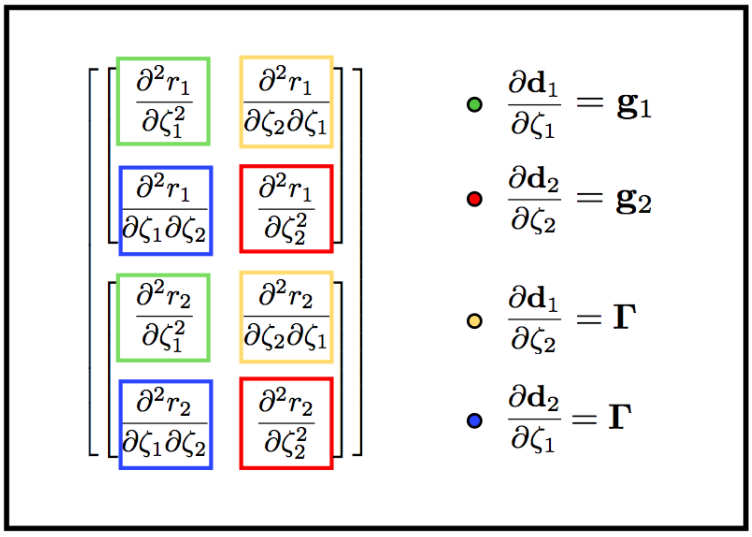

Figure 4.2: Hessian components and directional derivatives of tangent vectors to the images of coordinates lines

Given the two parametric families of coordinate curves $\left\{l_{\bar{\zeta}_1}\right\}_{\bar{\zeta}_1 \in I_1}$ and $\left\{l_{\bar{\zeta}_2}\right\}_{\bar{\zeta}_2 \in I_2}$ relative to our grid, we can introduce for each coordinate curve $l_{\bar{\zeta}_\alpha}$ its image ϕ under the introduced displacement field as

$$\begin{cases} \boldsymbol{\phi}_{\bar{\zeta}_1}(\zeta_2) = \mathbf{r}|_{l_{\bar{\zeta}_1}} & \forall \bar{\zeta}_1 \in I_1, \text{ with } \zeta_2 \in \mathfrak{D}_{\bar{\zeta}_1} \\ \boldsymbol{\phi}_{\bar{\zeta}_2}(\zeta_1) = \mathbf{r}|_{l_{\bar{\zeta}_2}} & \forall \bar{\zeta}_2 \in I_2 \text{ with } \zeta_1 \in \mathfrak{D}_{\bar{\zeta}_2} \end{cases}$$

for their images. According to definitions (4.1), it can be checked that

$$\mathbf{d}_1\left(\mathbf{r}\left(\zeta_1, \bar{\zeta}_2\right)\right) = \left.\frac{d\boldsymbol{\phi}_{\bar{\zeta}_2}}{d\zeta_1}\right|_{\mathbf{r}(\zeta_1, \bar{\zeta}_2)} \quad \text{and} \quad \mathbf{d}_2\left(\mathbf{r}\left(\bar{\zeta}_1, \zeta_2\right)\right) = \left.\frac{d\boldsymbol{\phi}_{\bar{\zeta}_1}}{d\zeta_2}\right|_{\mathbf{r}(\bar{\zeta}_1, \zeta_2)}.$$

In this way we can see that $\mathbf{d}_1$ and $\mathbf{d}_2$ can be seen to be tangent (generally non-unitary) vectors to the images of coordinate lines.

4.1.1 2D deformation measures

In order to give a geometric interpretation of the components of the second gradient of the placement field $\mathbf{r}$ given in (4.2), we first define the two unit vectors associated to $\mathbf{d}_1$ and $\mathbf{d}_2$ as

$$\boldsymbol{\tau}_1 = \frac{\mathbf{d}_1}{\lambda_1} \quad \text{and} \quad \boldsymbol{\tau}_2 = \frac{\mathbf{d}_2}{\lambda_2}, \tag{4.5}$$

where we set

$$\lambda_1 := \|\mathbf{d}_1\| \quad \text{and} \quad \lambda_2 := \|\mathbf{d}_2\|.$$

We can also define the four following angles:

$$\vartheta_1 := \arccos\langle \boldsymbol{\tau}_1, \mathbf{D}_1 \rangle, \qquad \vartheta_2 := \arccos\langle \boldsymbol{\tau}_2, \mathbf{D}_1 \rangle, \qquad \gamma = \frac{\pi}{2} - (\vartheta_2 - \vartheta_1), \qquad \vartheta = \frac{\pi}{2} - \gamma, \tag{4.6}$$

shown in figure (4.1.1). The fact of introducing such supplementary kinematical descriptors may be useful if one wants to interpret the results which we are going to present in the case in which

the coordinate lines coincides with preferred material directions inside an orthotropic medium. In particular, in the case of fibrous composite reinforcements such angles can be visualized as

- angle variations between fibers (for what concerns ϑ),
- angle variations from the reference configuration of the fibers to the current one (for what concerns γ).

In what follows, we will introduce all relevant quantities both in terms of the Eulerian vectors $\mathbf{d}_1$ and $\mathbf{d}_2$, and of the total angle variation γ in order to have the possibility of better interpret them when the particular case of orthotropic materials will be considered.

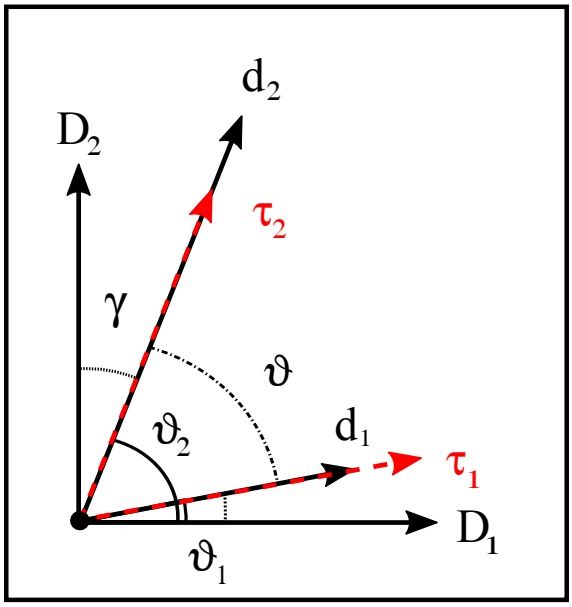

Figure 4.3: Defined angles

It can be checked that, introducing the quantity $S := \langle \mathbf{d}_1, \mathbf{d}_2 \rangle = \lambda_1 \lambda_2 \langle \boldsymbol{\tau}_1, \boldsymbol{\tau}_2 \rangle = \lambda_1 \lambda_2 \sin\gamma$, the Cauchy-Green deformation tensor associated to $\mathbf{r}$ can be written as

$$\mathbf{C} = \mathbf{F}^t \cdot \mathbf{F} = \lambda_1 \mathbf{D}_1 \otimes \mathbf{D}_1 + \lambda_2 \mathbf{D}_2 \otimes \mathbf{D}_2 + S\left(\mathbf{D}_1 \otimes \mathbf{D}_2 + \mathbf{D}_2 \otimes \mathbf{D}_1\right). \tag{4.7}$$

Now we can give a geometric interpretation of the components of the hessian.
A direct calculation shows that, recalling Eqs. (4.1), (4.4) and (4.5), the following identities hold

$$\begin{cases} \mathbf{g}_1\left(\zeta_1, \bar{\zeta}_2\right) = \dfrac{d}{d\zeta_1}\, \mathbf{d}_1|_{l_{\bar{\zeta}_2}} = \dfrac{d}{d\zeta_1}\left(\lambda_1 \boldsymbol{\tau}_1\right) = \dfrac{d\lambda_1}{d\zeta_1}\boldsymbol{\tau}_1 + \lambda_1 \dfrac{d\boldsymbol{\tau}_1}{d\zeta_1}, \\ \mathbf{g}_2\left(\bar{\zeta}_1, \zeta_2\right) = \dfrac{d}{d\zeta_2}\, \mathbf{d}_2|_{l_{\bar{\zeta}_1}} = \dfrac{d}{d\zeta_2}\left(\lambda_2 \boldsymbol{\tau}_2\right) = \dfrac{d\lambda_2}{d\zeta_2}\boldsymbol{\tau}_2 + \lambda_2 \dfrac{d\boldsymbol{\tau}_2}{d\zeta_2}. \end{cases}$$

Setting

$$b_\alpha = \left\| \frac{d\boldsymbol{\tau}_\alpha}{d\zeta_\alpha} \right\| \qquad \text{for} \qquad \alpha = 1, 2,$$

and being $\boldsymbol{\tau}_\alpha$ unitary, we have that $\boldsymbol{\tau}_\alpha \perp \frac{d\boldsymbol{\tau}_\alpha}{d\zeta_\alpha}$, so that introducing a unit vector $\boldsymbol{\nu}$ orthogonal to $\boldsymbol{\tau}$[2] we can finally write

[2] oriented in such a way that $\{\boldsymbol{\tau}, \boldsymbol{\nu}\}$ is obtained as a simple rotation of $\{\mathbf{D}_1, \mathbf{D}_2\}$

$$\frac{d\boldsymbol{\tau}_\alpha}{d\zeta_\alpha} = b_\alpha \boldsymbol{\nu}_\alpha \qquad \text{for} \qquad \alpha = 1, 2. \tag{4.8}$$

With these notations, we can finally express the two vectors $\mathbf{g}_1$ and $\mathbf{g}_2$ as

$$\mathbf{g}_\alpha = \lambda_{\alpha,\zeta_\alpha} \boldsymbol{\tau}_\alpha + \lambda_\alpha b_\alpha \boldsymbol{\nu}_\alpha, \tag{4.9}$$

that give a complete representation of the vectors $\mathbf{g}_1$ and $\mathbf{g}_2$ in the adapted (Eulerian) local basis $\{\boldsymbol{\tau}, \boldsymbol{\nu}\}$. The fact of rewriting the vectors $\mathbf{g}_1$ and $\mathbf{g}_2$ in this adapted basis is useful for catching the geometrical meaning of the quoted vectors. Indeed, the vectors $\mathbf{g}_\alpha$ account for a tangent component which contains informations about variations of elongations along the coordinate line (term $\lambda_{\alpha,\zeta_\alpha}$) and of a normal component which accounts for the the product of the elongation and bending strain (term $\lambda_\alpha b_\alpha$). We explicitly remark that in the particular case of inextensible coordinate lines (i.e. $\lambda_\alpha \equiv 1$), the vectors $\mathbf{g}_\alpha$ have only a normal component and the only intervening deformation mechanism is that of bending.
In an analogous way, we want to represent the vector $\boldsymbol{\Gamma}$ in such adapted basis, so that we start by noticing that by definition (4.4)

$$\boldsymbol{\Gamma} = \mathbf{d}_{1,2} = \mathbf{d}_{2,1}. \tag{4.10}$$

Being the two vector fields $\boldsymbol{\tau}_\alpha(\zeta_1, \zeta_2)$ unitary for every $(\zeta_1, \zeta_2) \in \mathscr{B}^\star$, we have also that

$$\boldsymbol{\tau}_{1,2} \perp \boldsymbol{\tau}_1, \qquad \text{and} \qquad \boldsymbol{\tau}_{2,1} \perp \boldsymbol{\tau}_2.$$

So, according to Eq. (4.5) we finally find that

$$\begin{aligned} \boldsymbol{\Gamma} &= \mathbf{d}_{1,2} = \lambda_{1,2}\boldsymbol{\tau}_1 + \lambda_1 \boldsymbol{\tau}_{1,2} = \lambda_{1,2}\boldsymbol{\tau}_1 + \lambda_1 \|\boldsymbol{\tau}_{1,2}\| \boldsymbol{\nu}_1 \\ &= \mathbf{d}_{2,1} = \lambda_{2,1}\boldsymbol{\tau}_2 + \lambda_2 \boldsymbol{\tau}_{2,1} = \lambda_{2,1}\boldsymbol{\tau}_2 + \lambda_2 \|\boldsymbol{\tau}_{2,1}\| \boldsymbol{\nu}_2. \end{aligned} \tag{4.11}$$

It is worth to remark that such decomposition of the vector $\boldsymbol{\Gamma}$ contains informations about the variation of elongation of a family of coordinate lines when moving on a coordinate line of the other family (term $\lambda_{1,2}$) and about the relative motion of two adjacent coordinate lines of the same family when moving on a coordinate line of the other one (see Fig. (4.4)).

Having identified the vectors $\mathbf{g}_\alpha$ and $\boldsymbol{\Gamma}$ in the local adapted basis, we have obtained a complete geometrical description of the second gradient of placement given in Eq. (4.3). Such second gradient of placement is a third order tensor field which is easily seen to contain informations about the deformation mechanisms of both families of coordinate lines. It is worth to introduce two new quantities which instead isolate informations concerning the two families of coordinate lines separately. To do so, we apply the tensor $\nabla^2\mathbf{r}$ to the vectors $\mathbf{D}_1$ and $\mathbf{D}_2$ so obtaining

$$\nabla^2\mathbf{r} \cdot \mathbf{D}_1 = \mathbf{g}_1 \otimes \mathbf{D}_1 + \boldsymbol{\Gamma} \otimes \mathbf{D}_2 \qquad \text{and} \qquad \nabla^2\mathbf{r} \cdot \mathbf{D}_2 = \mathbf{g}_2 \otimes \mathbf{D}_2 + \boldsymbol{\Gamma} \otimes \mathbf{D}_1.$$

4.1.2 Expression of the bending strain in terms of the geometric curvature

We have introduced in the previous subsection the bending strain $b_\alpha = \|d\boldsymbol{\tau}_\alpha / d\zeta_\alpha\|$ which can be seen to account for variations of the direction of the unitary tangent vector $\boldsymbol{\tau}_\alpha$ along the considered coordinate line. Hence, such quantity b_α is clearly related to a deformation mechanism which accounts for the fact that the coordinate line is curving. Nevertheless, the quantity which is classically introduced in differential geometry to account for such deformation mechanism is not b_α, but the curvature k_α, so that it appears useful to identify the relation between our bending strain and the classical curvature.

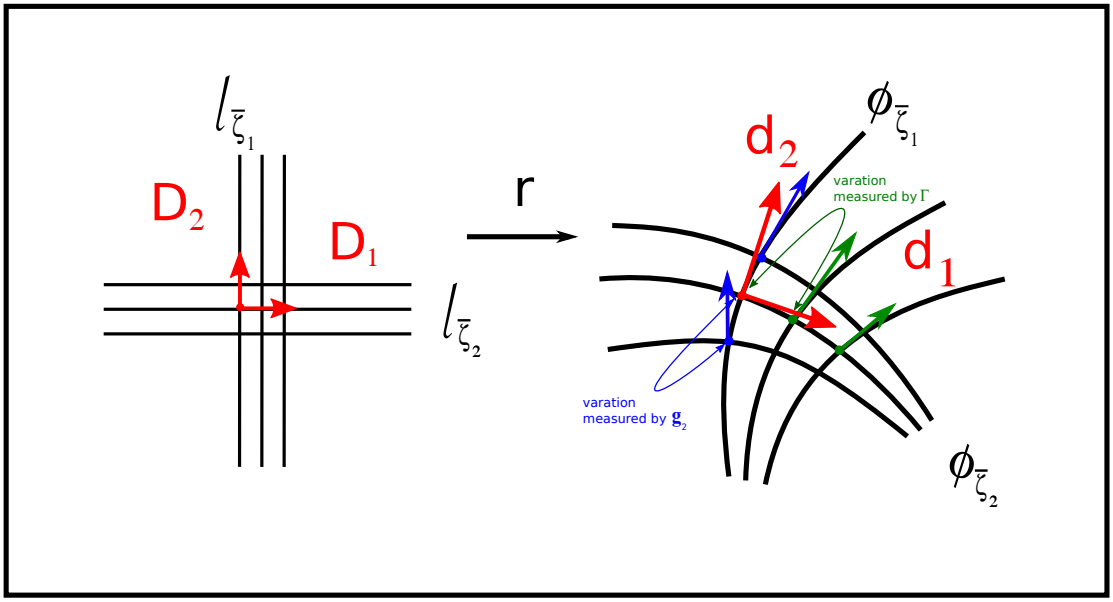

Figure 4.4: Geometrical interpretation of the introduced deformation measures.

Indeed, if we denote by $s$the arc length parameter of the considered curve, then we can write we have that

$$\frac{d\boldsymbol{\tau}_\alpha}{d\zeta_\alpha} = \frac{d\boldsymbol{\tau}_\alpha}{ds}\frac{ds}{d\zeta_\alpha} \qquad \text{for} \qquad \alpha = 1,2$$

and so

$$\underbrace{\left\|\frac{d\boldsymbol{\tau}_\alpha}{d\zeta_\alpha}\right\|}_{b_\alpha} = \underbrace{\left\|\frac{d\boldsymbol{\tau}_\alpha}{ds}\right\|}_{k_\alpha}\underbrace{\left|\frac{ds}{d\zeta_\alpha}\right|}_{\|\mathbf{d}_\alpha\|=\lambda_\alpha} \qquad \text{for} \qquad \alpha = 1,2$$

from which we finally recognize

$$b_\alpha = \lambda_\alpha k_\alpha \qquad \text{for} \qquad \alpha = 1,2.$$

Remark 35.

4.1.3 Deformation measures in terms of the angles variations

In this subsection we rewrite the previously introduced first and second gradient deformation measures in terms of the angles γ and ϑ
introduced in Eq. (4.6).
Since $\boldsymbol{\tau}_\alpha \perp \boldsymbol{\nu}_\alpha$ for all $(\zeta_1, \zeta_2) \in \mathscr{B}^\star$, then there exist two matrix rotation fields $\mathbf{R}_\alpha : \mathscr{B}^\star \to SO_2(\mathbb{R})$ such that

$$\mathbf{R}_\alpha \cdot \mathbf{D}_1 = \boldsymbol{\tau}_\alpha \qquad \text{and} \qquad \mathbf{R}_\alpha \cdot \mathbf{D}_2 = \boldsymbol{\nu}_\alpha,$$

and so two functions (introduced in (4.6)) $\vartheta_\alpha : \mathscr{B}^\star \to (-2\pi, 2\pi)$ such that (see also Fig. (4.5) and Eqs. (4.6))

$$\boldsymbol{\tau}_\alpha = \cos\vartheta_\alpha \mathbf{D}_1 + \sin\vartheta_\alpha \mathbf{D}_2, \qquad \boldsymbol{\nu}_\alpha = -\sin\vartheta_\alpha \mathbf{D}_1 + \cos\vartheta_\alpha \mathbf{D}_2. \tag{4.12}$$

Differentiating $\boldsymbol{\tau}_\alpha$ with respect to ζ_α one has

$$\boldsymbol{\tau}_{\alpha,\alpha} = \vartheta_{\alpha,\alpha}\left(-\sin\vartheta_\alpha \mathbf{D}_1 + \cos\vartheta_\alpha \mathbf{D}_2\right) = \vartheta_{\alpha,\alpha}\boldsymbol{\nu}_\alpha \qquad \text{for} \qquad \alpha = 1,2,$$

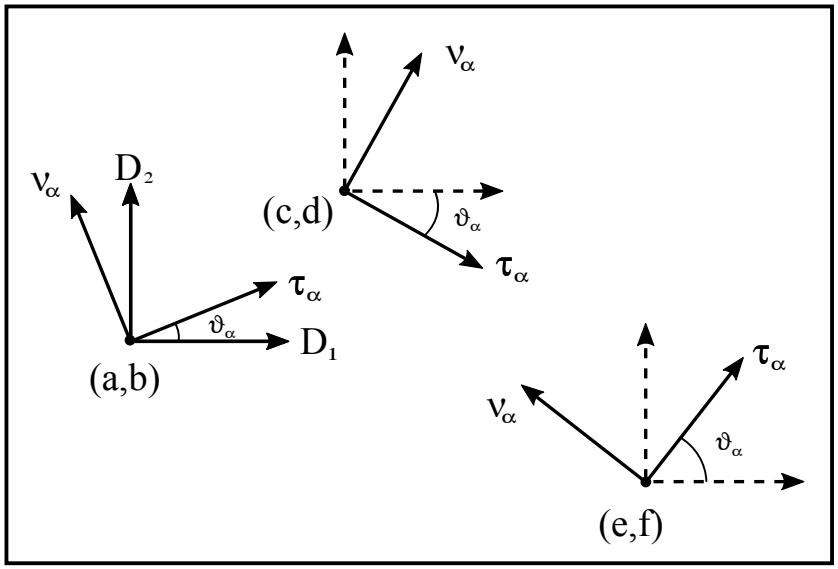

Figure 4.5: Representation of functions ϑ_α at different point of coordinates $(a,b)\,,(c,d)\,,(e,f)$ of $\mathscr{B}^\star$

which, recalling Eq. (4.8) implies

$$\vartheta_{\alpha,\alpha} = b_\alpha \tag{4.13}$$

On the other hand, differentiating $\boldsymbol{\tau}_1$ with respect to ζ_2 (analogously $\boldsymbol{\tau}_2$ with respect to ζ_1) one has

$$\boldsymbol{\tau}_{1,2} = \vartheta_{1,2}\boldsymbol{\nu}_1, \qquad \boldsymbol{\tau}_{2,1} = \vartheta_{2,1}\boldsymbol{\nu}_2. \tag{4.14}$$

Remark 36. The quantities $\vartheta_{1,2},\ \vartheta_{2,1}$ are called Tchebychev curvatures [49, 84].

At this point, recalling Eq. (4.9) and using (4.13), we can rewrite the two vector fields $\mathbf{g}_\alpha$ in terms of ϑ_α as

$$\mathbf{g}_\alpha = \lambda_{\alpha,\zeta_\alpha}\boldsymbol{\tau}_\alpha + \lambda_\alpha\vartheta_{\alpha,\alpha}\boldsymbol{\nu}_\alpha.$$

Analogously, recalling Eq. (4.11) and using 4.14, we have that the vector field $\boldsymbol{\Gamma}$ can be rewritten as

$$\boldsymbol{\Gamma} = \mathbf{d}_{1,2} = \lambda_{1,2}\boldsymbol{\tau}_1 + \lambda_1\vartheta_{1,2}\boldsymbol{\nu}_1 = \mathbf{d}_{2,1} = \lambda_{2,1}\boldsymbol{\tau}_2 + \lambda_2\vartheta_{2,1}\boldsymbol{\nu}_2. \tag{4.15}$$

We have thus identified the vectors $\mathbf{g}_\alpha$ and $\boldsymbol{\Gamma}$ in terms of the angles ϑ_α and their derivatives. Nevertheless, such angles ϑ_α are not the more natural ones, if one wants to associate a precise geometrical meaning to the deformation mechanisms that we want to describe. Indeed, the shear angle γ represents the total angle variation of the coordinate lines from their reference configuration to the current one (see Fig. 4.1.1), so that its geometrical meaning is much more direct in view of phenomenological interpretations.

In order to rewrite $\mathbf{g}_\alpha$ and $\boldsymbol{\Gamma}$ in terms of the shear angle γ we start to remark that

$$\vartheta_2 - \vartheta_1 = \frac{\pi}{2} - \gamma,$$

It follows that, taking the gradient of this formula

$$\nabla\gamma = \nabla\vartheta_1 - \nabla\vartheta_2.$$

On the other hand, we have

$$\nabla\vartheta_\alpha = (\nabla\vartheta_\alpha\cdot\mathbf{D}_1)\,\mathbf{D}_1 + (\nabla\vartheta_\alpha\cdot\mathbf{D}_2)\,\mathbf{D}_2 = \vartheta_{\alpha,1}\mathbf{D}_1 + \vartheta_{\alpha,2}\mathbf{D}_2.$$

Recalling Eq. (4.13)we can hence express the Tchebychev curvatures as functions of the bending strains and the shear angle γ as

$$\begin{cases} \gamma_{,1} = \vartheta_{1,1} - \vartheta_{2,1} \Longleftrightarrow \vartheta_{2,1} = b_1 + \gamma_{,1}, \\ \\ \gamma_{,2} = \vartheta_{1,2} - \vartheta_{2,2} \Longleftrightarrow \vartheta_{1,2} = b_2 + \gamma_{,2}. \end{cases} \tag{4.16}$$

In order to complete our reasoning and to finally write the Tchebychev curvatures as functions of the sole angle γ we project (4.15) on $\boldsymbol{\tau}_1$ and $\boldsymbol{\tau}_2$ so obtaining

$$\langle \mathbf{d}_{1,2}, \boldsymbol{\tau}_1 \rangle = \lambda_{1,2} = \langle \mathbf{d}_{2,1}, \boldsymbol{\tau}_1 \rangle = \lambda_{2,1} \langle \boldsymbol{\tau}_1, \boldsymbol{\tau}_2 \rangle + \lambda_2 \vartheta_{2,1} \langle \boldsymbol{\tau}_1, \boldsymbol{\nu}_2 \rangle = \lambda_{2,1} \sin\gamma - \lambda_2 \vartheta_{2,1} \cos\gamma,$$

and

$$\langle \mathbf{d}_{1,2}, \boldsymbol{\tau}_2 \rangle = \lambda_{1,2} \langle \boldsymbol{\tau}_1, \boldsymbol{\tau}_2 \rangle + \lambda_1 \vartheta_{1,2} \langle \boldsymbol{\nu}_1, \boldsymbol{\tau}_2 \rangle = \lambda_{1,2} \sin\gamma + \lambda_1 \vartheta_{1,2} \cos\gamma = \langle \mathbf{d}_{2,1}, \boldsymbol{\tau}_2 \rangle = \lambda_{2,1},$$

which finally implies

$$\begin{cases} \lambda_2 \vartheta_{2,1} \cos\gamma = \lambda_{2,1} \sin\gamma - \lambda_{1,2} \\ \\ \lambda_1 \vartheta_{1,2} \cos\gamma = \lambda_{2,1} - \lambda_{1,2} \sin\gamma. \end{cases}$$

Replacing the expressions of Tchebychev curvatures found in Eq. (4.16) in these last equations we have

$$\begin{cases} \lambda_2 (b_1 + \gamma_{,1}) \cos\gamma = \lambda_{2,1} \sin\gamma - \lambda_{1,2} \\ \\ \lambda_1 (b_2 + \gamma_{,2}) \cos\gamma = \lambda_{2,1} - \lambda_{1,2} \sin\gamma, \end{cases} \tag{4.17}$$

from which we can explicitly deduce the expression of b_α in terms of the shear angle γ.
Using the relationships (4.16) and (4.17) in the definitions of $\mathbf{g}_\alpha$ and $\boldsymbol{\Gamma}$, these latter can be rewritten in terms of λ_α, γ and their gradients.

4.1.4 Hypothesis of inextensibility

In this section, after having introduced the definition of inextensible field, we will explore the consequences of this assumption.

Definition 37. A map $\mathbf{r} : \mathbb{R}^2 \supseteq \mathscr{B}^\star \to \mathbb{R}^2$ is said ***inextensible*** if $\|\mathbf{d}_1\| = \|\mathbf{d}_2\| = 1$ for every $(\zeta_1, \zeta_2) \in \mathscr{B}^\star$.

If we explicitly write the two expressions $\|\mathbf{d}_1\| = \|\mathbf{d}_2\| = 1$ by recalling Eqs. (4.1), we get

$$\begin{cases} \left(\dfrac{\partial r_1}{\partial \zeta_1}\right)^2 + \left(\dfrac{\partial r_2}{\partial \zeta_1}\right)^2 = 1 \\ \\ \left(\dfrac{\partial r_1}{\partial \zeta_2}\right)^2 + \left(\dfrac{\partial r_2}{\partial \zeta_2}\right)^2 = 1. \end{cases}$$

Differentiating the first of such equations with respect to ζ_2 and the second with respect to ζ_1 we obtain

$$\begin{cases} \dfrac{\partial r_1}{\partial \zeta_1} \dfrac{\partial^2 r_1}{\partial \zeta_1 \partial \zeta_2} + \dfrac{\partial r_2}{\partial \zeta_1} \dfrac{\partial^2 r_2}{\partial \zeta_1 \partial \zeta_2} = 0 \\ \\ \dfrac{\partial r_1}{\partial \zeta_2} \dfrac{\partial^2 r_1}{\partial \zeta_1 \partial \zeta_2} + \dfrac{\partial r_2}{\partial \zeta_2} \dfrac{\partial^2 r_2}{\partial \zeta_1 \partial \zeta_2} = 0 \end{cases}$$

or in matrix notation

$$\begin{bmatrix} \dfrac{\partial r_1}{\partial \zeta_1} & \dfrac{\partial r_2}{\partial \zeta_1} \\ \dfrac{\partial r_1}{\partial \zeta_2} & \dfrac{\partial r_2}{\partial \zeta_2} \end{bmatrix} \begin{bmatrix} \dfrac{\partial^2 r_1}{\partial \zeta_1 \partial \zeta_2} \\ \dfrac{\partial^2 r_2}{\partial \zeta_1 \partial \zeta_2} \end{bmatrix} = \nabla \mathbf{r} \cdot \begin{bmatrix} \dfrac{\partial^2 r_1}{\partial \zeta_1 \partial \zeta_2} \\ \dfrac{\partial^2 r_2}{\partial \zeta_1 \partial \zeta_2} \end{bmatrix} = 0. \tag{4.18}$$

Having that the map $\mathbf{r}$ is $\mathscr{C}^2$ diffeomorphism, the only possibility, for every $(\zeta_1, \zeta_2) \in \mathscr{B}^\star$ to have a solution of (4.18) is that

$$\frac{\partial^2 r_1}{\partial \zeta_1 \partial \zeta_2} = \frac{\partial^2 r_2}{\partial \zeta_1 \partial \zeta_2} = 0, \tag{4.19}$$

Using such result in equation (4.2) we can find that the second gradient of the placement field in the case of inextensibility takes the following simplified form

$$\nabla^2 \mathbf{r}\left(\zeta_1, \zeta_2\right) = \begin{bmatrix} \begin{bmatrix} \dfrac{\partial^2 r_1}{\partial \zeta_1^2} & 0 \\ 0 & \dfrac{\partial^2 r_1}{\partial \zeta_2^2} \end{bmatrix} \\ \begin{bmatrix} \dfrac{\partial^2 r_2}{\partial \zeta_1^2} & 0 \\ 0 & \dfrac{\partial^2 r_2}{\partial \zeta_2^2} \end{bmatrix} \end{bmatrix}. \tag{4.20}$$

The equation (4.19) is the well known wave equation in the second form that, in connected domains has the solution

$$\mathbf{r}\left(\zeta_1, \zeta_2\right) = r_1\left(\zeta_1, \zeta_2\right) \mathbf{D}_1 + r_2\left(\zeta_1, \zeta_2\right) \mathbf{D}_2 = \left(\mu_1(\zeta_1) + \nu_2(\zeta_2)\right) \mathbf{D}_1 + \left(\nu_1(\zeta_1) + \mu_2(\zeta_2)\right) \mathbf{D}_2, \tag{4.21}$$

which we can rewrite in compact form as

$$\mathbf{r}\left(\zeta_1, \zeta_2\right) = \mathbf{r}_1\left(\zeta_1\right) + \mathbf{r}_2\left(\zeta_2\right) \tag{4.22}$$

with $\mathbf{r}_1$ and $\mathbf{r}_2$ vector valued maps of a real variable defined respectively (on the projection I_1 and I_2 of $\mathscr{B}^\star$ on coordinate axis) as

$$\begin{cases} \mathbf{r}_1\left(\zeta_1\right) = \mu_1\left(\zeta_1\right) \mathbf{D}_1 + \nu_1\left(\zeta_1\right) \mathbf{D}_2 \\ \\ \mathbf{r}_2\left(\zeta_2\right) = \nu_2\left(\zeta_2\right) \mathbf{D}_1 + \mu_2\left(\zeta_2\right) \mathbf{D}_2, \end{cases}$$

with μ_1, ν_1 and μ_2, ν_2 real valued functions of real variable defined respectively on I_1 and I_2. Consequently, according to Eq. (4.1), the vectors $\mathbf{d}_1$ and $\mathbf{d}_2$ will take following form

$$\begin{cases} \mathbf{d}_1\left(\zeta_1\right) = \mu_{1,1}\left(\zeta_1\right) \mathbf{D}_1 + \nu_{1,1}\left(\zeta_1\right) \mathbf{D}_2 \\ \\ \mathbf{d}_2\left(\zeta_2\right) = \nu_{2,2}\left(\zeta_2\right) \mathbf{D}_1 + \mu_{2,2}\left(\zeta_2\right) \mathbf{D}_2. \end{cases}$$

These last equations, together with the fact that in the inextensible case the vectors $\mathbf{d}_1$ and $\mathbf{d}_2$ are unitary, implies

$$\|\mathbf{d}_1\|^2 = 1 \Rightarrow \ (\mu_{1,1})^2 + (\nu_{1,1})^2 = 1 \ \Rightarrow \ \nu_{1,1} = \pm\sqrt{1-(\mu_{1,1})^2} \tag{4.23}$$

$$\|\mathbf{d}_2\|^2 = 1 \Rightarrow \ (\mu_{2,2})^2 + (\nu_{2,2})^2 = 1 \ \Rightarrow \ \nu_{2,2} = \pm\sqrt{1-(\mu_{2,2})^2}. \tag{4.24}$$

Integrating these last expressions we get

$$\nu_1(\zeta_1) - \nu_1(\zeta_{1\min}) = \pm\int_{\zeta_{1\min}}^{\zeta_1} \sqrt{1-(\mu_{1,1}(\eta))^2}d\eta, \qquad \forall\zeta_1 \in I_1$$

$$\nu_2(\zeta_2) - \nu_2(\zeta_{2\min}) = \pm\int_{\zeta_{2\min}}^{\zeta_2} \sqrt{1-(\mu_{2,2}(\eta))^2}d\eta, \qquad \forall\zeta_2 \in I_2,$$

where the points $\zeta_{1\min}$ and $\zeta_{2\min}$ can be defined as (see also Fig. 4.6)

$$\zeta_{1\min} := \min\{I_1\} \qquad \text{and} \qquad \zeta_{2\min} := \min\{I_2\}.$$

The existence of $\zeta_{1\min}$ and $\zeta_{2\min}$ is guaranteed by the fact that, since $\mathscr{B}^\star$ is a compact connected set and the projection maps are continuous maps, we also have that I_1 and I_2 are compact connected subsets of $\mathbb{R}$ (and so intervals). In what follows, whenever square roots appear in the formulas we will choose the sign + since only the corresponding specific families of deformations are involved in the problems that we will study.

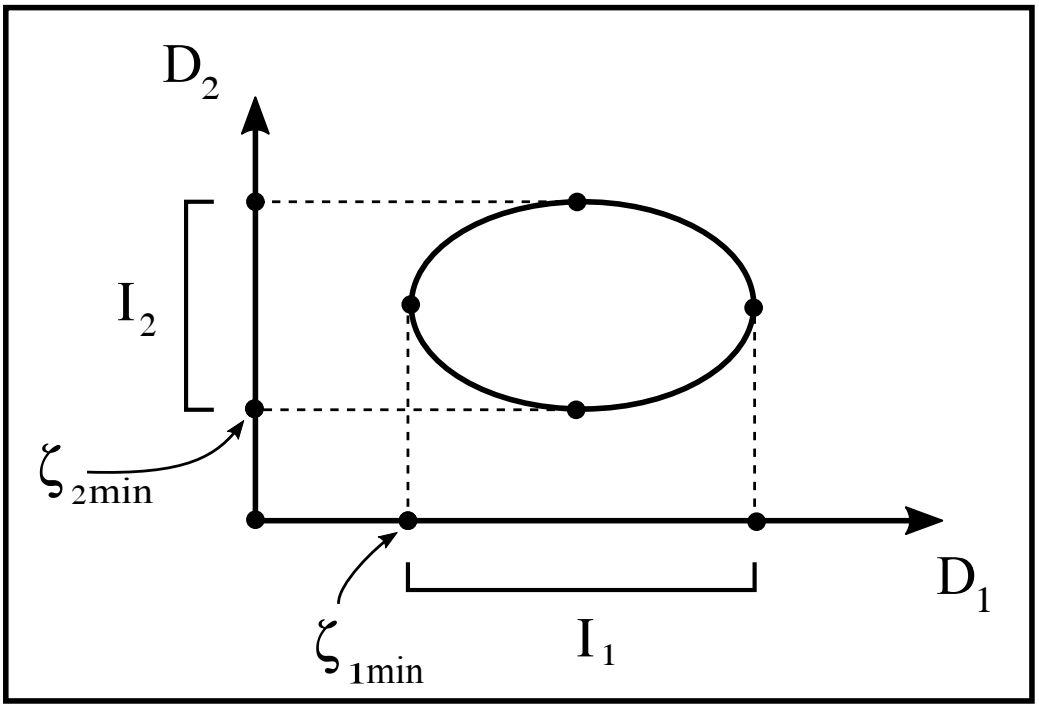

Figure 4.6: $\zeta_{1\min}$ and $\zeta_{2\min}$

Chapter 5

A 2D first gradient problem for rectangular specimens of fibrous materials with inextensible fibers

In the Fifties and Sixties decades of XX century Adkin, Rivlin [76, 77, 78, 81, 82, 1, 29, 68] and Pipkin [61, 73, 70, 62, 63, 71, 65, 66, 72, 84, 89, 90, 32, 69, 64, 67] developed a continuum model for inextensible fiber networks, to supply a predictive tool for many emerging and important technological applications. The mathematical problems which arose in their theoretical studies immediately appeared to be formidable. Indeed, they could not solve in a closed form a reasonably large number of exercises and, even if in Pipkin's works the analysis of some numerical problems is attempted, the numerical methods needed to supply meaningful solutions for applications could not be fully developed and exploited.
More recently, under the impulse of aeronautical and aerospace engineering, the attention of theoretical and applied mechanicians was attracted again to the study of mechanical systems and materials reinforced with "practically" inextensible fibers [33, 12, 6, 11]. However, the memory of the theoretical efforts produced by Adkin, Rivlin and Pipkin seemed to be lost and the standard first gradient Cauchy continuum model was used in a context which had been already recognized to be unsuitable. In particular, many numerical undesired effects, as locking (see e.g. [42, 17, 41]) or loss of convergence, cannot be easily avoided in the presence of inextensible material lines. Moreover the associated kinematical constraints have been recognized (see e.g. [5]) to cause the onset of ill-posedness in first gradient continuum models. Indeed, the incompressibility constraint is the only kind of kinematical constraint whose presence does not render inapplicable the standard proof strategy developed for proving existence and uniqueness results developed for not-constrained first gradient continua.
In the present paragraph:

- we start by characterizing the kinematics of considered mechanical system: we limit our attention to symmetric planar systems including two families of inextensible fibers in which any admissible configuration is specifiable by means of one real function of one real variable. More details about this one-to-one characterization of the set of admissible configurations can be found in Adkin and Rivlin [1, 78, 76];

- we then limit our attention to a suitable class of deformation energies [46, 64, 66, 47, 73] which depend on the variation of the angle between the fibers;

- we characterize the equilibrium configurations of considered mechanical systems as those admissible configurations which verify suitable imposed displacement conditions and for which the total potential energy attains its minima;

- we find that the conditions naturally associated to the introduced principle of minimum of total energy reduce to an integro-differential equations;
- we introduce an efficient iterative integration scheme, in the particular case of a specimen having length three times larger than width, in order to solve the integro-differential equation which govern the extensional bias-test.

Actually we call standard bias test the extension test where rectangular specimen whose length is exactly three times their width are clamped at their shorter sides and where a relative displacement (compatible with the presence of inextensible fiber) is imposed between the clamped specimen sides. Many further investigations are motivated by the presented results: for instance there is a great interest in the determination of internal stress induced in the inextensible fibers by imposed deformation, in order to completely describe experimental evidence (see e.g. [50, 51]) or in the design of non-standard bias extension tests where the specimen is longer or shorter, or in designing bias tests for specimen where the inextensible fibers are not orthogonal in the reference configuration.

Contents

5.1 Kinematics

The main conceptual tool used in this work is the principle of minimum total energy for the determination of equilibrium configurations. Therefore we must specify carefully and preliminarily the set of admissible configurations among which we look for in order to find the energy minimizers.

5.1.1 Geometry

We introduce an orthonormal reference system $(\mathcal{O}, X_1, X_2)$ on $\mathscr{S}$.
We assume that $\mathscr{B}^\star$ is a rectangle whose sides have length l and L, with $L = 3l$, described by the following conditions:

$$\mathscr{B}^\star = \left\{ (X_1, X_2) \in \mathscr{S} : \; X_1 \in [0, L] \,, \; X_2 \in \left[-\frac{l}{2}, \frac{l}{2} \right] \right\}.$$

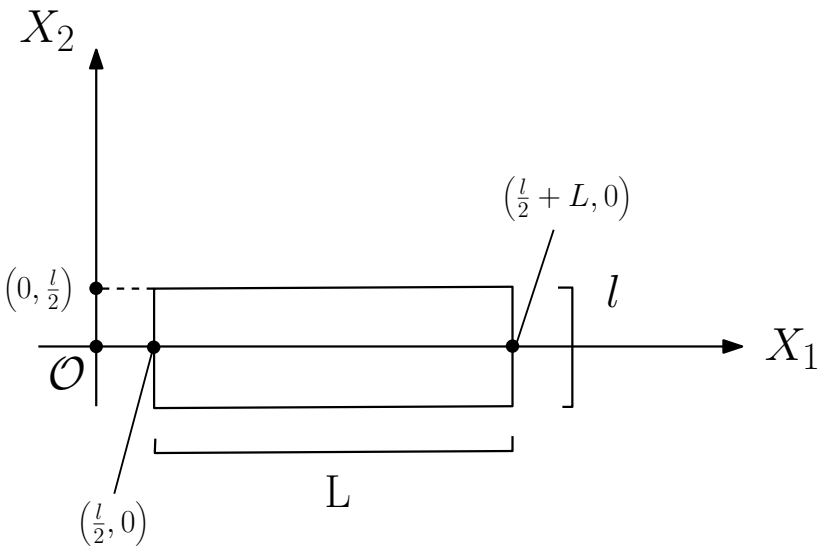

Figure 5.1: Space of material particles and the orthonormal system $(\mathcal{O}, X_1, X_2)$.

The body $\mathscr{B}^\star$ may be, in some conditions to be better determined, a model for a rectangular specimen of a woven fabric composed by two families of fibers which form a uniform orthogonal net intersecting the perimeter of $\mathscr{B}^\star$ with an angle of 45 degrees. It is therefore convenient to introduce another orthogonal reference system, $(\mathcal{O}, \xi_1, \xi_2)$, oriented according to the directions of the fibers of the fabric and shifted as shown in figure 5.2. In $(\mathcal{O}, \xi_1, \xi_2)$ we consider non-dimensional space coordinates, defined as follows:

$$\xi_1 := \frac{1}{l} (X_1 - X_2) + \frac{1}{2}, \qquad \xi_2 := \frac{1}{l} (X_1 + X_2) + \frac{1}{2}. \tag{5.1}$$

We call fiber reference the new reference system introduced and fiber directions the two directions in which the coordinates ξ_1, ξ_2 are spanning. It will be useful to represent all deformation measures also in the reference system $(\mathcal{O}, \xi_1, \xi_2)$, since ξ_1, ξ_2 represent the orthotropic directions of the material.
Let the two lines Σ_1 and Σ_2 be considered, in the fiber reference, which are described by the following algebraic equations (see also Fig. 5.3:

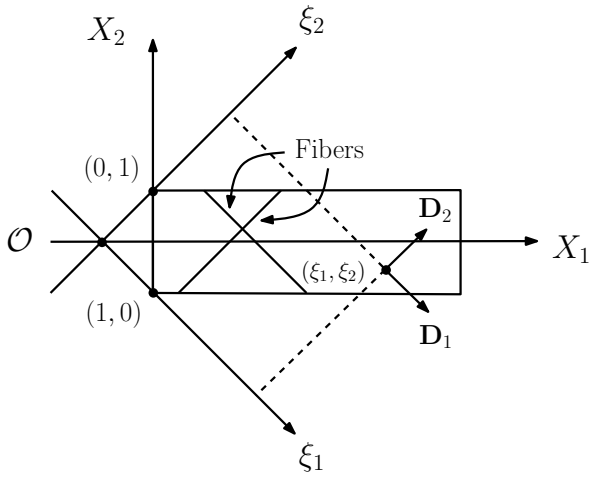

Figure 5.2: Material axes and fibers directions.

$$\Sigma_1 := \{(\xi_1,\xi_2) \in \mathscr{B}^\star : \ \xi_1 \in [0,1]\,, \xi_2 = 1-\xi_1\}\,, \tag{5.2}$$

$$\Sigma_2 := \{(\xi_1,\xi_2) \in \mathscr{B}^\star : \ \xi_1 \in [3,4]\,, \xi_2 = 7-\xi_1\}\,. \tag{5.3}$$

In this work, we impose the following boundary conditions on the two subsets Σ_1 and Σ_2 of the boundary of $\mathscr{B}^\star$:

1. vanishing displacement of the face Σ_1,
2. imposed displacement $\mathbf{u}_0 = u_0\,(\mathbf{D}_1 + \mathbf{D}_2)$ of the face Σ_2.

The kinematics of considered bias test naturally leads us to define 6 lines:

$$\begin{aligned} &S_1 := \{(\xi_1,\xi_2) \in \mathscr{B}^\star : \xi_1 \in [0,2]\,, \xi_2 = 1\}\,, \qquad S_2 := \{(\xi_1,\xi_2) \in \mathscr{B}^\star : \xi_1 = 1, \xi_2 \in [0,2]\}\,, \\ &S_3 := \{(\xi_1,\xi_2) \in \mathscr{B}^\star : \xi_1 \in [1,3]\,, \xi_2 = 2\}\,, \qquad S_4 := \{(\xi_1,\xi_2) \in \mathscr{B}^\star : \xi_1 = 2, \xi_2 \in [1,3]\} \\ &S_5 := \{(\xi_1,\xi_2) \in \mathscr{B}^\star : \xi_1 \in [2,4]\,, \xi_2 = 3\}\,, \qquad S_6 := \{(\xi_1,\xi_2) \in \mathscr{B}^\star : \xi_1 = 3, \xi_2 \in [2,4]\}\,. \end{aligned} \tag{5.4}$$

Indeed these lines are separating zones in which the inextensible fibers are subject to different kinematical conditions: as it is possible to check easily in Fig. 5.3 we remark that the part of the specimen characterized by the values of $\xi_2 \leq 1$ (i.e the part of the specimen below S_1) is constituted by all the fibers which i) are parallel to ξ_1 and ii) have one end blocked in Σ_1 while their other end is free. Exactly the same kinematical consideration is valid in the zone above S_5 (concerning all the fibers parallel to ξ_1 which have an end blocked in Σ_2 and the other one free) and in the zones above S_2 and under S_6 (where one has to consider the fibers parallel to ξ_2). The central part of the specimen is characterized kinematically as follows: the part between S_1 and S_3 is composed by fibers parallel to ξ_1 with both ends free that have interaction with fibers parallel to ξ_2 with an end fixed in Σ_1. Similarly, one can characterize kinematically all the subsets of the partition which we have introduced via the curves defined in equations (5.4).
If we indicate with π_1 and π_2 the projection maps respectively on ξ_1 and ξ_2, we introduce the notations (see also Fig. 5.4)

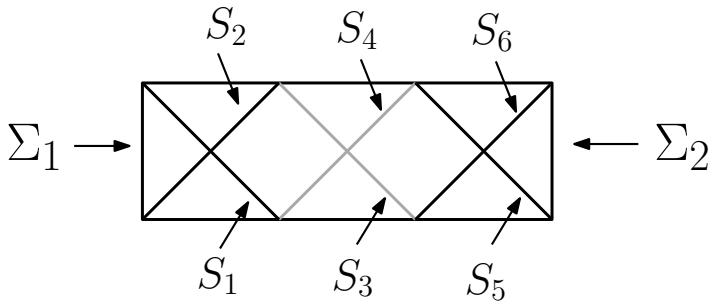

Figure 5.3: Discontinuity lines in the considered specimen.

$$I_{10} := \pi_1(\Sigma_1) = [0,1] \qquad I_{13} := \pi_1(\Sigma_2) = [3,4] \tag{5.5}$$

$$I_{20} := \pi_2(\Sigma_1) = [0,1] \qquad I_{23} := \pi_2(\Sigma_2) = [3,4]. \tag{5.6}$$

Analogously, we can define the projections of the whole $\mathscr{B}^\star$ on the fiber axes as (see also Fig. 5.4):

$$I_1 := \pi_1(\mathscr{B}^\star), \qquad I_2 := \pi_2(\mathscr{B}^\star). \tag{5.7}$$

Moreover, considering the projections of the lines S_i we define the following ranges:

$$I_{11} := [\pi_1(S_2), \pi_1(S_4)] = [1,2], \qquad I_{12} := [\pi_1(S_4), \pi_1(S_6)] = [2,3] \tag{5.8}$$

$$I_{21} := [\pi_2(S_1), \pi_2(S_3)] = [1,2] \qquad I_{23} := [\pi_2(S_3), \pi_2(S_5)] = [2,3]. \tag{5.9}$$

Therefore the following partition of the two intervals I_1 and I_2 are naturally introduced on the basis of the aforementioned kinematical considerations:

$$I_1 = I_{10} \cup I_{11} \cup I_{12} \cup I_{13} \qquad I_2 = I_{20} \cup I_{21} \cup I_{22} \cup I_{23} \tag{5.10}$$

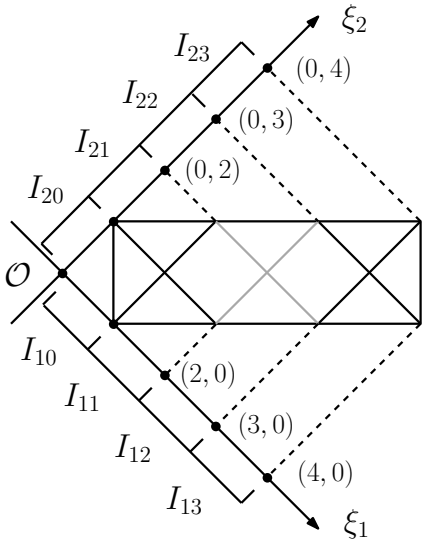

Figure 5.4: Projections of the domains on the fiber axes.

Furthermore, the partition of the axes naturally defines a partition of $\mathscr{B}^\star$ in regions Δ_{ij} as follows (see Fig. 5.5)

$$\Delta_{ij} := (I_{1i} \times I_{2j}) \cap \mathscr{B}^\star, \qquad \mathscr{B}^\star = \bigcup_{i,j=1}^{3} \Delta_{ij}. \tag{5.11}$$

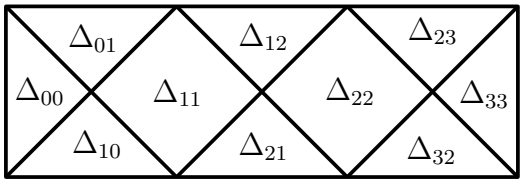

Figure 5.5: Partition of the body $\mathscr{B}^\star$ in different subdomains individuated by sets of fibers with different boundary conditions or different type of interaction with the orthogonal fibers.

5.2 Assumptions on admissible placement fields

We will assume that the placement field $\mathbf{r}$ is:

- continuous in the whole domain $\mathscr{B}^\star$;
- suffering some first-kind discontinuities in its first or in its second gradient at a finite number of inextensible fibers, at most;
- twice continuously differentiable in the other points of $\mathscr{B}^\star$.

We indicate with $\mathbf{F}$ the space gradient of $\mathbf{r}$ and we use the notation:

$$\mathbf{d}_1 = \mathbf{F} \cdot \mathbf{D}_1, \qquad \mathbf{d}_2 = \mathbf{F} \cdot \mathbf{D}_2. \tag{5.12}$$

The two vectors $\mathbf{d}_1$ and $\mathbf{d}_2$ represent the directions of the fibers in the current configuration. Because of our assumptions we can say that:

- the inextensible fibers are not cut in the passage from the reference to the current configuration;
- the current fiber directions are uniquely defined for every material point except on some inextensible fibers where they may suffer jumps;
- the domain $\mathscr{B}^\star$ can be partitioned into a finite number of convex subsets in each of which the placement is of class $\mathscr{C}^2$.

5.3 Inextensible continuum model

We assume that the placement field is twice continuously differentiable in any Δ_{ij}. If we indicate with $\mathbf{r}^{(i,j)}(\xi_1, \xi_2)$ the restriction of $\mathbf{r}$ to the Δ_{ij} component, for the propriety in (4.22) we have

$$\mathbf{r}^{(i,j)}(\xi_1, \xi_2) = \mathbf{r}_1^{(i)}(\xi_1) + \mathbf{r}_2^{(j)}(\xi_2) =: \left(\mu_1^{(i)}(\xi_1) + \nu_2^{(j)}(\xi_2)\right) \mathbf{D}_1 + \left(\nu_1^{(i)}(\xi_1) + \mu_2^{(j)}(\xi_2)\right) \mathbf{D}_2, \tag{5.13}$$

as the global continuity condition of $\mathbf{r}$ allows us to identify the vector fields $\mathbf{r}_1^{(i)}(\xi_1), \mathbf{r}_2^{(j)}(\xi_2)$ along straight lines included in B.
Indeed, if we consider two regions Δ_{ij} and Δ_{ik} then we have that $\mathbf{r}_1^{(\Delta_{ij})}(\xi_1) = \mathbf{r}_1^{\Delta_{ik}}(\xi_1) =: \mathbf{r}_1^{(i)}(\xi_1)$ and analogously, when considering two regions Δ_{ij} and Δ_{hj}, one has $\mathbf{r}_2^{(\Delta_{ij})}(\xi_2) = \mathbf{r}_2^{\Delta_{kj}}(\xi_2) =: \mathbf{r}_2^{(j)}(\xi_2)$.

5.3.1 Space of Configurations for considered system

A number of properties and results can be proven for the scalar fields determining the displacement field. The regularity assumptions, which we have accepted together with the condition of inextensibility of the fibers and the boundary conditions which we impose, will indeed determine the space of configurations inside which we can look for the equilibrium configurations: i.e. those configurations which minimize total energy.

5.3.1.1 Restrictions on the fields μ and ν imposed by boundary conditions

We prove here the three following properties of the displacement field relative to the considered bias test problem with inextensible fibers:

1. the boundary conditions on Σ_1 implies that $\mathbf{r}(\xi_1,\xi_2) = \xi_1\mathbf{D}_1 + \xi_2\mathbf{D}_2 \; \forall (\xi_1,\xi_2) \in \Delta_{00}$,
2. the boundary conditions on Σ_2 implies that $\mathbf{r}(\xi_1,\xi_2) = \xi_1\mathbf{D}_1 + \xi_2\mathbf{D}_2 + \mathbf{u}_0 \; \forall (\xi_1,\xi_2) \in \Delta_{33}$,
3. the continuity of $\mathbf{r}$ in the point $(3,3)$ implies a system (which is specified at the end of this section) of integral conditions for the two functions $\mu_1(\xi_1)$ and $\mu_2(\xi_2)$.

Proposition 38. *Let $\mathbf{r}^{(0,0)}$ be the restriction of $\mathbf{r}$ to the subdomain Δ_{00}. If the displacement vanishes on Σ_1, then we have $\mathbf{r}^{(0,0)}(\xi_1,\xi_2) = \xi_1\mathbf{D}_1 + \xi_2\mathbf{D}_2 \; \forall (\xi_1,\xi_2) \in \Delta_{00}$.*

Proof. We consider the following parametric description of Σ_1:

$$\Sigma_1 = \{(\xi_1(t), \xi_2(t)) : \xi_1(t) = t, \xi_2(t) = 1 - t \text{ with } t \in [0,1]\}. \tag{5.14}$$

We have that

$$\mathbf{r}^{(0,0)}(\xi_1(t), \xi_2(t)) = \mathbf{r}_1^{(0)}(\xi_1(t)) + \mathbf{r}_2^{(0)}(\xi_2(t)) =$$

$$= \left(\mu_1^{(0)}(\xi_1(t)) + \nu_2^{(0)}(\xi_2(t))\right)\mathbf{D}_1 + \left(\nu_1^{(0)}(\xi_1(t)) + \mu_2^{(0)}(\xi_2(t))\right)\mathbf{D}_2 \tag{5.15}$$

which, because of the imposed boundary conditions, imply

$$\begin{cases} \mu_1^{(0)}(\xi_1(t)) + \nu_2^{(0)}(\xi_2(t)) = t \\ \\ \nu_1^{(0)}(\xi_1(t)) + \mu_2^{(0)}(\xi_2(t)) = 1 - t. \end{cases} \tag{5.16}$$

By differentiating the two equations in (5.16) with respect to t we obtain (with obvious meaning of used notation)

$$\begin{cases} \left.\dfrac{d\mu_1^{(0)}}{d\xi_1}\right|_t - \left.\dfrac{d\nu_2^{(0)}}{d\xi_2}\right|_{1-t} = 1 \\ \\ \left.\dfrac{d\nu_1^{(0)}}{d\xi_1}\right|_t - \left.\dfrac{d\mu_2^{(0)}}{d\xi_2}\right|_{1-t} = -1 \end{cases} \Longrightarrow \begin{cases} \mu_{1,1}^{(0)} = 1 + \nu_{2,2}^{(0)} \\ \\ \nu_{1,1}^{(0)} = \mu_{2,2}^{(0)} - 1. \end{cases} \tag{5.17}$$

Recalling the relation $1 = \left(\mu_{1,1}^{(0)}\right)^2 + \left(\nu_{1,1}^{(0)}\right)^2$, we obtain

$$1 = \left(\mu_{1,1}^{(0)}\right)^2 + \left(\nu_{1,1}^{(0)}\right)^2 = \left(1+\nu_{2,2}^{(0)}\right)^2 + \left(\mu_{2,2}^{(0)} - 1\right)^2 = \tag{5.18}$$

$$= \underbrace{\left(\mu_{2,2}^{(0)}\right)^2 + \left(\nu_{2,2}^{(0)}\right)^2}_{=1} + 2 - 2\mu_{2,2}^{(0)} + 2\nu_{2,2}^{(0)} = 3 + 2\left(\nu_{2,2}^{(0)} - \mu_{2,2}^{(0)}\right). \tag{5.19}$$

As a consequence

$$1 = 3 + 2\left(\nu_{2,2}^{(0)} - \mu_{2,2}^{(0)}\right) \Longrightarrow \mu_{2,2}^{(0)} - \nu_{2,2}^{(0)} = 1. \tag{5.20}$$

Therefore we can easily find the fields $\mu_{2,2}^{(0)}$ and $\nu_{2,2}^{(0)}$. Indeed

$$\begin{cases} \left(\mu_{2,2}^{(0)}\right)^2 + \left(\nu_{2,2}^{(0)}\right)^2 = 1 \\ \\ \mu_{2,2}^{(0)} - \nu_{2,2}^{(0)} = 1 \end{cases} \Longrightarrow \nu_{2,2}^{(0)} = 0 \vee \nu_{2,2}^{(0)} = -1, \tag{5.21}$$

but, restricting to the case $\nu_{2,2}^{(0)} \in \left[0, \sqrt{2}/2\right]$, we can consider only the solution $\nu_{2,2}^{(0)} = 0$. As a consequence $\mu_{2,2}^{(0)} = 1$.
In the same way we find that $\nu_{1,1}^{(0)} = 0$ and $\mu_{1,1}^{(0)} = 1$ for any $\xi_1 \in I_{10}$.
Integrating the obtained expressions we have

$$\begin{cases} \mu_1^{(0)}(\xi_1) = \xi_1 + \mu_1^{(0)}(0) & \xi_1 \in I_{10} \\ \\ \nu_1^{(0)}(\xi_1) = \nu_1^{(0)}(0) & \xi_1 \in I_{10} \\ \\ \mu_2^{(0)}(\xi_2) = \xi_2 + \mu_2^{(0)}(0) & \xi_2 \in I_{20} \\ \\ \nu_2^{(0)}(\xi_2) = \nu_2^{(0)}(0) & \xi_2 \in I_{20}. \end{cases} \tag{5.22}$$

In the decomposition (5.13) the functions $\mathbf{r}_1$ and $\mathbf{r}_2$ are determined up to an additive vector constant (i.e. up to two scalar constants). We can choose it so to have:

$$\mu_1^{(0)}(0) = \nu_1^{(0)}(0) = \mu_2^{(0)}(0) = \nu_2^{(0)}(0) = 0. \tag{5.23}$$

□

In a similar way[1], we can prove also the following

Proposition 39. *Let $\mathbf{r}^{(3,3)}$ be the restriction of $\mathbf{r}$ to the subdomain Δ_{33} and $\mathbf{u}_0$ the imposed displacement on Σ_2. Then we have $\mathbf{r}^{(3,3)}(\xi_1, \xi_2) = \xi_1\mathbf{D}_1 + \xi_2\mathbf{D}_2 + \mathbf{u}_0$.*

Remark 40. It is very important to remark that in every region Δ_{ij} the two vector fields $\mathbf{r}_1^{(i)}(\xi_1)$ and$\mathbf{r}_2^{(j)}(\xi_2)$ in the decomposition

$$\mathbf{r}^{(i,j)}(\xi_1, \xi_2) = \mathbf{r}_1^{(i)}(\xi_1) + \mathbf{r}_2^{(j)}(\xi_2), \tag{5.24}$$

are defined up to two additive constants.
Indeed, if we take

[1] One could also apply the previous proposition to the function $\mathbf{r}^{(3,3)}(\xi_1, \xi_2) - \mathbf{u}_0$.

$$\mathbf{r}_1^{(i)}(\xi_1) = \mu_1^{(i)}(\xi_1)\,\mathbf{D}_1 + \nu_1^{(i)}(\xi_1)\,\mathbf{D}_2, \qquad \mathbf{r}_2^{(j)}(\xi_2) = \nu_2^{(j)}(\xi_2)\,\mathbf{D}_1 + \mu_2^{(j)}(\xi_2)\,\mathbf{D}_2, \tag{5.25}$$

then it is immediately evident that also for

$$\bar{\mathbf{r}}_1^{(i)}(\xi_1) = \left(\mu_1^{(i)}(\xi_1) + \alpha_i\right)\mathbf{D}_1 + \left(\nu_1^{(i)}(\xi_1) + \beta_j\right)\mathbf{D}_2 \quad \bar{\mathbf{r}}_2^{(j)}(\xi_2) = \left(\nu_2^{(j)}(\xi_2) - \alpha_i\right)\mathbf{D}_1 + \left(\mu_2^{(j)}(\xi_2) - \beta_j\right)\mathbf{D}_2 \tag{5.26}$$

with $\alpha_i, \beta_j \in \mathbb{R}$, we have

$$\mathbf{r}^{(i,j)}(\xi_1,\xi_2) = \bar{\mathbf{r}}_1^{(i)}(\xi_1) + \bar{\mathbf{r}}_2^{(j)}(\xi_2) = \mathbf{r}_1^{(i)}(\xi_1) + \mathbf{r}_2^{(j)}(\xi_2)\,. \tag{5.27}$$

Now, we can define the four functions μ_1, ν_1, μ_2 and ν_2 in the intervals I_1 and I_2 respectively as follows:

$$(\forall \xi_1 \in I_{1j}) \quad \left(\mu_1(\xi_1) = \mu_1^{(j)}(\xi_1)\,,\ \nu_1(\xi_1) = \nu_1^{(j)}(\xi_1)\right) \tag{5.28}$$

$$(\forall \xi_2 \in I_{2j}) \quad \left(\mu_2(\xi_2) = \mu_2^{(j)}(\xi_2)\,,\ \nu_2(\xi_2) = \nu_2^{(j)}(\xi_2)\right). \tag{5.29}$$

Obviously it is easy to see that we can determine (uniquely) the constants left arbitrary by the decomposition formula for displacement, after the initial choice in (5.23), simply by demanding the continuity on the intervals I_1 and I_2 of the just introduced four functions.

5.3.1.2 Continuity conditions in $(3,3)$

Because of (5.13), (4.23), (4.24), (5.28) and (5.29), the continuity conditions of the placement field $\mathbf{r}$ in $(3,3)$ with respect to the functions μ_1, μ_2 can be written as:

$$\begin{cases} \mu_1(3) + \int_1^3 \sqrt{1 - (\mu_{2,2}(\eta))^2}\,d\eta = 3 + u_0 \\ \\ \mu_2(3) + \int_1^3 \sqrt{1 - (\mu_{1,1}(\eta))^2}\,d\eta = 3 + u_0. \end{cases} \tag{5.30}$$

This condition is a consequence of the continuity of displacement in B and that its subbody Δ_{33} undergoes the translation $\mathbf{u}_0$.

5.3.2 Symmetry conditions

In this section we characterize the displacement fields which are symmetric with respect to the X_1-axis. This means that, given a point P of coordinates (ξ,η) and its symmetric P_s having coordinates (η,ξ) , the following conditions hold:

$$\begin{cases} \mathbf{d}_1(P)\cdot\mathbf{D}_1 = \mathbf{d}_2(P_s)\cdot\mathbf{D}_2 \\ \\ \mathbf{d}_1(P)\cdot\mathbf{D}_2 = \mathbf{d}_2(P_s)\cdot\mathbf{D}_1 \end{cases} \Longrightarrow \begin{cases} \mu_{1,1}(\xi) = \mu_{2,2}(\xi) \\ \\ \nu_{1,1}(\eta) = \nu_{2,2}(\eta) \end{cases} \tag{5.31}$$

Considering the symmetry of boundary conditions and the first equality in (5.31) we get directly the following identity:

$$\mu_1(\xi) = \mu_2(\xi) =: \mu(\xi) \quad \forall \xi \in [0,4]\,. \tag{5.32}$$

Therefore, considering the relations between μ_1, μ_2 and ν_1, ν_2 , the kinematics of the symmetric bias extension problem is completely described by means of a unique field μ. It is possible to determine another symmetry for the placement field. Indeed, our problem is equivalent (up to a translation) to the other one obtained imposing the following boundary conditions:

1. imposed displacement $-\mathbf{u}_0/2 = -u_0/2\,(\mathbf{D}_1 + \mathbf{D}_2)$ of the face Σ_1,
2. imposed displacement $\mathbf{u}_0/2 = u_0/2\,(\mathbf{D}_1 + \mathbf{D}_2)$ of the face Σ_2.

This implies the symmetry of $\mathbf{r}$ with respect to the line parallel to the X_2-axis passing through the point of coordinates $(2,2)$ in the $\xi_1\xi_2-$reference. It is straightforward to deduce that the functions $\mu_{1,1}$ and $\mu_{2,2}$ are even with respect to the points $\xi_1 = 2$ and $\xi_2 = 2$ in their domains of definition. Since the derivative of a even function is always an odd function, and in general the derivative of $\mu_{1,1}$ and $\mu_{2,2}$ is not equal to zero in $\xi_1 = 2$ and $\xi_2 = 2$, the second derivative of the fields μ_1 and μ_2 can be discontinuous in these points.

5.3.3 First variations of the fields belonging to the space of configurations

If we assume the hypothesis of symmetry, the configuration of considered body B is characterized by only one scalar field $\mu\,(\xi)$, defined on the real interval $[0,4]$. However, having already determined μ on $[0,1]$ and $[3,4]$ by means of imposed boundary conditions, we are left to find μ on $I = [1,3]$. Due to Proposition 1, continuity of the function μ and (5.30) we have also the conditions

$$\mu\,(1) = 1, \qquad \mu\,(3) + \int_1^3 \sqrt{1 - (\mu_{,\xi})^2}\,d\eta = 3 + u_0, \tag{5.33}$$

which must be verified by the functions in the space of configurations. Therefore the space of configurations is constituted by the set of functions μ in $\mathscr{C}^2_{pw}\,(I, \{2\})$, that is the space of two times continuously differentiable functions on I whose second derivatives can jump in 2, verifying the conditions (5.33).
Therefore, in order to be kinematically admissible, a variation $\delta\mu$ of μ has to verify the following conditions:

$$\delta\mu\,(1) = 0, \qquad \mu\,(3) + \delta\mu\,(3) + \int_1^3 \sqrt{1 - (\mu_{,\xi} + \delta\mu_{,\xi})^2}\,d\eta = u_0 + 3 \tag{5.34}$$

First we subtract the integral condition (5.33) to (5.34) to obtain:

$$\delta\mu\,(3) + \int_1^3 \sqrt{1 - (\mu_{,\xi} + \delta\mu_{,\xi})^2}\,d\eta - \int_1^3 \sqrt{1 - (\mu_{,\xi})^2}\,d\eta = 0. \tag{5.35}$$

Developing the argument of the first square root to the first order[2], we obtain

$$\delta\mu\,(3) + \int_1^3 \left(\sqrt{1 - (\mu_{,\xi})^2} - \frac{\mu'}{\sqrt{1 - (\mu_{,\xi})^2}}\delta\mu_{,\xi} \right) d\eta - \int_1^3 \sqrt{1 - (\mu_{,\xi})^2}\,d\eta = 0 \tag{5.36}$$

and consequently

$$\delta\mu\,(3) - \int_1^3 \frac{\mu_{,\xi}}{\sqrt{1 - (\mu_{,\xi})^2}}\delta\mu_{,\xi}\,d\eta = 0. \tag{5.37}$$

Remarking that we can write $\delta\mu\,(3)$ as $\int_1^3 \delta\mu_{,\xi}\,d\eta$, we find that (5.37) is equivalent to

$$\int_1^3 \left(1 - \frac{\mu_{,\xi}}{\sqrt{1 - (\mu_{,\xi})^2}} \right) \delta\mu_{,\xi}\,d\eta = 0. \tag{5.38}$$

This last orthogonality condition characterizes the admissible first variations of the functions in the space of configurations.

[2]Remark that this development is not possible in the neighborhood of the reference configuration.

5.3.4 First variation of energy

We assume the following expression for the energy density:

$$W(\xi_1,\xi_2)=\frac{1}{2}\left(\mathbf{d}_1\cdot\mathbf{d}_2\right)^2, \tag{5.39}$$

which, once expressed in terms of the kinematical field μ, becomes

$$W(\xi_1,\xi_2)=\frac{1}{2}\Bigg(\left(\mu_{,\xi}(\xi_1)\right)^2\left(1-\left(\mu_{,\xi}(\xi_2)\right)^2\right)+\left(\mu_{,\xi}(\xi_2)\right)^2\left(1-\left(\mu_{,\xi}(\xi_1)\right)^2\right)+ \tag{5.40}$$

$$+2\mu_{,\xi}(\xi_1)\,\mu_{,\xi}(\xi_2)\sqrt{\left(1-\left(\mu_{,\xi}(\xi_1)\right)^2\right)\left(1-\left(\mu_{,\xi}(\xi_2)\right)^2\right)}\Bigg).$$

In order to minimize the energy in the defined space of configurations, we have to introduce a Lagrange multiplier to take into account the integral constraint (5.33) imposed on μ. By using the notation

$$C(\mu_{,\xi}):=\mu(3)+\int_1^3\sqrt{1-(\mu_{,\xi})^2}d\eta-3-u_0$$

we must consider the following energy functional

$$\mathscr{A}_W=\int_B W\,dm+\Lambda C(\mu_{,\xi}),\quad \text{with}\,\Lambda\in\mathbb{R}. \tag{5.41}$$

Its first variation is

$$\delta\mathscr{A}_W=\int_B\delta W\,dm+\Lambda\delta C(\mu_{,\xi})+C(\mu_{,\xi})\,\delta\Lambda. \tag{5.42}$$

In the appendix we show all the details of the performed calculations for obtaining the aforementioned variation: to present them in the most effective way it is useful to introduce four integral operators $\mathscr{A}_i$ and $\mathscr{D}_i$, where $i=1,2$. These operators are assumed to map a function f defined in the interval $[0,4]$ into a function defined respectively in $J_1=[1,2]$, $J_2=[2,3]$ and are defined by means of the following equalities:

$$\begin{cases}[\mathscr{A}_1(f)](\xi)=\displaystyle\int_1^{\xi+1}f(\eta)\sqrt{1-(f(\eta))^2}d\eta\\[2ex] [\mathscr{D}_1(f)](\xi)=\left(1-\displaystyle\int_1^{\xi+1}\left(1-(f(\eta))^2\right)d\eta\right),\end{cases}\qquad\begin{cases}[\mathscr{A}_2(f)](\xi)=\displaystyle\int_{\xi-1}^{3}f(\eta)\sqrt{1-(f(\eta))^2}d\eta\\[2ex] [\mathscr{D}_2(f)](\xi)=\left(1-\displaystyle\int_{\xi-1}^{3}\left(1-(f(\eta))^2\right)d\eta\right).\end{cases} \tag{5.43}$$

Remark. It is easy to check that for every function f if $\sup|f|\le 1$ then $\sup|\mathscr{A}_i(f)|\le 1$ and $\sup|\mathscr{D}_i(f)|\le 1$, where $i=1,2$ and the sup is estimated in the corresponding domain of definition.

The stationarity condition finally obtained is expressed by the following integro-differential equations (to be complemented by suitable boundary conditions)

$$\frac{1-2(\mu_{,\xi})^2}{2\sqrt{1-(\mu_{,\xi})^2}}\mathscr{A}_i(\mu_{,\xi})-\mu_{,\xi}\mathscr{D}_i(\mu_{,\xi})+\Lambda\left(1-\frac{\mu_{,\xi}}{\sqrt{1-(\mu_{,\xi})^2}}\right)=0.\qquad\forall\xi\in J_i,\ i=1,2 \tag{5.44}$$

which can be transformed in the other one:

$$\left(\frac{1-2\left(\mu_{,\xi}\right)^2}{2\sqrt{1-\left(\mu_{,\xi}\right)^2}}\mathscr{A}_i\left(\mu_{,\xi}\right)-\mu_{,\xi}\mathscr{D}_i\left(\mu_{,\xi}\right)\right)\left(\frac{\mu_{,\xi}}{\sqrt{1-\left(\mu_{,\xi}\right)^2}}-1\right)^{-1}=\Lambda. \qquad \forall\xi\in J_i,\ i=1,2$$

To proceed in the study of the found integro-differential equation it is useful to introduce an auxiliary function F defined on the domain

$$\mathbb{R}^3\supseteq D:=\left[\frac{\sqrt{2}}{2},1\right)\times(0,1]\times(0,1]\,. \tag{5.45}$$

as follows:

$$F\left(x,a,d\right)=\left(\frac{1-2x^2}{2\sqrt{1-x^2}}a-xd\right)\left(\frac{x}{\sqrt{1-x^2}}-1\right)^{-1}, \tag{5.46}$$

It can be checked that $F(D)=\mathbb{R}^-$ and that there exists a function

$$G:(0,1]\times(0,1]\times\mathbb{R}^-\to\left[\frac{\sqrt{2}}{2},1\right) \tag{5.47}$$

such that

$$F(G(a,d,\Lambda),a,d)=\Lambda;\ G(a,d,F(x,a,d))=x \tag{5.48}$$

By means of the just introduced functions F and G the stationarity problem can be formulated in the two following more compact forms.

Problem 41. Find a function $\hat{\mu}\in\mathscr{C}^2_{pw}\left(I,\{2\}\right)$ such that i) $\hat{\mu}\left(1\right)=1$, and ii) there exists a negative real number Λ such that the following equations are verified:

$$\begin{cases} F\left(\hat{\mu}_{,\xi},\mathscr{A}_i\left(\hat{\mu}_{,\xi}\right),\mathscr{D}_i\left(\hat{\mu}_{,\xi}\right)\right)=\Lambda & \forall\xi\in J_i,\ i=1,2. \\ \\ C\left(\hat{\mu}_{,\xi}\right)=0 \end{cases} \tag{5.49}$$

By using the second of identities (5.48) and conditions (5.49) it can be easily seen that the just introduced problem is equivalent to the following one, which is more suitable to the application of the Picard-type iteration method we will use in the following section:

Problem 42. Find a function $\mu_*\in\mathscr{C}^2_{pw}\left(I,\{2\}\right)$ such that

$$\begin{cases} \mu_*(\xi)=1+\displaystyle\int_1^{\xi}G([\mathscr{A}_1\left(\mu_{*,\xi}\right)]\left(\eta\right),[\mathscr{D}_1\left(\mu_{*,\xi}\right)]\left(\eta\right),\Lambda)d\eta & \forall\xi\in[1,2] \\ \\ \mu_*(\xi)=\mu_*(2)+\displaystyle\int_2^{\xi}G([\mathscr{A}_2\left(\mu_{*,\xi}\right)]\left(\eta\right),[\mathscr{D}_2\left(\mu_{*,\xi}\right)]\left(\eta\right),\Lambda)d\eta & \forall\xi\in]2,3], \end{cases} \tag{5.50}$$

choosing the parameter Λ in order to verify the integral condition $C\left(\mu_{*,\xi}\right)=0$.
Postponing the study of the well-posedness of the formulated integro-differential problem to further investigations we show that the last presented form more easily lends itself to numerical integration.

5.3.5 Numerical resolution of the problem

The problem expressed by (5.49) cannot be, in general, solved in closed form: therefore we are obliged to resort to numerical methods.
In order to solve the problem (42) by means of numerical integration techniques we define an iterative scheme in which the initial function $\mu_{[0]}$ is chosen to be a first order polynomial satisfying the boundary conditions (5.33).
Given the approximation of the solution of the Picard-type problem formulated in (42) at the step $n-1$, that is the function $\mu_{[n-1]}$ we find the $n-th$ approximation as follows

$$\begin{cases} \mu_{[n]}(\xi) = 1 + \int_1^{\xi} G(\left[\mathscr{A}_1\left(\mu_{[n-1],\xi}\right)\right](\eta), \left[\mathscr{D}_1\left(\mu_{[n-1],\xi}\right)\right](\eta), \Lambda_n) d\eta & \forall \xi \in [1,2] \\ \mu_{[n]}(\xi) = \mu_{[n]}(2) + \int_2^{\xi} G(\left[\mathscr{A}_2\left(\mu_{[n-1],\xi}\right)\right](\eta), \left[\mathscr{D}_2\left(\mu_{[n-1],\xi}\right)\right](\eta), \Lambda_n) d\eta & \forall \xi \in]2,3], \end{cases} \quad (5.51)$$

choosing the parameter Λ_n in order to verify the boundary condition $C\left(\mu_{[n],\xi}\right) = 0$.
We iterate until the numerical convergence of the solution is obtained. In the following figure it is shown the flow chart of the algorithm.

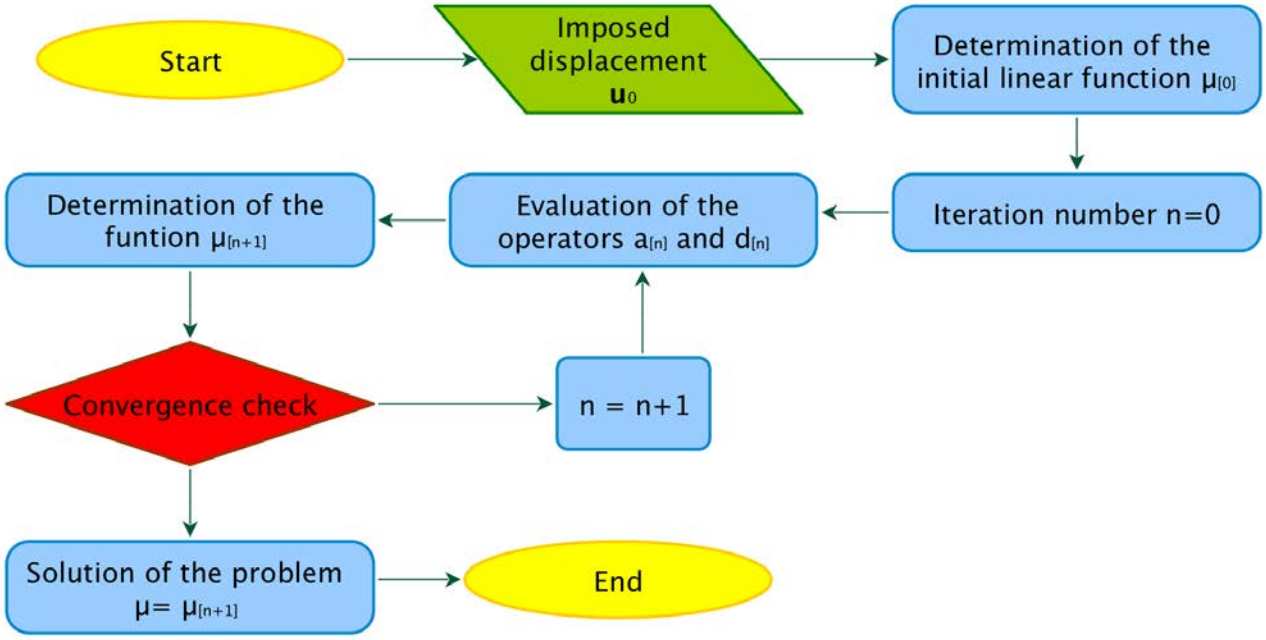

Figure 5.6: Resolutive algorithm

5.3.5.1 Numerical results

The algorithm is implemented in Mathematica® with different values of the imposed displacement u_0. In the figure (5.7) we show the deformed geometry for 3 different imposed displacements. The results match qualitatively the experimental results obtained with the standard bias extension text for composite fiber reinforcements.

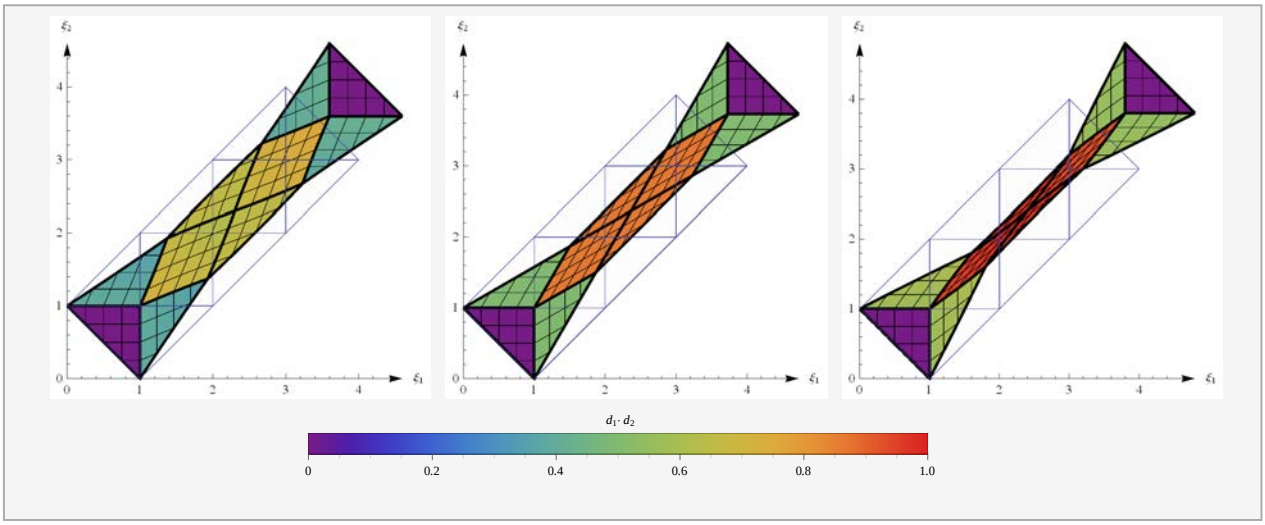

Figure 5.7: Deformed shape for imposed displacements u_0 of: 0.65, 0.73 and 0.8

The numerical analysis shows an interesting phenomenon which deserves some discussion and further theoretical, numerical and experimental investigations.
Indeed in the numerical solutions obtained, in general, one can check that the scalar field giving angle between the inextensible fibers (fiber shear angle), easily related to the field $\mathbf{d}_1 \cdot \mathbf{d}_2$, is not piece-wise constant in the kinematically determined (see previous sections) different zones of the domain as it is usually stated in the literature of fiber composite reinforcements. Actually the plots of this field along lines parallel to the long side of the specimen also show different concavities for different imposed displacements and it is also possible to observe the existence of a unique critical displacement for which the fiber shear angle is piece-wise constant.
This numerical results raises questions about their causes and implications. The questions to be addressed are, in particular, the following ones: is the numerical behavior detected related to some phenomena? Are these phenomena present in the fiber reinforcements which originated our investigations? Which complex mechanical structures show the behavior detected by the model which we consider in the present work?
The values of $\mathbf{d}_1 \cdot \mathbf{d}_2$ are plotted for the entire reference specimen in figure (5.8,5.9) and for particular sections in figure (5.10) to highlight the meaningful entity of the angle variation in each region. It is possible to find the critical value of displacement in correspondence of which the change of concavity occurs. This value is placed approximately at a displacement having a dimensionless value of 0.73 (which corresponds about to one quarter of the length of the specimen) and we can see in the presented figures that for the critical displacement $\mathbf{d}_1 \cdot \mathbf{d}_2$ it remains constant in all the different zones of the specimen.

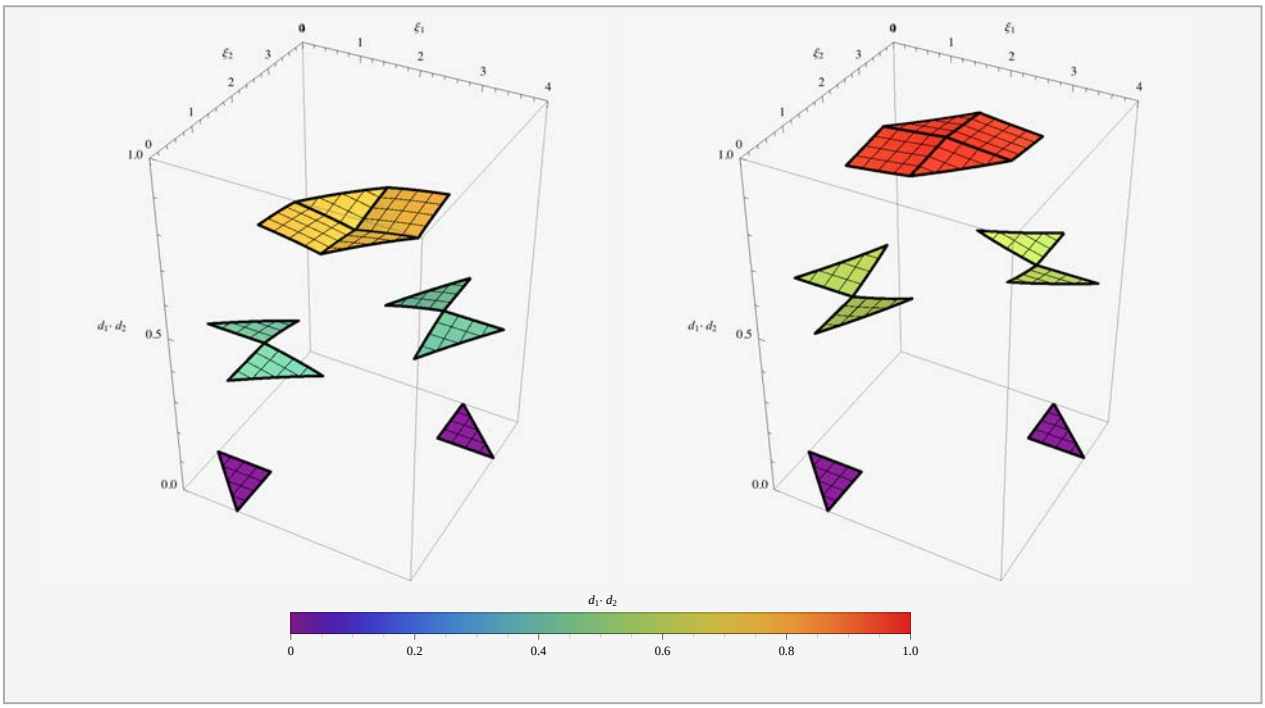

Figure 5.8: Cosine of the angle between the fibers for an imposed displacement u_0 of: 0.65 and 0.8

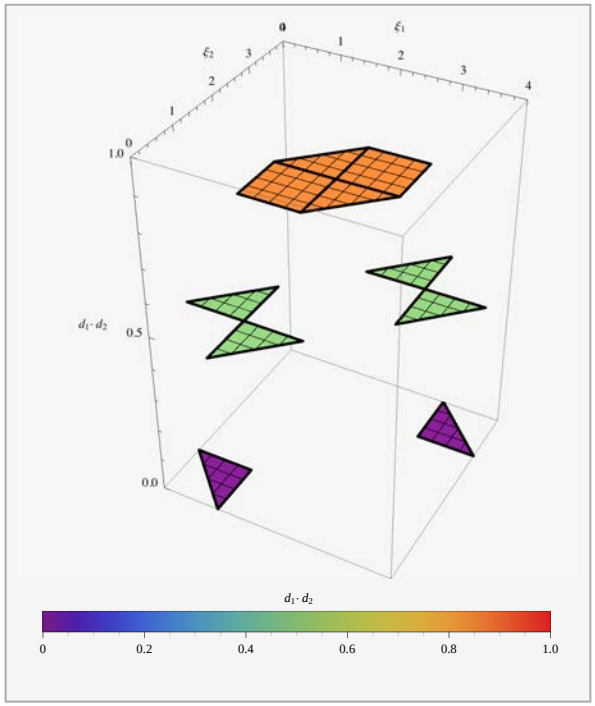

Figure 5.9: The critical value 0.73

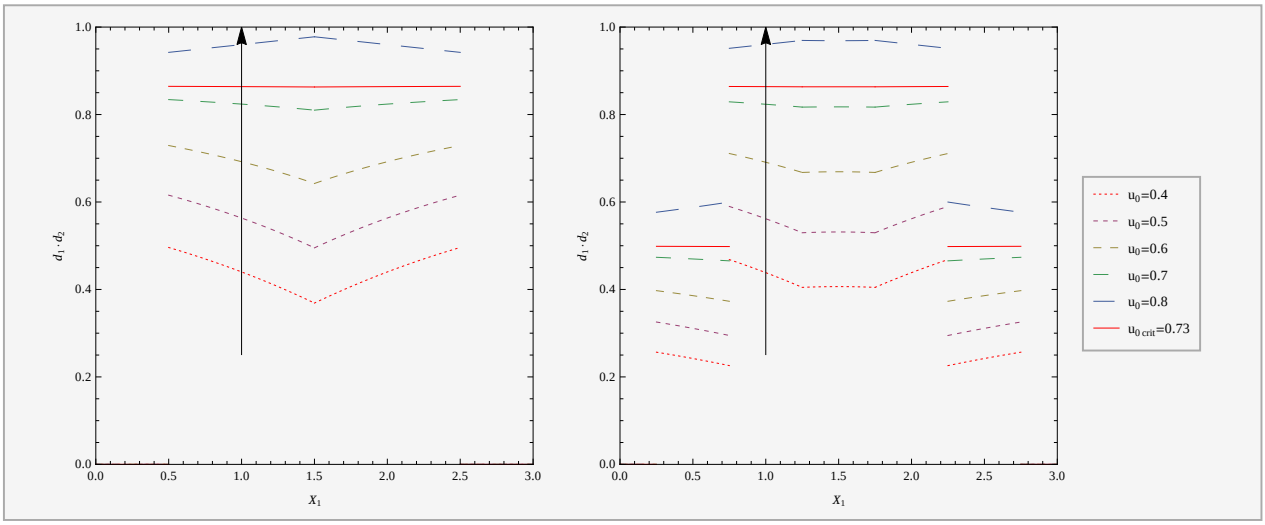

Figure 5.10: Cosine of the angle between the fibers in the symmetry axis X_1 and in the section $X_2 = 0.25$

5.3.6 Conclusion

In the present section the standard bias extension test for first gradient continua with inextensible fibers was studied assuming that the only deformation mechanism related to deformation energy consists in the change of angle between the fibers occurring in the passage from reference to current configuration: this change may be interpreted as a shear deformation of the considered continuum. Such a continuum seems suitable to describe the behavior of some complex materials in which very stiff fibers are embedded and can be applied, with some cautions, to describe the mechanical behavior of some fiber reinforcements.

The kinematics considered in this section is rather restrictive, even if the assumption of exact inextensibility of orthogonal families of fibers seems to be rather well-grounded from a physical point of view. Also the deformation energy considered (which depends quadratically only on the variation of the shear angle between the inextensible fibers) does not seem sufficient to describe completely many experimental evidences [33, 11, 12, 41, 42, 50, 51, 6]. It will be subject of further investigations the study of continua with extensible or inextensible fibers whose energy depend also on higher displacement gradients (by using the methods presented e.g. [22, 23, 24] e.g. [46, 64, 66, 47, 73].

The simple first gradient continuum considered here has been introduced mainly to move a first step towards a effective modeling of bias extension tests for fiber reinforcements or for newly conceived and built metamaterials. However it seems rich enough to catch some peculiarities of the mechanical behavior of fiber reinforcements. Indeed the results of presented analysis predict a sharp discontinuity in the angle variation (shear deformation between inextensible fibers) in the passage between the different (as kinematically characterized in terms of the imposed boundary conditions) zones of the specimen undergoing bias test. This circumstance catches some features of the experimentally observed evidence: indeed [33] in extension bias test shear deformation is concentrated in narrow regions in the neighborhood of some inextensible fibers. On the other hand the thickness of these regions is experimentally seen to be non-vanishing: therefore it seems a well-grounded conjecture to state that at least second gradient energies [20] are needed if one wants to get models capable to predict the onset of the boundary layers where high gradients of shear angle are concentrated.

Here it has to be underlined, once more, that it is very difficult to characterize, for considered mechanical systems, equilibrium configurations as those configurations where balance of force and momentum is to be verified. Indeed, as already implied in [90, 83], the postulation of continuum mechanics based on balance equations does not seem adapted to formulate the models needed here: the difficulties in formulating balance laws when introducing Lagrange multipliers in order to account

for all possible contact actions can be insurmountable. Only when mechanics is based on suitable variational principles then well-posed mathematical problems are easily obtained: the continuum models formulated in [1, 29, 68, 76, 77, 78, 81, 82, 69, 70, 62, 64, 71, 65, 66] give simply a further example of this statement.

General conclusion

The complete characterization of fibrous composite reinforcements must account for the description of their mechanical behavior at the mesoscopic and microscopic scales. In this manuscript we basically limit ourselves to the study of 2D fibrous reinforcements but approaching the problem of their modeling by treating a wealthy of different aspects.

- First of all we treat the case of bias extension test by introducing different discrete numerical simulations which allow us to conclude that the effect of the local bending of the fibers at the mesoscopic level cannot be neglected if one wants to fully characterize the behavior of fibrous composite reinforcements.
- On the basis of such observations, we introduce a second gradient continuum model which allows to properly describe the presence of such local bending of the yarns while still remaining in a macroscopic continuum framework. We present some numerical simulations, always concerning the bias extension test, which show the soundness of the proposed continuum model.
- We introduce the constraint of inextensibility of the yarns in order to investigate limit systems which can serve as a reference for more complicated material behaviors. We do so for first gradient continua and we show some numerical solutions for the bias extension test which allow to appreciate the well-posedness of the developed modeling.

Further studies should investigate the possibility of including the inextensibility constraint also for second gradient continua as it has been underlined in the first part of this thesis.
Moreover, the usefulness of higher gradient models for the description of the mechanical behavior of unbalanced fabrics could also be of use. Indeed, when the warp and weft have very different bending stiffnesses, the effect of such mesoscopic properties on the macroscopic behavior of the fabric could be unexpectedly important.

Appendix

First variation of the action functional of the first gradient inextensible model

In this appendix we supply some more details about the derivation of the Euler-Lagrange conditions found in the corresponding section.

Deformation energy functional

The functional whose first variation has to be calculated is:

$$\mathscr{A}_W\left(\mu\left(\bullet\right)\right)=\int_B W\,dm+\Lambda C\left(\mu_{,\xi}\right)=\int_B\left[\frac{1}{2}\left(\left(\mu_{,\xi}\left(\xi_1\right)\right)^2\left(1-\left(\mu_{,\xi}\left(\xi_2\right)\right)^2\right)+\left(\mu_{,\xi}\left(\xi_2\right)\right)^2\left(1-\left(\mu_{,\xi}\left(\xi_1\right)\right)^2\right)+\right.$$

$$\left.+2\mu_{,\xi}\left(\xi_1\right)\mu_{,\xi}\left(\xi_2\right)\sqrt{\left(1-\left(\mu_{,\xi}\left(\xi_1\right)\right)^2\right)\left(1-\left(\mu_{,\xi}\left(\xi_2\right)\right)^2\right)}\right)\right]dm \tag{5.52}$$

$$+\left(\mu\left(H-1\right)+\int_1^3\sqrt{1-\left(\mu_{,\xi}\right)^2}d\eta-3-u_0\right)\Lambda.$$

Remark. The reader must remark that the just introduced functional maps a real function μ defined in the interval $[1,3]$ into a real number. However the function μ is calculated in some occurrences in the variable ξ_1 and in some other occurrences in the variable ξ_2 when forming the integrand function appearing inside the square brackets of the previous equation. This integrand is indeed a function of the two variables (ξ_1,ξ_2) and its domain of integration is the two-dimensional domain B.

Considering the partition (5.11) of the domain B and defining $\underline{\Delta}=\Delta_{11}\cup\Delta_{21}\cup\Delta_{22}\cup\Delta_{21}$, it is possible to rewrite the functional as follows:

$$\begin{aligned}\mathscr{A}_W = &\int_{\Delta_{01}\cup\Delta_{32}} \frac{1}{2}\left(1-\left(\mu_{,\xi}\left(\xi_2\right)\right)^2\right) dm + \int_{\Delta_{10}\cup\Delta_{23}} \frac{1}{2}\left(1-\left(\mu_{,\xi}\left(\xi_1\right)\right)^2\right) dm + \\ &+ \int_{\underline{\Delta}} \frac{1}{2}\Bigg[\left(\mu_{,\xi}\left(\xi_1\right)\right)^2\left(1-\left(\mu_{,\xi}\left(\xi_2\right)\right)^2\right) + \left(\mu_{,\xi}\left(\xi_2\right)\right)^2\left(1-\left(\mu_{,\xi}\left(\xi_1\right)\right)^2\right) + \\ &+ 2\mu_{,\xi}\left(\xi_1\right)\mu_{,\xi}\left(\xi_2\right)\sqrt{\left(1-\left(\mu_{,\xi}\left(\xi_1\right)\right)^2\right)\left(1-\left(\mu_{,\xi}\left(\xi_2\right)\right)^2\right)}\Bigg] dm \\ &+ \left(\int_1^3 \left(\mu_{,\xi}\left(\xi_1\right) + \sqrt{1-\left(\mu_{,\xi}\left(\xi_1\right)\right)^2}\right) d\xi_1 - 2 - u_0\right)\Lambda,\end{aligned} \tag{5.53}$$

which, by using the assumed symmetry of the solution, becomes

$$\begin{aligned}\mathscr{A}_W = &\int_{\Delta_{01}\cup\Delta_{32}} \frac{1}{2}\left(1-\left(\mu_{,\xi}\left(\xi_2\right)\right)^2\right) dm + \int_{\Delta_{10}\cup\Delta_{23}} \frac{1}{2}\left(1-\left(\mu_{,\xi}\left(\xi_1\right)\right)^2\right) dm + \\ &+ \int_{\underline{\Delta}} \Bigg[\left(\mu_{,\xi}\left(\xi_1\right)\right)^2\left(1-\left(\mu_{,\xi}\left(\xi_2\right)\right)^2\right) + \mu_{,\xi}\left(\xi_1\right)\mu_{,\xi}\left(\xi_2\right)\sqrt{\left(1-\left(\mu_{,\xi}\left(\xi_1\right)\right)^2\right)\left(1-\left(\mu_{,\xi}\left(\xi_2\right)\right)^2\right)}\Bigg] dm \\ &+ \left(\int_1^3 \left(\mu_{,\xi}\left(\xi_1\right) + \sqrt{1-\left(\mu_{,\xi}\left(\xi_1\right)\right)^2}\right) d\xi_1 - 2 - u_0\right)\Lambda.\end{aligned} \tag{5.54}$$

Calculation of the first variation of the deformation energy functional

The first variation of the deformation energy functional can be expressed as:

$$\delta\mathscr{A}_W = \int_B \delta W\, dm + \Lambda\delta C\left(\mu_{,\xi}\right) + C\left(\mu_{,\xi}\right)\delta\Lambda. \tag{5.55}$$

We have

$$\int_B \delta W\, dm + \Lambda \delta C\left(\mu_{,\xi}\right) = -\int_{\Delta_{01}\cup\Delta_{32}} \mu_{,\xi}\left(\xi_2\right)\delta\mu_{,\xi}\left(\xi_2\right) dm - \int_{\Delta_{10}\cup\Delta_{23}} \mu_{,\xi}\left(\xi_1\right)\delta\mu_{,\xi}\left(\xi_1\right) dm +$$

$$+\int_{\underline{\Delta}} \left(2\mu_{,\xi}\left(\xi_1\right)\left(1-\left(\mu_{,\xi}\left(\xi_2\right)\right)^2\right) + \frac{1-2\left(\mu_{,\xi}\left(\xi_1\right)\right)^2}{\sqrt{1-\left(\mu_{,\xi}\left(\xi_1\right)\right)^2}}\mu_{,\xi}\left(\xi_2\right)\sqrt{1-\left(\mu_{,\xi}\left(\xi_2\right)\right)^2} + \right. \tag{5.56}$$

$$\left. + \left(1 - \frac{\mu_{,\xi}\left(\xi_1\right)}{\sqrt{1-\left(\mu_{,\xi}\left(\xi_1\right)\right)^2}}\right)\Lambda\right)\delta\mu_{,\xi}\left(\xi_1\right) +$$

$$+\int_{\underline{\Delta}} \left(-2\mu_{,\xi}\left(\xi_2\right)\left(\left(\mu_{,\xi}\left(\xi_1\right)\right)^2\right) + \frac{1-2\left(\mu_{,\xi}\left(\xi_2\right)\right)^2}{\sqrt{1-\left(\mu_{,\xi}\left(\xi_2\right)\right)^2}}\mu_{,\xi}\left(\xi_1\right)\sqrt{1-\left(\mu_{,\xi}\left(\xi_1\right)\right)^2}\right)\delta\mu_{,\xi}\left(\xi_2\right) dm.$$

Due to the symmetry condition, we have that

$$\int_{\underline{\Delta}} \left(-2\mu_{,\xi}\left(\xi_2\right)\left(\left(\mu_{,\xi}\left(\xi_1\right)\right)^2\right) + \frac{1-2\left(\mu_{,\xi}\left(\xi_2\right)\right)^2}{\sqrt{1-\left(\mu_{,\xi}\left(\xi_2\right)\right)^2}}\mu_{,\xi}\left(\xi_1\right)\sqrt{1-\left(\mu_{,\xi}\left(\xi_1\right)\right)^2}\right)\delta\mu_{,\xi}\left(\xi_2\right) dm =$$

$$= \int_{\underline{\Delta}} \left(-2\mu_{,\xi}\left(\xi_1\right)\left(\left(\mu_{,\xi}\left(\xi_2\right)\right)^2\right) + \frac{1-2\left(\mu_{,\xi}\left(\xi_1\right)\right)^2}{\sqrt{1-\left(\mu_{,\xi}\left(\xi_1\right)\right)^2}}\mu_{,\xi}\left(\xi_2\right)\sqrt{1-\left(\mu_{,\xi}\left(\xi_2\right)\right)^2}\right)\delta\mu_{,\xi}\left(\xi_1\right) dm, \tag{5.57}$$

and

$$\int_{\Delta_{01}\cup\Delta_{32}} \mu_{,\xi}\left(\xi_2\right)\delta\mu_{,\xi}\left(\xi_2\right) dm = \int_{\Delta_{10}\cup\Delta_{23}} \mu_{,\xi}\left(\xi_1\right)\delta\mu_{,\xi}\left(\xi_1\right) dm. \tag{5.58}$$

So, replacing (5.57) and (5.58) in (5.56), we obtain:

$$\int_B \delta W\, dm + \Lambda \delta C\left(\mu_{,\xi}\right) = -2\int_{\Delta_{10}\cup\Delta_{23}} \mu_{,\xi}\left(\xi_1\right)\delta\mu_{,\xi}\left(\xi_1\right) dm + \int_{\underline{\Delta}} \left(2\mu_{,\xi}\left(\xi_1\right) - 4\mu_{,\xi}\left(\xi_1\right)\left(\mu_{,\xi}\left(\xi_2\right)\right)^2 + \right.$$

$$\left. + 2\frac{1-2\left(\mu_{,\xi}\left(\xi_1\right)\right)^2}{\sqrt{1-\left(\mu_{,\xi}\left(\xi_1\right)\right)^2}}\mu_{,\xi}\left(\xi_2\right)\sqrt{1-\left(\mu_{,\xi}\left(\xi_2\right)\right)^2} + \left(1 - \frac{\mu_{,\xi}\left(\xi_1\right)}{\sqrt{1-\left(\mu_{,\xi}\left(\xi_1\right)\right)^2}}\right)\Lambda\right)\delta\mu_{,\xi}\left(\xi_1\right). \tag{5.59}$$

Now, applying the Fubini Theorem we find:

$$\int_B \delta W\, dm + \Lambda \delta C\left(\mu_{,\xi}\right) = \int_1^2 \Bigg[4\mu\left(\xi_1\right)\left(-1 + \int_1^{1+\xi_1} \left(1 - \left(\mu_{,\xi}\left(\xi_2\right)\right)^2\right) d\xi_2\right) +$$

$$+ 2\frac{1 - 2\left(\mu_{,\xi}\left(\xi_1\right)\right)^2}{\sqrt{1 - \left(\mu_{,\xi}\left(\xi_1\right)\right)^2}} \int_1^{1+\xi_1} \mu_{,\xi}\left(\xi_2\right) \sqrt{1 - \left(\mu_{,\xi}\left(\xi_2\right)\right)^2} d\xi_2 + \tag{5.60}$$

$$+ \left(1 - \frac{\mu_{,\xi}\left(\xi_1\right)}{\sqrt{1 - \left(\mu_{,\xi}\left(\xi_1\right)\right)^2}}\right) \Lambda \Bigg] \delta\mu_{,\xi}\left(\xi_1\right)\, d\xi_1 +$$

$$+ \int_2^3 \Bigg[4\mu_{,\xi}\left(\xi_1\right)\left(-1 + \int_{\xi_1 - 1}^3 \left(1 - \left(\mu_{,\xi}\left(\xi_2\right)\right)^2\right) d\xi_2\right) +$$

$$+ 2\frac{1 - 2\left(\mu_{,\xi}\left(\xi_1\right)\right)^2}{\sqrt{1 - \left(\mu_{,\xi}\left(\xi_1\right)\right)^2}} \int_{\xi_1 - 1}^3 \mu_{,\xi}\left(\xi_2\right) \sqrt{1 - \left(\mu_{,\xi}\left(\xi_2\right)\right)^2} d\xi_2 +$$

$$+ \left(1 - \frac{\mu_{,\xi}\left(\xi_1\right)}{\sqrt{1 - \left(\mu_{,\xi}\left(\xi_1\right)\right)^2}}\right) \Lambda \Bigg] \delta\mu_{,\xi}\left(\xi_1\right)\, d\xi_1.$$

Renaming the variables by means of the equalities $\xi_2 = \eta$ and $\xi_1 = \xi$, we are lead to define two functions F_i in the following way :

$$F_1\left(\mu_{,\xi}, \xi, \Lambda\right) = \frac{1 - 2\left(\mu_{,\xi}\left(\xi\right)\right)^2}{2\sqrt{1 - \left(\mu_{,\xi}\left(\xi\right)\right)^2}} \underbrace{\int_1^{1+\xi} \mu_{,\xi}\left(\eta\right) \sqrt{1 - \left(\mu_{,\xi}\left(\eta\right)\right)^2} d\eta}_{a_1(\xi)} +$$

$$- \mu\left(\xi\right) \underbrace{\left(1 - \int_1^{1+\xi} \left(1 - \left(\mu_{,\xi}\left(\eta\right)\right)^2\right) d\eta\right)}_{d_1(\xi)} + \left(1 - \frac{\mu_{,\xi}\left(\xi\right)}{\sqrt{1 - \left(\mu_{,\xi}\left(\xi\right)\right)^2}}\right) \Lambda, \tag{5.61}$$

$$F_2\left(\mu_{,\xi}, \xi, \Lambda\right) = \frac{1 - 2\left(\mu_{,\xi}\left(\xi\right)\right)^2}{2\sqrt{1 - \left(\mu_{,\xi}\left(\xi\right)\right)^2}} \underbrace{\int_{\xi-1}^3 \mu_{,\xi}\left(\eta\right) \sqrt{1 - \left(\mu_{,\xi}(\eta)^2\right)} d\eta}_{a_2(\xi)} +$$

$$- \mu_{,\xi}\left(\xi\right) \underbrace{\left(1 - \int_{\xi-1}^3 \left(1 - \left(\mu_{,\xi}\left(\eta\right)\right)^2\right) d\eta\right)}_{d_2(\xi)} + \left(1 - \frac{\mu_{,\xi}\left(\xi\right)}{\sqrt{1 - \left(\mu_{,\xi}\left(\xi\right)\right)^2}}\right) \Lambda.$$

Therefore the first variation of the deformation energy can be represented as follows:

$$\delta\mathscr{A}_W = 4\int_1^2 F_1(\mu_{,\xi},\xi,\Lambda)\delta\mu_{,\xi}d\xi + 4\int_2^3 F_2(\mu_{,\xi},\xi,\Lambda)\delta\mu_{,\xi}d\xi + C(\mu_{,\xi})\delta\Lambda. \tag{5.62}$$

Integration by parts and the final expression for Euler-Lagrange stationarity condition

Thanks to an integration by parts, it is possible to rewrite the variation of the deformation energy functional as follows:

$$\delta\mathscr{A}_W = 4\int_1^2 F_1(\mu_{,\xi},\xi,\Lambda)\delta\mu_{,\xi}d\xi + 4\int_2^3 F_2(\mu_{,\xi},\xi,\Lambda)\delta\mu_{,\xi}d\xi + C(\mu_{,\xi})\delta\Lambda = \tag{5.63}$$

$$= 4\left[F_1(\mu_{,\xi},\xi,\Lambda)\delta\mu\right]_1^2 + 4\left[F_2(\mu_{,\xi},\xi,\Lambda)\delta\mu\right]_2^3 - 4\int_1^2 \frac{\partial F_1(\mu_{,\xi},\xi,\Lambda)}{\partial\xi}\delta\mu\, d\xi + \tag{5.64}$$

$$- 4\int_2^3 \frac{\partial F_2(\mu_{,\xi},\xi,\Lambda)}{\partial\xi}\delta\mu\, d\xi + C(\mu_{,\xi})\delta\Lambda. \tag{5.65}$$

Because of the arbitrariness of the variation $\delta\mu$, we get that:

$$\begin{cases} \dfrac{\partial F_i(\mu_{,\xi},\xi,\Lambda)}{\partial\xi} = 0 & \forall\xi\in I_i \implies F_i(\mu_{,\xi},\xi,\Lambda) = K_i \\ F_2(\mu_{,\xi},3,\Lambda) = 0 & \implies K_2 = 0 \\ F_1(\mu_{,\xi},2,\Lambda) = F_2(\mu_{,\xi},2,\Lambda) & \implies K_1 = K_2 = 0 \\ C(\mu_{,\xi}) = 0 \end{cases} \tag{5.66}$$

Therefore, the stationarity condition is given by the system of equations:

$$\begin{cases} F_i(\mu_{,\xi},\xi,\Lambda) = 0 & \forall\xi\in I_i \\ C(\mu_{,\xi}) = 0 \end{cases} \tag{5.67}$$

with $I_1 = [1,2]$, $I_2 = [2,3]$.

Bibliography

[1] JE Adkins and RS Rivlin. Large elastic deformations of isotropic materials X. Reinforcement by inextensible cords. *Philosophical Transactions of the Royal Society of London. Series A, Mathematical and Physical Sciences*, 248(944):201–223, 1955.

[2] Jean-Jacques Alibert, Pierre Seppecher, and Francesco Dell'Isola. Truss modular beams with deformation energy depending on higher displacement gradients. *Mathematics and Mechanics of Solids*, 8(1):51–73, 2003.

[3] Nicolas Auffray, Francesco dell'Isola, VA Eremeyev, Angela Madeo, and Giuseppe Rosi. Analytical continuum mechanics à la Hamilton-Piola least action principle for second gradient continua and capillary fluids. *Mathematics and Mechanics of Solids*, page 1081286513497616, 2013.

[4] Pierre Badel, S Gauthier, Emmanuelle Vidal-Sallé, and Philippe Boisse. Rate constitutive equations for computational analyses of textile composite reinforcement mechanical behaviour during forming. *Composites Part A: Applied Science and Manufacturing*, 40(8):997–1007, 2009.

[5] J.M. Ball. Convexity conditions and existence theorems in nonlinear elasticity. *Arch. Rat. Mech. Anal.*, 63:337–403, 1977.

[6] Sylvain Bel, Philippe Boisse, and Francois Dumont. Analyses of the deformation mechanisms of non-crimp fabric composite reinforcements during preforming. *Applied Composite Materials*, 19(3-4):513–528, 2012.

[7] Philippe Boisse. Composite fiber reinforcement forming. *Wiley Encyclopedia of Composites*, 2012.

[8] Philippe Boisse, Nahiene Hamila, Emmanuelle Vidal-Sallé, and Francois Dumont. Simulation of wrinkling during textile composite reinforcement forming. influence of tensile, in-plane shear and bending stiffnesses. *Composites Science and Technology*, 71(5):683–692, 2011.

[9] M Camar-Eddine and P Seppecher. Closure of the set of diffusion functionals with respect to the mosco-convergence. *Mathematical Models and Methods in Applied Sciences*, 12(08):1153–1176, 2002.

[10] Mohamed Camar-Eddine and Pierre Seppecher. Determination of the closure of the set of elasticity functionals. *Archive for rational mechanics and analysis*, 170(3):211–245, 2003.

[11] J Cao, R Akkerman, P Boisse, J Chen, HS Cheng, EF De Graaf, JL Gorczyca, P Harrison, G Hivet, J Launay, et al. Characterization of mechanical behavior of woven fabrics: experimental methods and benchmark results. *Composites Part A: Applied Science and Manufacturing*, 39(6):1037–1053, 2008.

[12] A. Charmetant and P. Boisse J.G. Orliac, E. Vidal Sallée. Hyperelastic model for large deformation analyses of 3d interlock composite preforms. *Composites Science and Technology*, 72 1352–1360:1352–1360, 2012.

[13] Adrien Charmetant. *Approches hyperélastiques pour la modélisation du comportement mécanique de préformes tissées de composites*. PhD thesis, INSA de Lyon, 2011.

[14] Adrien Charmetant, Emmanuelle Vidal-Sallé, and Philippe Boisse. Hyperelastic modelling for mesoscopic analyses of composite reinforcements. *Composites Science and Technology*, 71(14):1623–1631, 2011.

[15] Philippe G Ciarlet. *Mathematical elasticity: Three-dimensional elasticity*, volume 1. Elsevier, 1993.

[16] Massimo Cuomo and Mario Fagone. Finite deformation non-isotropic elasto-plasticity with evolving structural tensors. a framework. *Il Nuovo Cimento*, 32(1):55–72, 2009.

[17] M.V. d'Agostino, I. Giorgio, L. Greco, A. Madeo, and P. Boisse. Continuum and discrete models for structures including (quasi-)inextensible elasticae with a view to the design and modeling of composite reinforcements. *International Journal of Solids and Structures*, doi: http://dx.doi.org/10.1016/j.ijsolstr.2014.12.014, 2014.

[18] Francesco Dell'Isola, Ugo Andreaus, and Luca Placidi. At the origins and in the vanguard of peridynamics, non-local and higher-gradient continuum mechanics: An underestimated and still topical contribution of gabrio piola. *Mathematics and Mechanics of Solids*, page 1081286513509811, 2014.

[19] Francesco dell'Isola, Ugo Andreaus, Luca Placidi, and Daria Scerrato. Intorno alle equazioni fondamentali del movimento di corpi qualsivogliono, considerati secondo la naturale loro forma e costituzione. In *The complete works of Gabrio Piola: Volume I*, pages 1–370. Springer, 2014.

[20] Francesco dell'Isola, Henri Gouin, and Giacomo Rotoli. Nucleation of spherical shell-like interfaces by second gradient theory: numerical simulations. *European journal of mechanics. B, Fluids*, 15(4):545–568, 1996.

[21] Francesco Dell'Isola, Giulio Sciarra, and Stefano Vidoli. Generalized hooke's law for isotropic second gradient materials. In *Proceedings of the Royal Society of London A: Mathematical, Physical and Engineering Sciences*, pages rspa–2008. The Royal Society, 2009.

[22] Francesco dell'Isola and Pierre Seppecher. The relationship between edge contact forces, double forces and interstitial working allowed by the principle of virtual power. *Comptes Rendus de l Académie des Sciences-Series IIB-Mechanics-Physics-Astronomy*, 1995.

[23] Francesco dell'Isola and Pierre Seppecher. Edge contact forces and quasi-balanced power. *Meccanica*, 32(1):33–52, 1997.

[24] Francesco dell'Isola and David Steigmann. A two-dimensional gradient-elasticity theory for woven fabrics. *Journal of Elasticity*, 118(1):113–125, 2015.

[25] M Duhovic, P Mitschang, and D Bhattacharyya. Modelling approach for the prediction of stitch influence during woven fabric draping. *Composites Part A: Applied Science and Manufacturing*, 42(8):968–978, 2011.

[26] Francois Dumont, Gilles Hivet, Rene Rotinat, Jean Launay, Philippe Boisse, and Pierre Vacher. Mesures de champs pour des essais de cisaillement sur des renforts tissés. *Mécanique & industries*, 4(6):627–635, 2003.

[27] Francois19 Dumont et al. *Contribution à l'expérimentation et à la modélisation du comportement mécanique de renforts de composites tissés*. PhD thesis, Paris 6, 2003.

[28] Marek ElŻanowski and Marcelo Epstein. The symmetry group of second-grade materials. *International journal of non-linear mechanics*, 27(4):635–638, 1992.

[29] JL Ericksen and RS Rivlin. Large elastic deformations of homogeneous anisotropic materials. *Journal of rational mechanics and analysis*, 3(3):281–301, 1954.

[30] A Cemal Eringen and ES Suhubi. Nonlinear theory of simple micro-elastic solids—i. *International Journal of Engineering Science*, 2(2):189–203, 1964.

[31] Ahmed Cemal Eringen. *Microcontinuum field theories*. Springer, 2001.

[32] GC Everstine and AC Pipkin. Boundary layers in fiber-reinforced materials. *Journal of Applied Mechanics*, 40(2):518–522, 1973.

[33] Manuel Ferretti, Angela Madeo, Francesco dell'Isola, and Philippe Boisse. Modeling the onset of shear boundary layers in fibrous composite reinforcements by second-gradient theory. *Zeitschrift für angewandte Mathematik und Physik*, 65(3):587–612, 2014.

[34] Thomas Gereke, Oliver Döbrich, Matthias Hübner, and Chokri Cherif. Experimental and computational composite textile reinforcement forming: A review. *Composites Part A: Applied Science and Manufacturing*, 46:1–10, 2013.

[35] Paul Germain. La méthode des puissances virtuelles en mécanique des milieux continus. *J. Mécanique*, 12:236–274, 1973.

[36] Paul Germain. The method of virtual power in continuum mechanics. part 2: Microstructure. *SIAM Journal on Applied Mathematics*, 25(3):556–575, 1973.

[37] AE Green and RS Rivlin. Simple force and stress multipoles. *Archive for Rational Mechanics and Analysis*, 16(5):325–353, 1964.

[38] Albert E Green and Ronald S Rivlin. On cauchy's equations of motion. *Zeitschrift für Angewandte Mathematik und Physik (ZAMP)*, 15(3):290–292, 1964.

[39] Albert Edward Green and Ronald S Rivlin. Multipolar continuum mechanics. *Archive for Rational Mechanics and Analysis*, 17(2):113–147, 1964.

[40] Albert Edward Green and Ronald Samuel Rivlin. Multipolar continuum mechanics: functional theory i. In *Proceedings of the Royal Society of London A: Mathematical, Physical and Engineering Sciences*, volume 284, pages 303–324. The Royal Society, 1965.

[41] Nahiene Hamila and Philippe Boisse. Locking in simulation of composite reinforcement deformations. analysis and treatment. *Composites Part A: Applied Science and Manufacturing*, 53:109–117, 2013.

[42] Nahi'ene Hamila and Philippe Boisse. Tension locking in finite-element analyses of textile composite reinforcement deformation. *Comptes Rendus Mécanique*, 341(6):508 – 519, 2013.

[43] Nahiene Hamila, Philippe Boisse, Francis Sabourin, and Michel Brunet. A semi-discrete shell finite element for textile composite reinforcement forming simulation. *International journal for numerical methods in engineering*, 79(12):1443–1466, 2009.

[44] Philip Harrison. Normalisation of biaxial bias extension test results considering shear tension coupling. *Composites Part A: Applied Science and Manufacturing*, 43(9):1546–1554, 2012.

[45] Philip Harrison, Jo Wiggers, and Andrew C Long. Normalization of shear test data for rate-independent compressible fabrics. *Journal of composite materials*, 2008.

[46] MG Hilgers and AC Pipkin. Elastic sheets with bending stiffness. *The Quarterly Journal of Mechanics and Applied Mathematics*, 45(1):57–75, 1992.

[47] MG Hilgers and AC Pipkin. Energy-minimizing deformations of elastic sheets with bending stiffness. *Journal of elasticity*, 31(2):125–139, 1993.

[48] MJ King, P Jearanaisilawong, and S Socrate. A continuum constitutive model for the mechanical behavior of woven fabrics. *International Journal of Solids and Structures*, 42(13):3867–3896, 2005.

[49] EN Kuznetsov. Underconstrained structural systems. *International journal of solids and structures*, 24(2):153–163, 1988.

[50] Jean Launay, Gilles Hivet, Ahn V. Duong, and Philippe Boisse. Experimental analysis of the influence of tensions on in plane shear behaviour of woven composite reinforcements. *Composites Science and Technology*, 68(2):506 – 515, 2008.

[51] W. Lee, J. Padvoiskis, J. Cao, E. de Luycker, P. Boisse, F. Morestin, J. Chen, and J. Sherwood. Bias-extension of woven composite fabrics. *International Journal of Material Forming*, 1(1):895–898, 2008.

[52] Angela Madeo, Ionel-Dumitrel Ghiba, Patrizio Neff, and Ingo Münch. Incomplete traction boundary conditions in the grioli-koiter-mindlin-toupin indeterminate couple stress model. *arXiv preprint arXiv:1505.00995*, 2015.

[53] Angela Madeo, Patrizio Neff, Ionel-Dumitrel Ghiba, Luca Placidi, and Giuseppe Rosi. Wave propagation in relaxed micromorphic continua: modeling metamaterials with frequency band-gaps. *Continuum Mechanics and Thermodynamics*, pages 1–20, 2013.

[54] J Merodio and RW Ogden. Mechanical response of fiber-reinforced incompressible non-linearly elastic solids. *International Journal of Non-Linear Mechanics*, 40(2):213–227, 2005.

[55] Raymond David Mindlin. Micro-structure in linear elasticity. *Archive for Rational Mechanics and Analysis*, 16(1):51–78, 1964.

[56] Raymond David Mindlin. Second gradient of strain and surface-tension in linear elasticity. *International Journal of Solids and Structures*, 1(4):417–438, 1965.

[57] RD Mindlin and NN Eshel. On first strain-gradient theories in linear elasticity. *International Journal of Solids and Structures*, 4(1):109–124, 1968.

[58] Patrizio Neff, Ionel-Dumitrel Ghiba, Angela Madeo, Luca Placidi, and Giuseppe Rosi. A unifying perspective: the relaxed linear micromorphic continuum. *Continuum Mechanics and Thermodynamics*, 26(5):639–681, 2014.

[59] Jean-Guillaume Orliac. *Analyse et simulation du comportement anisotrope lors de la mise en forme de renforts tissés interlock*. PhD thesis, INSA de Lyon, 2012.

[60] Catherine Pideri and Pierre Seppecher. A second gradient material resulting from the homogenization of an heterogeneous linear elastic medium. *Continuum Mechanics and Thermodynamics*, 9(5):241–257, 1997.

[61] AC Pipkin. Finite deformations of ideal fiber-reinforced composites. *Mechanics of composite materials.(A 75-24868 10-39) New York, Academic Press, Inc., 1974*, pages 251–308, 1974.

[62] AC Pipkin. Generalized plane deformations of ideal fiber-reinforced materials. *Quarterly of Applied Mathematics*, 32:253–263, 1974.

[63] AC Pipkin. Finite deformations in materials reinforced with inextensible cords. *Finite Elasticity*, 27:92–102, 1977.

[64] AC Pipkin. Energy changes in ideal fiber-reinforced composites. *Quarterly of Applied Mathematics*, 35:455–463, 1978.

[65] AC Pipkin. Some developments in the theory of inextensible networks. *Quarterly of Applied Mathematics*, 38(3):343–355, 1980.

[66] AC Pipkin. Plane traction problems for inextensible networks. *The Quarterly Journal of Mechanics and Applied Mathematics*, 34(4):415–429, 1981.

[67] AC Pipkin. Stress channelling and boundary layers in strongly anisotropic solids. In *Continuum theory of the mechanics of fibre-reinforced composites*, pages 123–145. Springer, 1984.

[68] AC Pipkin and RS Rivlin. Minimum-weight design for pressure vessels reinforced with inextensible fibers. *Journal of Applied Mechanics*, 30(1):103–108, 1963.

[69] AC Pipkin and TG Rogers. A mixed boundary-value problem for fiber-reinforced materials (mixed boundary value problem for fiber reinforced materials, analyzing shear response in multiply admissible kinematic deformations). *Quarterly of Applied Mathematics*, 29:151–155, 1971.

[70] AC Pipkin and TG Rogers. Plane deformations of incompressible fiber-reinforced materials. *Journal of Applied Mechanics*, 38(3):634–640, 1971.

[71] Allen C Pipkin. Stress analysis for fiber-reinforced materials. *Advances in applied mechanics.*, 19:1–51, 1979.

[72] Allen C Pipkin. Equilibrium of tchebychev nets. In *The Breadth and Depth of Continuum Mechanics*, pages 287–303. Springer, 1986.

[73] Allen C Pipkin and VM Sanchez. Existence of solutions of plane traction problems for ideal composites. *SIAM Journal on Applied Mathematics*, 26(1):213–220, 1974.

[74] GY Qiu and TJ Pence. Remarks on the behavior of simple directionally reinforced incompressible nonlinearly elastic solids. *Journal of Elasticity*, 49(1):1–30, 1997.

[75] Annie Raoult. Symmetry groups in nonlinear elasticity: An exercise in vintage mathematics. *Communications on Pure and Applied Mathematics*, 8(1):435–456, 2009.

[76] RS Rivlin. Plane strain of a net formed by inextensible cords. *Journal of Rational Mechanics and Analysis*, 4(6):951–974, 1955.

[77] RS Rivlin. Constitutive equation for a fiber-reinforced lamina. In *IUTAM Symposium on Anisotropy, Inhomogeneity and Nonlinearity in Solid Mechanics*, pages 379–384. Springer, 1995.

[78] RS Rivlin. Networks of inextensible cords. In *Collected Papers of RS Rivlin*, pages 566–579. Springer, 1997.

[79] Lucio Russo. *The forgotten revolution*. Springer Science & Business Media, 2004.

[80] Pierre Seppecher, Jean-Jacques Alibert, and Francesco Dell Isola. Linear elastic trusses leading to continua with exotic mechanical interactions. In *Journal of Physics: Conference Series*, volume 319, page 012018. IOP Publishing, 2011.

[81] GF Smith and Richard S Rivlin. Stress-deformation relations for anisotropic solids. *Archive for Rational Mechanics and Analysis*, 1(1):107–112, 1957.

[82] GF Smith and RS Rivlin. The strain-energy function for anisotropic elastic materials. In *Collected Papers of RS Rivlin*, pages 541–559. Springer, 1997.

[83] Anthony James Merrill Spencer et al. *Continuum theory of the mechanics of fibre-reinforced composites*, volume 282. Springer, 1984.

[84] DJ Steigmann and AC Pipkin. Equilibrium of elastic nets. *Philosophical Transactions of the Royal Society of London. Series A: Physical and Engineering Sciences*, 335(1639):419–454, 1991.

[85] RHW Ten Thije, R Akkerman, and J Huétink. Large deformation simulation of anisotropic material using an updated lagrangian finite element method. *Computer methods in applied mechanics and engineering*, 196(33):3141–3150, 2007.

[86] Richard A Toupin. Elastic materials with couple-stresses. *Archive for Rational Mechanics and Analysis*, 11(1):385–414, 1962.

[87] Richard A Toupin. Theories of elasticity with couple-stress. *Archive for Rational Mechanics and Analysis*, 17(2):85–112, 1964.

[88] J Wang, R Paton, and JR Page. The draping of woven fabric preforms and prepregs for production of polymer composite components. *Composites Part A: Applied Science and Manufacturing*, 30(6):757–765, 1999.

[89] WB Wang and AC Pipkin. Inextensible networks with bending stiffness. *The Quarterly Journal of Mechanics and Applied Mathematics*, 39(3):343–359, 1986.

[90] WB Wang and AC Pipkin. Plane deformations of nets with bending stiffness. *Acta mechanica*, 65(1-4):263–279, 1987.

[91] Woong-Ryeol Yu, Philip Harrison, and Andrew Long. Finite element forming simulation for non-crimp fabrics using a non-orthogonal constitutive equation. *Composites Part A: Applied Science and Manufacturing*, 36(8):1079–1093, 2005.

INSA INSTITUT NATIONAL DES SCIENCES APPLIQUÉES LYON

FOLIO ADMINISTRATIF

THÈSE SOUTENUE DEVANT L'INSTITUT NATIONAL DES SCIENCES APPLIQUÉES DE LYON

NOM : D'AGOSTINO
(avec précision du nom de jeune fille, le cas échéant)

DATE de SOUTENANCE : 07/09/2015

Prénoms : Marco Valerio

TITRE : Generalized continua and applications to finite deformations of quasi-inextensible fiber reinforcements.
(Milieux continus généralisés: application aux grandes transformations des renforts de composites quasi- inextensibles)

NATURE : Doctorat

Numéro d'ordre : 2015ISAL0061

Ecole doctorale : MEGA

Spécialité : Mécanique, génie mécanique

RESUME : La microstructure des matériaux constitue un outil essentiel pour optimiser les propriétés mécaniques des structures et ainsi améliorer leurs performances.

Ce manuscrit est organisé comme suit :

- Dans le chapitre 1 nous introduisons les aspects généraux de la mécanique des renforts fibreux.

- Dans le chapitre 2 nous rappelons certains concepts fondamentaux concernant la mécanique des milieux continus classiques et les théories de deuxième gradient.

- Dans le chapitre 3 nous nous proposons de présenter une première modélisation des renforts fibreux de composites en mettant en place des modèles numériques discrets. Dans un deuxième moment nous introduisons une modélisation continue de deuxième gradient et nous montrons que les termes d'ordre supérieur permettent une description satisfaisante des effets de flexion locale sur-cités.

- Dans le chapitre 4 on particularise le cadre général de la mécanique des milieux continus introduit dans le chapitre 2 au cas particulier des milieux continus 2D.

- Dans le chapitre 5 nous introduisons une hypothèse cinématique forte sur les déformations admissibles, en supposant que les mèches du renfort considéré sont inextensibles. Une méthode numérique permettant de montrer certaines solutions concernant le cas du bias extension test est codée en Mathematica et les résultats obtenus sont discutés.

MOTS-CLÉS : Renforts fibreux de composite, théories de second gradient, milieux continus généralisés, bias extension test, matériaux fibreux quasi inextensibles .

Laboratoire (s) de recherche :
LaMCoS-CNRS, INSA-Lyon, France.

Directeur de thèse:
BOISSE Philippe, INSA-Lyon, France

Président de jury :

Composition du jury :
BOISSE Philippe, CARON Jean-François, CHABRAND Patrick , DELL'ISOLA Francesco, LIMAM Ali, MADEO Angela, SEPPECHER Pierre.